

UNIVERSITY OF RIJEKA  
FACULTY OF BIOTECHNOLOGY AND  
DRUG DEVELOPMENT

Josip Peradinović

**IMMUNE-MEDIATED PATHOLOGIES IN AN  
OPTINEURIN INSUFFICIENCY MOUSE MODEL**

DOCTORAL THESIS

Rijeka, 2025.



UNIVERSITY OF RIJEKA  
FACULTY OF BIOTECHNOLOGY AND  
DRUG DEVELOPMENT

Josip Peradinović

**IMMUNE-MEDIATED PATHOLOGIES IN AN  
OPTINEURIN INSUFFICIENCY MOUSE MODEL**

DOCTORAL THESIS

Supervisor: Professor Ivana Munitić, MD, PhD

Rijeka, 2025.

SVEUČILIŠTE U RIJECI  
FAKULTET BIOTEHNOLOGIJE I  
RAZVOJA LIJEKOVA

Josip Peradinović

**IMUNOSNO-POSREDOVANE PATOLOGIJE U  
MIŠJEM MODELU INSUFICIJENCIJE OPTINEURINA**  
DOKTORSKA DISERTACIJA

Mentor: Prof. dr. sc. Ivana Munitić, dr. med.

Rijeka, 2025.

Supervisor: Professor Ivana Munitić, MD, PhD

Doctoral thesis was defended on \_\_\_\_\_ at the Faculty of Biotechnology and Drug Development, University of Rijeka, in front of the Evaluation Committee:

1. Professor Antonija Jurak Begonja, PhD
2. Professor Kristina Pilipović, MD, PhD
3. Associate Professor Ilija Brizić, PhD

## **Zahvale**

## **Scientific support**

This research was supported by the Croatian Science Foundation (CSF) grant (IP-2018-01-8563) and the support of the University of Rijeka (18-211-1369 and 23-186-3163) to Professor Ivana Munitić. Josip Peradinović is financed by CSF PhD grant to Professor Ivana Munitić. The equipment used for the study was financed by European Regional Development Fund (ERDF), within the project “Research Infrastructure for Campus-based Laboratories at University of Rijeka”.

## Abstract

Amyotrophic lateral sclerosis (ALS) and frontotemporal dementia (FTD) are adult-onset neurodegenerative diseases characterized by neuronal loss, neuroinflammation and TAR DNA-binding protein 43 (TDP-43) protein aggregation in distinct regions of the central nervous system (CNS). Both diseases may be caused by mutations in the same genes, one of which is *OPTN*, encoding for optineurin. Optineurin is a ubiquitin-binding adaptor protein that regulates various cellular functions, including inflammatory signaling, autophagy, vesicular and mitochondrial trafficking. To study its role in disease, a truncation mouse model of optineurin insufficiency that lacks the ubiquitin-binding region (Optn<sup>470T</sup>) was generated by our group. Aging is the major risk factor for neurodegenerative diseases, which strongly affects the immune system and results in a chronic low-grade inflammation (inflammaging). Since optineurin plays a role in inflammatory signaling, which was shown to be impaired in ALS/FTD patients, we have performed detailed analyses of Optn<sup>470T</sup> mice during aging, which include evaluations of motor and cognitive abilities, neuropathology (neuronal loss, TDP-43 aggregation and lipofuscin accumulation) and neuroinflammation. We observed that aging of Optn<sup>470T</sup> mice did not exaggerate the decrease in motor and cognitive abilities found in wild-type (WT) mice. This was corroborated by the absence of neuropathology and exaggerated neuroinflammation in aged Optn<sup>470T</sup> mice. Given that peripheral immune cells are also affected in ALS patients and during aging, we analyzed T cell polarization. We found a decreased percentage of tumor necrosis factor (TNF)- and interleukin (IL)-17A-producing CD4<sup>+</sup> helper T cells and an increased percentage of TNF-producing CD8<sup>+</sup> T cells in Optn<sup>470T</sup> mice in comparison to WT mice. One of the new potential ALS hallmarks is decreased phagocytosis of microglia and macrophages, reported during aging and in ALS patients. Here, we reported a decreased percentage of phagocytic bone-marrow derived macrophages (BMDMs) from aging mice, which was unaffected by optineurin insufficiency. To test if additional genetic hits will precipitate the disease phenotype, we crossed Optn<sup>470T</sup> mice with TDP-43<sup>G348C</sup> mice, where the latter have been reported to develop ALS/FTD-like symptoms. We successfully confirmed the generation of Optn<sup>470T</sup>/TDP-43<sup>G348C</sup>, which showed lower expression levels of TDP-43<sup>G348C</sup> transgene compared to TDP-43<sup>G348C</sup> mice, suggesting a potential protective mechanism of Optn<sup>470T</sup> truncation. TDP-43 was previously reported to directly regulate inflammatory nuclear factor (NF)- $\kappa$ B-mediated signaling, which we did not observe in our experiments in BMDMs. In



contrast, lipopolysaccharide (LPS)-stimulated BMDMs from Optn<sup>470T</sup>/TDP-43<sup>G348C</sup> mice have shown unaffected NF-κB and decreased TANK-binding kinase (TBK1) signaling when compared to BMDMs from TDP-43<sup>G348C</sup> mice. Aged Optn<sup>470T</sup>/TDP-43<sup>G348C</sup> mice have shown decreased body weight and improved motor and cognitive abilities compared to TDP-43<sup>G348C</sup> mice of the same age. We also analyzed these mice in inflammatory conditions, which were reported to aggravate ALS/FTD phenotype. A three-day LPS administration resulted in a significant body weight loss and higher mortality of TDP-43<sup>G348C</sup> mice, which was rescued in Optn<sup>470T</sup>/TDP-43<sup>G348C</sup> mice. LPS-administered Optn<sup>470T</sup>/TDP-43<sup>G348C</sup> mice have shown decreased numbers of splenocytes, B cells, classical dendritic (cDC) and natural killer cells. Lastly, we observed an increase in chemokine (C-C motif) ligand 2 (CCL2) and IL-10 serum levels in TDP-43<sup>G348C</sup> and Optn<sup>470T</sup>/TDP-43<sup>G348C</sup> mice, respectively. Altogether, the presence of Optn<sup>470T</sup> truncation was insufficient to cause ALS/FTD-like neuropathology during aging. In contrast, Optn<sup>470T</sup> truncation has shown a protective effect in the presence of TDP-43<sup>G348C</sup> transgene in the basal state and during inflammation in aged mice, which could have been caused by decreased TDP-43<sup>G348C</sup> transgene levels in Optn<sup>470T</sup>/TDP-43<sup>G348C</sup> mice. Analysis of neuropathology and neuroinflammation in the hippocampus (region responsible for memory) and denervation of neuromuscular junctions will be performed to confirm this.

**Keywords:** amyotrophic lateral sclerosis, frontotemporal dementia, aging, optineurin, neurodegeneration, inflammatory signaling

## Sažetak

Amiotrofična lateralna skleroza (ALS) i frontotemporalna demencija (FTD) su neurodegenerativne bolesti odraslih ljudi koje su karakterizirane gubitkom neurona, neuroinflamacijom i agregacijom TAR DNA-vezujućeg proteina 43 (TDP-43) u različitim dijelovima središnjeg živčanog sustava (SŽS). Obje bolesti mogu biti uzrokovane mutacijama istih gena, jedan od kojih je *OPTN*, koji kodira protein optineurin. Optineurin je ubikvitin-vezujući adaptorski protein koji regulira razne stanične funkcije, uključujući upalnu signalizaciju, autofagiju, vezikularno i mitohondrijalno prometovanje. Kako bismo izučili ulogu optineurina u bolesti, naša istraživačka skupina generirala je mišji model insuficijencije optineurina (*Optn*<sup>470T</sup>) kojem nedostaje ubikvitin-vezujuća regija. Starenje je glavni faktor rizika neurodegenerativnih bolesti koji znatno utječe na imunosni sustav te rezultira kroničnom upalom slabog intenziteta, odnosno „upalnim starenjem“. S obzirom na ulogu optineurina u upalnoj signalizaciji, koja je poremećena u ALS/FTD pacijenata, proveli smo detaljnu analizu *Optn*<sup>470T</sup> miševa tijekom starenja. Evaluirali smo simptome ALS/FTD-a analizirajući motoričke i kognitivne sposobnosti, neuropatologiju (gubitak neurona, TDP-43 agregacija i akumulacija lipofuscina) i neuroinflamaciju. Zamijetili smo da starenje *Optn*<sup>470T</sup> miševa nije pogoršalo gubitak motoričkih i kognitivnih sposobnosti pronađenih u miševima divljeg tipa (WT). Ove nalaze potvrdili smo nedostatkom neuropatologije i pojačane neuroinflamacije u starim *Optn*<sup>470T</sup> miševima. S obzirom da ALS i starenje također utječu na periferne imunosne stanice, analizirali smo polarizaciju T stanica. Pronašli smo smanjeni postotak CD4<sup>+</sup> pomoćničkih T stanica koje proizvode faktor nekroze tumora (TNF) i interleukin (IL)-17A te povećan postotak CD8<sup>+</sup> T stanica u *Optn*<sup>470T</sup> miševima u odnosu na WT miševe. Jedan od novih potencijalnih obilježja ALS-a je smanjena fagocitoza mikroglije i makrofaga koja je pronađena tijekom starenja i u ALS pacijenata. Ovdje smo pronašli smanjeni postotak fagocitirajućih makrofaga deriviranih iz koštane srži (BMDM-ovi) starih miševa, koja nije bila poremećena u prisustvu insuficijencije optineurina. Kako bismo testirali ukoliko će dodatne genetske mutacije doprinijeti razvoju bolesti, proveli smo križanje *Optn*<sup>470T</sup> i TDP-43<sup>G348C</sup> miševa, gdje je za potonjeg pokazano da razvija ALS/FTD simptome. Uspješno smo potvrdili generaciju *Optn*<sup>470T</sup>/TDP-43<sup>G348C</sup> miševa, koji su pokazali nižu razinu ekspresije TDP-43<sup>G348C</sup> transgena u usporedbi s TDP-43<sup>G348C</sup> miševima, što je potencijalni protektivni mehanizam *Optn*<sup>470T</sup> trunkacije. Pronađeno je kako TDP-43 direktno regulira upalnu

signalizaciju posredovanu nuklearnim faktorom (NF)- $\kappa$ B, što mi nismo zamijetili u našim eksperimentima s BMDM-ovima. Suprotno tome, BMDM-ovi iz Optn<sup>470T</sup>/TDP-43<sup>G348C</sup> miševa stimulirani lipopolisaharidom (LPS-om) su pokazali normalnu NF- $\kappa$ B te smanjenu aktivaciju TANK-vezujuće kinaze 1 (TBK1) signalizacije u usporedbi s BMDM-ovima iz TDP-43<sup>G348C</sup> miševa. Ostarjeli Optn<sup>470T</sup>/TDP-43<sup>G348C</sup> miševi pokazali su nižu tjelesnu masu te unaprijeđene motoričke i kognitivne sposobnosti u usporedbi s TDP-43<sup>G348C</sup> miševima iste dobi. Ove miševe smo također analizirali u upalnim uvjetima za koje je pokazano da pogoršavaju ALS/FTD fenotip. Trodnevna administracija LPS-a rezultirala je značajnim gubitkom tjelesne mase i visokom smrtnošću TDP-43<sup>G348C</sup> miševa, koje su bile značajno ublažene u Optn<sup>470T</sup>/TDP-43<sup>G348C</sup> miševima. U Optn<sup>470T</sup>/TDP-43<sup>G348C</sup> miševa administriranih LPS-om pronađen je niži broj splenocita, B stanica, klasičnih dendritičkih stanica (cDC) i prirodnih stanica ubojica. Na kraju smo pronašli povećanje kemokinog C-C liganda 2 (CCL2) i interleukina-10 u TDP-43<sup>G348C</sup> i Optn<sup>470T</sup>/TDP-43<sup>G348C</sup> miševima. Sveukupno, prisustvo Optn<sup>470T</sup> trunkacije je nedovoljno za izazivanje ALS/FTD neuropatologije tijekom starenja. Međutim, Optn<sup>470T</sup> trunkacija je pokazala protektivni učinak u prisustvu TDP-43<sup>G348C</sup> transgena u bazalnom stanju i tijekom upale u starih miševa, što bi moglo biti uzorkovano smanjenim razinama TDP-43<sup>G348C</sup> transgena u Optn<sup>470T</sup>/TDP-43<sup>G348C</sup> miševima. Analiza neuropatologije i neuroinflamacije u hipokampusu (regiji odgovornoj za memoriju) te denervacije neuromišićnih spojnica će biti provedene kako bismo to potvrdili.

**Ključne riječi:** amiotrofična lateralna skleroza, frontotemporalna demencija, starenje, optineurin, neurodegeneracija, upalna signalizacija

# Table of Contents

|   |    |
|---|----|
| 1. Introduction.....  | 1  |
| 1.1. Amyotrophic lateral sclerosis .....                                      | 1  |
| 1.1.1. Genetics, mechanisms and risk factors of ALS .....                     | 2  |
| 1.1.2. ALS/FTD spectrum disorder.....   | 4  |
| 1.1.3. ALS therapy .....  | 5  |
| 1.2. Optineurin .....   | 6  |
| 1.2.1. Optineurin protein domains and interaction partners.....               | 6  |
| 1.2.1.1. Ubiquitin-binding region .....                                       | 8  |
| 1.2.1.2. Receptor-interacting serine/threonine-protein kinase 1 (RIPK1) ..... | 9  |
| 1.2.1.3. Cyldromatosis (CYLD).....  | 9  |
| 1.2.1.4. TANK-binding kinase 1 (TBK1) .....                                   | 10 |
| 1.2.2. Optineurin in ALS and FTD .....  | 10 |
| 1.2.3. Mouse model of optineurin insufficiency (Optn <sup>470T</sup> ).....   | 12 |
| 1.3. Immune response during aging .....                                       | 12 |
| 1.4. Immune response in ALS.....  | 13 |
| 1.4.1. Microglia and neuroinflammation .....                                  | 13 |
| 1.4.2. Neuroinflammation in ALS.....  | 15 |
| 1.4.3. Peripheral immunity in ALS .....                                       | 17 |
| 1.4.4. NF-κB signaling pathway .....  | 18 |
| 1.4.4.1. The role of optineurin in the NF-κB signaling pathway.....           | 20 |
| 1.4.4.2. NF-κB signaling in ALS .....   | 24 |
| 1.4.5. TBK1 signaling.....  | 25 |
| 1.4.5.1. The role of optineurin in the TBK1 signaling.....                    | 26 |

|          |   |    |
|----------|---|----|
| 1.4.5.2. | TBK1 signaling in ALS .....   | 28 |
| 1.5.     | TAR DNA-binding protein 43 (TDP-43).....  | 29 |
| 1.5.1.   | TDP-43 <sup>G348C</sup> mouse model .....   | 30 |
| 2.       | Thesis aims and hypotheses .....  | 31 |
| 3.       | Materials and methods .....   | 34 |
| 3.1.     | Materials .....   | 34 |
| 3.1.1.   | Reagents for mouse genotyping.....  | 34 |
| 3.1.2.   | Reagents for mouse perfusion and fixation .....   | 34 |
| 3.1.3.   | Reagents for immunofluorescence on tissue sections (IF) .....   | 34 |
| 3.1.4.   | Reagents for cell culture .....   | 35 |
| 3.1.4.1. | Primary neonatal microglia.....   | 35 |
| 3.1.4.2. | Bone marrow-derived macrophages (BMDMs) .....   | 35 |
| 3.1.4.3. | T-cell restimulation medium .....   | 36 |
| 3.1.4.4. | Neuro2A (N2A) cell line.....  | 36 |
| 3.1.4.5. | Agonists, inhibitors and dyes.....  | 36 |
| 3.1.5.   | Reagents for protein isolation and SDS-polyacrylamide gel electrophoresis (SDS-PAGE) and western blot (WB)..... | 37 |
| 3.1.6.   | Reagents for Enzyme-linked immunosorbent assay (ELISA).....   | 38 |
| 3.1.6.1. | IFN- $\beta$ .....  | 38 |
| 3.1.6.2. | IL-10 and TNF .....   | 38 |
| 3.1.7.   | Reagents for flow cytometry.....  | 39 |
| 3.1.8.   | Antibodies .....  | 40 |
| 3.1.8.1. | Primary antibodies for western blot and immunofluorescence.....   | 40 |
| 3.1.8.2. | Secondary antibodies for western blot and immunofluorescence.....   | 41 |
| 3.1.8.3. | Antibodies used for IFN- $\beta$ ELISA.....   | 41 |

|            |  |    |
|------------|--|----|
| 3.1.8.4.   | Antibodies used for flow cytometry – surface markers .....                 | 42 |
| 3.1.8.5.   | Antibodies used for flow cytometry – intracellular staining .....          | 42 |
| 3.2.       | Methods.....   | 43 |
| 3.2.1.     | Mouse models .....   | 43 |
| 3.2.2.     | Mouse genotyping.....  | 44 |
| 3.2.2.1.   | DNA isolation from mouse tail .....  | 44 |
| 3.2.2.2.   | Polymerase chain reaction (PCR) .....                                      | 44 |
| 3.2.2.3.   | Agarose gel electrophoresis .....  | 46 |
| 3.2.3.     | Motor tests and cognitive tests.....                                       | 46 |
| 3.2.3.1.   | Accelerating rotarod.....  | 46 |
| 3.2.3.2.   | Grid- and wire-hanging tests.....  | 47 |
| 3.2.3.3.   | Novel object recognition.....  | 47 |
| 3.2.4.     | Stimulation of mice with LPS and measurement of sickness behavior .....    | 47 |
| 3.2.5.     | Mouse perfusion and fixation for isolation of tissue and serum .....       | 47 |
| 3.2.6.     | Cell culture.....  | 48 |
| 3.2.6.1.   | Isolation and cultivation of primary neonatal microglia.....               | 48 |
| 3.2.6.2.   | Isolation and cultivation of bone marrow-derived macrophages (BMDMs) ..... | 49 |
| 3.2.6.2.1. | Complete BMDM medium preparation .....                                     | 50 |
| 3.2.7.     | Functional and biochemical assays .....                                    | 50 |
| 3.2.7.1.   | Immunoblotting.....  | 50 |
| 3.2.7.1.1. | Protein isolation and quantification for SDS-PAGE.....                     | 50 |
| 3.2.7.1.2. | SDS-PAGE.....  | 51 |
| 3.2.7.1.3. | Western blot and antibody incubation.....                                  | 51 |
| 3.2.7.1.4. | Western blot band quantification .....                                     | 52 |
| 3.2.7.2.   | ELISA .....  | 52 |

|            |  |    |
|------------|--|----|
| 3.2.7.3.   | Immunofluorescence on tissue sections.....   | 53 |
| 3.2.7.3.1. | Imaging and image analysis.....  | 53 |
| 3.2.7.4.   | Analysis of gene expression.....   | 53 |
| 3.2.7.4.1. | RNA isolation.....   | 53 |
| 3.2.7.4.2. | Synthesis of complementary DNA (cDNA) by reverse transcription.....  | 54 |
| 3.2.7.4.3. | Reverse transcription quantitative polymerase chain reaction (RT-qPCR)   | 55 |
| 3.2.7.4.4. | Analysis of RT-qPCR results .....  | 56 |
| 3.2.7.5.   | Flow cytometry .....   | 57 |
| 3.2.7.5.1. | Immune cell isolation from the spleen and <i>in vitro</i> T-cell restimulation ...   | 57 |
| 3.2.7.5.2. | Staining for flow cytometry .....  | 57 |
| 3.2.7.5.3. | Phagocytosis assay.....  | 58 |
| 3.2.7.5.4. | Flow cytometry-based multiplex analysis of cytokine concentration.....   | 60 |
| 3.2.7.5.5. | Analysis by flow cytometry .....   | 61 |
| 3.2.7.5.6. | Analysis of flow cytometry data .....  | 61 |
| 3.2.8.     | Statistical analysis.....  | 65 |
| 4.         | Results.....   | 66 |
| 4.1.       | Analysis of the role of optineurin during aging in the central nervous system .....  | 66 |
| 4.1.1.     | Optn <sup>470T</sup> mice showed similar motor coordination, cognitive functions, and lipofuscin accumulation as WT mice during aging .....          | 66 |
| 4.1.2.     | Optn <sup>470T</sup> mice did not develop ALS-like neuropathology during aging .....   | 67 |
| 4.1.3.     | Aging increased wild-type optineurin levels in the spinal cord, but its insufficiency did not exacerbate aging-induced microgliosis.....             | 70 |
| 4.1.4.     | Optineurin insufficiency led to increased microgliosis in the whole brain lysates of aged mice, but did not affect TNF and IFN- $\beta$ levels ..... | 73 |
| 4.2.       | Analysis of the role of optineurin in phagocytosis .....   | 76 |

|        |  |     |
|--------|--|-----|
| 4.2.1. | Basal and inflammatory phagocytosis in BMDMs during aging and in primary neonatal microglia were unaffected by optineurin insufficiency .....  | 76  |
| 4.3.   | Analysis of the role of optineurin on splenic T cell function during aging .....   | 79  |
| 4.3.1. | Similar T <sub>H1</sub> , but decreased T <sub>H17</sub> CD4 <sup>+</sup> T cell polarization during aging was observed in male but not female Optn <sup>470T</sup> compared to WT mice .....          | 79  |
| 4.3.2. | Aged Optn <sup>470T</sup> male mice showed an increased percentage of CD8 <sup>+</sup> T cells positive for TNF, whereas positivity for IFN- $\gamma$ and IL-2 remained similar compared to WT mice... | 82  |
| 4.4.   | Characterization of a new double-hit Optn <sup>470T</sup> /TDP-43 <sup>G348C</sup> mouse model during aging and upon LPS stimulation.....  | 84  |
| 4.4.1. | Characterization of a new Optn <sup>470T</sup> /TDP-43 <sup>G348C</sup> mouse model.....   | 84  |
| 4.4.2. | NF- $\kappa$ B and TBK1 signaling activation between TDP-43 <sup>G348C</sup> and WT BMDMs was comparable.....  | 86  |
| 4.4.3. | LPS stimulation of Optn <sup>470T</sup> /TDP-43 <sup>G348C</sup> led to a similar NF- $\kappa$ B, but reduced TBK1 activation compared to TDP-43 <sup>G348C</sup> BMDMs .....                          | 89  |
| 4.4.4. | Optn <sup>470T</sup> /TDP-43 <sup>G348C</sup> mice had lower body weight, and improved motor and cognitive functions compared to TDP-43 <sup>G348C</sup> mice.....                                     | 92  |
| 4.4.5. | LPS-mediated body weight loss and death were rescued by the presence of Optn <sup>470T</sup> truncation in TDP-43 <sup>G348C</sup> mice.....   | 93  |
| 4.4.6. | The spleens of LPS-treated Optn <sup>470T</sup> /TDP-43 <sup>G348C</sup> mice had reduced B cell percentage and number compared to Optn <sup>470T</sup> mice .....                                     | 95  |
| 4.4.7. | The spleens of LPS-treated Optn <sup>470T</sup> /TDP-43 <sup>G348C</sup> mice had lower numbers of classical dendritic and NK cells compared to Optn <sup>470T</sup> mice.....                         | 97  |
| 4.4.8. | Three-day LPS administration led to increased serum CCL2 and IL-10 levels in TDP-43 <sup>G348C</sup> and Optn <sup>470T</sup> /TDP-43 <sup>G348C</sup> mice, respectively .....                        | 99  |
| 5.     | Discussion .....   | 102 |
| 5.1.   | The role of optineurin in the central nervous system during aging .....  | 102 |
| 5.1.1. | Optn <sup>470T</sup> mice did not show ALS/FTD-like neuropathology during aging.....   | 102 |



|        |   |     |
|--------|---|-----|
| 5.1.2. | Optineurin insufficiency did not alter phagocytosis in primary myeloid cells...   | 106 |
| 5.1.3. | The role of optineurin in splenic T cell polarization during aging .....  | 107 |
| 5.2.   | Characterization of a novel double-hit ALS/FTD mouse model during aging and upon inflammation .....   | 108 |
| 5.2.1. | Optineurin insufficiency reduces TDP-43 levels in the brains of TDP-43 <sup>G348C</sup> mice  | 108 |
| 5.2.2. | Optineurin insufficiency alters LPS-induced NF-κB signaling and decreases TBK1 activation in TDP-43 <sup>G348C</sup> BMDMs.....   | 109 |
| 5.2.3. | Optn <sup>470T</sup> /TDP-43 <sup>G348C</sup> mice showed decreased body weight, but improved motor and cognitive functions compared to TDP-43 <sup>G348C</sup> mice.....   | 111 |
| 5.2.4. | Compared to TDP-43 <sup>G348C</sup> mice, Optn <sup>470T</sup> /TDP-43 <sup>G348C</sup> mice had prolonged survival and decreased splenocyte number, without difference in innate immune cell activation and cytokine profiles upon <i>in vivo</i> three-day LPS administration ..... | 112 |
| 6.     | Conclusions.....  | 115 |
| 7.     | Literature.....   | 116 |
| 8.     | Abbreviations.....  | 148 |
| 9.     | List of figures.....  | 152 |
| 10.    | List of tables.....   | 154 |
| 11.    | Biography.....  | 155 |

# 1. Introduction

## 1.1. Amyotrophic lateral sclerosis

Amyotrophic lateral sclerosis (ALS) or Lou Gehrig's disease, is a neurodegenerative disease leading to death of upper and lower motor neurons (Masrori & Van Damme, 2020). It was first described by Jean-Martin Charcot in the 19<sup>th</sup> century, where ALS was described as disease leading to muscle denervation (amyotrophy) and scarring of the spinal cord (sclerosis). Upper motor neurons are located in the motor cortex of the brain, whereas lower motor neurons are located in the brainstem and the spinal cord. The information is spread from upper to lower motor neurons, where the latter innervate the muscles (Fig. 1). When motor neurons die, the connection between the central nervous system (CNS) and the muscles is lost, leading to muscle atrophy, paralysis and death 3-5 years upon diagnosis, which is mostly caused by respiratory failure (Brown & Al-Chalabi, 2017).

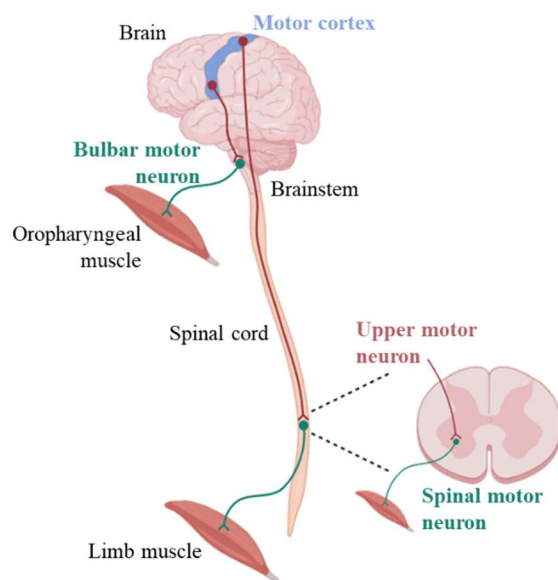


**Figure 1. Central nervous system regions and neurons affected in ALS.** Upper motor neurons (located in the motor cortex of the brain; marked in red) send information through lower (bulbar and spinal; marked in green) motor neurons to skeletal muscles. Adapted and modified from (Brown & Al-Chalabi, 2017) and made in Biorender.com

Regarding the site of disease onset, ALS can be clinically distinguished as bulbar (33% of cases) and spinal (66% of cases). Bulbar ALS, in which brainstem motor functions are affected first, is characterized by oropharyngeal muscle stiffness and spasticity, and difficulties in speaking (dysarthria) and swallowing (dysphagia), whereas spinal ALS is characterized by upper and lower limb muscle twitching (fasciculations), hyporeflexia and atrophy (Es et al., 2017). It was also shown that bulbar ALS has faster disease progression rate compared to spinal ALS (Brown & Al-

Chalabi, 2017). The age of symptom onset varies from 40 to 63 years of age (Masrori & Van Damme, 2020). ALS was reported to affect men slightly more than women in a ratio 1.2-1.5:1 (Es et al., 2017). The incidence for people with European ancestry is about 2-3 cases per 100 000 people with lifetime risk of 1 in 350 for men and 1 in 400 for women, although this can vary between different populations and geographic regions (Es et al., 2017; Hardiman et al., 2017).

### **1.1.1. Genetics, mechanisms and risk factors of ALS**

ALS patients are usually classified as sporadic (90% of cases) or familial (10% of cases) regarding to the absence or presence of the disease in family history, respectively (Masrori & Van Damme, 2020). However, some of the sporadic patients may have relatives that died before they developed ALS, therefore making them a part of familial cases (Al-Chalabi & Lewis, 2011). It was found that mutations in more than 40 different genes may cause ALS (Mead et al., 2022). Genes that are most frequently affected by mutations are chromosome 9 open reading frame 72 (*C9ORF72*), superoxide dismutase 1 (*SOD1*), fused in sarcoma (*FUS*) and TAR DNA-binding protein-43 (*TARDBP*; encoding for protein TDP-43) and are involved in the regulation of various cellular functions including autophagy, oxidative stress, nucleic acid metabolism and nucleocytoplasmic transport (Hardiman et al., 2017; Mead et al., 2022; Akçimen et al., 2023). Also, it is worth mentioning that sporadic and familial ALS may be caused by mutations in the same genes, making both types of ALS a genetic ALS, regardless of heritability (Fig. 2). In addition, mutations in genes involved in the regulation of inflammation were also found, and those are TANK-binding kinase 1 (*TBKI*), cylindromatosis (*CYLD*) and optineurin (*OPTN*), meaning that dysregulation of inflammation may play a role in ALS pathogenesis, and will be discussed later (De Marchi et al., 2023). Other disease mechanisms involve excitotoxicity, mitochondrial dysfunction, dysregulated vesicle transport, impaired protein homeostasis, endoplasmic reticulum stress, impaired DNA repair and axonopathy (Mead et al., 2022). Therefore, multiple cellular mechanisms are affected in ALS, which makes the disease difficult to treat and investigate.

The first ALS-causing mutations were found in the *SOD1* gene, which encodes for Cu/Zn SOD1 and is involved in the clearance of reactive oxygen species (H. X. Deng et al., 1993; Rosen et al., 1993). Based on that, the first ALS mouse model was generated, named *SOD1*<sup>G93A</sup> mouse, which is a transgenic mouse overexpressing human G93A mutation (Gurney et al., 1994). This mutation

led to toxic gain-of-function, which was initially thought to result in toxicity to motor neurons due to a high concentration of free radicals. However, it was soon discovered that mutated SOD1 forms cytoplasmic aggregates, which were toxic to motor neurons, resulting in their death (Bruijn et al., 1998; Watanabe et al., 2001). Other proteins were also found to aggregate, and those are TDP-43, FUS and C9ORF72 (Neumann et al., 2006; Arai et al., 2006; Vance et al., 2009; Kwiatkowski et al., 2009; DeJesus-Hernandez et al., 2011). It was shown that SOD1, FUS and TDP-43 protein aggregates show prion-like properties, or more precisely, that they can be spread from cell-to-cell resulting in disease dissemination across various regions and cells of the CNS (Polymenidou & Cleveland, 2011; Lee & Kim, 2015). Of note, TDP-43 aggregates were found in more than 97% of ALS cases regardless of gene mutation (Ling et al., 2013), whereas the exceptions are patients with mutations in *SOD1* and *FUS*, where TDP-43 aggregates are absent (Mackenzie et al., 2007; Vance et al., 2009). Therefore, TDP-43 is considered a major hallmark of ALS patients and will be further discussed later.

Various risk factors have been reported to be associated to ALS such as smoking, alcohol intake, physical activity and trauma, electric and magnetic fields, metals, chemical agents and pesticides, and hazardous air pollutants (Talbot et al., 2016). However, these have relatively small effects, and the only risk factor that clearly stands out is aging, which was shown to be the major risk factor for all neurodegenerative diseases (Hou et al., 2019). Aging leads to defects in various cellular processes such as genomic instability, loss of proteostasis, cellular senescence and mitochondrial dysfunction (López-Otín et al., 2023), which are also linked to neurodegenerative diseases (Wilson et al., 2023). In addition, the immune system is also strongly affected by aging through inflammaging and immunosenescence, which will be discussed in more detail later. To this day, the impact of environmental factors is still under debate, whereas aging is confirmed as the strongest risk factor for all neurodegenerative diseases. To account for such complexity in disease pathogenesis, a multistep pattern of disease development was suggested, where the presence of genetic mutation is not sufficient for disease development, but rather requires additional genetic and/or environmental hits (Al-Chalabi et al., 2014)

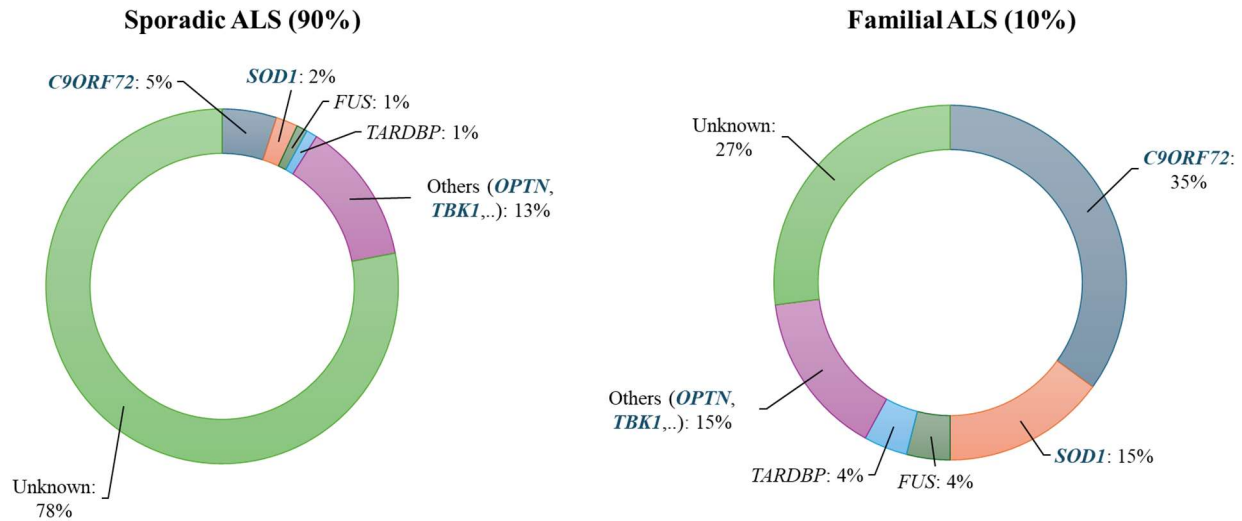


**Figure 2. Most frequent genes affected by mutations in ALS.** Genes mostly affected by mutations in ALS patients were found to be *C9ORF72*, *SOD1*, *FUS* and *TARDBP*. Additionally, mutations in *TBK1* and *OPTN* were also found, but in a lesser frequency. It is noteworthy that the same genes are affected in both familial and sporadic ALS cases. Genes linked to immune response are marked in blue. The figure is modified from Volk *et al.*, 2018.

### 1.1.2. ALS/FTD spectrum disorder

Frontotemporal dementia (FTD) represents a variety of neurodegenerative diseases characterized by neuron loss in the frontal and temporal lobes (illustrated in Fig. 2 A) (Bang *et al.*, 2015; Grossman *et al.*, 2023). It is classified based on the protein aggregates found in the brain, such as TDP-43 (FTD-TDP), tau (encoded by *MAPT* gene; FTD-tau) and FUS (FTD-FUS) (Ling *et al.*, 2013). It was reported that 15% of ALS patients develop FTD (Ringholz *et al.*, 2005) and 15% of FTD patients developed ALS (Lomen-Hoerth *et al.*, 2002). Additionally, mutations in some genes were reported to cause solely ALS (e.g. *SOD1*), FTD (e.g. *GRN*, encoding for protein progranulin; *MAPT*, encoding for protein tau) and both diseases (e.g. *OPTN*, *C9ORF72*, *TARDBP*, *TBK1*, *FUS*) (De Marchi *et al.*, 2023). This led to a new conclusion that ALS and FTD represent an ALS/FTD disease spectrum rather than two distinct diseases (Fig. 2 B).

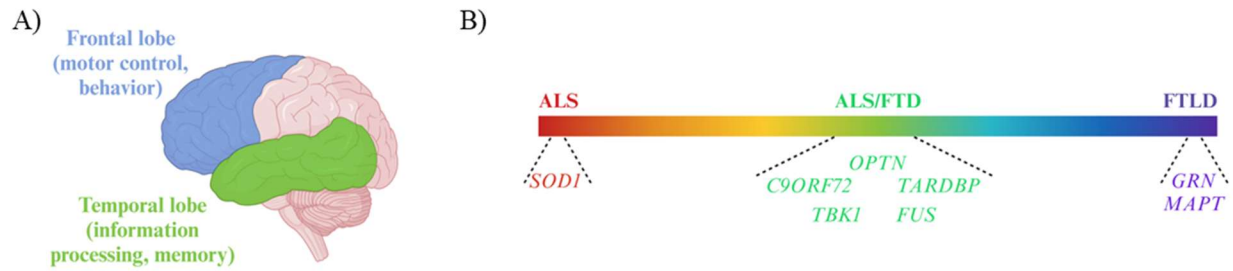


**Figure 3. ALS/FTD represents a spectrum disorder, rather than distinct diseases.** FTD is a name for a group of diseases characterized by neurodegeneration in the frontal and temporal lobes (A). Genes affected solely in ALS (e.g. *SOD1*), FTD (e.g. *GRN*, *MAPT*) and both (e.g. *OPTN*, *C9ORF72*, *TARDBP*, *TBK1*, *FUS*) (B). As most of these genes are involved in the pathogenesis of both diseases, ALS and FTD are considered as a spectrum (ALS/FTD).

### 1.1.3. ALS therapy

The treatment of ALS is still mostly symptomatic, requires a multidisciplinary team of specialists, but still prolongs life merely by a matter of months. The most widely used drug is Riluzole, which is approved by European Medicines Agency and U.S. Food and Drug Administration Agency (FDA). It is considered to act by decreasing glutamate-mediated toxicity and was shown to prolong life for 6-19 months (Andrews et al., 2020). Another drug in use is Edaravone, which has antioxidant properties and is approved for use only in the USA, Canada and Japan. In the original study, it slowed the disease progression with a questionable effect on survival due to a small cohort of patients (Abe et al., 2017; Al-Chalabi et al., 2017). Also, a slowed disease progression was observed in a small cohort of patients that administered Riluzole and Edaravone, with a short-term effect (Samadhiya et al., 2022). Another disease-modifying therapies involve treatments of symptoms such as hypersalivation (atropine, hyoscine), pain (nonsteroidal anti-inflammatory drugs, opioids), muscle cramps (quinine sulphate), depression (tricyclic antidepressants) and respiratory insufficiency (non-invasive ventilation) (Hardiman et al., 2017). Some recent approaches include AMX0035 (phenylbutyrate/taurursodiol, also known as Pb/TURSO or Pb/TUDCA) and Tofersen (antisense oligonucleotides for *SOD1*). The former acts by a decrease in mitochondrial and ER stress, whereas the latter downregulates the levels of misfolded superoxide dismutase 1 (SOD1) (Mead et al., 2022). Various preclinical and clinical studies

targeting protein aggregate removal, restoring normal gene function (gene therapy), neuroinflammation and others are still ongoing, so the results are still unavailable.

## **1.2. Optineurin**

Optineurin is a cytoplasmic multifunctional ubiquitin-binding adaptor protein that lacks enzymatic activity (Markovinovic et al., 2017). It was first discovered in 1998, when it was found that it interacts with an adenovirus E3 14.7-kDa protein and was therefore named 14.7-kDa-interacting protein or FIP-2 (Y. Li et al., 1998). Later, it acquired other names such as transcription factor IIIA-interacting protein (TFIIIA-intP) and nuclear factor (NF)-kB essential modulator-related protein (NEMO-related protein or NRP) due to the findings of its new interacting partner and homology to NEMO, respectively (Moreland et al., 2000; Schwamborn et al., 2000). Finally, the same protein was named optineurin (for optic neuropathy-inducing) upon relating its mutations to normal tension primary open-angle glaucoma (NTG or POAG) (Rezaie et al., 2002).

Optineurin gene (*OPTN*) is located at chromosome 10p13 in humans and encodes for a protein containing 577 amino acids (Slowicka, Vereecke, & Van Loo, 2016). A mouse optineurin gene (*Optn*) is located on chromosome 2 and shows an 80% homology with human optineurin, with a similar size of 584 amino acids (Rezaie & Sarfarazi, 2005). The highest expression of optineurin protein levels was detected in tissues such as the brain, bone marrow, lymphoid tissues, muscles and the reproductive system (*Tissue Expression of OPTN - Summary - The Human Protein Atlas*).

### **1.2.1. Optineurin protein domains and interaction partners**

Optineurin contains several functional protein domains: coiled-coil 1 (CC1), CC2, LC3-interacting region (LIR), and ubiquitin-binding region. This enables optineurin to interact with proteins involved in various cellular processes such as inflammatory signaling, autophagy, vesicle trafficking, etc. (Prtenjaca, 2020). The main proteins that were found to interact with optineurin are listed in Table 1 and shown in Figure 4. Given the focus of this work on the role of optineurin in inflammatory signaling, interaction partners involved in inflammation will be further discussed in the subsequent chapters.

**Table 1. List of optineurin interaction partners and their cellular function.** Abbreviations: amino acids (aa), myosin phosphatase target subunit 1 (MYPT1), metabotropic glutamate receptor type 1a (mGluR1a), huntingtin (Htt), cylindromatosis (CYLD), receptor-interacting serine/threonine protein kinase 1 (RIPK1). Modified from: (Toth & Atkin, 2018).

| <b>Binding partner</b> | <b>Binding site (aa)</b>  | <b>Cellular function</b>  | <b>References</b>  |
|------------------------|---------------------------|---------------------------|--|
| <b>TBK1</b>            | 26-103                    | Inflammation, autophagy   | (Morton et al., 2008; Wild et al., 2011; Gleason et al., 2011; F. Li et al., 2016; Munitic et al., 2013; Meena et al., 2016; Pourcelot et al., 2016; Richter et al., 2016; Brenner et al., 2024) |
| <b>Caspase 8</b>       | 121-230                   | Apoptosis                 | (Nakazawa et al., 2016)  |
| <b>MYPT1</b>           | 131-170                   | Mitosis                   | (Kachaner et al., 2012)  |
| <b>Rab8</b>            | 133-170                   | Vesicle trafficking       | (Hattula & Peränen, 2000; Chi et al., 2010; Vaibhava et al., 2012; J. Zhang et al., 2024)  |
| <b>TFIIIA</b>          | 160-469                   | Transcription             | (Moreland et al., 2000)  |
| <b>LC3</b>             | 178-181                   | Autophagy                 | (Wild et al., 2011)  |
| <b>p62</b>             | 193 (upon ubiquitination) | Autophagy                 | (Z. Liu et al., 2014)  |
| <b>mGLUR1a</b>         | 202-246                   | Excitotoxicity            | (Anborgh et al., 2005)   |
| <b>HACE1</b>           | 411-456                   | Autophagy                 | (Z. Liu et al., 2014)  |
| <b>Htt</b>             | 411-461                   | Vesicle trafficking       | (Hattula & Peränen, 2000)  |
| <b>Myosin VI</b>       | 412-520                   | Exocytosis                | (Sahlender et al., 2005; Tumbarello et al., 2012; Sundaramoorthy et al., 2015)   |
| <b>CYLD</b>            | 424-529                   | Inflammation              | (Nagabhushana et al., 2011; Obaid et al., 2015)  |
| <b>RIPK1</b>           | 461-493                   | Inflammation, necroptosis | (Zhu et al., 2007; Y. Ito et al., 2016; Nakazawa et al., 2016)   |



### 1.2.1.1. Ubiquitin-binding region

Optineurin is a ubiquitin-binding protein that possesses the ubiquitin-binding region (UBR) in the C-terminus. UBR consists of ubiquitin-binding region of ABIN proteins and NEMO (UBAN) and zinc finger (ZF), illustrated in Figure 4. It was reported that NEMO and optineurin share 53% of homology in their sequence, with even higher conservation found in UBAN and ZF regions between optineurin, NEMO and ABINs (Laplantine et al., 2009; Schwamborn et al., 2000; Zhu et al., 2007). The binding of ubiquitin, which is an evolutionary conserved post-translational modification of proteins, is important for regulation of cellular signaling (Komander & Rape, 2012). It is characterized by formation of polyubiquitin chains on target proteins linked through different intrinsic sites of the ubiquitin molecule, involving methionine 1 (M1) and 7 lysines (K6, K11, K27, K29, K33, K48 and K63). For example, K63 polyubiquitin chains are generated by binding of ubiquitin molecules to the lysine 63 in the next ubiquitin. More precisely, the chain type decides the fate of the targeted protein. For example, K11-, 48- and K29-labeled proteins are directed to proteasomal degradation via ubiquitin-proteasomal system (UPS) (Komander & Rape, 2012). In contrast, K63 labeling takes part in autophagy-mediated degradation (Pohl & Dikic, 2019) and inflammatory signaling (Hu & Sun, 2016), whereas M1 labeling takes part only in the latter. It was reported that ZF strongly increases the affinity for K63-linked polyubiquitin chains of UBR (Laplantine et al., 2009), whereas the UBAN region alone prefers M1 chains (Nakazawa et al., 2016). Optineurin is involved in regulation of signaling pathways such as NF- $\kappa$ B and TBK1 signaling through interactions with M1- and K63-polyubiquitinated partners, respectively (Nakazawa et al., 2016).

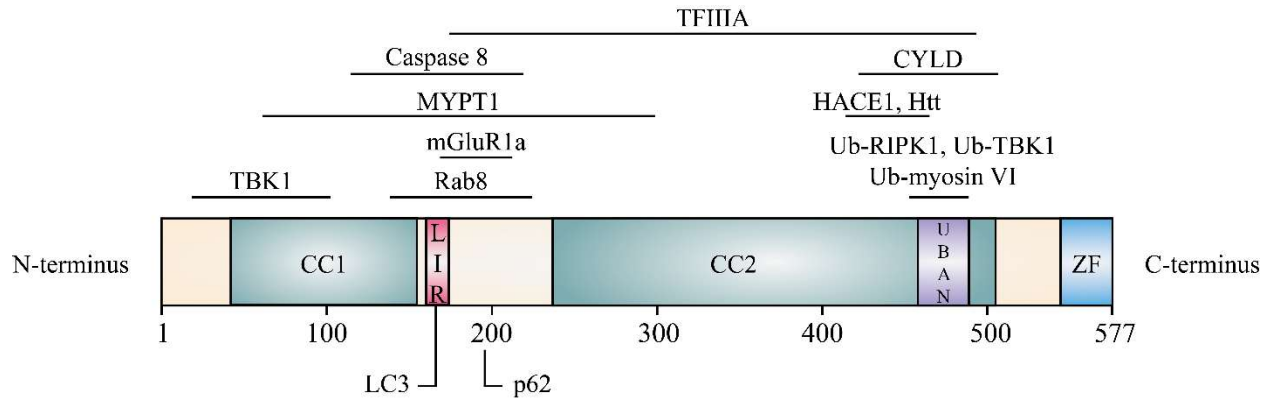


**Figure 4. Protein domains and interaction partners of optineurin.** The major protein domains of optineurin are marked as coiled-coil 1 (CC1; 38-170 aa), LC3-interacting region (LIR; 178-181 aa), CC2 (238-509 aa), ubiquitin-binding region of ABIN and NEMO (UBAN; 461-493 aa), zinc finger (ZF; 553-577 aa); ubiquitin-binding region includes UBAN and ZF. Interaction partners mentioned in Table 1 are shown according to their binding region. Some of the interaction partners need to be M1- and/or K63-polyubiquitinated to be bound by UBR of optineurin, and those are RIPK1, TBK1, and myosin VI. Modified from: Markovinovic *et al.*, 2017.

#### 1.2.1.2. Receptor-interacting serine/threonine-protein kinase 1 (RIPK1)

RIPK1 is a molecule involved in transduction of immune and cell death signaling. It is recruited in NF- $\kappa$ B signaling upon stimulation of various pattern recognition (PRR) or cytokine receptors, such as Toll-like receptor 4 (TLR4) and tumor necrosis factor receptor 1 (TNFR1), respectively (Clucas & Meier, 2023). Importantly, it was reported that optineurin competes with NEMO to bind polyubiquitinated RIPK1 upon NF- $\kappa$ B activation with TNF, suggesting that optineurin acts a negative regulator of the NF- $\kappa$ B pathway (Zhu et al., 2007).

#### 1.2.1.3. Cylindromatosis (CYLD)

CYLD is a molecule involved in the regulation of NF- $\kappa$ B signaling. More precisely, it is a deubiquitinase that hydrolyses K63 polyubiquitin chains and thus dampens signaling transduction (Marín-Rubio et al., 2023). It was shown that region around UBR of optineurin has a binding site

for CYLD (Nagabhushana et al., 2011; Obaid et al., 2015). Moreover, Nagabhushana *et al.* suggested that optineurin recruits CYLD to the NF- $\kappa$ B signalosome to inhibit excessive signaling (Nagabhushana et al., 2011).

#### **1.2.1.4. TANK-binding kinase 1 (TBK1)**

TBK1 is a major kinase involved in the production of interferon (IFN)- $\beta$  (Ahmad et al., 2016). It is activated through autophosphorylation upon stimulation of various PRRs, including TLR4, which will be discussed in more detail below. Optineurin binding to TBK1 is achieved through both termini of the protein. More precisely, via N-terminal TBK1-binding region (26-103 aa) and C-terminal UBR (UBAN + ZF; 461-577 aa) of optineurin (Gleason et al., 2011; Munitic et al., 2013; F. Li et al., 2016; Pourcelot et al., 2016), since TBK1 is K63-polyubiquitinated during activation of inflammatory signaling (Tu et al., 2013).

#### **1.2.2. Optineurin in ALS and FTD**

The first optineurin mutations were linked to NTG, such as E50K, which is of proven pathogenicity (Rezaie et al., 2002). The E50K mutation was shown to be gain-of-function mutation, which increased optineurin aggregation and binding to TBK1 (Morton et al., 2008; Minegishi et al., 2013; F. Li et al., 2016). Subsequently, Maruyama *et al.* discovered the first ALS-linked mutations, which included homozygous deletion of exon 5 ( $\Delta$ ex5), homozygous Q398X truncation and heterozygous E478G point mutation (Maruyama et al., 2010). Therefore, the latter is thought to act by a dominant-negative effect.  $\Delta$ ex5 resulted in protein deficiency, whereas Q398X truncation resulted in protein insufficiency, which is thought to result from nonsense-mediated mRNA decay due to premature stop codon (Maruyama et al., 2010; Kamada et al., 2014). It is noteworthy that these mutations lack either the whole protein ( $\Delta$ ex5) or directly affect the UBR (Q398X and E478G) of optineurin. ALS patients carrying Q398X and E478G mutations were also found to have FTD (H. Ito et al., 2011; Kamada et al., 2014), meaning that optineurin plays a role in both pathologies. Most of the ALS-linked mutations are concentrated around UBAN and ZF (Fig. 5), whereas some ALS- (Q165X and S174X) and FTD- (K238ETer11) linked mutations occurring earlier in the sequence lead to a premature stop codon and translation of the protein lacking the UBR (Tümer et

al., 2012; Van Blitterswijk et al., 2012; Özoğuz et al., 2015; Dominguez et al., 2021; Gotkine et al., 2021). Thereby, these mutations were proposed to act by loss-of-function since the functional part of the protein is missing. Importantly, ALS patients with *OPTN* mutations that affect the UBR have shown TDP-43 cytoplasmic aggregation in neuronal and non-neuronal (glial) cells in the brain and the spinal cord (H. Ito et al., 2011; Kamada et al., 2014; Parvizi et al., 2024). Altogether, the ubiquitin-binding function of optineurin is important for a normal cellular function. Truncations, mutations, or loss of the whole protein have been identified as contributing factors in ALS and FTD.

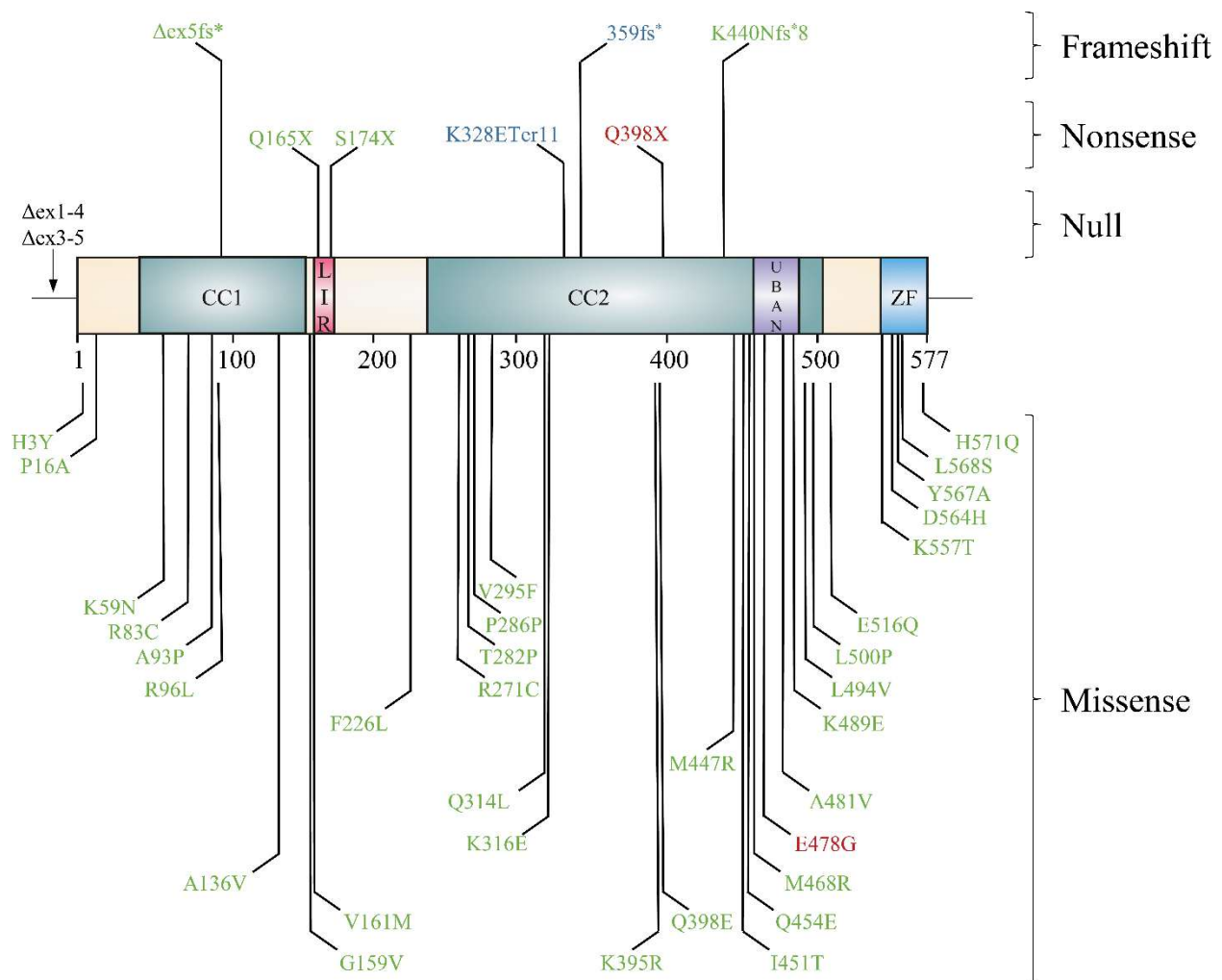


**Figure 5. Optineurin mutations found in ALS, FTD and both.** The list of frameshift, nonsense, null and missense mutations linked to ALS (green), FTD (blue) or both (red). Reviewed in (Markovinovic et al., 2017; Franjkic T, Peradinovic J, Munitic I: unpublished data). Abbreviations:  $\Delta ex$  (exon deletion), fs (frameshift), \* (stop codon).

### 1.2.3. Mouse model of optineurin insufficiency (Optn<sup>470T</sup>)

To investigate the role of optineurin in the pathogenesis of ALS, various mouse models were generated to resemble patient mutations. Those are Optn<sup>-/-</sup> (null mutation that results in protein deficiency), Optn<sup>D474N</sup> (mimicking human E478G mutation) and Optn<sup>470T</sup> (mimicking human Q398X truncation). Since this research will be conducted on Optn<sup>470T</sup> mice, it will be the model we will further focus on. In Optn<sup>470T</sup> mouse model, only the first 470 amino acids are translated instead of a full-length protein containing 584 amino acids, where the whole UBR is lacking (Munitic et al., 2013). This mouse model mimics the Q398X human truncation in terms of: 1) homozygosity, 2) absence of the UBR and 3) protein insufficiency. Due to the presence of premature stop codon, nonsense-mediated mRNA decay was suggested to be the reason of decreased mRNA and protein levels of the truncated version in humans (Kamada et al., 2014) and mice (Munitic et al., 2013). In conclusion, due to its similarity to the pathogenic human *OPTN* mutation, Optn<sup>470T</sup> mouse model represents a valuable model for investigating the role of ALS pathogenesis.

### 1.3. Immune response during aging

In 2000s, Franceschi *et al.* were the first to describe the term inflammaging, which represents aging of the immune system and is caused by chronic exposure to antigenic load and stress (Franceschi et al., 2000). Inflammaging is characterized by chronic low-grade inflammation due to inefficiency of dealing with inflammatory stimuli (infections, tissue damage, etc.) and is therefore marked by increased expression of pro-inflammatory markers, such as TNF and IL-6 (López-Otín et al., 2013; Franceschi et al., 2018). More precisely, the diminished regenerative potential and accumulation of senescent cells results in chronic low-grade inflammation marked by increased pro-inflammatory cytokine secretion. However, the senescent cells themselves are hyporesponsive to the inflammatory stimuli (X. Li et al., 2023). The cells that were described to have a major impact on inflammaging were macrophages, due to their propensity of secreting high levels of various cytokines and chemokines in response to inflammatory stimuli (Franceschi et al., 2000). Macrophages were shown to have decreased phagocytosis and cytokine secretion, whereas the production of reactive oxygen species was increased (Moss et al., 2023). The other innate immune cells were also shown to be affected by aging. For example, aging resulted in decreased

phagocytosis by neutrophils and dendritic cells (Wenisch et al., 2000; Agrawal & Gupta, 2011). In addition, T cells are also a major component of inflammaging. The pool of naïve T cells is decreasing during aging, whereas memory T cell number increases (Mittelbrunn & Kroemer, 2021). Aged individuals were also shown to have increased numbers of T<sub>H1</sub> (proinflammatory; secreting TNF and IFN- $\gamma$ ) and T<sub>H17</sub> (proinflammatory; secreting IL-17A and linked to autoimmune disorders) CD4<sup>+</sup> T cells, which support inflammation by releasing their signature pro-inflammatory cytokines (Mittelbrunn & Kroemer, 2021). For cytotoxic CD8<sup>+</sup> T cells, an aging-induced percentage of IFN- $\gamma$ -producing cells was reported as well (Pulko et al., 2016). This pro-inflammatory milieu of aged individuals is linked to susceptibility to age-related diseases such as metabolic and cardiovascular diseases (Franceschi et al., 2018). Furthermore, the CNS is also strongly affected by aging, which correlates with the development of neurodegenerative diseases (Mattson & Arumugam, 2018). Microglia in aged individuals show activated morphology (increased cell body area and shorter processes), accompanied by increased pro-inflammatory marker expression and decreased phagocytosis (von Bernhardi et al., 2015). Astrocytes were shown to have increased glial fibrillary acidic protein (GFAP) expression, changed morphology and pro-inflammatory profile during aging (Gudkov et al., 2023). The pro-inflammatory microenvironment is toxic to neurons and may lead to their death and neurodegeneration. In conclusion, inflammaging affects the peripheral and CNS immune system, supporting pro-inflammatory and toxic environment linked to immune cell dysfunction.

## **1.4. Immune response in ALS**

### **1.4.1. Microglia and neuroinflammation**

Microglia are the only innate immune cells present in the CNS parenchyma. They are tissue-specific macrophages of the CNS (Ginhoux et al., 2010). During embryonic development, their precursors migrate from the yolk sac and populate the CNS parenchyma, where they acquire their specific markers. Colony-stimulating factor 1 (CSF1) and interleukin (IL)-34 were shown to be important trophic factors that are crucial for microglial survival and proliferation, with both acting through CSF1 receptor (CSF1R) (Ginhoux et al., 2010; Y. Wang et al., 2012). The main role of microglia is surveillance of the CNS. They play a role in important mechanisms such as response to pathogens or tissue injury, synaptic pruning, and phagocytosis of cellular debris or pathogens

(Q. Li & Barres, 2018). These microglial roles are possible due to possession of diverse receptors, such as pattern recognition receptors (PRRs), which enable detection of pathogen-associated and damage-associated molecular patterns (PAMPs and DAMPs) (Bsibsi et al., 2002). Sensing of PAMPs and DAMPs via PRRs activates two distinct signaling pathways, nuclear factor (NF)- $\kappa$ B and TBK1 signaling (D. Li & Wu, 2021), which are further described in sections 1.4.4. and 1.4.5. Activation of glial cells (microglia and astrocytes) can be achieved upon stimulation of PRRs, which triggers their proliferation and changes in morphology, cytokine profile and expression of various activation markers (Matejuk & Ransohoff, 2020). This glial cell activation is termed neuroinflammation (Kwon & Koh, 2020). Due to the focus of this study on immune response, the role of microglia in neuroinflammation will be discussed in more detail.

Based on the nature of the microenvironment, microglia may acquire M1 (pro-inflammatory) or M2 (anti-inflammatory) phenotype (Fig. 4). M1 phenotype is acquired by classical activation upon stimulation with lipopolysaccharide (LPS), marked by NF- $\kappa$ B signaling pathway activation (Tang & Le, 2016). It is characterized by upregulation of various pro-inflammatory molecules, such as tumor necrosis factor (TNF), IL-1 $\beta$ , IL-6 and inducible nitric oxide synthase (iNOS). On the other hand, M2 phenotype is acquired upon alternative activation by IL-4 and IL-13, which is characterized by upregulation of IL-4, arginase 1 (Arg1), insulin-like growth factor (IGF)-1 and transforming growth factor (TGF)- $\beta$  (Tang & Le, 2016). However, the dichotomization to M1 and M2 is considered as an oversimplification and is believed that there is a gradient between those two phenotypes (Tang & Le, 2016; S. Guo et al., 2022). Nevertheless, a fine regulation of switching between those phenotypes is important. Prolonged M1 polarization leads to chronic neuroinflammation with a neurotoxic effect, whereas M2 phenotype is shown to have neuroprotective properties (Béland et al., 2020). In addition, various microglial phenotypes were described in neurodegenerative diseases, such as disease-associated microglia (DAM) and microglial neurodegenerative phenotype (MGnD) (Paolicelli et al., 2022), which further increases the complexity of neurodegenerative disease pathogenesis.

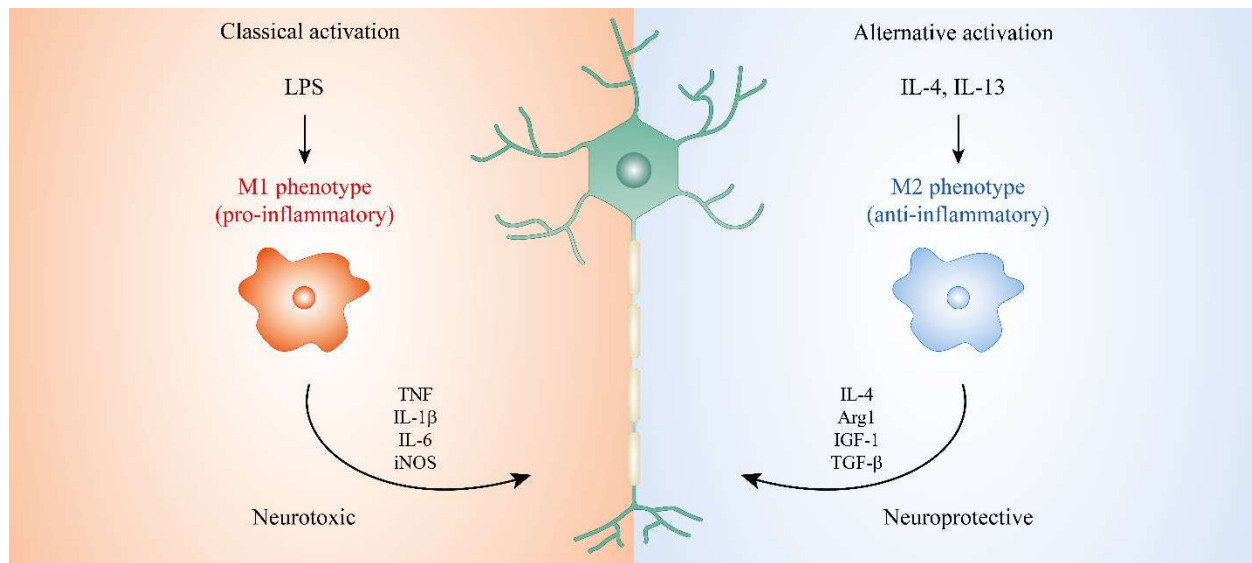


**Figure 6. Microglial phenotypes and their characteristic markers.** Upon classical activation by LPS stimulation, microglia acquire M1 (pro-inflammatory) phenotype characterized by increased expression of TNF, IL-1 $\beta$ , IL-6 and iNOS. Microglia may also acquire M2 (anti-inflammatory) phenotype characterized by expression of IL-4, Arg1, IGF-1 and TGF- $\beta$ . Modified from: Tang & Le, 2016.

#### 1.4.2. Neuroinflammation in ALS

Neuroinflammation is one of the major hallmarks of ALS patients (McCauley & Baloh, 2019; De Marchi et al., 2023). Activated microglia and astrocytes can be seen adjacent to motor neuron loss in ALS-affected parts of the brain, brainstem and the spinal cord (McGeer et al., 1991; Kawamata et al., 1992). Therefore, even though motor neurons are the main cells dying in ALS, non-neuronal (glial) cells were shown to be also affected, meaning that ALS has both an autonomous and a non-cell autonomous component. This was further confirmed by manipulating neuronal and glial cells in various SOD1 mouse models. Kriz *et al.* have shown that depletion of microglia by minocycline, which inhibits microglial activation, extended survival of SOD1<sup>G37R</sup> mice, demonstrating that microglia indeed plays an important role in ALS pathogenesis (Kriz et al., 2002). However, whether mutant SOD1 overexpression in microglia and/or other cells directly affected the disease pathogenesis was not deciphered. Therefore, mouse models with restricted overexpression of SOD1 mutants to certain CNS cell types were generated. It was shown that selective mutant SOD1



overexpression in motor neurons (Pramatarova et al., 2001; Lino et al., 2002) and astrocytes (Gong et al., 2000) did not precipitate the disease, which means that the mutation needs to be present in different CNS cell types. A study done on chimeric mice (generated from blastocytes containing a mixture of WT and mutant SOD1 cells) has shown that increase in the percentage of WT cells led to delay in disease progression and extended lifespan (Clement et al., 2003). To address the importance of non-neuronal cells, mice with a conditional knockout of mutant SOD1 in glial cells were generated. Microglia- and astrocyte-specific Cre-mediated deletion of mutant SOD1 resulted in survival prolongation and slowed disease progression, without an effect on disease onset, whereas the delay in onset was observed only upon mutant SOD1 deletion in motor neurons (Boillée et al., 2006; Yamanaka et al., 2008). This suggests that motor neurons overexpressing mutant SOD1 are more susceptible to death mediated by surrounding glial cells. An additional importance of microglia was shown by Beers *et al.*, where they have crossed SOD1<sup>G93A</sup> mice with PU.1 knockout (PU.1<sup>-/-</sup>) mice, which lacked immune cells, including microglia. After transplantation of WT bone marrow into SOD1<sup>G93A</sup> × PU.1<sup>-/-</sup> mice, macrophages repopulated the CNS parenchyma, disease progression was slowed and survival was prolonged (Beers et al., 2006). This group has also shown that primary microglia derived from SOD1<sup>G93A</sup> mice showed increased release of oxidative stress molecules in basal state and LPS-induced inflammation. In addition, SOD1<sup>G93A</sup> primary microglia has shown to be toxic to motor neurons *in vitro* in basal and LPS-induced states (Beers et al., 2006; Liao et al., 2012). An interesting finding was shown by Beers *et al.* in 2011, where they analyzed M1 and M2 markers during ALS disease course in SOD1<sup>G93A</sup> mice (Beers et al., 2011). In these mice, they have shown that microglia first acquired M2 phenotype, which upon constant damage load transformed to M1 phenotype. This meant that microglia acquired neuroprotective phenotype in the early stage, whereas neurotoxic phenotype prevailed in the late stage of the disease (Beers et al., 2011). To conclude, glial cells play an important role in ALS pathogenesis and their manipulation should be done according to the disease stage. Of note, all of those studies were done in mice overexpressing human SOD1 mutants due to the lack of overt phenotypes in other mouse ALS models (De Marchi et al., 2021).

### 1.4.3. Peripheral immunity in ALS

In addition to dysregulated immune response in the CNS, pathological changes were also reported for various immune cells in the periphery (outside the CNS) (Beers & Appel, 2019; Béland et al., 2020; De Marchi et al., 2021, 2023). In ALS patients' blood, monocytes were shown to be polarized towards a pro-inflammatory state based on increased expression of MHC-II (R. Zhang et al., 2005) and IL-1 $\beta$ , IL-8 and CXCL10 mRNA (Zhao et al., 2017). Similar was confirmed in SOD1<sup>G93A</sup> mouse model, where monocytes exhibited increased mRNA expression for TNF and IL-1 $\beta$  (Butovsky et al., 2012). Mouse and rat models overexpressing mutant SOD1 have also shown an accumulation of activated macrophages at the neuromuscular junction (NMJ) (Chiu et al., 2009; Graber et al., 2010; Lincecum et al., 2010). Macrophages derived from monocytes of ALS patients had stronger M1 polarization marker expression in terms of TNF and IL-6 mRNA and protein upon LPS stimulation (Du et al., 2020), confirming the finding of activated macrophages in mice. Dendritic cell (DC) transcripts were found in the spinal cord of ALS patients (Henkel et al., 2004) and were shown to be decreased in number with altered production of CCL2 and IL-8 (Rusconi et al., 2017). Natural-killer (NK) cells were shown to infiltrate the CNS of ALS patients and mouse models, where they mediate motor neuron death and M1 microglial polarization (Garofalo et al., 2020). Mast cells and neutrophils were found to act in concert by accumulating at the NMJs, where they degranulate and recruit neutrophils, which prevent reinnervation by phagocytosing degenerating axons (Trias et al., 2018). This evidence shows that peripheral innate immune cells are also involved in the pathogenesis of ALS.

The cells of adaptive immunity (B and T cells) were also of interest to many ALS research groups. Although, B cells were found to have no impact on disease progression in the SOD1 mouse model (Naor et al., 2009), immunoglobulins were shown to accumulate in motor neurons and to activate microglia, astrocytes and motor neurons *in vitro* (Engelhardt & Appel, 1990; Demestre et al., 2005; Milošević et al., 2017). However, the pathogenicity of immunoglobulins and the role of B cells are still incompletely understood. On the other hand, much more is known about T cells, which depending on their polarization state, differently affect macrophage/microglial polarization (Tang & Le, 2016; Tuzlak et al., 2021). Increased polarization to T<sub>H1</sub> and T<sub>H17</sub> was shown in ALS patients and mouse models at the late stage of the disease (Beers et al., 2011; Henkel et al., 2013; Saresella et al., 2013). On the contrary, T<sub>H2</sub> (anti-inflammatory; secreting IL-4) and regulatory cells (T<sub>reg</sub>;

secreting IL-10 and TGF- $\beta$ ) mitigate microglial activation (Béland et al., 2020; De Marchi et al., 2021). Furthermore, T<sub>reg</sub> cells were shown to be dysfunctional in ALS patients, with a reduced number correlating with faster disease progression and shorter survival (Henkel et al., 2013; Beers et al., 2017). In the SOD1<sup>G93A</sup> mouse model it was shown that in the early stages of the disease T<sub>H2</sub> and T<sub>reg</sub> cells were prevalent, whereas in the late stage T<sub>H1</sub> polarization took place (Beers et al., 2011), suggesting that the former support neuroprotective, whereas the latter supports neurotoxic microenvironment. CD8<sup>+</sup> T cells were shown to be toxic to motor neurons *in vitro*, which was mediated by granzymes, Fas ligand and IFN- $\gamma$  (Coque et al., 2019). However, T cell-deficiency in SOD1 mice did not affect the survival. Additionally, pro-inflammatory cytokines and chemokines (such as TNF, IFN- $\gamma$ , IL-6, CCL2, and IL-8) in the blood and cerebrospinal fluid correlated with more rapid disease progression, whereas anti-inflammatory cytokines (such as IL-4 and IL-10) ameliorated disease symptoms (Béland et al., 2020). In conclusion, cytokines released from innate and adaptive immune cells directly affect each other, having an impact on microglial polarization and the disease course.

#### **1.4.4. NF- $\kappa$ B signaling pathway**

NF- $\kappa$ B signaling pathway is a major signaling pathway with an important role in immune signaling, cell survival and proliferation (T. Liu et al., 2017; Q. Guo et al., 2024). It can be activated canonically and non-canonically. Canonical activation is achieved upon stimulation of different PRRs, cytokine receptors, T- and B-cell receptors. It results in translocation of the NF- $\kappa$ B (p65:p50 heterodimer) from cytoplasm to the nucleus, where it starts transcription of various pro-inflammatory genes. Non-canonical pathway is activated upon stimulation of receptors such as CD40, RANK, lymphotoxin- $\beta$  receptor and B-cell activating factor receptor. It results in translocation of a different NF- $\kappa$ B heterodimer (p100:RelB) and acts on cell proliferation and differentiation (T. Liu et al., 2017; Q. Guo et al., 2024). In this study, we will focus on canonical signaling, which will be further described in detail.

PRR signaling is crucial for detection and resolution of bacterial and viral infection. The most well-known PRRs are Toll-like receptors (TLRs), which recognize different parts of bacteria and viruses (D. Li & Wu, 2021). One example is TLR4, which senses LPS, a component of Gram-

negative bacterial cell wall. When it binds to TLR4, TIR-domain-containing adapter-inducing IFN- $\beta$  (TRIF) and TRIF-related adapter molecule (TRAM) are recruited to the cytoplasmic domain of TLR4 (Fitzgerald et al., 2003). Then, ubiquitin ligases tumor necrosis factor receptor-associated factor 6 (TRAF6) and linear ubiquitin chain assembly complex (LUBAC) catalyze formation of K63 and M1 polyubiquitin chains on RIPK1, respectively (L. Deng et al., 2000; Tokunaga et al., 2009). Polyubiquitinated RIPK1 serves as an anchor for binding the inhibitor of  $\kappa$ B (I $\kappa$ B) kinase (IKK) complex and TGF- $\beta$  activated kinase 1 (TAK1) (Poyet et al., 2000; C. Wang et al., 2001). IKK complex is formed from three subunits: the kinases IKK- $\alpha$  and IKK- $\beta$ , and regulatory unit IKK- $\gamma$ , also known as NEMO. NEMO recognizes K63 and M1 polyubiquitinated RIPK1 and therefore mediates binding of IKK complex to the latter (Ea et al., 2006; Wu et al., 2006; Rahighi et al., 2009). Then, IKK complex phosphorylates I $\kappa$ B- $\alpha$ , which at the steady state keeps the p65:p50 dimer in the cytoplasm thus restricting its activity as a transcription factor (Zandi et al., 1997). Phosphorylated I $\kappa$ B- $\alpha$  undergoes K48 polyubiquitination and proteasomal degradation (Chen et al., 1996). This frees the p65:p50 dimer, which also gets phosphorylated on the p65 subunit by the IKK complex, enabling its translocation to the nucleus, where it regulates the transcription of various pro-inflammatory molecules such as TNF, IL-1 $\beta$  and IL-6 (Fig. 7).

Importantly, NF- $\kappa$ B activation is tightly controlled. I $\kappa$ B- $\alpha$  is resynthesized after degradation to promote NF- $\kappa$ B signaling inhibition, and I $\kappa$ B- $\alpha$  expression is directly regulated by p65 (Sun et al., 1993; Arenzana-Seisdedos et al., 1997). Additionally, deubiquitinases CYLD and A20 play an important role in inhibition of the NF- $\kappa$ B pathway. A20 cleaves K63 polyubiquitin chains from RIPK1 through its N-terminus, whereas its C-terminus performs K48 polyubiquitination of RIPK1, leading to RIPK1 degradation via the proteasome (Wertz et al., 2004). CYLD hydrolyses K63-linked polyubiquitin chains on RIPK1 (Kovalenko et al., 2003). Therefore, this prevents excessive NF- $\kappa$ B signaling activation, which would have detrimental effects on the cells and the whole organism.

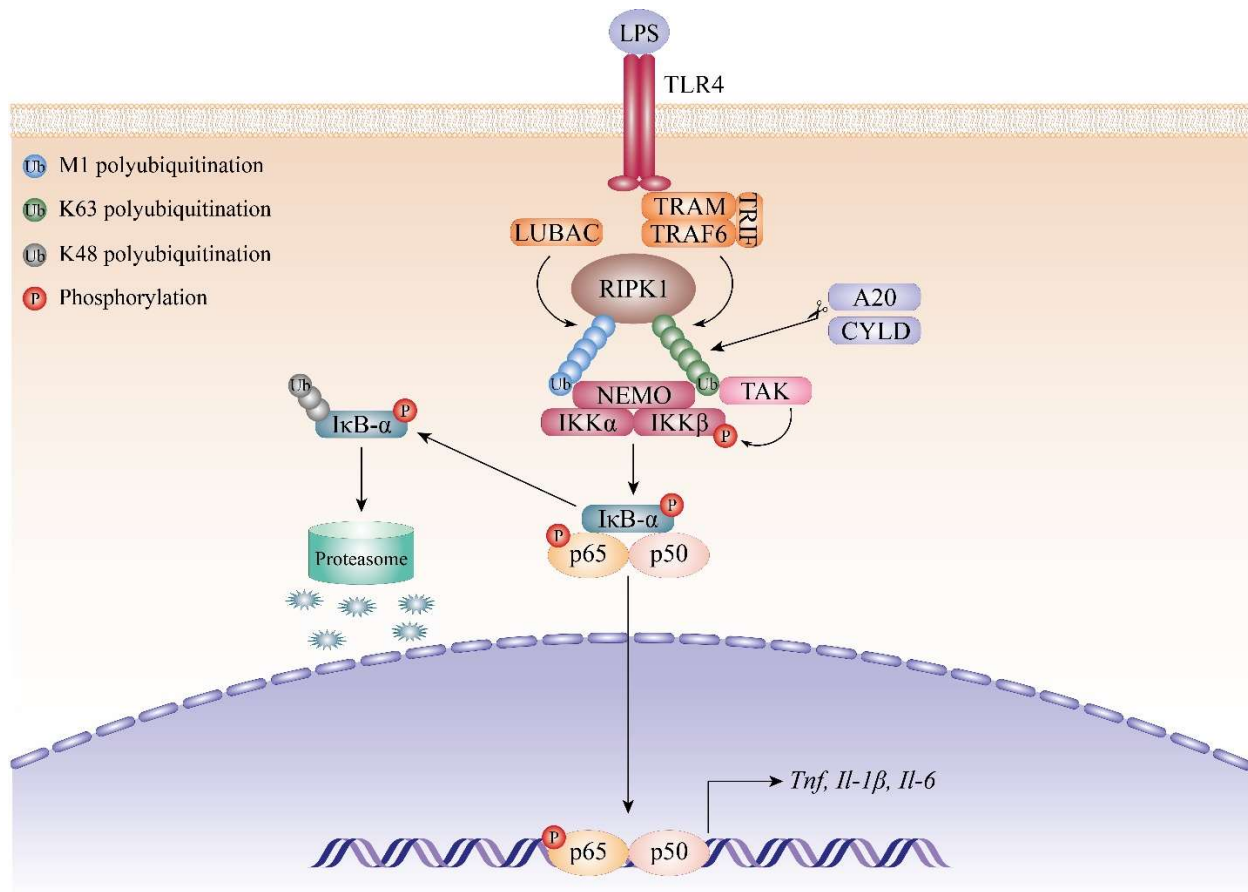


**Figure 7. NF- $\kappa$ B signaling upon TLR4 stimulation with LPS.** TLR4 stimulation by LPS leads to the recruitment of ubiquitin ligases TRAF6 and LUBAC, which mediate M1 and K63 polyubiquitination of RIPK1, respectively. Then, IKK (comprising NEMO, IKK $\alpha$  and IKK $\beta$ ) and TAK1 complexes bind to polyubiquitinated RIPK1, whereby TAK1 activates the IKK complex. Kinase subunits of the IKK complex (IKK $\alpha$  and IKK $\beta$ ) phosphorylate I $\kappa$ B- $\alpha$ , which is bound to the p65:p50 (NF- $\kappa$ B) dimer and is further K48 polyubiquitinated and degraded via the proteasome. Free p65:p50 dimer is phosphorylated by the IKK complex and as such translocates to the nucleus, where it regulates the transcription of pro-inflammatory cytokines such as TNF, IL-1 $\beta$  and IL-6. Modified from: Markovinovic *et al.*, 2017.

#### 1.4.4.1. The role of optineurin in the NF- $\kappa$ B signaling pathway

Optineurin was shown to share a high homology with NEMO and their UBRs show the same specificity for ubiquitin chains on RIPK1 (Schwamborn *et al.*, 2000; Zhu *et al.*, 2007; Wagner *et*

al., 2008; Laplantine et al., 2009). Zhu *et al.* have shown that optineurin competes with NEMO for polyubiquitinated RIPK1, thus acting as a negative regulator of the NF- $\kappa$ B pathway (Zhu et al., 2007). Another proposed mechanism was that optineurin recruits CYLD deubiquitinase, which hydrolyses K63-linked polyubiquitin chains from RIPK1. However, the lack of the ubiquitin binding capacity (D477N mutation) of optineurin showed stronger phenotype compared to loss of CYLD binding (H486R mutation) (Nagabhushana et al., 2011). Therefore, the proposed function of optineurin in NF- $\kappa$ B signaling inhibition is dual: 1) competition with NEMO for polyubiquitinated RIPK1 and 2) CYLD recruitment. Notably, most of these studies used overexpression systems, which may have resulted in artefacts. In addition, they used cell lines (HEK293T and HeLa) or primary cells that were not of the CNS origin (mouse embryonic fibroblasts). To test these mechanisms in primary cells, mouse models lacking optineurin in the whole body (Optn<sup>-/-</sup> or optineurin knockout) or with defective UBR (Optn<sup>D477N</sup> and Optn<sup>470T</sup>) were generated. However, only one *in vivo* study showed that optineurin suppresses the NF- $\kappa$ B pathway, but these results were not as clear-cut as the overexpression findings. Notably, Obaid *et al.* have shown that optineurin acted as a negative regulator of the NF- $\kappa$ B signaling only at the late time points (peaking on the third day of stimulation), but was dispensable in early time points during RANKL-mediated differentiation of bone marrow-derived macrophages (BMDMs) to osteoclasts (Obaid et al., 2015). Additionally, Ito *et al.* showed increased basal TNF secretion from primary microglia derived from Optn<sup>-/-</sup> mice. However, the NF- $\kappa$ B signaling activation was not assessed and the slightly increased spinal cord TNF protein level (~15%) was attributed to excessive RIPK1-mediated necroptosis, a type of inflammatory TNF-mediated cell death (Y. Ito et al., 2016). In conclusion, some of the reported studies suggested the role of optineurin as the negative regulator of the NF- $\kappa$ B signaling and TNF production.

In contrast, multiple studies in various primary mouse cells have shown no effect of optineurin deficiency or insufficiency on the NF- $\kappa$ B signaling. Specifically, optineurin was dispensable for the NF- $\kappa$ B signaling in primary mouse embryonic fibroblasts (MEFs) and BMDMs derived from Optn<sup>-/-</sup> mice. In addition, upon intraperitoneal stimulation of WT and Optn<sup>-/-</sup> mice with recombinant TNF, comparable NF- $\kappa$ B activation markers were found in the liver (Slowicka et al., 2016a). Gleason *et al.* generated BMDMs from Optn<sup>D477N</sup> mice, which carry a point mutation in the UBR. Even though they have shown abrogated binding of ubiquitin, NF- $\kappa$ B activation was

similar to WT cells (Gleason et al., 2011). Primary cells (BMDMs, bone marrow-derived dendritic cells or BMDCs, B cells, T cells and primary microglia) derived from the *Optn*<sup>470T</sup> mouse model of optineurin insufficiency, which lacks the whole UBR (described in 1.2.3.), showed normal NF- $\kappa$ B signaling compared to WT cells (Munitic et al., 2013; Markovinovic et al., 2018). Additionally, we have performed CRISPR/Cas9-mediated optineurin knockout in Neuro2A (neuronal cell line) and BV2 (microglial cell line) cells, and confirmed the results found in primary cells (Rob, 2018). Therefore, results from overexpression and physiological systems differ, which makes the role of optineurin in the NF- $\kappa$ B pathway still debatable (summarized in table 2).

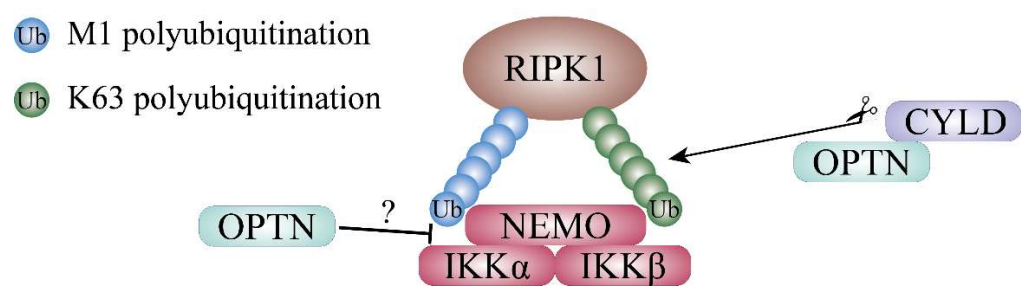


**Figure 8. The proposed role of optineurin in the NF- $\kappa$ B signaling pathway.** It was shown that optineurin acts as a negative regulator of the NF- $\kappa$ B signaling by two mechanisms: 1) it competes with NEMO for polyubiquitinated RIPK1 (Zhu et al., 2007); 2) it recruits CYLD, which hydrolyses K63-linked polyubiquitin chains on RIPK1 (Nagabhushana et al., 2011).

**Table 2. Summary of findings regarding the role of optineurin in the NF- $\kappa$ B signaling.** The chronological order of findings, which have (YES) and have not (NO) corroborated the hypothesis that optineurin is a negative regulator of the NF- $\kappa$ B signaling pathway. Abbreviations: HEK (human embryonic kidney), HeLa (Henrietta Lacks cervical cancer cells), NSC-34 (mouse motor neuron-like cell line), RGC-5 (mouse retinal ganglion cell line), BMDM (bone marrow-derived macrophages), RPE (human retinal pigment epithelium), BMDC (bone marrow-derived dendritic cells), Neuro2A (mouse neuronal cell line), BV2 (mouse microglial cell line).

| Optineurin is a negative regulator of the NF- $\kappa$ B signaling pathway |     |           |
|--|-----|-----------|
| Cell type  | YES | Reference |

|                            |  |                             |
|----------------------------|--|-----------------------------|
| HEK293T                    | Optineurin overexpression (D474N) and silencing (miRNA)  | (Zhu et al., 2007)          |
| HeLa                       | Optineurin overexpression (D474N) and silencing (shRNA)  | (Sudhakar et al., 2009)     |
| NSC-34                     | Optineurin overexpression (E478G, Q398X)   | (Maruyama et al., 2010)     |
| HeLa, RGC-5                | Optineurin overexpression (D474N, H486R) and silencing (shRNA)   | (Nagabhushana et al., 2011) |
| Neuro2A                    | Optineurin overexpression (Q398X) and silencing (shRNA)  | (Akizuki et al., 2013)      |
| HEK293                     | Optineurin overexpression (D474N, 467T)  | (Munitic et al., 2013)      |
| BMDM-derived osteoclasts   | Optn <sup>D474N</sup> osteoclasts upon RANKL-mediated differentiation  | (Obaid et al., 2015)        |
| Primary neonatal microglia | Increased TNF secretion from unstimulated Optn <sup>-/-</sup> cells, without analysis of the NF-κB signaling | (Y. Ito et al., 2016)       |
| HEK293T                    | Optineurin overexpression (Q165X, Q398X, D474N, E478G and other mutants)                                     | (Nakazawa et al., 2016)     |
| HeLa                       | Optineurin silencing (siRNA)   |                             |
| Primary MEFs               | Optineurin overexpression (Q165X, Q398X, D474N, E478G and other mutants)                                     | (Z. Liu et al., 2018)       |
| Brain                      | Optineurin overexpression (E478G)  |                             |
| RPE                        | Optineurin overexpression (E478G)  | (O'Loughlin et al., 2020)   |
| Primary MEFs               | Derived from Optn <sup>-/-</sup> mice  | (Fukushi et al., 2023)      |
|                            | <b>NO</b>  |                             |
| BMDMs                      | Derived from Optn <sup>D477N</sup> mice  | (Gleason et al., 2011)      |



|  |  |                                |
|--|--|--------------------------------|
| BMDMs,<br>BMDCs, B and T<br>cells        | Derived from Optn <sup>470T</sup> mice   | (Munitic et al.,<br>2013)      |
| HEK293T<br>HeLa<br>Primary MEFs<br>BMDMs | Optineurin silencing (siRNA)<br>CRISPR/Cas9-mediated optineurin knockout<br>Derived from Optn <sup>470T</sup> mice<br>Derived from Optn <sup>470T</sup> mice | (Pourcelot et al.,<br>2016)    |
| Primary MEFs,<br>BMDMs                   | Derived from Optn <sup>-/-</sup> mice  | (Slowicka et al.,<br>2016a)    |
| Neuro2A, BV2                             | CRISPR/Cas9-mediated optineurin knockout   | (Rob, 2018)                    |
| Primary neonatal<br>microglia            | Derived from Optn <sup>470T</sup> mice   | (Markovinovic et<br>al., 2018) |

#### 1.4.4.2. NF-κB signaling in ALS

NF-κB activity in ALS tissues was confirmed to be increased compared to healthy controls, measured by increased protein levels of either phosphorylated or non-phosphorylated p65 (Swarup et al., 2011b; Sako et al., 2012; Nakazawa et al., 2016). Since microglia and astrocytes are the main sources of cytokines and chemokines, they represent interesting targets for manipulation of the NF-κB signaling in ALS animal models. Frakes *et al.* inhibited NF-κB signaling specifically in microglia in SOD1<sup>G93A</sup> mouse model and have shown rescue of motor neuron death, extended survival, decreased microgliosis and astrogliosis, without an effect on disease onset (Frakes et al., 2014). In another ALS mouse model, overexpressing WT TDP-43 resulted in increased NF-κB activation, and its inhibition ameliorated neurotoxicity, microgliosis and astrogliosis (Swarup et al., 2011b). This group reported that TDP-43 acted as a co-activator of p65 by stabilizing its localization in the nucleus, thus prolonging its effect on expression of pro-inflammatory cytokines. In addition, constitutively active NF-κB only in microglia of WT mice resulted in ALS-like pathology, characterized by microgliosis, astrogliosis, motor neuron loss and motor impairments (Frakes et al., 2014). On the contrary, inhibition of NF-κB signaling specifically in astrocytes affected neither motor neuron death nor the disease course (Crosio et al., 2011; Frakes et al., 2014).

To conclude, microglia-specific NF- $\kappa$ B regulation is essential for regulation of neuroinflammation and neurodegeneration.

#### 1.4.5. TBK1 signaling

TBK1 signaling pathway is the major pathway for the production of IFN- $\beta$ , one of the key antiviral cytokines (Ahmad et al., 2016). It is activated upon stimulation of different PRRs, including TLR4 (Fitzgerald et al., 2003). Upon TLR4 stimulation with LPS, TRIF and TRAM are recruited to the cytoplasmic domain of TLR4, which serve for further recruitment of K63 ubiquitin ligase TRAF3 (Fitzgerald et al., 2003; Häcker et al., 2006). TRAF3 polyubiquitinates TBK1 (Lin et al., 2023), leading to its autophosphorylation and activation (Clark et al., 2011; Ma et al., 2012). Active TBK1 phosphorylates interferon regulatory factor 3 (IRF3), which dimerizes, translocates into the nucleus and regulates the transcription of IFN- $\beta$  (Sharma et al., 2003). The signaling pathway is illustrated in Figure 9.

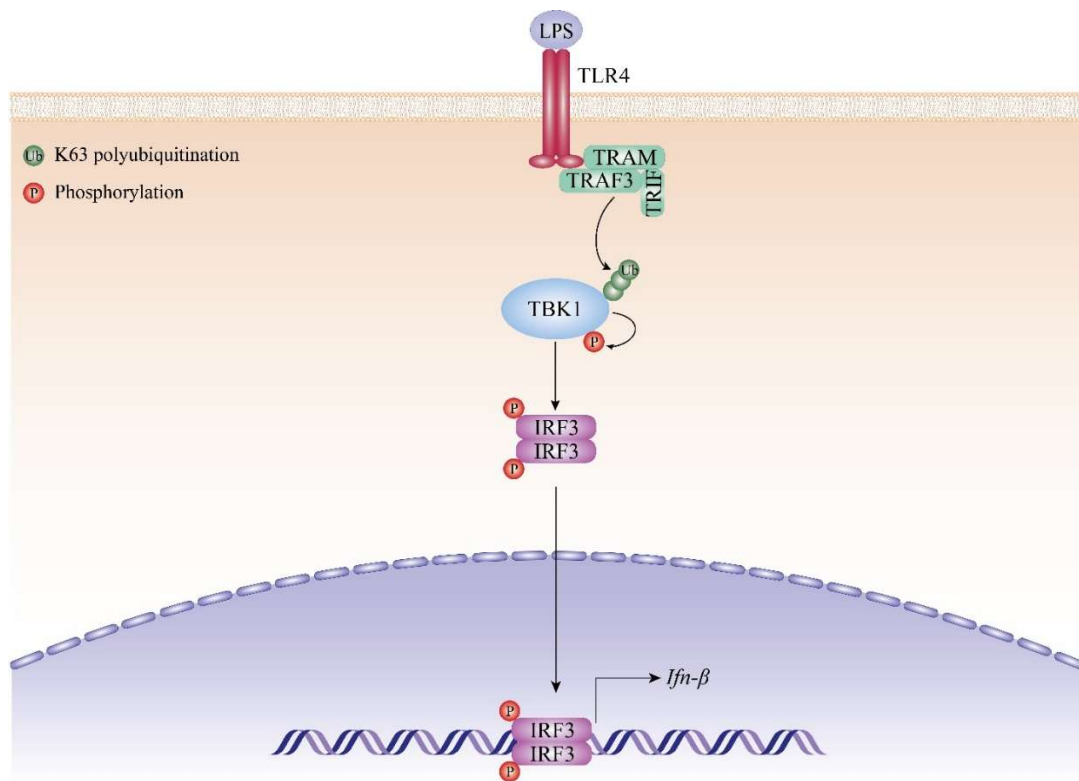


**Figure 9 TBK1 signaling pathway.** Stimulation of TLR4 by LPS leads to recruitment of TRAM, TRIF and ubiquitin ligase TRAF3. TRAF3 ligates K63 ubiquitin chains to TBK1, enabling its

activation by autophosphorylation. Such activated form of TBK1 further phosphorylates IRF3, which dimerizes and translocates into the nucleus, where it regulates transcription of IFN- $\beta$ . Modified from: Chau *et al.*, 2008.

#### **1.4.5.1. The role of optineurin in the TBK1 signaling**

Optineurin was proposed to take part in the TBK1 signaling (Markovinovic et al., 2018; Prtenjaca, 2020). Optineurin binding of TBK1 is bivalent. TBK1 is recognized and bound by N-terminal TBK1-binding region and C-terminal UBR of optineurin (Gleason et al., 2011; F. Li et al., 2016; Meena et al., 2016). Additionally, K63-polyubiquitin chains on activated TBK1 are recognized by the UBR of optineurin. Gleason *et al.* have shown that deficient binding of ubiquitin via UBR in Optn<sup>D477N</sup> BMDMs decreased TBK1 activation, but did not affect TBK1 binding. However, it was sufficient to decrease IFN- $\beta$  production upon LPS stimulation (Gleason et al., 2011). A study done by Munitic *et al.* has confirmed the importance of the UBR in TBK1 activation. BMDMs derived from UBR-deficient mice (Optn<sup>470T</sup>) have shown decreased TBK1 signaling in various primary cells, even though the absence of UBR had the opposite effects in cell lines upon overexpression (Munitic et al., 2013). These results were further confirmed in various other primary cells and cell lines upon inflammatory stimulation with RANKL, LPS, poly (I:C) and Sendai virus (Obaid et al., 2015; Pourcelot et al., 2016; Markovinovic et al., 2018). HEK263T cells overexpressing Optn <sup>$\Delta$ 157</sup>, which lacks the TBK1-binding domain, have shown absence of TBK1 binding (Meena et al., 2016). This was further confirmed by decreased TBK1 signaling and IFN- $\beta$  production upon LPS stimulation of BMDMs generated from Optn <sup>$\Delta$ 157</sup> mice. The lack of whole protein (optineurin knockout mouse and cellular models) confirmed the role of optineurin as a positive regulator of the TBK1 signaling (Slowicka, Vereecke, Mc Guire, et al., 2016; Rob, 2018), which is illustrated in Figure 10.

Nevertheless, as observed for the NF- $\kappa$ B signaling (see section 1.3.3.1.), the role of optineurin in TBK1 signaling is also controversial. Overexpression studies have shown that optineurin negatively regulated TBK1 signaling (Munitic et al., 2013; O'Loughlin et al., 2020). Additionally, primary Optn<sup>-/-</sup> MEFs, J774.1 and BV2 cell lines with silenced optineurin and patient-derived fibroblasts with E478G mutation and Q398X truncation showed that optineurin suppressed TBK1

signaling upon viral infection (Fukushi et al., 2023). However, the detailed analysis as performed in primary cells is still missing. A brief overview of findings related to the role of optineurin in the TBK1 signaling is summarized in Table 3.

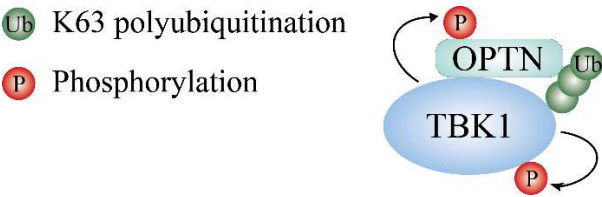


**Figure 10. The proposed role of optineurin in the TBK1 signaling pathway.** It was shown that optineurin acts as a positive regulator of the TBK1 signaling by stabilizing its autophosphorylation, downstream signaling and subsequent IFN-β production. This is achieved by binding of TBK1 and its K63-linked polyubiquitin chain by optineurin (Gleason et al., 2011; Meena et al., 2016; Pourcelot et al., 2016). As mentioned before, the TBK1 binding by optineurin is bivalent. More precisely, N-terminal TBK1-binding region binds TBK1, whereas C-terminal UBR binds K63-polyubiquitin chains, which are added upon activation of signaling. The latter is required for optimal TBK1 kinase activity.

**Table 3. Summary of findings regarding the role of optineurin in the TBK1 signaling.** The chronological order of findings, which have (YES) and have not (NO) corroborated the hypothesis that optineurin is a positive regulator of the TBK1 signaling pathway. Abbreviations: HEK (human embryonic kidney), HeLa (Henrietta Lacks; cervical cancer cells), BMDM (bone marrow-derived macrophages), RPE (human retinal pigment epithelium), BMDC (bone marrow-derived dendritic cells), BV2 (mouse microglial cell line), J774.1 (mouse macrophage cell line).

| Optineurin is a positive regulator of the TBK1 signaling pathway |   |                        |
|--|---|------------------------|
| Cell type  | YES                                     | Reference              |
| BMDMs  | Derived from Optn <sup>D477N</sup> mice | (Gleason et al., 2011) |
| BMDMs, BMDCs   | Derived from Optn <sup>470T</sup> mice  | (Munitic et al., 2013) |

|   |  |                           |
|---|--|---------------------------|
| BMDM-derived osteoclasts                      | Optn <sup>D474N</sup> osteoclasts upon RANKL-mediated differentiation  | (Obaid et al., 2015)      |
| BMDMs   | Derived from Optn <sup>Δ157</sup> mice   | (Meena et al., 2016)      |
| HEK293T<br>HeLa<br>Primary MEFs<br>BMDMs      | Optineurin silencing (siRNA)<br>CRISPR/Cas9-mediated optineurin knockout<br>Derived from Optn <sup>470T</sup> mice<br>Derived from Optn <sup>470T</sup> mice | (Pourcelot et al., 2016)  |
| BMDMs   | Derived from Optn <sup>-/-</sup> mice  | (Slowicka et al., 2016a)  |
| BV2   | CRISPR/Cas9-mediated optineurin knockout   | (Rob, 2018)               |
|   | <b>NO</b>  |                           |
| HEK293  | Optineurin overexpression (D474N, 467T)  | (Munitic et al., 2013)    |
| RPE   | Optineurin overexpression (E478G)  | (O'Loughlin et al., 2020) |
| Primary MEFs<br>J774.1 and BV2<br>Fibroblasts | Derived from Optn <sup>-/-</sup> mice<br>Optineurin silencing (shRNA)<br>Derived from ALS patients (E478G, Q398X)  | (Fukushi et al., 2023)    |

#### 1.4.5.2. TBK1 signaling in ALS

Impaired signaling was described for *TBK1* loss-of-function mutations found in ALS- and FTD patients (Freischmidt et al., 2015; De Majo et al., 2018; Brenner et al., 2024). Specifically, in *in vitro* systems and in the *in vivo* mouse model of TBK1 haploinsufficiency (*Tbk1*<sup>+/-</sup>), it was shown that those mutations led to decreased IRF3 phosphorylation and optineurin binding. Diminished TBK1 signaling reduces production of IFN-β, which may play an important role in ALS pathogenesis. Interestingly though, Brenner *et al.* have shown that TBK1 haploinsufficiency in SOD1<sup>G93A</sup> mice had detrimental effect in the early and beneficial effect in the late stage of the disease, where the latter was associated with decreased microgliosis (Brenner et al., 2019). This means that IFN-β may be neurotoxic and neuroprotective, depending on the disease stage.

### 1.5. TAR DNA-binding protein 43 (TDP-43)

TDP-43 was discovered as a protein that binds to trans-activation response element of human immunodeficiency virus-1 (HIV-1), which acts as a transcription repressor (Ou et al., 1995). TDP-43, encoded by *TARDBP* gene, is ubiquitously expressed protein of 414 amino acids (Fig. 11). Its RNA recognition motifs (RRM1 and 2) enable the binding of RNA molecules, by which TDP-43 regulates various aspects of nucleic acid metabolism (Prasad et al., 2019; Jo et al., 2020). TDP-43 is mainly located in the nucleus, with a small proportion in the cytoplasm, which is controlled by the nuclear localization signals (Prasad et al., 2019; Jo et al., 2020). Its expression is tightly regulated via the negative feedback regulation of its own expression (Ayala et al., 2011). Mutations in TDP-43, such as A315T, G348C and Q331K, were found in a small percentage of ALS and FTD patients, (Prasad et al., 2019; Jo et al., 2020). These mutations are concentrated in the glutamine-, asparagine- and glycine-rich region (also known as prion-like region), located in the C-terminus (Prasad et al., 2019; Jo et al., 2020). This region dictates the solubility and stability of the protein, so mutations in this region often lead to an increased propensity for TDP-43 aggregation. In addition, toxic C-terminal fragments, which are the result of proteolytic cleavage of a full-length protein, were found in neurons of ALS and FTD patients (Neumann et al., 2006). Importantly, despite the low frequency of *TARDBP* mutation carriers in patients, cytoplasmic inclusions of WT TDP-43 were found in 97% and 45% of ALS and FTD patients, respectively (Ling et al., 2013). These inclusions were found to be hyperphosphorylated and ubiquitinated and were found in neuronal and glial cells (Arai et al., 2006; Neumann et al., 2006; Inukai et al., 2008). The exact cause of TDP-43 cytoplasmic aggregation in ALS/FTD patients is still unknown. However, Correia *et al.* have shown that LPS stimulation *in vitro* and *in vivo* led to TDP-43 aggregation and nuclear loss, respectively (Correia et al., 2015), suggesting that inflammation may precede TDP-43 aggregation.

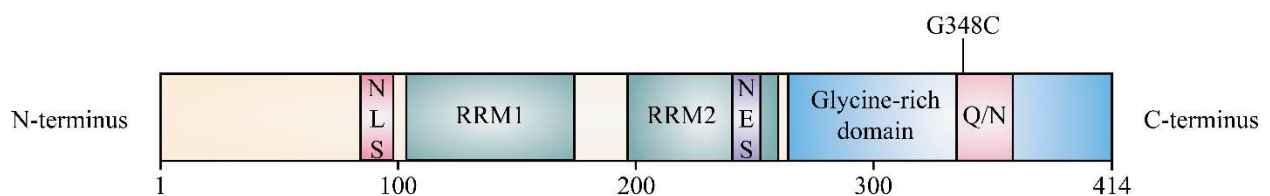


**Figure 11. TDP-43 protein domains.** Protein domains of TDP-43 are marked as nuclear localization signal (NLS; 82-98 aa), RNA recognition motif 1 (RRM1; 104-176 aa), RRM2 (192-

262 aa), nuclear export signal (239-250 aa), glycine-rich domain (274-414 aa) and glutamine/asparagine-rich region (Q/N; 345-366 aa). G348C mutation found in ALS patients is depicted. Based on it, a TDP-43<sup>G348C</sup> mouse model was generated, which will be used in our studies. Modified from: Prasad *et al.*, 2019.

### **1.5.1. TDP-43<sup>G348C</sup> mouse model**

To investigate the role of TDP-43 in the pathogenesis of ALS/FTD, various transgenic mouse models were generated. The most used ones include those with overexpression of TDP-43<sup>WT</sup>, TDP-43<sup>A315T</sup>, TDP-43<sup>G348C</sup> and TDP-43<sup>Q331K</sup>. In this study, we will utilize TDP-43<sup>G348C</sup> mouse model, which overexpresses G348C mutation, found in sporadic and familial ALS patients. This mouse model has shown age-related ALS and FTD symptoms. At 10 months of age, it showed TDP-43 cytoplasmic aggregation and neuroinflammation in the brain and the spinal cord. Also, these mice developed cognitive and motor deficits with onset from 7-8 and 10 months of age, respectively (Swarup et al., 2011). Therefore, this mouse model represents a valuable ALS/FTD mouse model since it develops major hallmarks of ALS/FTD, TDP-43 aggregation and neuroinflammation, which are age-dependent. Here we utilized this mouse model to investigate the role of optineurin in ALS by crossing Optn<sup>470T</sup> mice to TDP-43<sup>G348C</sup> mice.

## 2. Thesis aims and hypotheses

Optineurin is a multifunctional adaptor protein involved in the regulation of inflammatory signaling via NF- $\kappa$ B and TBK1 pathways. *OPTN* mutations found in ALS patients were reported to lead to dysregulation of inflammatory signaling in multiple *in vitro* model systems (Zhu et al., 2007; Maruyama et al., 2010; Nagabhushana et al., 2011). Since inflammation was also found to be affected by aging, the major risk factor for neurodegenerative diseases, the aging process was predicted to represent a sufficient second hit for developing neurodegeneration in the presence of optineurin mutation. To study this, several groups generated optineurin mouse models and examined them for signs of neuropathology (Y. Ito et al., 2016; Dermentzaki et al., 2019; Kurashige et al., 2021; Slowicka et al., 2016b). However, more detailed analyses are necessary to understand the role of optineurin mutations in disease pathogenesis.

We have utilized our original Optn<sup>470T</sup> mouse model, which mimics Q398X truncation found in ALS patients and performed a detailed neurological, neuropathological and neuroimmunological analysis to test for the potential development of ALS or FTD during aging. We also crossed the Optn<sup>470T</sup> to TDP-43<sup>G348C</sup> transgenic mice to analyse the potential aggravation of phenotype in mice carrying two ALS/FTD mutations. For the *in vitro* studies, we have used BMDMs, neonatal microglia and T cells from these mice, in which we analyzed immune signaling, phagocytosis and polarization.

The main aims and hypotheses of this research were:

- 1) To test if aging will act as a second hit that will trigger neurodegeneration in Optn<sup>470T</sup> mice. We hypothesized that aging would lead to ALS/FTD-like symptom development in Optn<sup>470T</sup> mice. We thus compared motor and cognitive performances, and tested various neuropathological signs of neurodegeneration and neuroinflammation, including neuronal loss, astrogliosis, microgliosis, lipofuscin accumulation and the presence of TDP-43 pathology in the motor cortex and the spinal cord of young-adult and aged Optn<sup>470T</sup> mice.
- 2) To test the role of optineurin in the process of phagocytosis in inflammatory conditions and during aging. It was recently reported that microglia-like cells derived from sporadic ALS patients (Quek et al., 2022) and adult primary microglia from SOD1<sup>G93A</sup> mice (Barreto-



Núñez et al., 2024) showed decreased phagocytosis, which may represent a new disease hallmark. Therefore, we have compared phagocytosis in primary neonatal microglia, and BMDMs derived from young adult and aged mice from WT and Optn<sup>470T</sup> mice. We hypothesized that Optn<sup>470T</sup> primary cells would have decreased phagocytosis, and that aging-induced decline in phagocytosis will be more pronounced in cells derived from Optn<sup>470T</sup> mice compared to WT cells.

- 3) To analyze T cell polarization in the spleens of Optn<sup>470T</sup> mice during aging. T cell polarization is affected in ALS patients and animal models (Béland et al., 2020; De Marchi et al., 2021), and aging is known to affect CD4<sup>+</sup> (increased pro-inflammatory T<sub>H1</sub> and T<sub>H17</sub> polarization) (Mittelbrunn & Kroemer, 2021) and CD8<sup>+</sup> T cells (increased percentage of IFN- $\gamma$ -producing cells) (Pulko et al., 2016). We hypothesized that aged Optn<sup>470T</sup> mice would have increased CD4<sup>+</sup> T<sub>H1</sub> and T<sub>H17</sub> polarization and more IFN- $\gamma$ -producing CD8<sup>+</sup> T cells compared to WT mice.
- 4) To test if ALS/FTD will be exacerbated by crossing Optn<sup>470T</sup> with TDP-43<sup>G348C</sup> transgenic mice. The latter model was reported to develop ALS- and FTD-like neuropathology, and cognitive and motor decline from 6 and 9 months of age, respectively (Swarup et al., 2011). By breeding these mice, we generated a new potential double-mutant ALS/FTD mouse model Optn<sup>470T</sup>/TDP-43<sup>G348C</sup>. We have let these mice age up to 18 months and analyzed them for motor and cognitive impairments. We hypothesized that Optn<sup>470T</sup>/TDP-43<sup>G348C</sup> mice would develop more pronounced motor and cognitive impairments compared to mice carrying only one mutation (Optn<sup>470T</sup> and TDP-43<sup>G348C</sup>) and WT mice.
- 5) To analyze NF- $\kappa$ B and TBK1 signaling pathways in Optn<sup>470T</sup>/TDP-43<sup>G348C</sup> BMDMs. We have shown that optineurin was dispensable for NF- $\kappa$ B but positively regulated TBK1 signaling (Markovinovic et al., 2018; Munitic et al., 2013), whereas TDP-43 stabilizes NF- $\kappa$ B activation (Swarup et al., 2011) without a known role in the TBK1 signaling. We hypothesized that Optn<sup>470T</sup>/TDP-43<sup>G348C</sup> BMDMs will have more pronounced NF- $\kappa$ B but decreased TBK1 signaling upon LPS stimulation.

- 6) To test if inflammation will differentially affect aged Optn<sup>470T</sup>/TDP-43<sup>G348C</sup>, single mutant Optn<sup>470T</sup> and TDP-43<sup>G348C</sup>, and control mice. To this end, we intraperitoneally administered mice with LPS for three consecutive days. Long-term stimulation was applied because it was reported that chronic LPS stimulation of TDP-43<sup>A315T</sup> mice resulted in nuclear loss of TDP-43 (Correia et al., 2015). We measured the sickness behavior signs, cytokines in the CNS and serum, and analyzed innate immune cell composition and activation in the spleen. We hypothesized that repetitive LPS administration would lead to the breakdown of immune regulation, which would be more pronounced in Optn<sup>470T</sup>/TDP-43<sup>G348C</sup> mice. We expected that these mice would have dysbalanced cytokine profiles and altered splenic immune cell composition and activation compared to their single mutant counterparts and WT mice.

### **3. Materials and methods**

#### **3.1. Materials**

##### **3.1.1. Reagents for mouse genotyping**

DNA lysing buffer: 10 mM Tris (#4855.3, Carl Roth), 150 mM NaCl (#31434-1KG, Honeywell Fluka), 10 mM EDTA (#A3145,0500, AppliChem), 0.2% sodium dodecyl sulphate (SDS; #0183.2, Carl Roth).

2X EmeraldAmpGT PCR Master Mix (#RR310A, Takara Bio) contains optimized buffer, DNA polymerase, dNTP mixture, green gel loading dye, and a density reagent (all at 2X concentration).

50X TAE: 2 M Tris, 1 mM EDTA, 20 mM CH<sub>3</sub>COOH (#64-19-7, Alkaloid); diluted 1:50 in dH<sub>2</sub>O.

##### **3.1.2. Reagents for mouse perfusion and fixation**

10X Phosphate-buffered saline (PBS): 1.37 M NaCl, 27 mM KCl (#7447-40-7, T.T.T. d.o.o.), 96 mM Na<sub>2</sub>HPO<sub>4</sub> × 7 H<sub>2</sub>O (#S9390, Honeywell Fluka or #X987.2, Carl Roth), 15 mM KH<sub>2</sub>PO<sub>4</sub> (#3904.2, Carl Roth); diluted 1:10 in dH<sub>2</sub>O and the pH was adjusted to 7.4.

1X PBS (137 mM NaCl, 2.7 mM KCl, 9.6 mM Na<sub>2</sub>HPO<sub>4</sub> × 7 H<sub>2</sub>O, 1.5 mM KH<sub>2</sub>PO<sub>4</sub>), pH = 7.4.

Fixation buffer: 4% paraformaldehyde (PFA; #0335.3, Carl Roth) in 1X PBS, pH = 7.5.

##### **3.1.3. Reagents for immunofluorescence on tissue sections (IF)**

Tissue storage solution: 30% sucrose (#4621.1, Carl Roth) in 1X PBS.

Phosphate buffer: 244 mM NaH<sub>2</sub>PO<sub>4</sub> (#P143790, Gram-mol), 200 mM NaOH (#P147090, Gram-mol).

Cryoprotectant solution: 30% glycerol (#P121003, Gram-mol), 30% ethylene glycol (#P116701, Gram-mol), 24.4 mM phosphate buffer; pH was adjusted to 7.4.

Permeabilization/blocking (Perm/Block) buffer: 10% horse serum (#P30-0702, Pan Biotech) in 0.25% Triton X-100 (#9002-93-1, Fisher Scientific)/1X PBS + 0.05% NaN<sub>3</sub> (#K305.1, Carl Roth).

Antibody probing solution: 1% horse serum in 0.25% Triton X-100/1X PBS.

1X true black: dilute 20X TrueBlack stock solution (#23007, Biotium) in 70% ethanol in 1:20 ratio.

Wash buffer: 1X PBS.

Other materials used: Vectashield Plus Antifade Mounting Medium (#VE-H-1900, Vector Laboratories), ImmEdge Hydrophobic Barrier PAP Pen (#H-4000, Vector Laboratories), VitroGnost Plus Ultra adhesive slides (#103001A72, BioGnost), Tissue-Tek O.C.T. Compound Medium (#4583-1, Sakura Finetek).

### **3.1.4. Reagents for cell culture**

#### **3.1.4.1. Primary neonatal microglia**

Complete DMEM: Dulbecco's Modified Eagle Medium (DMEM; #P04-04510, Pan Biotech) supplemented with 10% fetal bovine serum (FBS; #P30-3306, Pan Biotech or #FBS-11A, Capricorn Scientific) that was heat-inactivated (1 h at 60 °C), 1X Antibiotic/Antimycotic Solution (#AAS-B, Capricorn Scientific; 100 000 U/mL penicillin, 10 mg/mL streptomycin and 25 µg/mL amphotericin B) and 2 mM L-glutamine (#GLN-B, Capricorn Scientific).

Trypsin solution: 0.25% trypsin (#15090-46, Invitrogen) in 1X Hanks' Balanced Salt Solution without Ca<sup>2+</sup> and Mg<sup>2+</sup> (HBSS<sup>-/-</sup>).

DNase I solution (≥ 400 Kunitz units/mg protein; #DN25-100MG, Sigma Aldrich) was prepared at 5 mg/mL stock in sterile 0.9% NaCl and was used at final concentration of 0.625 mg/mL.

Poly-L-Lysine (mol wt 70,000-150,000; #P1274 Sigma Aldrich) was prepared at stock concentration of 10 mg/mL in sterile dH<sub>2</sub>O and was further diluted to 100 µg/mL for coating.

#### **3.1.4.2. Bone marrow-derived macrophages (BMDMs)**

Complete RPMI: RPMI 1640 (#RPMI-A, Capricorn Scientific) supplemented with 10% fetal bovine serum that was heat-inactivated (1 h at 60 °C), 1X Antibiotic/Antimycotic Solution, 2 mM L-glutamine and 10 mM HEPES (#HEP-B, Capricorn Scientific).

Complete BMDM medium: 30% L929 medium in complete RPMI.

L929 medium: as mentioned in section 3.1.4.1. with addition of 10 mM HEPES.

#### **3.1.4.3. T-cell restimulation medium**

Complete RPMI supplemented with 50  $\mu$ M  $\beta$ -mercaptoethanol ( $\beta$ -ME; #M3148-100ML, Sigma Aldrich), 50 ng/mL phorbol myristate acetate (PMA; #P1585, Sigma Aldrich), 500 ng/mL ionomycin (Iono; #I0634, Sigma Aldrich), and BD Golgi Stop (#554724, BD; 1:1500).

#### **3.1.4.4. Neuro2A (N2A) cell line**

Complete MEM: Eagle's Minimum Essential Medium (EMEM; #P04-09500, Pan Biotech) supplemented with 10% fetal bovine serum that was heat-inactivated (1 h at 60 °C), 1X Antibiotic/Antimycotic Solution, 2 mM L-glutamine, 10 mM, 1 mM sodium pyruvate (#P04-43100, Pan Biotech) and 1X non-essential amino acid solution (#P08-32100, Pan Biotech).

#### **3.1.4.5. Agonists, inhibitors and dyes**

Lipopolysaccharide (LPS) from *E. coli* O55:B5 (#L2880, Sigma Aldrich) was dissolved in sterile 1X PBS (#PBS-1A, Capricorn Scientific) at stock concentration of 5 mg/mL; used for *in vivo* studies.

LPS from *E. coli* O111:B4 (#L4391, Sigma Aldrich) was dissolved in sterile milliQ-H<sub>2</sub>O at stock concentration of 1 mg/mL; used for *in vitro* studies.

Tumor necrosis factor (TNF; #12343014, ImmunoTools) was dissolved in sterile milliQ-H<sub>2</sub>O at stock concentration of 100  $\mu$ g/mL.

Staurosporine (STS; #sc-3510, Santa Cruz) was dissolved in DMSO at stock concentration of 10 mM.

Cytochalasin D (Cyto D; #C8273, Sigma Aldrich) was dissolved in DMSO at stock concentration of 1 mM.

Carboxyfluorescein succinimidyl ester (CFSE; #65-0850-85, eBioscience) was dissolved in DMSO at stock concentration of 10 mM.

PKH26 Red Fluorescent Cell Linker Kit for General Cell Membrane Labeling (#PKH26GL-1KT, Sigma Aldrich).

CellTrace™ Far Red (#C34564, Invitrogen).

### **3.1.5. Reagents for protein isolation and SDS-polyacrylamide gel electrophoresis (SDS-PAGE) and western blot (WB)**

Radioimmunoprecipitation assay (RIPA) buffer for cell lysis: 50 mM Tris, 150 mM NaCl, 0.5% sodium deoxycholate (#D6750-10G, Sigma Aldrich), 1% Triton X-100; pH was adjusted to 8.0.

RIPA buffer for protein isolation from tissues: 50 mM Tris, 150 mM NaCl, 1 mM EDTA, 0.5% sodium deoxycholate, 1% NP-40 (#85124, Thermo Scientific), 0.1% SDS; pH was adjusted to 8.0.

10 mL of RIPA buffer was supplemented with 1 tablet of protease inhibitor cocktail (cOmplete™, EDTA-free Protease Inhibitor Cocktail; #11873580001, Roche) and 1 tablet of phosphatase inhibitor cocktail (PhosSTOP™; #04906837001, Roche).

4X Laemmli buffer: 217 mM Tris pH = 6.8, 35% glycerol, 9% SDS, bromophenol blue (#T116.1, Carl Roth); 8% β-ME was added freshly before use.

Stacking gel: 125 mM Tris-HCl pH = 6.8, 5% acrylamide (#3030.1, Carl Roth), 0.1% SDS, 0.1% ammonium peroxydisulphate (APS; #9592.2, Carl Roth), 0.1% N,N,N',N'-tetramethylethylenediamine (TEMED; #2367.3, Carl Roth).

Separating gel: 375 mM Tris-HCl pH = 8.8, 10% or 8-16% (gradient) acrylamide, 0.1% SDS, 0.1% APS, 0.1% TEMED.

10X SDS-running buffer: 250 mM Tris, 2 M glycine (#3908.4, Carl Roth), 1% SDS; diluted 1:10 in dH<sub>2</sub>O.

1X Transfer buffer: 25 mM Tris, 153 mM glycine, 20% methanol (#20847.295, VWR).

10X Tris-buffered saline (TBS): 248 mM Tris, 1.4 M NaCl, 27 mM KCl, pH was adjusted to 7.4; diluted 1:10 in dH<sub>2</sub>O.

0.1% TBS-Tween-20 (TBS-T): 0.1% Tween-20 (#9055-64-5, J.T. Baker) in 1X TBS.

Blocking buffer: 3% bovine serum albumin (BSA; #3854.3, Carl Roth) or 5% milk (#A0830,0500, AppliChem) in 0.1% TBS-T.

Primary antibody probing solution: blocking buffer + 0.05% NaN<sub>3</sub>.

Secondary antibody probing solution: blocking buffer.

Other materials used: PageRuler™ Prestained Protein Ladder (10 to 180 kDa; #26616, Thermo Scientific), nitrocellulose membrane (0.2 mm pore size; #10600001, Cytiva), Lumi-Light Western Blotting Substrate (#12015200001, Roche), Supersignal West Femto Maximum Sensitivity Substrate (#34095, Thermo Scientific).

### **3.1.6. Reagents for Enzyme-linked immunosorbent assay (ELISA)**

Wash buffer: 0.05% Tween-20 in 1X PBS.

3,3',5,5'-Tetrametilbenzidine (TMB; #ES001-100ML, Merck Millipore).

STOP solution: 8.5% H<sub>3</sub>PO<sub>4</sub> (#30417-1L-M, Sigma Aldrich).

#### **3.1.6.1. IFN-β**

Coating buffer: 50 mM carbonate buffer (45 mM NaHCO<sub>3</sub>; #S5761-500G, Sigma Aldrich, 4.5 mM Na<sub>2</sub>CO<sub>3</sub>; #497-19-8, Merck Millipore), pH = 9.0

Blocking buffer: 1% BSA in 1X PBS.

#### **3.1.6.2. IL-10 and TNF**

Mouse IL-10 DuoSet ELISA kit (#DY417-05, R&D Systems) and Mouse TNF alpha Uncoated ELISA Kit (#88-7324-88, Invitrogen).

Coating buffer: 1X PBS.

### **3.1.7. Reagents for flow cytometry**

For flow cytometry we used FACS flow buffer (2% FBS, 0.05% NaN<sub>3</sub> in 1X PBS), ammonium-chloride-potassium (ACK) lysing buffer (#A1049201, Gibco), UltraComp eBeads™ Compensation Beads (#01-2222-42, Invitrogen), Perm/Wash Buffer (#554723, BD Pharmingen), Fixable Viability Dye eFluor450 (#65-0863-14, eBioscience; used 1:20 000 in 1X PBS).



### 3.1.8. Antibodies

#### 3.1.8.1. Primary antibodies for western blot and immunofluorescence

**Table 4. List of primary antibodies used in western blot (WB) and immunofluorescence (IF).**

| <b>Antigen</b>                     | <b>Host</b> | <b>Catalog number</b> | <b>Manufacturer</b> | <b>Dilution</b>         |
|------------------------------------|-------------|-----------------------|---------------------|-------------------------|
| <b>β-actin-HRP</b>                 | mouse       | A3854                 | Sigma Aldrich       | WB 1:25 000             |
| <b>ChAT</b>                        | goat        | AB144P                | Sigma Aldrich       | IF 1:100                |
| <b>GAPDH</b>                       | rabbit      | 5174S                 | Cell Signaling      | WB 1:10 000 (tissues)   |
| <b>GFAP</b>                        | goat        | ab53554               | Abcam               | WB 1:1000<br>IF 1:200   |
| <b>Iba1</b>                        | rabbit      | 019-19741             | Wako                | WB 1:1000*<br>IF 1:1000 |
| <b>IκB-α</b>                       | rabbit      | sc-371                | Santa Cruz          | WB 1:1000*              |
| <b>NeuN</b>                        | mouse       | MAB377                | Merck Millipore     | IF 1:200                |
| <b>Optineurin<br/>(N-terminal)</b> | mouse       | sc-166576             | Santa Cruz          | WB 1:1000*              |
| <b>p-p65</b>                       | rabbit      | 3033S                 | Cell Signaling      | WB 1:1000               |
| <b>TBK</b>                         | rabbit      | 3013S                 | Cell Signaling      | WB 1:1000               |
| <b>p-TBK1</b>                      | rabbit      | 5483S                 | Cell Signaling      | WB 1:1000               |
| <b>TDP-43<br/>(N-terminal)</b>     | rabbit      | 10782-2-AP            | Proteintech         | WB 1:1000               |
| <b>TDP-43<br/>(C-terminal)</b>     | rabbit      | 12892-1-AP            | Proteintech         | IF 1:200                |
| <b>p-TDP-43</b>                    | rabbit      | SAB4200223            | Sigma Aldrich       | IF 1:200                |

**Information:** Antibodies incubated in 5% milk-based solutions are marked with \*, whereas others were incubated in 3% BSA-based solutions (only for WB).

### 3.1.8.2. Secondary antibodies for western blot and immunofluorescence

**Table 5. List of secondary antibodies used in western blot (WB) and immunofluorescence (IF).**

| <b>Antibody</b>    | <b>Conjugate</b> | <b>Catalog number</b> | <b>Manufacturer</b>    | <b>Dilution</b> |
|--------------------|------------------|-----------------------|------------------------|-----------------|
| <b>Anti-goat</b>   | HRP              | 805-035-180           | Jackson ImmunoResearch | WB 1:2500       |
| <b>Anti-mouse</b>  | HRP              | 115-035-174           | Jackson ImmunoResearch | WB 1:2500       |
| <b>Anti-rabbit</b> | HRP              | 111-035-144           | Jackson ImmunoResearch | WB 1:2500       |
| <b>Anti-goat</b>   | Alexa Fluor 488  | A11055                | Invitrogen             | IF 1:500        |
| <b>Anti-mouse</b>  | Alexa Fluor 488  | A21202                | Invitrogen             | IF 1:500        |
| <b>Anti-rabbit</b> | Alexa Fluor 488  | A32731                | Invitrogen             | IF 1:500        |
| <b>Anti-rabbit</b> | Alexa Fluor 555  | A31572                | Invitrogen             | IF 1:500        |

### 3.1.8.3. Antibodies used for IFN- $\beta$ ELISA

**Table 6. List of antibodies used for IFN- $\beta$  ELISA.**

| <b>Antibody</b>                           | <b>Host</b> | <b>Catalog number</b> | <b>Manufacturer</b>    | <b>Dilution</b> |
|---|-------------|-----------------------|------------------------|-----------------|
| <b>IFN-<math>\beta</math> (capture)</b>   | rat         | sc-57201              | Santa Cruz             | 1:400           |
| <b>IFN-<math>\beta</math> (detection)</b> | rabbit      | 32400-1               | PBL Assay Science      | 1:6000          |
| <b>Anti-rabbit-HRP</b>                    | goat        | 111-035-144           | Jackson ImmunoResearch | 1:1500          |

#### 3.1.8.4. Antibodies used for flow cytometry – surface markers

**Table 7. Antibodies used for staining surface markers by flow cytometry.**

| <b>Antibody</b>    | <b>Conjugate</b> | <b>Catalog number</b> | <b>Manufacturer</b> | <b>Dilution for cells</b> | <b>Dilution for beads</b> |
|--------------------|------------------|-----------------------|---------------------|---------------------------|---------------------------|
| B220               | Alexa Fluor 700  | 103231                | BioLegend           | 1:1000                    | 1:1000                    |
| CD4                | APC-H7           | 560181                | BD Pharmingen       | 1:1000                    | 1:500                     |
| CD8a               | BV605            | 100744                | BioLegend           | 1:1000                    | 1:1500                    |
| CD11b              | APC              | 553312                | BD Pharmingen       | 1:400                     | 1:400                     |
| CD11c              | PE               | 12-0114-82            | eBioscience         | 1:200                     | 1:100                     |
| CD86               | PE-Cy7           | 25-0862-80            | eBioscience         | 1:200                     | 1:1000                    |
| CD90.2<br>(Thy1.2) | BV786            | 105331                | BioLegend           | 1:2000                    | 1:2000                    |
| F4/80              | PerCP-Cy5.5      | 45-4801-82            | eBioscience         | 1:200                     | 1:50                      |
| Ly6C               | APC-eFluor780    | 47-5932-82            | eBioscience         | 1:100                     | 1:100                     |
| Ly6G               | FITC             | 127606                | BioLegend           | 1:1000                    | 1:400                     |
| MHC-II             | PE/Dazzle        | 107648                | BioLegend           | 1:8000                    | 1:200                     |
| NK1.1              | BV605            | 108739                | BioLegend           | 1:100                     | 1:1000                    |

#### 3.1.8.5. Antibodies used for flow cytometry – intracellular staining

**Table 8. Antibodies used for intracellular staining by flow cytometry.**

| <b>Antibody</b> | <b>Conjugate</b> | <b>Catalog number</b> | <b>Manufacturer</b> | <b>Dilution for cells</b> | <b>Dilution for beads</b> |
|-----------------|------------------|-----------------------|---------------------|---------------------------|---------------------------|
| IFN- $\gamma$   | PE/Dazzle        | 505845                | BioLegend           | 1:800                     | 1:600                     |
| IL-2            | APC              | 17-7021-81            | eBioscience         | 1:500                     | 1:800                     |
| IL-17A          | PE               | 12-7177-81            | eBioscience         | 1:1000                    | 1:1000                    |
| TNF             | PE-Cy7           | 25-7321-82            | eBioscience         | 1:2000                    | 1:800                     |

## 3.2. Methods

### 3.2.1. Mouse models

Mouse model of optineurin insufficiency (hereafter referred to as Optn<sup>470T</sup>) was generated as previously described (Munitic et al., 2013). Briefly, mice with flanked exon 12 by loxP-neo<sup>R</sup>-loxP cassette (subsequently deposited in Jackson Laboratory, #029708) were crossed with mice expressing Cre recombinase under the control of endogenous  $\beta$ -actin promoter, which resulted in the whole-body truncation of the C-terminal ubiquitin-binding region of optineurin. More precisely, truncation led to the loss of the last 114 amino acids in the C-terminus, resulting in protein with 470 amino acids (instead of the full-size protein of 584 amino acids). Optn<sup>470T</sup> mice were backcrossed to the C57BL/6 (hereafter referred to as *wild-type*, WT; Jackson Laboratory) for 9-11 generations. Homozygous Optn<sup>470T</sup> (Optn<sup>470T/470T</sup>) mice were used in this research and were compared to sex- and age-matched WT mice.

To generate a new double-hit mouse model, Optn<sup>470T</sup> mice were crossed with transgenic mice overexpressing human TDP-43 mutation under its endogenous promoter (TDP-43<sup>G348C</sup>) (Swarup et al., 2011) to obtain double-mutant Optn<sup>470T</sup>/TDP-43<sup>G348C</sup> mice (Mohović, 2023). Optn<sup>470T</sup>/TDP-43<sup>G348C</sup> mice of both sexes were compared to their age-matched WT, Optn<sup>470T</sup> and TDP-43<sup>G348C</sup> littermates.

The mice were housed in the Laboratory of Mouse Engineering and Breeding Facility at the Medical Faculty of Rijeka on 12 h light/12 h dark cycle and had access to food and water *ad libitum*. For this research, we used four groups of either male or female mice according to age: young-adult (3-6-month-old), adult (6-10-month-old), middle-aged (11-15-month-old), and aged (16-24-month-old). Experiments were performed according to the European Communities Council Directive of 24<sup>th</sup> November 1986 (86/609/EEC) and were approved by the Ministry of Agriculture of the Republic of Croatia, Ethics Committees of the Medical Faculty and Faculty of Biotechnology and Drug Development.

### **3.2.2. Mouse genotyping**

#### **3.2.2.1. DNA isolation from mouse tail**

A small piece of tail was digested in 400  $\mu$ L of DNA lysing buffer supplemented with 0.4 mg/mL proteinase K (#70663-4, Merck Millipore) overnight on a shaker at 55°C and 900 rpm, which was followed by centrifugation at 4°C, 12 000 rpm for 1 min to remove hair residues. Next, the supernatants (~400  $\mu$ L) were transferred to a new 1.5 mL Eppendorf tube where they were mixed with an equal volume (~400  $\mu$ L) of 100% isopropanol (#KE00.0906, LabExpert) and were vortexed to precipitate DNA. After the centrifugation at 4°C, 12 000 rpm for 10 min, the supernatants were discarded, and the pellet was washed with 1 mL of 70% ethanol and centrifuged again at 12 000 rpm for 10 min. The supernatants were discarded, and the DNA pellets were let to dry for 1 h at RT, resuspended in 50-200  $\mu$ L (depending on the pellet size) of sterile milliQ-H<sub>2</sub>O and dissolved by shaking at 55°C, 900 rpm for 1 h. The DNA concentration was determined on a BioDrop Duo spectrophotometer (#80-3006-61, Biochrom) based on the A<sub>260</sub>/A<sub>280</sub> ratio, which was ~1.8 (indicates for “pure” DNA). DNA concentration was set to approximately 0.1 – 0.15  $\mu$ g/ $\mu$ L.

#### **3.2.2.2. Polymerase chain reaction (PCR)**

WT, Optn<sup>470T</sup>, TDP-43<sup>G348C</sup> and Optn<sup>470T</sup>/TDP-43<sup>G348C</sup> mice were identified by polymerase chain reaction (PCR). Three PCR reaction mixes were prepared (Table 9.) and after 1  $\mu$ L of DNA was added, the reaction mixes were put in Mastercycler (#6345, Eppendorf), which was set to a specific program (Table 10.) to amplify the desired DNA by use of specific primers (Table 11.).

**Table 9. PCR reaction mixes per one sample for amplification of WT and Optn<sup>470T</sup> and TDP-43<sup>G348C</sup> DNA fragments.** Note: The same calculation was used for preparation of mixes for amplification of WT and Optn<sup>470T</sup> DNA fragment, with different primers for each mix, as depicted below.

| PCR reaction mix for WT and Optn <sup>470T</sup> |             | PCR reaction mix for TDP-43 <sup>G348C</sup> |             |
|--|-------------|--|-------------|
| Component  | Volume (μL) | Component                                    | Volume (μL) |
| 2X EmeraldAmpGT PCR Master Mix                   | 10          | 2X EmeraldAmpGT PCR Master Mix               | 10          |
| Forward primer (10 μM)                           | 0.4         | Forward primer (20 μM)                       | 1           |
| Reverse primer (10 μM)                           | 0.4         | Reverse primer (10 μM)                       | 1           |
| H <sub>2</sub> O                                 | 8.2         | H <sub>2</sub> O                             | 7           |
| Total volume                                     | 19          | Total volume                                 | 19          |
| → 19 μL master mix + 1 μL DNA                    |             |  |             |

**Table 10. PCR programs for genotyping.**

| Step                 | Temperature  | Time | Number of cycles |
|----------------------|--|------|------------------|
| Initial denaturation | 95°C   | 30 s | 1x               |
| Denaturation         | 95°C   | 30 s | 35x              |
| Primer annealing     | 55°C (WT and Optn <sup>470T</sup> )<br>59°C (TDP-43 <sup>G348C</sup> ) | 30 s |                  |
| Elongation           | 72°C   | 60 s |                  |
| Final elongation     | 72°C   | 60 s | 1x               |
| Cooling              | 4°C  | ∞    | /                |

**Table 11. Primers used for PCR, ordered from Metabion at stock concentration of 100  $\mu$ M.**

| Gene                    | Primer  | Sequence (5' $\rightarrow$ 3') | Final concentration |
|-------------------------|---------|--------------------------------|---------------------|
| Optn <sup>WT</sup>      | Forward | GCTACCATGCTCAGCCAGAGTTTC       | 0.2 $\mu$ M         |
|                         | Reverse | GGCTTCAGGGATGCATGAATC          | 0.2 $\mu$ M         |
| Optn <sup>470T</sup>    | Forward | GCAACACAGACCTGAACAGACG         | 0.2 $\mu$ M         |
|                         | Reverse | ACTCCACCCATAAGTCATCAAAGC       | 0.2 $\mu$ M         |
| TDP-43 <sup>G348C</sup> | Forward | CTCTTTGTGGAGAGGAC              | 1 $\mu$ M           |
|                         | Reverse | TTATTACCCGATGGGCA              | 0.5 $\mu$ M         |

### 3.2.2.3. Agarose gel electrophoresis

The presence of the amplified DNA fragment was confirmed by electrophoresis on 2% agarose gel, which was prepared in 1X TAE with addition of 1  $\mu$ L of GelStar (#50535, Lonza) for band visualization. The electrophoresis was performed at 110 V, after loading 3  $\mu$ L of 100 bp DNA ladder (#N3231S, New England BioLabs) and 15  $\mu$ L of amplified DNA, until the front reached the edge of the gel. DNA was then visualized on ChemiDoc<sup>TM</sup> MP Imaging System (Bio-Rad). The product sizes were detected at 363 bp (Optn<sup>wt</sup>), 288 bp (Optn<sup>470T</sup>) and at 365 bp (TDP-43<sup>G348C</sup>).

### 3.2.3. Motor tests and cognitive tests

#### 3.2.3.1. Accelerating rotarod

To check the motor coordination of mice, a rotarod test was performed on a rotating rod device (#47600, Ugo Basile). Mice were trained by giving them three trial sessions with fixed speed (1<sup>st</sup> and 2<sup>nd</sup> trial: 5 rpm for 4 min; 3<sup>rd</sup> trial: 8 rpm for 3 min) with at least 1 h of rest between the trials. Latency to fall was measured on the test day (at least 24 h after the training), when the mice were given three trials with accelerating speed (from 5 to 50 rpm during 300 s) with rest such as in the training session. Average value was calculated from all three trials for each mouse.

#### **3.2.3.2. Grid- and wire-hanging tests**

For grid- and wire-hanging motor coordination tests, the grid or 3-mm-thick wire were placed 30 cm above the surface that was covered with soft bedding, respectively. Each mouse was placed in the center of the grid or wire and was given three trials of max 180 s, with at least 10 min rest between the trials. The average of three trials was calculated.

#### **3.2.3.3. Novel object recognition**

Novel object recognition test was performed to check for the cognitive capability of the mice, and was performed as previously described (Leger et al., 2013), with minor modifications. On the first day (habituation), the mouse was placed in an empty plexiglass box (42 cm × 26.5 cm × 15 cm) and on the second day (familiarization) two same objects were given. On the third (test) day, one familiar object was replaced with a novel one and the time of interaction with both objects was individually measured with a stopwatch. Each session lasted for 5 min. To assess cognitive capability, the percentages of time spent on interaction with familiar and novel object were determined and compared.

#### **3.2.4. Stimulation of mice with LPS and measurement of sickness behavior**

At 18 months of age, WT, Optn<sup>470T</sup>, TDP-43<sup>G348C</sup> and Optn<sup>470T</sup>/TDP-43<sup>G348C</sup> mice were stimulated with 1.5 mg/kg dose of LPS (from *Escherichia coli* O55:B5, #L2880, Sigma Aldrich) for three consecutive days, which represents a model of sepsis. The sickness behavior was assessed 24 h after every dose by measurement of body weight and temperature.

For stock preparation, LPS was dissolved in sterile 1X PBS (#PBS-1A, Capricorn Scientific) at concentration of 5 mg/mL, stored at -20°C and diluted in 1X PBS before injection.

#### **3.2.5. Mouse perfusion and fixation for isolation of tissue and serum**

Before tissue isolation, mice were anesthetized with a mixture of 100 mg/kg ketamine (#000786, Bioveta) and 20 mg/kg xylazine (#001338, Bioveta) prepared in sterile 1X PBS. After reaching deep anesthesia, the sternum was lifted with forceps and the thoracic cavity was opened with iris



scissors. Next, the ribs and the diaphragm were cut to expose the heart, where a small cut with iris scissors was made in the right atrium and the 25G butterfly needle was inserted into the left ventricle. The mice were perfused with 60 mL of ice-cold 1X PBS to remove erythrocytes (a source of autofluorescence) and contaminant leukocytes, and the spleen was isolated. Immediately after that, the mice were laid on their abdomen and decapitated. The skin on the head was pulled to expose the skull and the parietal bones were cut on both sides to enable removal of the occipital lobe. Then, another cut was made through the sagittal suture (located in-between parietal bones) to expose the brain, which was carefully removed with the spatula. The olfactory bulbs and cerebellum were removed. For the spinal cord isolation, the mice were laid on their abdomen and the skin was cut from the cervical to the sacral part. The excess of muscles was removed with iris scissors and the vertebrae were cut on each side of the spine. The whole spinal cord was extracted by scraping with spatula. The tissues were then flash frozen in liquid nitrogen and stored at -80°C or were processed for analysis on flow cytometer (see section 3.2.8.6.).

For immunofluorescence studies, the mice were perfused with 60 mL of ice-cold 1X PBS and fixed with the same amount of 4% paraformaldehyde (PFA). The brain and the spinal cord were isolated with the help of spring scissors and post-fixed in 4% PFA for 24-72 h at 4°C. Next, the tissues were stored in a tissue preservation solution until they sank to the bottom of the 50 mL Falcon tube (min 72 h), which is an indication for successful dehydration.

Serum isolation: before perfusion, the blood was drawn from the left ventricle with 21G needle, let to clot for 2 h at RT and centrifuged at 4°C, 1000 × g for 10 min. The sera (supernatants) were transferred to a new 1.5 mL Eppendorf tube and stored at -80°C.

### **3.2.6. Cell culture**

All cells were maintained in an incubator with 5% CO<sub>2</sub> and at 37°C.

#### **3.2.6.1. Isolation and cultivation of primary neonatal microglia**

For isolation of primary neonatal microglia, pups on postnatal day 0-3 (P0-3) were taken and decapitated with iris scissors. The skin on the head and skull was cut with micro dissecting scissors to expose the brain, which was carefully removed and transferred into a 6 cm Petri dish containing

3 mL of 1X HBSS<sup>-/-</sup>. Under the dissecting microscope (#SMZ-168, Motic) the meninges, olfactory bulbs and cerebellum were removed with Dumont forceps. After pooling three brains of the same genotype into one 6 cm Petri dish, they were chopped into small pieces with a blade and 3 mL of 0.25% trypsin was added (to the final volume of 6 mL). After incubation at 37°C for 15 min, trypsin was neutralized by transferring 6 mL of suspension into a 15 mL Falcon tube containing 6 mL of complete DMEM. After the tissue chunks reached the bottom of the tube, the supernatants were carefully removed with a 10 mL serological pipette. Another 3 mL of complete DMEM and 375 µL of DNase I were added to the tube and the tissues were triturated by pipetting up and down until a homogenous suspension was formed. The suspension was then passed through a 70 µm filter (#542070, Greiner) into another 50 mL Falcon tube, which was centrifuged at 500 rpm for 5 min. The supernatant was removed with a 10 mL serological pipette and the cells were resuspended in 10 mL of complete DMEM and seeded into a poly-L-lysine-coated T75 flasks. The medium was changed the next day and then every two to three days until the cell reached complete confluency (after 7-10 days). The culture resulted in a co-culture consisting of astrocytes and microglia. To detach microglia from the astrocyte layer, 500 µL of 1 M HEPES was added to the culture medium, the cap was sealed with parafilm, and the flask was put on a shaker at 120 rpm, 37°C overnight. Next day, the cells were shaken for another 4 h at 300 rpm. The supernatants were collected (pooled for each genotype) and centrifuged at 1500 rpm for 5 min. The viable cells were counted by using trypan blue (#17-924E, Lonza), stained for phagocytosis assay (see section 3.2.8.6.4.) and plated in a poly-L-lysine-coated 24-well plates at a density of 200 000 cells/well. The cells were treated 48 h after plating.

### **3.2.6.2. Isolation and cultivation of bone marrow-derived macrophages (BMDMs)**

The mice were sacrificed by cervical dislocation, put on their backs and sprayed with 70% ethanol. The skin on the legs was removed and a cut above the hip joint was made. The legs containing tibia and femur were then transferred to an empty Petri dish, where the feet and residual muscles were removed. After the tibia and femur were separated, both ends of the bones were cut to expose the bone marrow and were put in a new Petri dish filled with 20 mL of complete RPMI. Next, the bone marrow was flushed using a 3 mL syringe (#309658, BD) and a 25G needle, and was filtered through a 70 µm cell strainer into a 50 mL Falcon tube. The remaining bone marrow chunks left

on the strainer were mashed with a blunt end of a syringe, followed by washing with additional 5 mL of complete medium. The suspension was centrifuged at 1500 rpm for 5 min and the supernatant was discarded. The cells were resuspended in 3 mL of freezing medium (10% FBS/90% DMSO) and frozen at -80°C in 1 mL aliquots. After thawing, the cells were washed with complete RPMI, centrifuged at 1500 rpm for 5 min and plated in 20 mL of complete BMDM medium (see section 3.2.6.2.1.). The cells were differentiated to macrophages for 5-7 days in culture. The cells were lifted with 10 mM EDTA/PBS, rinsed in complete RPMI and plated in 24-well plates at a density of 150 000 cells/well in complete BMDM medium. The cells were treated 24-48 h after plating.

#### **3.2.6.2.1. Complete BMDM medium preparation**

L929 cell line (a mouse fibroblast cell line that is a source of macrophage colony-stimulating factor or M-CSF, which is a trophic factor that drives macrophage differentiation from bone marrow precursors; a kind gift from Jonathan D. Ashwell) was thawed and expanded in a T75 flask until reaching 90-100% cell confluency. Then, the cells were trypsinized, centrifuged at 1500 rpm for 5 min, resuspended in 5 mL of complete DMEM and split equally to five T125 flasks (100 mL of complete DMEM + 1 mL of cell suspension). When the cells reached 100% confluency, the culture was kept in an incubator for 10 days for enrichment of the medium with M-CSF. After 10 days, L929 medium was filtered through a 0.22 µm filter unit (#15913307, Fisherbrand), aliquoted (10 aliquots of 50 mL) and stored at -80°C. For BMDM differentiation, complete BMDM medium was prepared by mixing 35 mL of complete RPMI and 15 mL of L929 medium (30% L929 medium in complete RPMI).

### **3.2.7. Functional and biochemical assays**

#### **3.2.7.1. Immunoblotting**

##### **3.2.7.1.1. Protein isolation and quantification for SDS-PAGE**

After the cell treatment, the wells were washed with 1 mL of ice-cold 1X PBS. The cells were lysed by addition of 110 µL of RIPA buffer (supplemented with protease and phosphatase inhibitors) and subsequent scraping with the pipette tip. The lysates were transferred to a 1.5 mL

Eppendorf tubes, kept on ice for the next 30 min, and centrifuged at 4°C, 14 000 rpm for 10 min. Next, 90 µL of lysate was transferred to a new 1.5 mL Eppendorf tube, where it was mixed with 30 µL of 4X Laemmli buffer.

For protein isolation from tissues, ½ of the brain or the whole spinal cord were lysed in a glass homogenizer (#AA731, Thomas Scientific) for 2 min in 700 or 500 µL of RIPA buffer (supplemented with protease and phosphatase inhibitors), respectively. The lysates were incubated on ice for 30 min and subsequently centrifuged at 13 000 rpm for 20 min. The supernatants were aliquoted and stored at -80°C. Before mixing with 4X Laemmli buffer, protein concentration was determined with Pierce BCA Protein Assay Kit (#23227, Thermo Scientific) according to the manufacturer's instructions. Briefly, the BSA concentration range (from 2000 to 25 µg/mL) and tissue lysates (diluted 1:40) were diluted in RIPA buffer and loaded (25 µL/well) on a polystyrene flat-bottom 96-well plate. Then, 200 µL of mixture of reagent A and B (reagent A:reagent B = 50:1) was added to each well, the plate was sealed with parafilm and incubated in the dark at 37°C for 30 min. The absorbance was read on a spectrophotometer (#16039400, Tecan) at 570 nm. The final protein concentration per lysate was calculated to be 10 mg/mL after mixing with 4X Laemmli buffer. For SDS-PAGE, 5 µg of protein was loaded into each lane.

#### **3.2.7.1.2. SDS-PAGE**

Mini-PROTEAN Tetra Vertical Electrophoresis Cell (#1658037, Bio-Rad) was used for protein separation based on size in 1X SDS-running buffer. Cell and tissue lysates were heated at 95°C for 10 min and were loaded on 10% or 8-16% polyacrylamide gels. Prestained protein ladder was used for protein size assessment. The gels were first run at 110 V until the proteins reached the separating gel, when the voltage was increased to 130 V until the front reached the end of the separating gel.

#### **3.2.7.1.3. Western blot and antibody incubation**

After protein separation, the proteins were transferred to a nitrocellulose membrane by assembling a sandwich (from cathode (-) to anode (+): sponge – Whatman paper – gel – membrane – Whatman paper – sponge) in a cassette. The transfer was performed in a western blot tank filled with 1X

transfer buffer, and lasted for 95 min. The membranes were then cut according to the protein size, blocked with blocking buffer on a shaker for 1 h at RT and subsequently incubated with primary antibody at +4°C overnight (or 30 min at RT for incubation with  $\beta$ -actin-HRP). Next day, the membranes were washed with 0.1% TBS-T ( $3 \times 10$  min), which was followed by 1 h incubation with a corresponding HRP-conjugated secondary antibody. After the next three washes, the bands were visualized with visualizing substrates (see section 3.1.5.) on ChemiDoc™ MP Imaging System (Bio-Rad).

#### **3.2.7.1.4. Western blot band quantification**

The bands were quantified using ImageJ Fiji software (National Institutes of Health). Each band intensity was normalized to the intensity of the loading control ( $\beta$ -actin or GAPDH).

#### **3.2.7.2. ELISA**

TNF and IL-10 ELISA were performed according to the manufacturer's instructions, while IFN- $\beta$  ELISA was performed as previously described (Weinstein et al., 2000) with minor modifications. Flat-bottom polystyrene 96-well plates (#M9410-1CS, Nunc) were coated with capture antibody and incubated overnight at +4°C (for TNF and IFN- $\beta$ ) or RT (for IL-10). Next day, the plates were washed with washing buffer and blocked with blocking buffer for 1 h at RT and washed again. Supernatants were loaded undiluted (for IFN- $\beta$ ) or diluted (1:5 to 1:50 for TNF and IL-10) and were incubated for 2 h at RT. The plates were then washed and incubated with biotinylated HRP-labeled (for TNF and IL-10) or unlabeled (for IFN- $\beta$ ) detection antibody for 1 h at RT. The plates were washed and incubated with avidin-HRP conjugate (for TNF and IL-10) or HRP-labeled detection antibody (for IFN- $\beta$ ) for 30 min or 1 h at RT, respectively. Next, the plates were washed again, incubated with TMB reagent and after 20 min incubation in the dark (until the blue color developed) the reaction was stopped with 8.5%  $\text{H}_3\text{PO}_4$ . The absorbance was read at 450 nm on a spectrophotometer. The standard curve and cytokine concentrations were analyzed on GraphPad Prism 8.0.

### **3.2.7.3. Immunofluorescence on tissue sections**

Post-fixed and dehydrated brains and spinal cords were embedded in O.C.T. medium on dry ice until completely frozen. The tissues were coronally cut on a cryostat (#CM1850, Leica) on which 25 µm thick slices were obtained, transferred to cryoprotectant solution and stored at -20°C until use.

For staining, the slices were transferred to adherent slides, let to dry for 1 h at RT and encircled with hydrophobic pen. This was followed by permeabilization and blocking with perm/block buffer for 1 h at RT in a humid chamber (used for all subsequent incubations). After the buffer was removed, the slices were incubated with primary antibodies (Table 4.) overnight at RT. Next day, the slices were washed (3 × 10 min) with washing buffer, incubated with fluorophore-conjugated secondary antibodies (Table 5.) for 1 h at RT, and stained with 500 ng/mL DAPI for 15 min. The slices were washed again (3 × 10 min) and incubated with 1X TrueBlack for 30 s to quench autofluorescence. TrueBlack was omitted when autofluorescence caused by lipofuscin was imaged. After the last series of washing, the tissues were mounted and stored at 4°C.

#### **3.2.7.3.1. Imaging and image analysis**

The motor cortex (brain) and ventral horns (spinal cord) were imaged with Olympus IX83 fluorescent microscope using 10X or 20X objective, respectively. Z-stacking (step number: 30, step size: 1 µm) and subsequent EFI processing were done on cellSens Dimension software (Olympus) for analysis of Iba1<sup>+</sup> and GFAP<sup>+</sup> cells. Mean fluorescence intensity (MFI; integrated density) was normalized to and shown as % of one-year-old WT mice, which was used for assessment of microglial and astrocyte activation. Additionally, microglial morphology (cell body area and longest process length) was also analyzed in the context of activation. Analyses were performed using ImageJ Fiji software.

### **3.2.7.4. Analysis of gene expression**

#### **3.2.7.4.1. RNA isolation**

RNA isolation from cells was performed with RNeasy Mini Kit (#74106, Qiagen) according to the manufacturer's instructions. Briefly, after treatment, the cells were washed with 1 mL of 1X PBS

and frozen at  $-80^{\circ}\text{C}$  upon addition of 350  $\mu\text{L}$  of RLT buffer. On the day of isolation, the plate was brought to RT (until RLT buffer thawed completely) and 350  $\mu\text{L}$  of 70% ethanol (prepared in RNase-free water) was added to each well, and the cells were lysed by scraping with pipette tip. The suspension ( $\sim 700$   $\mu\text{L}$ ) was transferred to RNeasy Mini spin column, centrifuged at  $8000 \times g$  for 1 min, and the flow-through was discarded. Next, 700  $\mu\text{L}$  of RW1 buffer was added to the column, which was subsequently centrifuged at  $8000 \times g$  for 1 min. Two washes with RPE buffer were performed at  $8000 \times g$  for 1 and 2 min, respectively. Lastly, the column was transferred to a new RNase-free 1.5 mL tube and 30  $\mu\text{L}$  of RNase-free water was added to the column, which was centrifuged at  $8000 \times g$  for 1 min to elute RNA. RNA concentration was determined on BioDrop Duo spectrophotometer based on the A260/280 ratio, which was  $\sim 2$  (indicates for “pure” RNA).

#### 3.2.7.4.2. Synthesis of complementary DNA (cDNA) by reverse transcription

Complementary DNA (cDNA) was synthesized from RNA by using High-Capacity cDNA Reverse Transcription Kit (#4368814, Applied Bioscience) and RNase Inhibitor (#N8080119, Applied Bioscience) following manufacturer’s instructions. Reverse transcription reaction mix was prepared (see Table 12.) and run on Mastercycler (see program in Table 13.). Synthesized cDNA was diluted in sterile milliQ  $\text{H}_2\text{O}$  in 1:5 ratio, quantified on BioDrop Duo spectrophotometer and stored at  $-20^{\circ}\text{C}$ .

**Table 12. Reverse transcription reaction mix.**

| Reverse transcription master mix                     |                          |
|--|--------------------------|
| Kit component  | Volume ( $\mu\text{L}$ ) |
| 10X RT buffer  | 2                        |
| 25X dNTP mix (100 mM)                                | 0.8                      |
| 10X Random primers                                   | 2                        |
| RNase inhibitor (20 U/ $\mu\text{L}$ )               | 1                        |
| Reverse transcriptase (50 U/ $\mu\text{L}$ )         | 1                        |
| Nuclease-free $\text{H}_2\text{O}$                   | 3.2                      |
| → 10 $\mu\text{L}$ master mix + 10 $\mu\text{L}$ RNA |                          |

**Table 13. Reverse transcription PCR program.**

| Step                  | Temperature | Time    |
|-----------------------|-------------|---------|
| Primer annealing      | 25°C        | 10 min  |
| Reverse transcription | 37°C        | 125 min |
| Enzyme inactivation   | 85°C        | 5 min   |
| Cooling               | 4°C         | ∞       |

**3.2.7.4.3. Reverse transcription quantitative polymerase chain reaction (RT-qPCR)**

Analysis of gene expression was done by RT-qPCR by using qPCRBIO SyGreen Mix Lo-ROX (#PB20.11-20, PCR Biosystems), following manufacturer's instructions. RT-qPCR master mix (Table 14.) with primers (Table 15.) was loaded into LightCycler 480 Multiwell Plate (#4729692001, Roche), with total volume of 20 µL/well. The reactions were loaded in duplicates for each gene. RT-qPCR was performed on LightCycler® 96 Instrument (#05815916001, Roche) based on the program listed in Table 13.

**Table 14. RT-qPCR master mix.**

| RT-qPCR master mix             |             |
|--------------------------------|-------------|
| Component                      | Volume (µL) |
| 2X Master mix                  | 10          |
| Forward primer (10 µM)         | 0.8         |
| Reverse primer (10 µM)         | 0.8         |
| H <sub>2</sub> O               | 3.4         |
| Total volume                   | 15          |
| → 15 µL master mix + 5 µL cDNA |             |



**Table 15. List of primers used for RT-qPCR ordered from Metabion at stock concentration of 100  $\mu$ M.**

| Gene         | Primer               | Sequence (5' $\rightarrow$ 3') | Final concentration |
|--------------|----------------------|--------------------------------|---------------------|
| GAPDH        | Forward (10 $\mu$ M) | GGTGCTGAGTATGTCGTGGA           | 0.4 $\mu$ M         |
|              | Reverse (10 $\mu$ M) | GTGGTTCACACCCATCACAA           | 0.4 $\mu$ M         |
| TNF          | Forward (10 $\mu$ M) | TCTTCTCATTCCTGCTTG             | 0.4 $\mu$ M         |
|              | Reverse (10 $\mu$ M) | GGTCTGGGCCATAGAACTGA           | 0.4 $\mu$ M         |
| IFN- $\beta$ | Forward (10 $\mu$ M) | CTGGCTTCCATCATGAACAA           | 0.4 $\mu$ M         |
|              | Reverse (10 $\mu$ M) | AGAGGGCTGTGGTGGAGAA            | 0.4 $\mu$ M         |

**Table 16. RT-qPCR program.**

| Step                 | Temperature | Time    | Number of cycles |
|----------------------|-------------|---------|------------------|
| Preincubation        | 95°C        | 600 sec | 1x               |
| 3 step amplification | 95°C        | 10 sec  | 45x              |
|                      | 55°C        | 10 sec  |                  |
|                      | 72°C        | 30 sec  |                  |
| Melting              | 95°C        | 10 sec  | 1x               |
|                      | 65°C        | 60 sec  |                  |
|                      | 97°C        | 1 sec   |                  |
| Cooling              | 37°C        | 30 sec  | 1x               |

#### 3.2.7.4.4. Analysis of RT-qPCR results

Gene expression was analyzed in LightCycler<sup>®</sup> 96 software (Roche). The genes were first analyzed based on the melting peak. If more than one melting peak was present, the measurement was excluded because this indicates non-specific amplification. The mean value of cycle threshold (Ct) of a specific gene was subtracted from the mean Ct value of housekeeping gene, glyceraldehyde-3-phosphate dehydrogenase (*Gapdh*), to obtain a difference in threshold cycles ( $\Delta$ CT). Then, mean of  $\Delta\Delta$ CT value was calculated by subtraction of mean  $\Delta$ CT for each condition from mean  $\Delta$ CT for

WT unstimulated cells. Relative gene expression was calculated from formula  $2^{-\Delta\Delta CT}$ , normalized to WT cells treated with LPS for 2 h, and shown as % of WT.

### **3.2.7.5. Flow cytometry**

#### **3.2.7.5.1. Immune cell isolation from the spleen and *in vitro* T-cell restimulation**

After cervical dislocation or perfusion with 1X PBS, the spleens were taken and smashed with a blunt end of a syringe on a 70  $\mu$ m cell strainer (pre-wet with 1 mL of FACS flow buffer). The residual tissue was washed with 4 mL of FACS flow buffer. The suspensions were centrifuged at 1500 rpm for 5 min and the supernatants were discarded. Pelleted splenocytes were resuspended in 1 mL of ACK lysis buffer (results in erythrocyte lysis) for 5 min on ice, which was then neutralized by addition of 10 mL of FACS flow buffer. The suspension was filtered, resuspended and enumerated on flow cytometer by using 123 count eBeads™ (#01-1234-42, Invitrogen) following manufacturer's instructions. For staining,  $10^6$  cells were plated in a U-bottom 96-well plate (see section 3.2.8.6.3.).

For *in vitro* restimulation, splenocytes were plated as mentioned above, centrifuged at 1500 rpm for 5 min and resuspended in T-cell restimulation medium (see section 3.1.4.3.). The plates were incubated in an incubator (5% CO<sub>2</sub> and 37°C) for 4 h and were further processed for intracellular staining (see section 3.2.8.6.3.).

#### **3.2.7.5.2. Staining for flow cytometry**

After the cells were plated in U-bottom 96-well plates, the plates were centrifuged at 1500 rpm for 5 min and the supernatants were discarded by inverting, and the remaining pellets were vortexed. To each well, 50  $\mu$ L of Fc block (anti-CD16/CD32, clone 2.4G2; #553142, BD Pharmingen; diluted 1:1000; blocks unspecific antibody binding via Fc receptor) was added and incubated for 5 min on ice. The purpose of Fc block is to bind to Fc receptors on phagocytes to ensure the binding of fluorochrome-labeled antibodies to their specific antigen, and not the Fc receptor. Next, 50  $\mu$ L of 2X concentrated antibody mix for surface staining was added and incubated for 30 min at 4°C in the dark. Simultaneously, UltraComp Beads were stained with only individual antibodies from the mix for single color compensation. Afterwards, the cells and beads were washed twice with

FACS flow buffer and centrifuged at 1500 rpm for 5 min. The cells were stained with 500 ng/mL DAPI for 5 min in the dark, washed twice and centrifuged at 1500 rpm for 5 min. The cells and the beads were resuspended with 200  $\mu$ L of FACS flow buffer, transferred (and filtered through 70  $\mu$ m filter – for cells only) to a FACS flow tube (already contained 200  $\mu$ L of FACS flow buffer) and kept on ice in the dark until flow cytometry analysis.

For intracellular staining for cytokines Perm/Wash Buffer was used according to the manufacturer's instructions. Briefly, after the cells were centrifuged upon isolation, they were washed once in 1X PBS and stained with Fixable Viability Dye eFluor450 (1:20 000 in 1X PBS) for 30 min at 4°C. The cells were washed with 1X PBS again, centrifuged and stained for extracellular markers (B220, CD90.2, CD4, and CD8) as mentioned above. This was followed by washing with FACS flow buffer, centrifugation and fixation in 4% PFA at RT for 20 min in the dark. The cells were washed twice with FACS flow buffer, permeabilized for 15 minutes at RT, Fc blocked and stained for cytokines for 30 min in the dark at 4°C. The cells were washed twice in FACS flow buffer, resuspended in 200  $\mu$ L of FACS flow buffer and filtered as mentioned above.

### **3.2.7.5.3. Phagocytosis assay**

Phagocytosis assay was performed on BMDMs (derived from three- and 24-month-old mice) and primary neonatal microglia stained with PKH26 or CellTrace Far Red, respectively, following manufacturer's instructions. The staining of these phagocytes was performed to distinguish intracellular from extracellular debris. Briefly,  $3 \times 10^6$  BMDMs were washed twice in RPMI (without supplements), stained with PKH26 (1:1000 in 1X PBS) for 3 min at RT or CellTrace Far Red (1:5000 in 1X PBS) for 20 min at 37°C. Unincorporated dye was neutralized with complete RPMI medium. Microglia were washed once in PBS, stained with CellTrace Far Red, which was followed by dye neutralization with complete DMEM, washing with complete medium again and centrifugation at  $500 \times g$  for 5 min. After staining, BMDMs and microglia were seeded in a 24-well plate at a density of 100 000 and 200 000 cells/well, respectively. Apoptotic N2A or *E. coli* bioparticles were used as phagocytic materials. N2A cells were treated with 2  $\mu$ M staurosporine (STS; an apoptosis-inducing bacterial toxin) for 24 h to generate apoptotic cell debris. N2A cell debris was collected, washed once in 1X PBS and stored at -80°C (in aliquots of  $10^6$  cells). On the day of the experiment, N2A cell debris was thawed and stained with 10  $\mu$ M CFSE for 20 min at

RT in the dark, following the manufacturer's instructions. After washing and addition of CFSE-stained N2A debris to phagocytes (in 3:1 ratio), the plate was centrifuged at  $200 \times g$  for 5 min, incubated for 5 h and processed for the flow cytometry analysis. BMDMs and microglia were treated with 500 ng/mL of LPS (24 h before addition of phagocytic material) to induce pro-inflammatory polarization. Cytochalasin D (CytoD), an inhibitor of actin-mediated phagocytosis, was used as a control to show that detected CFSE signal came from phagocytosed material and not from debris stuck on the cell surface. The experimental setup for phagocytosis of CFSE-stained N2A debris is illustrated in Figure 12.

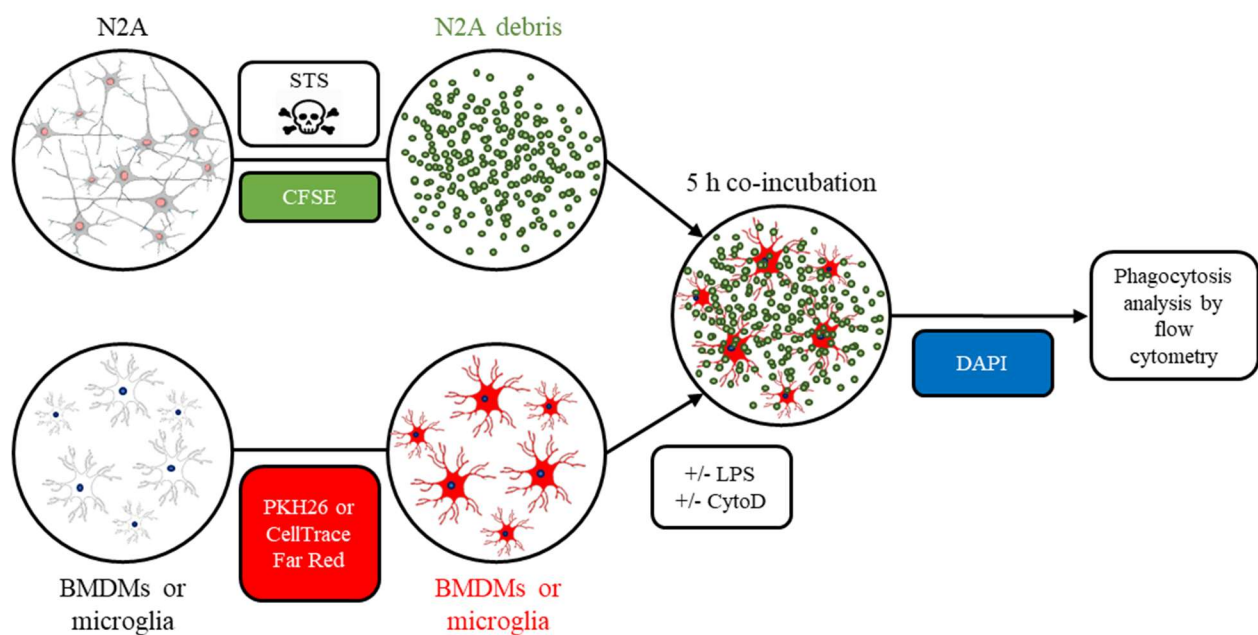


**Figure 12. Phagocytosis assay setup.** BMDMs and microglia were stained with PKH26 or CellTrace Far Red to distinguish them from CFSE-stained apoptotically killed N2A (N2A debris). For some tests, phagocytes were pretreated for 24 h with 500 ng/mL LPS (to induce pro-inflammatory polarization) or 30 min with 2 mM CytoD (to inhibit phagocytosis) before CFSE-stained N2A debris was added. After 5 h co-incubation of stained phagocytes and dN2A debris, the cells were stained for DAPI (to distinguish between live and dead cells) and analyzed by flow cytometry.

#### **3.2.7.5.4. Flow cytometry-based multiplex analysis of cytokine concentration**

##### **3.2.7.5.4.1. Protein isolation for cytokine analysis**

The whole spinal cord and ½ of the brain were homogenized in 500 µL of sterile-filtered 1X TBS (pH = 7.4) supplemented with protease and phosphatase inhibitors. Homogenization was done by using MagNALyser green beads (#3358941001, Roche) and MagNALyser instrument (#03358976001, Roche). The program was set at 6000 rpm and 30 seconds, and was repeated three times in total, with two minutes of cooling of the samples on ice between the sessions. The tubes were then centrifuged at 4°C and 13 000 rpm for 20 min. The supernatants were analyzed for protein concentration by BCA assay (see section 3.2.8.1.1.), aliquoted, and stored at -80°C.

##### **3.2.7.5.4.2. LEGENDplex procedure for cytokine analysis**

To analyze 13 different cytokines simultaneously, LEGENDplex MU Anti-Virus Response Panel (#740622, BioLegend) was used according to the manufacturer's instructions. Upon kit receipt, the standard and matrix A were reconstituted in assay buffer, aliquoted and stored at -80°C until use. The procedure was performed in V-bottom plates (#BZ-740379, BioLegend). On the day of the experiment, the standard was serially diluted in an assay buffer (when analyzing cell supernatants or tissue homogenates) or matrix A (when analyzing sera). The sample wells were first loaded with 8 µL of assay buffer, whereas the standard wells were loaded either with assay buffer or matrix A (as previously mentioned), and then 8 µL of standard and samples were added to appropriate wells. The sera were diluted in 1:2 ratio in assay buffer, whereas the brain and spinal cord lysates were loaded undiluted or were diluted 1:10 in assay buffer if the concentration exceeded the standard curve. When 8 µL of capture beads were added (total volume/well was 24 µL), the plate was incubated on a shaker at RT and 800 rpm for 2 h in the dark. The plate was then centrifuged at 500 × g for 5 min, slightly inverted and lightly pressed on paper. The wells were washed with 200 µL of 1X wash buffer, which was followed by addition of 8 µL of detection antibodies and incubation on shaker at RT and 800 rpm for 1 h in the dark. Without washing, another 8 µL of streptavidin-phycoerythrin (SA-PE) conjugate was added (total volume/well was 16 µL) and the plate was incubated on shaker at RT and 800 rpm for 30 min in the dark. The plate was centrifuged at 500 × g for 5 min, resuspended in 150 µL FACS flow buffer and transferred to FACS tube with additional 200 µL of FACS buffer. The samples were then analyzed on a flow

cytometer. Quantification of cytokine concentration was done in Qognit software according to the manufacturer's instructions.

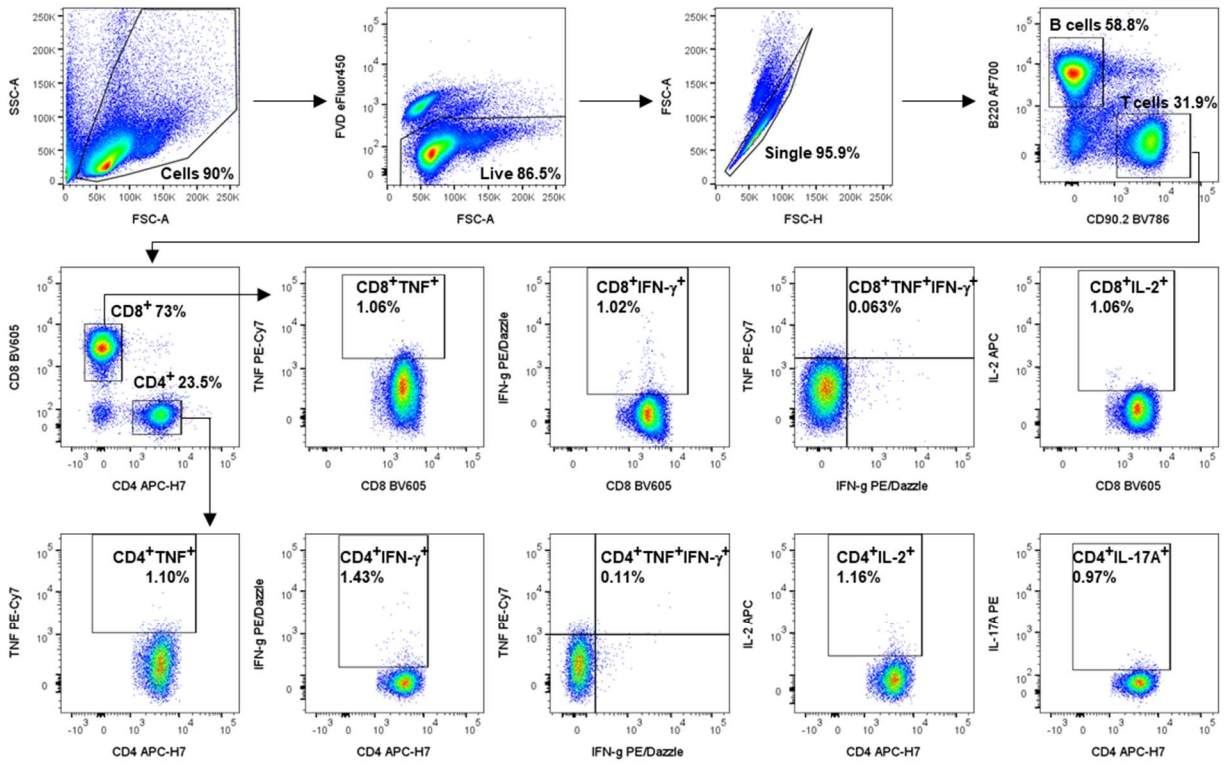
#### **3.2.7.5.5. Analysis by flow cytometry**

Flow cytometry analysis was performed on BD FACSAria III flow cytometer equipped with BD FACSDiva software (both from BD). Unstained, single-color stained cells and beads were recorded to perform compensation to prevent fluorescent spillover because fluorochrome-emitted fluorescence may be detected with more than one detector. Approximately  $3\text{-}5 \times 10^5$  (for extra- and intracellular staining) or  $2.5\text{-}5 \times 10^5$  (for phagocytosis) cells were recorded with a flow rate ranging from 8 to 10.

#### **3.2.7.5.6. Analysis of flow cytometry data**

Data acquired by flow cytometry was analyzed in FlowJo software (TreeStar) as illustrated in Figures 13-15. Briefly, cell doublets exclusion was done based on FSC-A (area) and FSC-H (height) gating. Single live cells (negative for DAPI staining) were further gated based on positivity for B220 (B cells) and CD90.2 (T cells). For restimulation studies, T<sub>H</sub> cells were classified based on the positivity for certain cytokines, such as T<sub>H1</sub> (CD4<sup>+</sup>TNF<sup>+</sup>IFN- $\gamma$ <sup>+</sup>) and T<sub>H17</sub> (CD4<sup>+</sup>IL-17A<sup>+</sup>). Cytotoxic CD8<sup>+</sup> T cells were defined based on positivity for TNF (CD8<sup>+</sup>TNF<sup>+</sup>), IFN- $\gamma$  (CD8<sup>+</sup>IFN- $\gamma$ <sup>+</sup>) or both. Proliferating/stimulated helper or cytotoxic T cells were defined based on positivity for IL-2. The cytokine content was analyzed based on the MFI for each cytokine in helper and cytotoxic T cell populations. For innate immune analysis, non-T/non-B (B220<sup>-</sup>CD90.2<sup>-</sup>) cells were further divided to classic or conventional dendritic cells (cDC; CD11c<sup>+</sup>MHC-II<sup>hi</sup>), neutrophils (Ly6C<sup>+</sup>Ly6G<sup>+</sup>), macrophages/monocytes (Ly6G<sup>-</sup>Ly6C<sup>+</sup>CD11b<sup>+</sup>), and natural killer (NK) cells (NK1.1<sup>+</sup>). Macrophage and cDC activation was assessed based on the MFI of activation markers such as CD11c, CD86 and MHC-II. For phagocytosis assay, single and live cells (negative for Fixable Viability Dye eFluor450) were distinguished as phagocytes (BMDMs or primary neonatal microglia) and were analyzed for the percentage of cells that performed phagocytosis and amount of phagocytic material (phagocytic capacity) based on CFSE MFI.

### A) Unstimulated



### B) 4 h PMA/Ionomycin

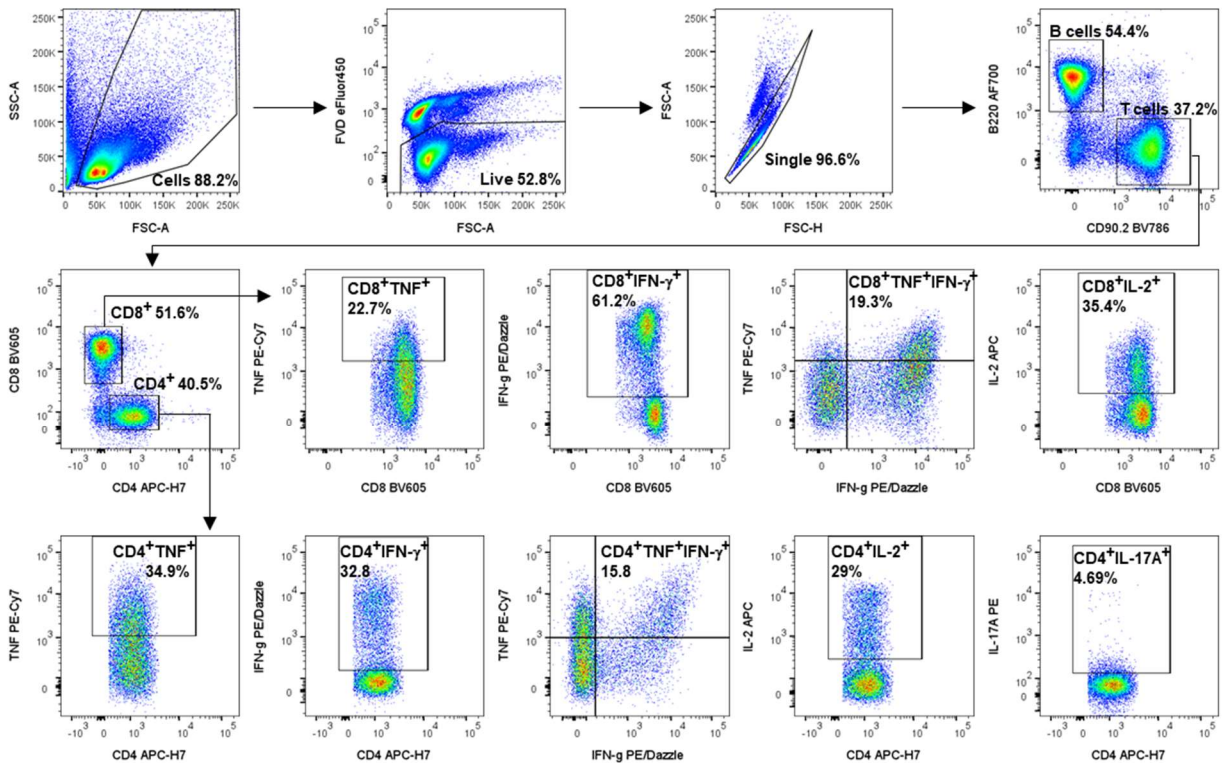


**Figure 13. Gating strategy for *in vitro* T cell restimulation.** Splenocytes were isolated from spleens of three- 12- and 24-month-old WT and Optn<sup>470T</sup> mice and were restimulated for 4 h with PMA/Ionomycin in the presence of inhibitor of degranulation (BD Golgi Stop). After the main cell population gated, live cells were gated, and cell aggregates were removed. B and T cells were distinguished based on B220 and CD90.2 (THY1.2) positivity, respectively. T cells were further divided into CD4 and CD8 populations. CD4<sup>+</sup> cells were analyzed for positivity for TNF, IFN- $\gamma$ , IL-2 and IL-17A. CD8<sup>+</sup> cells were analyzed in the same manner, but without IL-17A. The amount of cytokine per cell was quantified based on the MFI for each cytokine. Representative gating is shown for restimulation of splenocytes isolated from 24-month-old WT male mouse without (A) and with (B) restimulation.

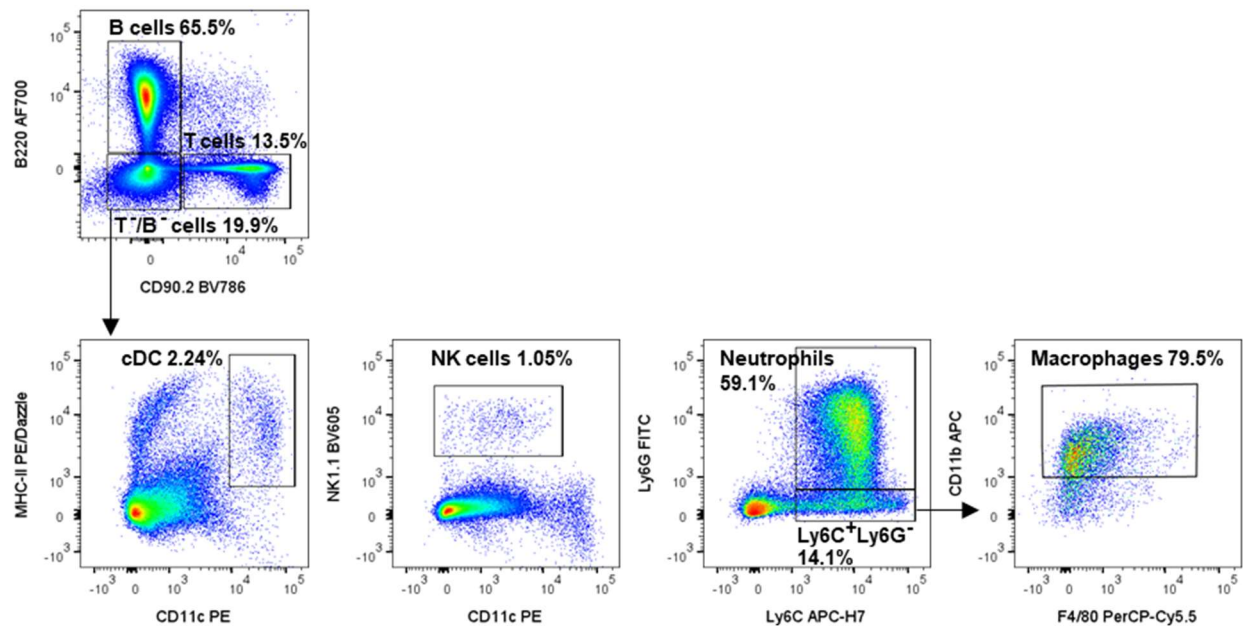


**Figure 14. Gating strategy for analysis of spleens upon consecutive LPS stimulation.** Splenocytes were isolated from spleens of 18-month-old WT, Optn<sup>470T</sup>, TDP-43<sup>G348C</sup> and Optn<sup>470T</sup>/TDP-43<sup>G348C</sup> mice 24 h after the last LPS dose (stimulation with 1.5 mg/kg LPS for three consecutive days). After the main cell population gated, live cells were gated, and cell aggregates were removed. B and T cells were distinguished based on B220 and CD90.2 (THY1.2) positivity, respectively. Non-T/non-B cells (CD90.2<sup>-</sup>B220<sup>-</sup>) were further classified as classic or conventional dendritic cells (cDC; CD11c<sup>+</sup>MHC-II<sup>+</sup>), natural-killer cells (NK; NK1.1<sup>+</sup>), neutrophils



(Ly6C<sup>+</sup>Ly6G<sup>+</sup>) and macrophages (Ly6C<sup>+</sup>Ly6G<sup>-</sup>CD11b<sup>+</sup>). Activation of cDC and macrophages was assessed based on MFI for CD11c, CD86 and MHC-II. Representative gating is shown for splenocytes isolated from LPS-stimulated 18-month-old WT mouse.

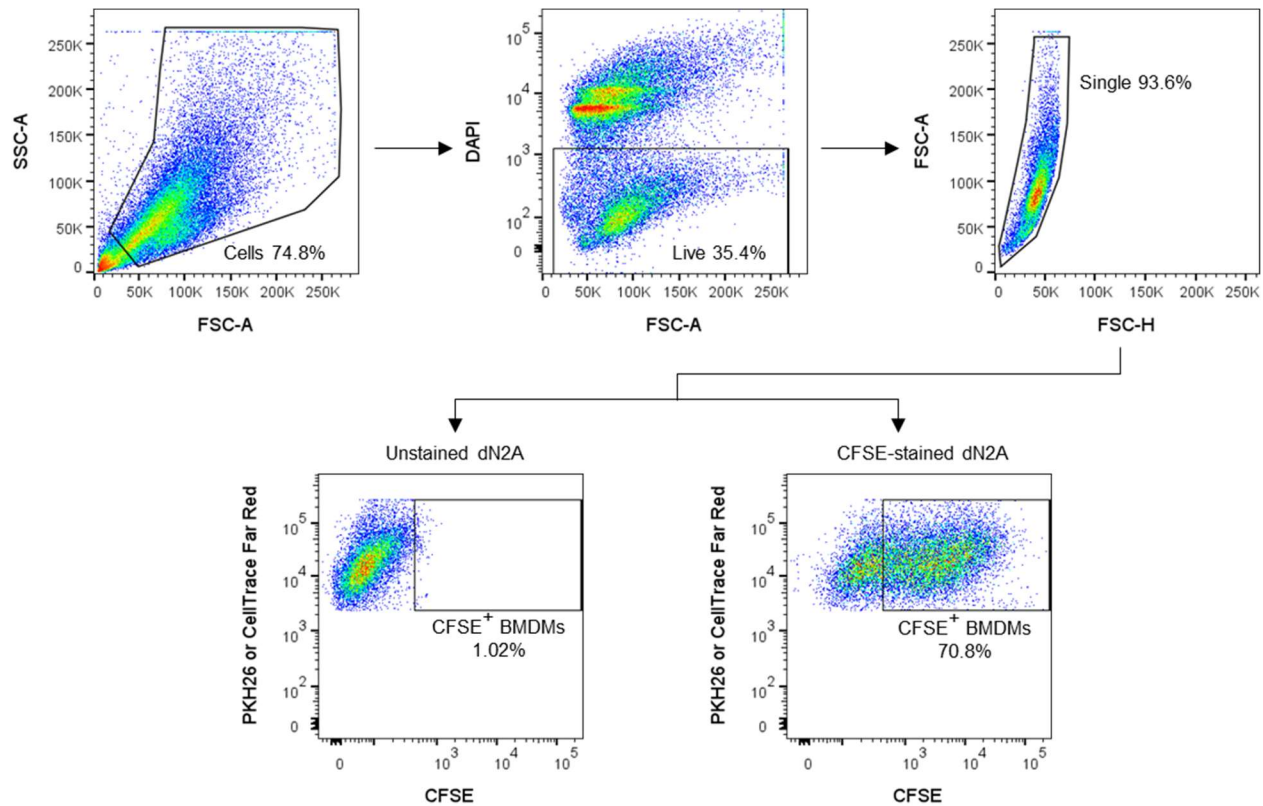


**Figure 15. Gating strategy for phagocytosis assay.** The main cell population was gated based on forward (FSC) and side (SSC) scatter; cells negative for DAPI were gated as live cells; cell aggregates were excluded based on FSC-A and FSC-H gating; BMDMs or primary neonatal microglia were detected as cells positive for PKH26 or CellTrace Far Red; the percentage of phagocytosed CFSE-stained N2A debris (dN2A) as well as the phagocytic capacity were quantified.

### **3.2.8. Statistical analysis**

Statistical analysis was performed in GraphPad Prism Software 8.0.1. The data was first tested for normality by Shapiro-Wilk normality test. For comparisons between two individual groups, unpaired Student's *t*-test (for normal distribution) or Mann-Whitney test (for non-normal distribution) was used. For comparisons between multiple groups, one- or two-way ANOVA with Tukey's post-hoc test (for normal distribution), or Kruskal-Wallis test with Dunn's multiple comparisons test (for non-normal distribution) was used. A p-value of  $< 0.05$  was considered as statistically significant.

## 4. Results

### 4.1. Analysis of the role of optineurin during aging in the central nervous system

#### 4.1.1. Optn<sup>470T</sup> mice showed similar motor coordination, cognitive functions, and lipofuscin accumulation as WT mice during aging

Aging is considered a major risk factor for all neurodegenerative diseases, therefore Optn<sup>470T</sup> mice were aged up to 18 and 24 months and their neurological functions were compared to WT mice. We have previously tested motor coordination by rotarod and found no differences between the genotypes (Mohović, 2023), so potentially more delicate defects in motor coordination were analyzed by wire-hanging test. No aging-induced decline was found between 12- and 24-month-old males in any of the genotypes (Fig. 16 A). In contrast, females showed a strong aging-induced decline in motor coordination, which was similar between the genotypes (Fig. 16 B). Since optineurin mutations were also found in FTD (Pottier et al., 2018), we have assessed cognitive function by the novel object recognition test. In 18-month-old WT and Optn<sup>470T</sup> males and females a higher preference for the novel object over the familiar one was observed (Fig. 16 C and D), which was more pronounced in males. This demonstrated preserved cognitive functions in Optn<sup>470T</sup> mice. At 24 months the preference for the novel object was lost in both sexes without a major difference between the genotypes, which indicated a similar aging-mediated memory loss (Fig. 16 C and D). In conclusion, aging did not enhance the impairment of motor and cognitive functions of Optn<sup>470T</sup> mice.

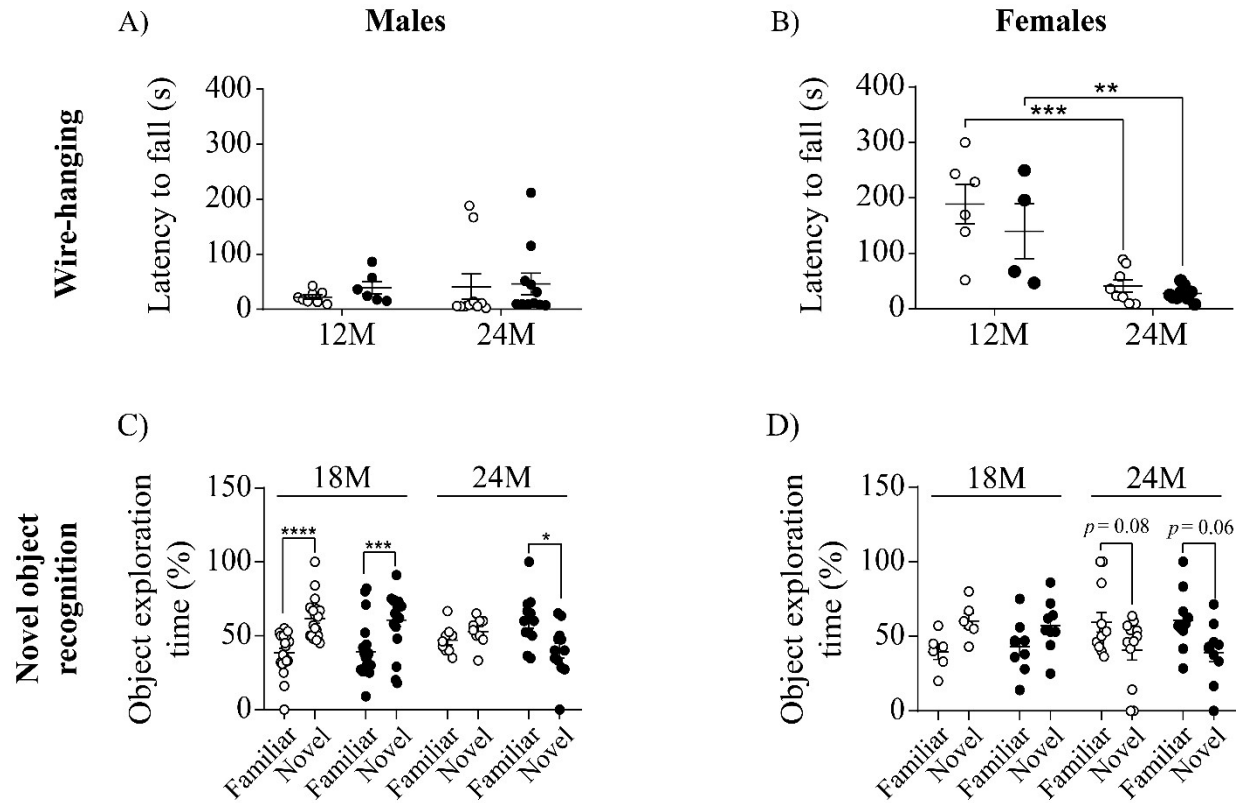
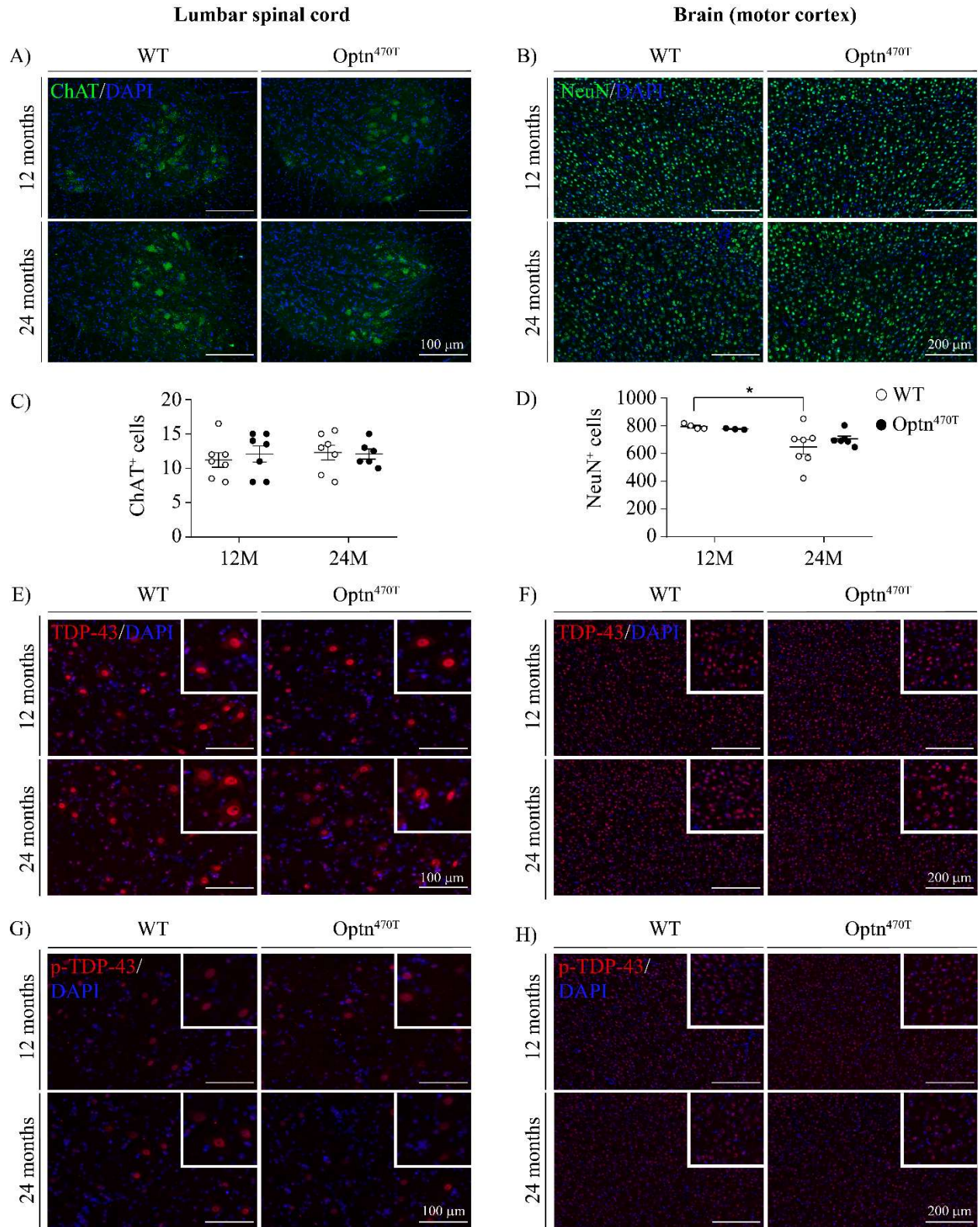


**Figure 16. Aging did not accelerate motor and cognitive decline in *Optn*<sup>470T</sup> mice.** Motor coordination was tested by wire-hanging test and an average of three measurements is shown for 12-month-old (8 WT, 6 *Optn*<sup>470T</sup>) and 24-month-old (10 WT, 11 *Optn*<sup>470T</sup>) males (A), and 12-month-old (6 WT, 4 *Optn*<sup>470T</sup>) and 24-month-old (8 WT, 10 *Optn*<sup>470T</sup>) females (B). Cognitive function was tested by novel object recognition test and is shown as percentages of interaction with familiar and novel object for 18- (20 WT, 19 *Optn*<sup>470T</sup>) and 24-month-old (9 WT, 12 *Optn*<sup>470T</sup>) males (C) and females (6 WT, 9 *Optn*<sup>470T</sup> and 12 WT, 10 *Optn*<sup>470T</sup>) (D). The data is shown as average  $\pm$  SEM and was analyzed by Kruskal-Wallis test (A) and two-way ANOVA (B-D); \*\*  $p < 0.01$ , \*\*\*  $p < 0.001$ , \*\*\*\*  $p < 0.0001$ .

#### 4.1.2. *Optn*<sup>470T</sup> mice did not develop ALS-like neuropathology during aging

ALS symptoms occur after  $\geq 50\%$  of motor neurons in the spinal cord are lost (Hardiman et al., 2017). So, even though *Optn*<sup>470T</sup> mice did not develop pronounced motor deficits, we analyzed the signs of ALS-like neuropathology (neuronal loss and TDP-43 aggregation) to check if they are already present but yet insufficient to lead to the development of ALS symptoms. Therefore, we

analyzed the lumbar spinal cord and the motor cortex of 12- and 24-month-old mice for (motor) neuron loss. During aging, WT and Optn<sup>470T</sup> mice have shown a preserved number of ChAT-positive motor neurons in the lumbar spinal cord (Fig. 17 A, C). In contrast, in the motor cortex we found a 10% neuronal loss in Optn<sup>470T</sup> mice during aging that did not reach the statistical significance, whereas the 20% loss in WT mice reached statistical significance (Fig. 17 B, D). Notably though, no statistical difference was found between the genotypes at 24 months, suggesting that optineurin insufficiency did not affect neuronal numbers in the motor cortex. Interestingly, Kurashige *et al.* reported TDP-43 cytoplasmic aggregation in 24-month-old Optn<sup>-/-</sup> mice, without development of motor deficits (Kurashige et al., 2021). Therefore, we analyzed the presence of TDP-43 pathology with the use of two antibodies: anti-C-terminal TDP-43 and anti-phospho-TDP-43<sup>Ser409</sup>; the latter was used since TDP-43 aggregates were reported to be hyperphosphorylated (Neumann et al., 2006). The lumbar spinal cord (Fig. 17 E) and motor cortex (Fig. 17 F) sections of 12- and 24-month-old WT and Optn<sup>470T</sup> mice revealed that most of TDP-43 was in the nucleus with a substantially lesser amount in the cytoplasm, without the presence of cytoplasmic aggregates. To corroborate the absence of TDP-43 cytoplasmic aggregates, we performed the staining with an antibody against phospho-TDP-43<sup>Ser409</sup> (Fig 17 G, H). We observed similar results since the localization of phospho-TDP-43<sup>Ser409</sup> was mostly nuclear, without cytoplasmic aggregates in the lumbar spinal cord (Fig. 17 G) and motor cortex (Fig. 17 H) of WT and Optn<sup>470T</sup> mice. Lipofuscin, an undegraded lipid-containing cargo, accumulates during aging (Nakanishi & Wu, 2009) and can be measured as autofluorescence in the red channel (Eichhoff et al., 2008). Indeed, we observed a significant lipofuscin accumulation during aging in the lumbar spinal cord (Fig. 17 I, K) and motor cortex (Fig. 17 J, L), which was unaffected by optineurin insufficiency. In conclusion, we have shown that optineurin insufficiency did not lead to intensified neuronal loss, the development of TDP-43 pathology or altered aging-mediated lipofuscin accumulation in the motor cortex and lumbar spinal cord.





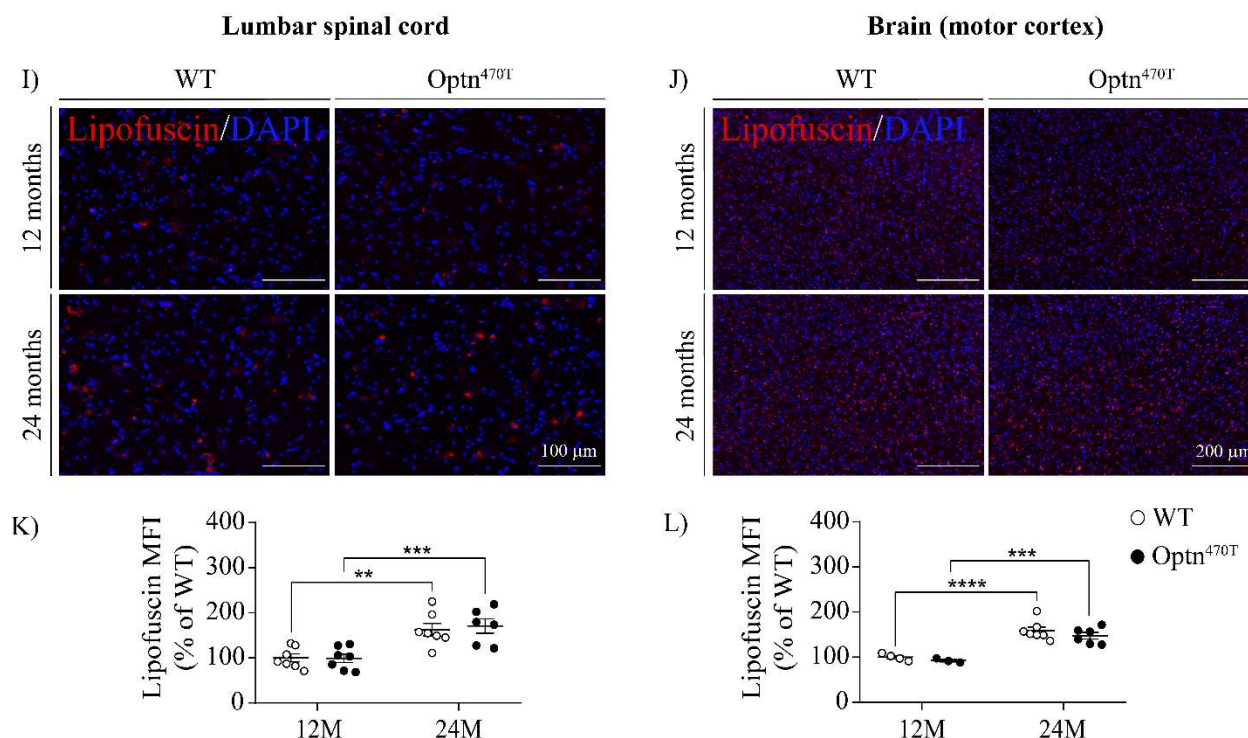


**Figure 17. Aging did not trigger ALS-like neuropathology in Optn<sup>470T</sup> mice.** Ventral horn of the lumbar spinal cord (left column) and motor cortex (right column) sections of 12- and 24-month-old male mice were stained for ChAT (A; motor neuron marker in the spinal cord; quantification shown in C), NeuN (B; neuronal marker, used for staining of the motor cortex, quantification shown in D), C-terminal TDP-43 (E, F) and phospho-TDP-43<sup>Ser409</sup> (G, H). Lipofuscin accumulation was measured by autofluorescence in the red channel of the ventral horn of the lumbar spinal cord (6-7 WT and Optn<sup>470T</sup> 12- and 24-month-old males) (I, K), and motor cortex (3-7 WT and Optn<sup>470T</sup> 12- and 24-month-old males) (J, L). MFI was normalized and shown as % of 12-month-old WT. The data is shown as average of 6-7 (left column) or 3-7 (right column) mice  $\pm$  SEM and was analyzed by two-way ANOVA (C, D, K, L); \*  $p < 0.05$ .

#### 4.1.3. Aging increased wild-type optineurin levels in the spinal cord, but its insufficiency did not exacerbate aging-induced microgliosis

Neuroinflammation, characterized as astrogliosis (increase in astrocyte activation) and microgliosis (increase in microglial activation), was found to be a prominent sign of aging (Sikora et al., 2021) and a hallmark of neurodegenerative diseases, including ALS (Wilson et al., 2023).

We analyzed the ventral horns of the lumbar spinal cord tissue sections of 12- and 24-month-old WT and Optn<sup>470T</sup> male mice for astrogliosis and microgliosis by staining for GFAP (Fig. 18 A, B) and Iba1, respectively (Fig. 18 C-F). We observed a slight but non-significant increase in GFAP MFI in Optn<sup>470T</sup> mice during aging (Fig. 18 B), similar to WT mice. The Iba1 MFI did not change during aging and was similar in both genotypes (Fig. 18 D). However, we observed a similar aging-mediated decrease in the longest process length (Fig. 18 E) and an increase in cell body area (Fig. 18 F) in Optn<sup>470T</sup> and WT mice, indicating the presence of microgliosis in both genotypes. Since the changes in neuroinflammation markers were not very prominent between 12- and 24-month-old mice, we also used young-adult (3-4-month-old) mice for comparison by western blot. Specifically, we compared the whole spinal cord lysates between 3-4- and 18-20-month-old mice (Fig. 18 G). We analyzed the expression of optineurin by using an N-terminal optineurin antibody to measure the levels of WT and truncated form during aging and observed a ~40% increase in the expression of WT but not the truncated form of optineurin during aging (Fig. 18 G, H). GFAP levels dropped during aging (Fig. 18 G, I), whereas Iba1 levels significantly increased (Fig. 18 G, J), without a difference between the genotypes. We measured the TNF concentration in the spinal cord homogenates by ELISA and showed no differences between WT and Optn<sup>470T</sup> mice (Fig. 18 K). To conclude, in both genotypes aging between 12 to 24 months revealed a trend of an increased GFAP expression in the lumbar spinal cord when analyzed by immunofluorescence, however, in western blot analysis of the whole spinal cord homogenates we found a decrease in GFAP expression between 3-4- and 18-20-month-old mice. These conflicting results need to be further clarified by immunofluorescence analysis of the lumbar spinal cords of mice of the same age groups. Regarding microgliosis, we observed aging-induced microglial activation by immunofluorescence and western blot analyses in both genotypes. Additionally, we were the first to show that optineurin levels substantially increased during aging, without that effect on the expression of the truncated form. Lastly, WT and Optn<sup>470T</sup> mice showed similar TNF levels in the spinal cords.



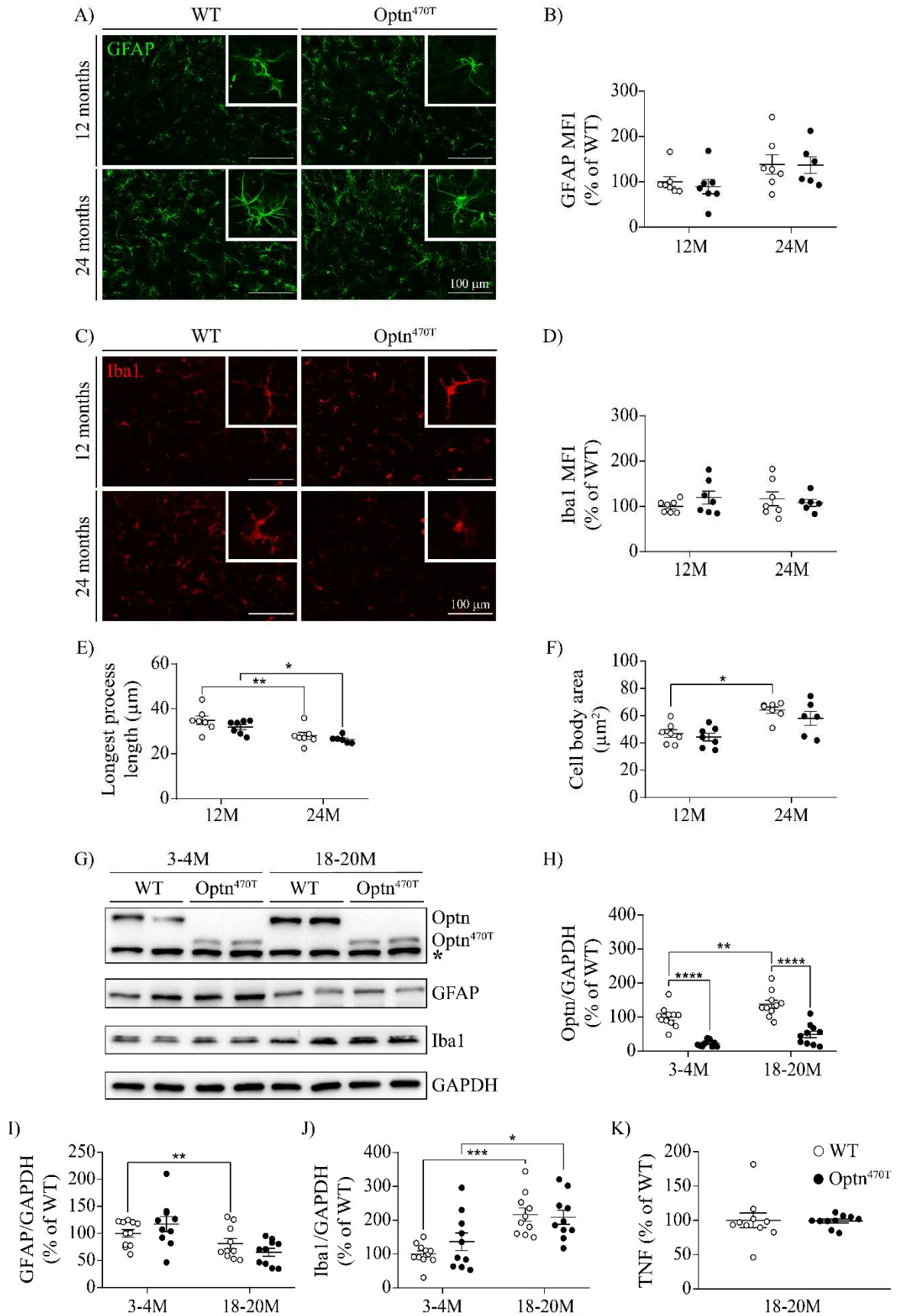


**Figure 18. Optineurin levels increased during aging in the spinal cord, but its insufficiency did not increase microgliosis.** The ventral horns of the lumbar spinal cord sections of 12- and 24-month-old WT and Optn<sup>470T</sup> males were stained for GFAP (A) and Iba1 (C). MFI of GFAP and Iba1 (B and D; shown as % of 12-month-old WT mice), microglial longest process length (E) and cell body area (F) are shown. Western blot analysis (G) of optineurin (H; marked as Optn), GFAP (I) and Iba1 (J) expression in the whole spinal cord homogenates; results were normalized to GAPDH as the loading control and shown as % of 3-4-month-old WT mice; two representative mice of each genotype are shown. The non-specific band in (G) is marked with \*. TNF ELISA (K) of the whole spinal cord homogenates (shown as % of 18-20-month-old WT mice). The data is shown as average  $\pm$  SEM of 6-7 (A-F) and 10-11 male mice (G-K) and was analyzed by Kruskal-Wallis test (B, D), two-way ANOVA (E, F, H-J) and Mann-Whitney test (K); \*  $p < 0.05$ , \*\*  $p < 0.01$ , \*\*\*  $p < 0.001$ , \*\*\*\*  $p < 0.0001$ .

#### **4.1.4. Optineurin insufficiency led to increased microgliosis in the whole brain lysates of aged mice, but did not affect TNF and IFN- $\beta$ levels**

To check the signs of neuroinflammation in the brain, we performed similar analyses as in the spinal cord (see section 4.1.3.). Briefly, motor cortex sections of WT and Optn<sup>470T</sup> 12- and 24-month-old male mice were stained for Iba1 (Fig. 19 A). We observed no change in Iba1 MFI (Fig. 19 B) and longest process length (Fig. 19 C) between 12- and 24-month-old mice, with a tendency of an increase in the cell body area (Fig. 19 D) in both genotypes. To compare 3-4- and 18-20-month-old mice, we performed western blot analysis of the whole brain homogenate (Fig. 19 E). We observed a strong aging-induced increase (~50%) in WT optineurin levels, but not in the truncated form (Fig. 19 E, F). GFAP levels did not change during aging and were unaffected by the genotype (Fig. 19 E, G). Iba1 levels increased during aging in both genotypes, but this was more prominent in Optn<sup>470T</sup> brains compared to the WT (Fig. 19 E, G). However, the concentrations of TNF (Fig. 19 I) and IFN- $\beta$  (Fig. 19 J) in the brain homogenates were similar in both genotypes. In conclusion, we showed that optineurin levels increased during aging in the brain, similar to our observation in the spinal cord. In contrast to the spinal cord, optineurin insufficiency in the whole brain led to a stronger aging-induced Iba1 increase, although this

difference was not present in the motor cortex. Finally, the concentrations of TNF and IFN- $\beta$  in the brains were unaffected by optineurin insufficiency.

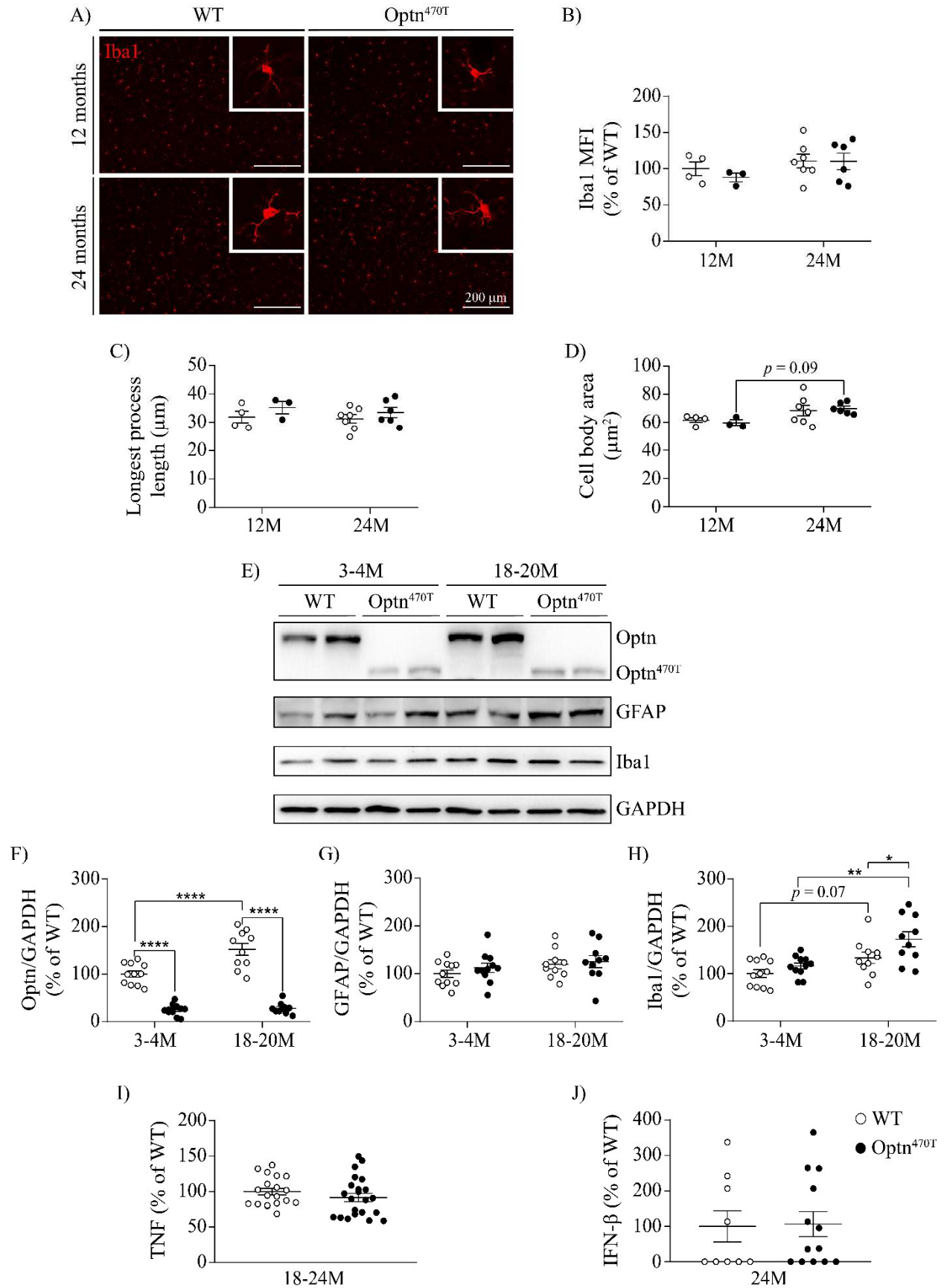


**Figure 19. Optineurin insufficiency led to an increase of aging-induced Iba1 expression in the brain homogenates, but similar cytokine profiles.** The motor cortex sections of 12- and 24-month-old WT and Optn<sup>470T</sup> males were stained for Iba1 (A). MFI of Iba1 (B; shown as % of 12-month-old WT mice), microglial longest process length (C) and cell body area (D) are shown. Western blot analysis (E) of optineurin (F; marked as Optn), GFAP (G) and Iba1 (H) expression in the whole brain homogenates; results were normalized to GAPDH as the loading control and shown as % of 3-4-month-old WT mice; two representative mice of each genotype are shown. TNF (I) and IFN- $\beta$  (J) ELISA of the whole brain homogenates (shown as % of 18-24 or 24-month-old WT mice). The data is shown as average  $\pm$  SEM of 3-7 (A-D), 10-11 (E-H), 19-23 (I) and 8-13 (J) male mice and was analyzed by two-way ANOVA (B-D, F-H), unpaired Student's *t*-test (I) and Mann-Whitney test (J); \*  $p < 0.05$ , \*\*  $p < 0.01$ , \*\*\*\*  $p < 0.0001$ .

## **4.2. Analysis of the role of optineurin in phagocytosis**

### **4.2.1. Basal and inflammatory phagocytosis in BMDMs during aging and in primary neonatal microglia were unaffected by optineurin insufficiency**

It was reported that phagocytosis was decreased in both microglia-like cells derived from ALS patients (Quek et al., 2022) and the primary microglia derived from the spinal cord of the SOD1<sup>G93A</sup> ALS mouse model (Barreto-Núñez et al., 2024), thus we assessed phagocytosis in BMDMs and primary neonatal microglia derived from Optn<sup>470T</sup> mice. We first analyzed phagocytosis in BMDMs derived from three- (young-adult) and 24-month-old (aged) mice in the basal state under pro-inflammatory polarization with LPS (Fig. 20 A, B). The percentage of phagocytic BMDMs was ~60% and did not differ between the genotypes. In contrast, aging led to an almost 50% decrease in phagocytosis (Fig. 20 A). The amount of phagocytosed material per cell was measured based on the CFSE MFI (Fig. 20 B). CytoD, a phagocytosis inhibitor, was used to test if the fluorescent signal came from the phagocytosed material rather than from the material attached to the cell surface. It reduced CFSE MFI by approximately 50%, showing a partial inhibition of phagocytosis (Fig. 20 B). In basal conditions, the amount of phagocytosed material remained the same between the genotypes. We also tested phagocytosis upon pro-inflammatory polarization with LPS to check if inflammation will affect the phagocytosis of Optn<sup>470T</sup> BMDMs. The amount of phagocytic material increased upon pro-inflammatory polarization, especially in

BMDMs derived from aged mice (Fig. 20 B). To assess BMDM function during aging in more detail, we analyzed the secretion of TNF (Fig. 20 C) and IL-10 (Fig. 20 D) under basal and LPS-stimulated conditions in the presence of phagocytic material. The secretion of TNF (a pro-inflammatory cytokine) was almost undetectable in the basal state phagocytosis, whereas its levels increased in LPS-stimulated conditions. In contrast, TNF secretion from BMDMs derived from aged mice was significantly decreased. IL-10 secretion was detectable in basal conditions (~130 pg/mL) and increased by ~20-fold in BMDMs derived from young-adults and to a substantially lesser extent in those from aged mice (Fig. 20 D). Therefore, we have shown that the percentage of phagocytic BMDMs and cytokine secretion were reduced in BMDMs derived from aged mice, but without an effect of optineurin insufficiency.

We next analyzed phagocytosis in primary neonatal microglia, since microglia are more relevant for neurodegeneration. In the basal and LPS-stimulated state, we observed a high percentage (~90%) of phagocytic microglia, which was similar between the genotypes (Fig. 20 E). The amount of phagocytosed material was comparable between the genotypes in the basal and LPS-stimulated conditions, whereas LPS stimulation led to a ~70% increase in the CFSE signal (Fig. 20 F). The function of microglia was further analyzed for TNF (Fig. 20 G) and IL-10 (Fig. 20 H) in the presence of phagocytic material. Both TNF and IL-10 were almost undetectable in the basal state, whereas LPS stimulation led to a prominent secretion of both cytokines, which was similar between the genotypes. In conclusion, phagocytosis of primary neonatal microglia derived from *Optn*<sup>470T</sup> mice was similar to microglia derived from WT mice.

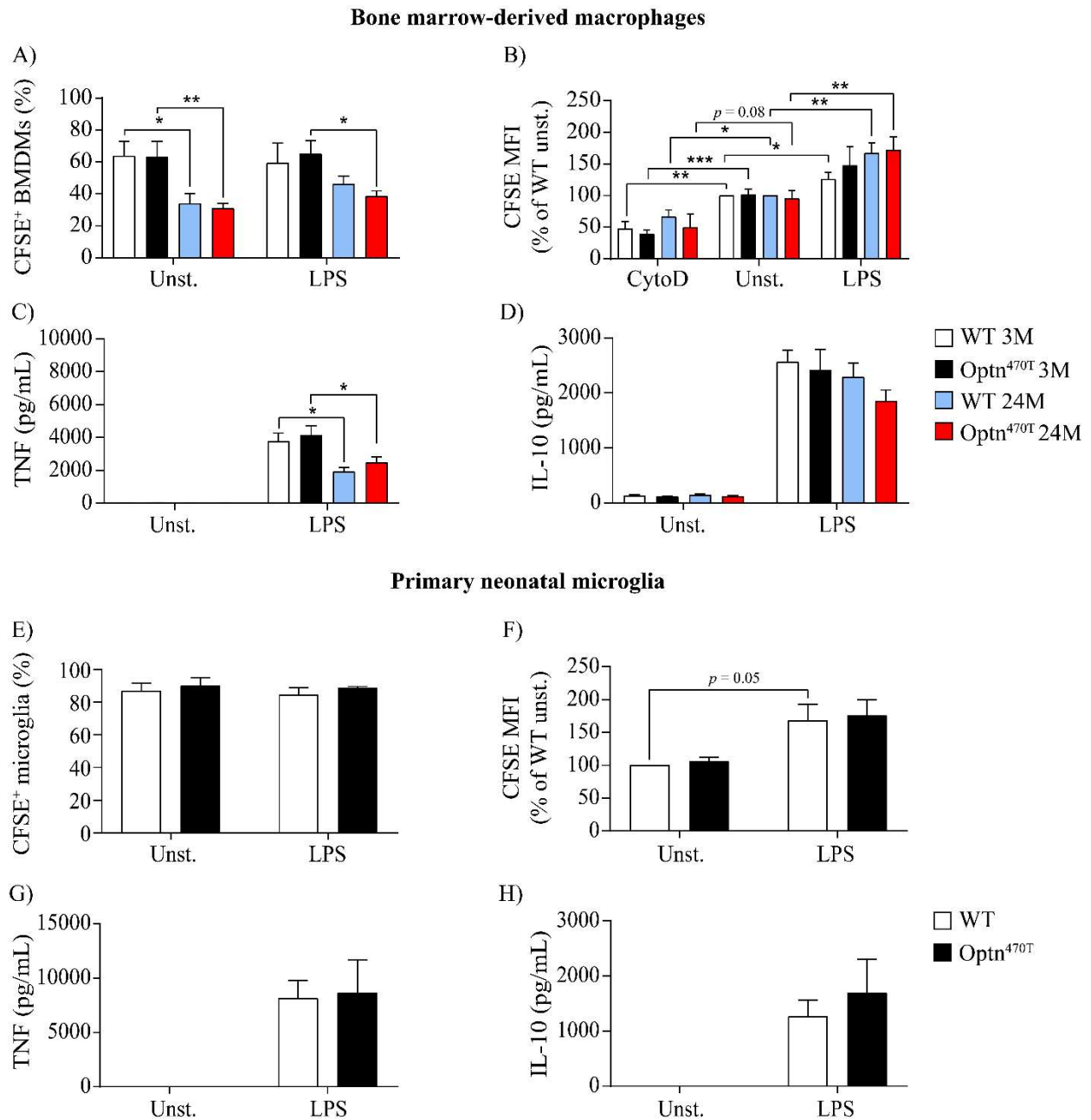


**Figure 20. Optineurin insufficiency did not affect basal and inflammatory phagocytosis neither in BMDMs during aging nor in primary neonatal microglia.** BMDMs derived from three- or 24-month-old mice and primary neonatal microglia were left unstimulated (Unst.) or were pretreated for 24 h with 500 ng/mL of LPS before the addition of the CFSE-stained N2A debris. Some samples were pretreated for 30 min with 2  $\mu$ M of CytoD to block phagocytosis, as indicated. The percentage of phagocytic BMDMs (positive for CFSE-stained N2A debris) is shown in (A). The quantity of phagocytosed material (B) is shown as CFSE MFI (normalized to WT untreated

cells and shown as % of WT). TNF (C) and IL-10 (D) ELISA for unstimulated and LPS-stimulated BMDMs are shown. Primary neonatal microglia were left untreated or stimulated with LPS and incubated with CFSE-stained N2A debris, as indicated for BMDMs. The percentage of phagocytic microglia (E), the quantity of phagocytosed material (F), and ELISA for TNF (G) and IL-10 (H) are shown. The data is shown as average  $\pm$  SEM of 3-6 (A-D; BMDMs) and 2-4 (E-H; primary neonatal microglia) independent experiments and was analyzed by unpaired Student's t-test; \*  $p < 0.05$ , \*\*  $p < 0.01$ , \*\*\*  $p < 0.001$ .

### **4.3. Analysis of the role of optineurin on splenic T cell function during aging**

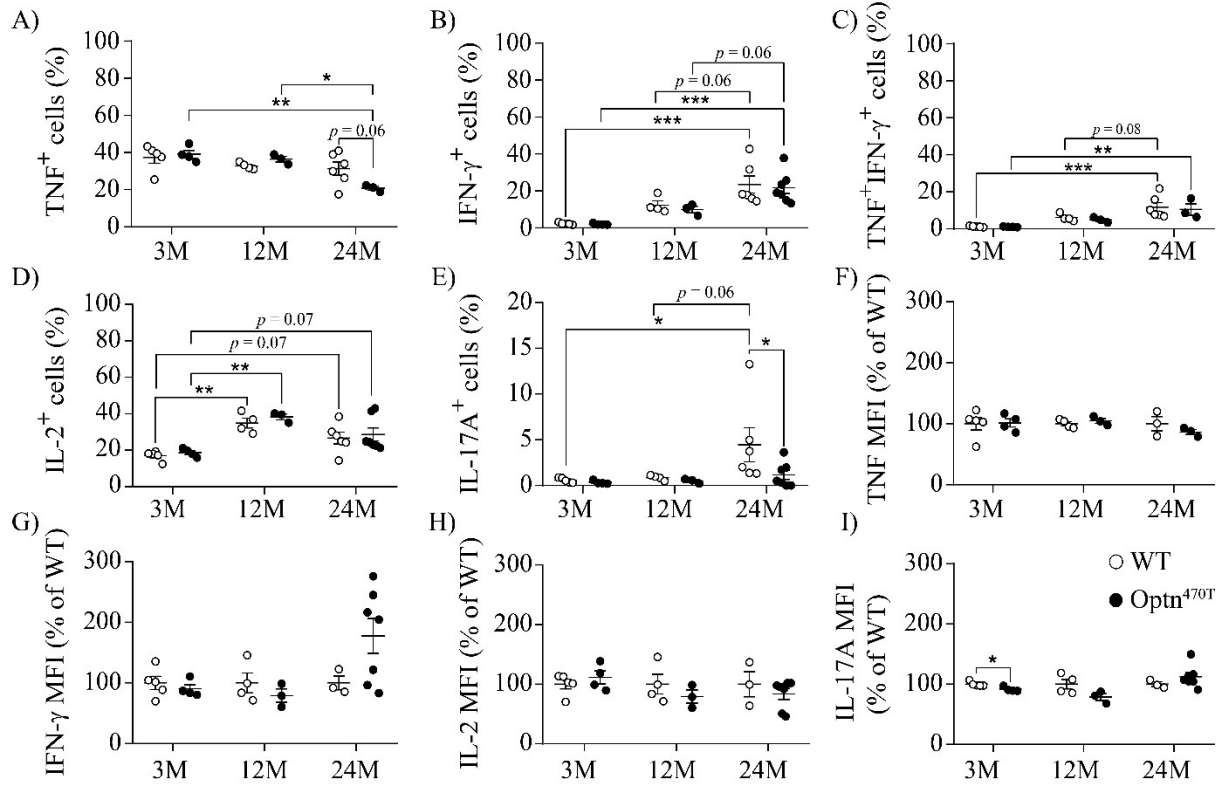
#### **4.3.1. Similar $T_H1$ , but decreased $T_H17$ $CD4^+$ T cell polarization during aging was observed in male but not female $Optn^{470T}$ compared to WT mice**

Even though the ALS/FTD disease spectrum affects the central nervous system, impairments in various subsets of peripheral immune cells, including T cells, are commonly present (Béland et al., 2020). Also, it was shown that optineurin plays a role in immune signaling (Markovinovic et al., 2017), so it might affect T-cell polarization. We first analyzed helper T cell ( $T_H$ ,  $CD4^+$ ) subpopulations in young-adult (three-month-old), middle-aged (12-month-old), and aged (24-month-old) males after a short-term *in vitro* stimulation with PMA/Ionomycin. We observed a decrease in  $CD4^+TNF^+$  cells in aged  $Optn^{470T}$  mice compared to aged WT mice, and young-adult and middle-aged  $Optn^{470T}$  mice (Fig. 21 A).  $CD4^+IFN-\gamma^+$  cell percentage increased significantly in aged mice of both genotypes compared to young adults, and almost significantly compared to middle-aged mice (Fig. 21 B), and we showed the similar for the  $CD4^+TNF^+IFN-\gamma^+$  ( $T_H1$ ) cell population (Fig. 21 C).  $CD4^+IL-2^+$  T cell percentage peaked in middle-aged and was reduced in aged mice, but was still higher when compared to young adults, without a difference between genotypes (Fig. 21 D). The  $CD4^+IL-17A^+$  ( $T_H17$ ) cell population significantly increased in aged WT mice compared to WT young adults and was significantly higher compared to aged  $Optn^{470T}$  mice (Fig. 21 E), suggesting that optineurin enhances  $T_H17$  polarization. The amount of each cytokine per cell was calculated based on the MFI value for each cytokine. We found almost no differences between the genotypes at any age point in the level of production of TNF (Fig. 21 F), IFN- $\gamma$  (Fig. 21 G), IL-2 (Fig. 21 H), and IL-17A (Fig. 21 I). The exceptions were in IFN- $\gamma$  with a tendency of higher production in aged  $Optn^{470T}$  mice compared to WT mice (Fig. 21 G) and IL-



17A where we observed 9% lower production in young-adult Optn<sup>470T</sup> compared to WT mice (Fig. 21 I). In females, CD4<sup>+</sup>TNF<sup>+</sup> percentage did not change during aging (Fig. 21 J), whereas CD4<sup>+</sup>IFN- $\gamma$ <sup>+</sup> and CD4<sup>+</sup>TNF<sup>+</sup>IFN- $\gamma$ <sup>+</sup> percentages significantly increased during aging (Fig. 21 K, L), without differences between the genotypes. CD4<sup>+</sup>IL-2<sup>+</sup> (Fig. 10 M) and CD4<sup>+</sup>IL-17A<sup>+</sup> (Fig. 10 N) cell percentage did not change during aging and between the genotypes. The production of TNF (Fig. 21 O), IFN- $\gamma$  (Fig. 21 P), IL-2 (Fig. 21 R) and IL-17A (Fig. 21 S) was comparable between WT and Optn<sup>470T</sup> mice. To conclude, a strong increase in the percentage of CD4<sup>+</sup>IFN- $\gamma$ <sup>+</sup> and CD4<sup>+</sup>TNF<sup>+</sup>IFN- $\gamma$ <sup>+</sup> cells was observed in both genders and genotypes during aging. Additionally, an increase in CD4<sup>+</sup>IL-2<sup>+</sup> and CD4<sup>+</sup>IL-17A<sup>+</sup> was more prominent in males compared to females. Finally, we also found a decreased percentage of CD4<sup>+</sup>IL-17A<sup>+</sup> cells in aged Optn<sup>470T</sup> compared to WT males.

### Analysis of CD4<sup>+</sup> T cells in male mice



### Analysis of CD4<sup>+</sup> T cells in female mice

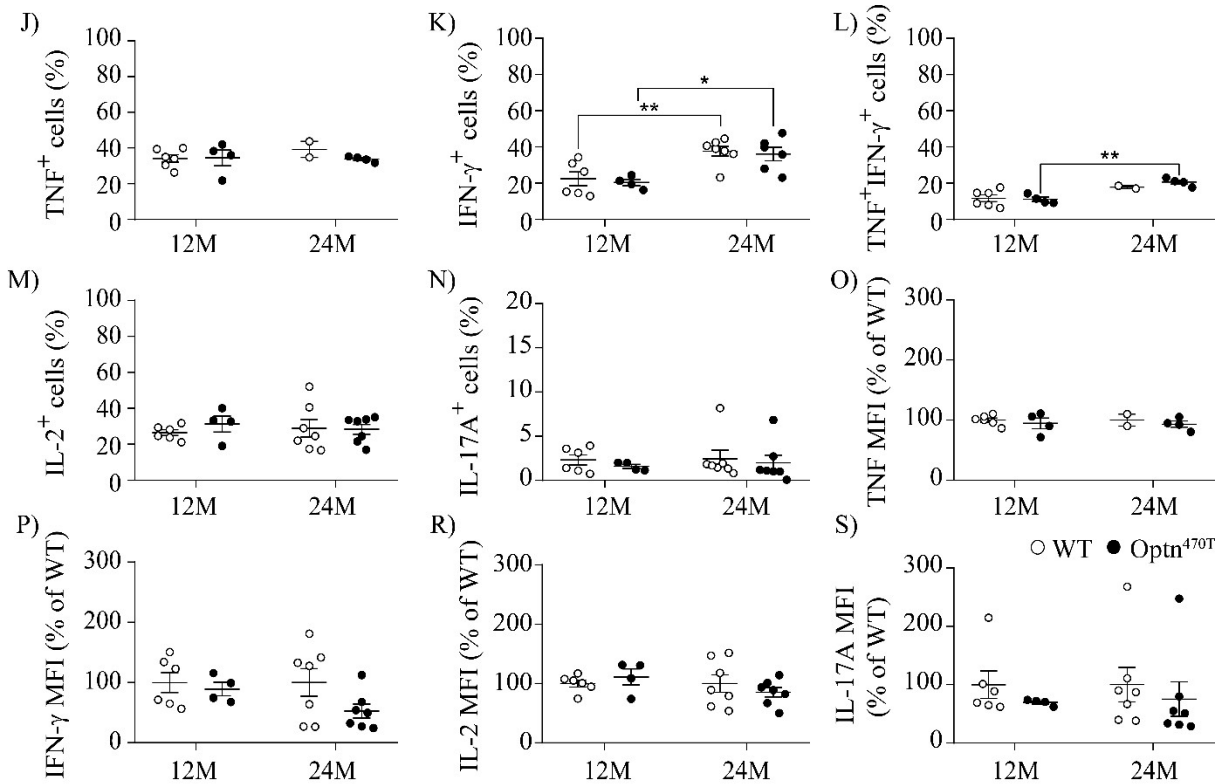
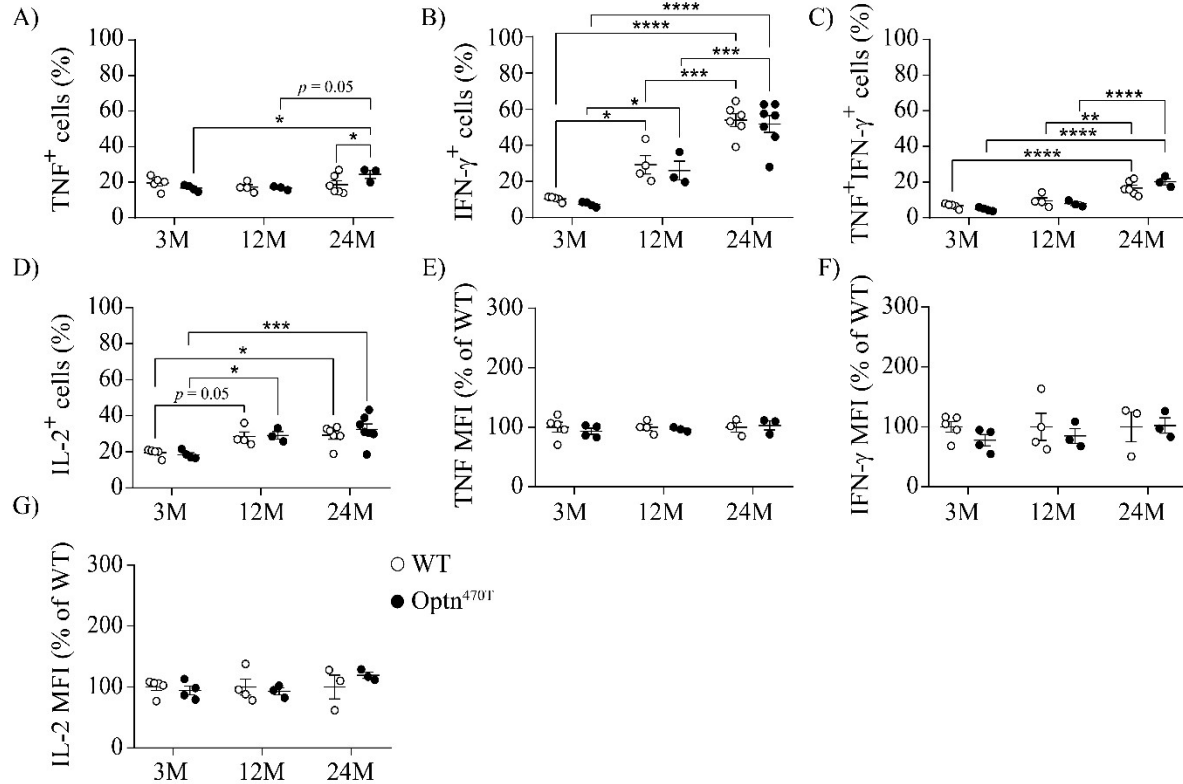


**Figure 21. Male  $\text{Optn}^{470\text{T}}$ , but not female mice, had similar  $\text{T}_{\text{H}1}$  but decreased  $\text{T}_{\text{H}17}$   $\text{CD4}^+$  T cell polarization during aging compared to WT mice.** Analysis of  $\text{CD4}^+$  T cells for the positivity for TNF (A, J),  $\text{IFN-}\gamma$  (B, K), both TNF and  $\text{IFN-}\gamma$  (C, L), IL-2 (D, M) and IL-17A (E, N) upon splenocyte restimulation with PMA/Ionomycin for 4 h is shown. The cytokine content per cell was analyzed based on MFI for each cytokine (F-I, O-S) and was expressed as % of WT for each age group independently. The data is shown as average  $\pm$  SEM of 4-7 (A-I, males) and 2-7 (J-S; females) mice and was analyzed by two-way ANOVA (A-E, J-N), unpaired Student's *t*-test (F-H, O-R) and Mann-Whitney test (I, S); \*  $p < 0.05$ , \*\*  $p < 0.01$ , \*\*\*  $p < 0.001$ .

#### **4.3.2. Aged $\text{Optn}^{470\text{T}}$ male mice showed an increased percentage of $\text{CD8}^+$ T cells positive for TNF, whereas positivity for $\text{IFN-}\gamma$ and IL-2 remained similar compared to WT mice**

We analyzed  $\text{CD8}^+$  T cell polarization in the same fashion as in  $\text{CD4}^+$  T cells. We first analyzed male mice and observed an increase in  $\text{CD8}^+\text{TNF}^+$  cell percentage between young-adult and aged mice, which was more prominent in  $\text{Optn}^{470\text{T}}$  mice compared to WT mice (Fig. 22 A), in contrast to what we found in  $\text{CD4}^+$  cells. Interestingly, aged  $\text{Optn}^{470\text{T}}$  mice had an increased percentage of  $\text{CD8}^+\text{TNF}^+$  cells compared to WT mice. A strong increase during aging was found in  $\text{CD8}^+\text{IFN-}\gamma^+$  (Fig. 22 B) and  $\text{CD8}^+\text{TNF}^+\text{IFN-}\gamma^+$  (Fig. 22 C) cell percentage and was similar in both genotypes.  $\text{CD8}^+\text{IL-2}^+$  cell percentage was significantly higher in aged mice compared to young-adult and middle-aged mice and was similar between genotypes (Fig. 22 D). The production of TNF (Fig. 22 E),  $\text{IFN-}\gamma$  (Fig. 22 F), and IL-2 (Fig. 22 G) in  $\text{Optn}^{470\text{T}}$  mice was comparable to WT mice at all age points. In females, we found an aging-induced increase in  $\text{CD8}^+\text{TNF}^+$  (Fig. 22 H) and  $\text{CD8}^+\text{IFN-}\gamma^+$  (Fig. 22 I) cell percentage, similar in both genotypes, whereas the increase in  $\text{CD8}^+\text{TNF}^+\text{IFN-}\gamma^+$  (Fig. 22 J) and  $\text{CD8}^+\text{IL-2}^+$  (Fig. 22 K) cell percentage was not so prominent or even absent. The amount of TNF (Fig. 22 L),  $\text{IFN-}\gamma$  (Fig. 22 M) and IL-2 (Fig. 22 N) production was comparable between the genotypes at any age point. Here, we have shown that aging resulted in a stronger increase in  $\text{CD8}^+$  T cells positive for TNF,  $\text{IFN-}\gamma$ , both TNF and  $\text{IFN-}\gamma$ , and IL-2 in males compared to females and was similar between  $\text{Optn}^{470\text{T}}$  and WT mice. However, a conclusion cannot be made for females since the analysis of young adults is missing, and a higher number of mice for TNF measurements is needed.

### Analysis of CD8<sup>+</sup> T cells in male mice



### Analysis of CD8<sup>+</sup> T cells in female mice

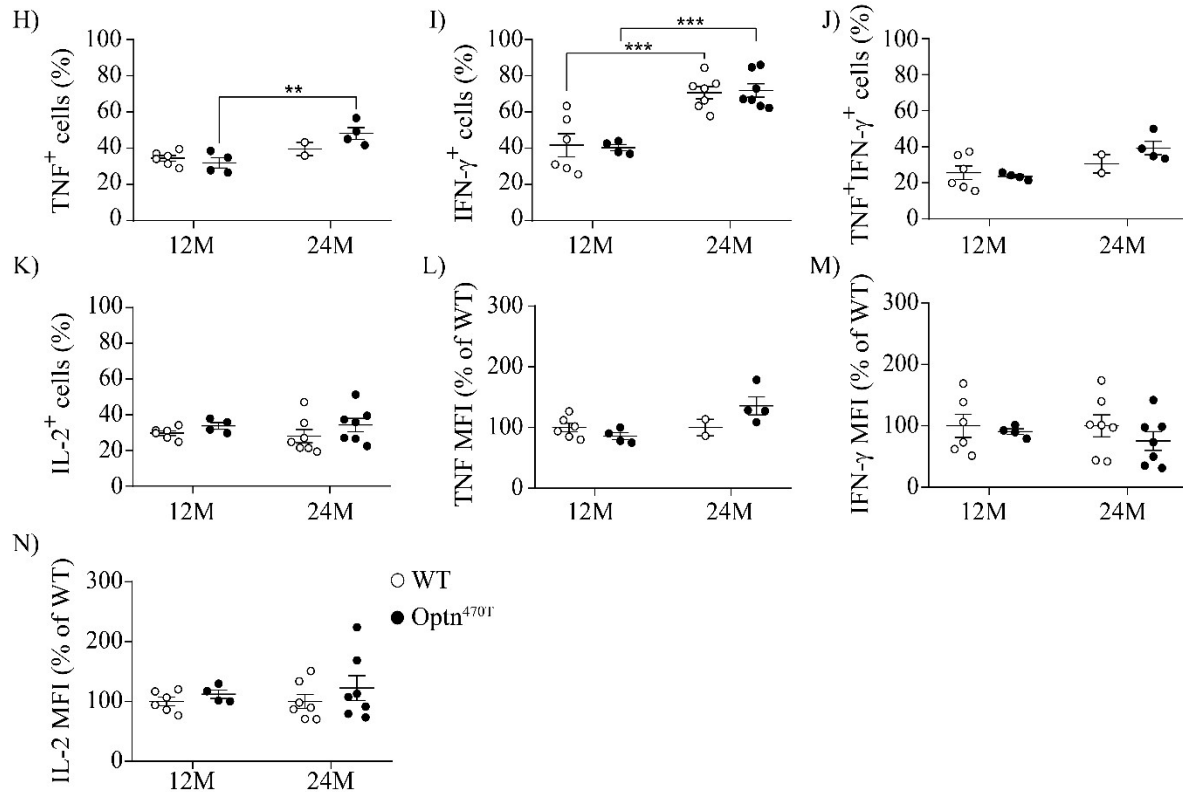


**Figure 22. Aging induced an increase in CD8<sup>+</sup> T cells positive for TNF in Optn<sup>470T</sup> male mice, whereas IFN- $\gamma$  and IL-2 were similar to WT mice.** Analysis of CD8<sup>+</sup> T cells for the positivity for TNF (A, H), IFN- $\gamma$  (B, I), both TNF and IFN- $\gamma$  (C, J), and IL-2 (D, K) upon splenocyte restimulation with PMA/Ionomycin for 4 h is shown. The cytokine content per cell was analyzed based on MFI for each cytokine (E-G, L-N) and was expressed as % of WT for each age group independently. The data is shown as average  $\pm$  SEM of 4-7 (A-G, males) and 2-7 (H-N; females) mice and was analyzed by two-way ANOVA (A-D, H-K) and unpaired Student's *t*-test (E-G, L-N) \*  $p < 0.05$ , \*\*  $p < 0.01$ , \*\*\*  $p < 0.001$ .

#### **4.4. Characterization of a new double-hit Optn<sup>470T</sup>/TDP-43<sup>G348C</sup> mouse model during aging and upon LPS stimulation**

##### **4.4.1. Characterization of a new Optn<sup>470T</sup>/TDP-43<sup>G348C</sup> mouse model**

Due to the lack of an overt ALS/FTD-like phenotype in Optn<sup>470T</sup> mice during aging (Mohovic, Peradinovic et al., 2023), we crossed Optn<sup>470T</sup> mice with mice that harbor a patient mutation in TDP-43 (human TDP-43<sup>G348C</sup> transgene), which has been shown to develop cytoplasmic TDP-43 aggregation, neuroinflammation, and motor and cognitive deficits from 7 months of age onwards (Swarup et al., 2011). Briefly, we first crossed Optn<sup>470T/470T</sup> to Optn<sup>WT/WT</sup> TDP-43<sup>G348C</sup> mice, both of which were of C57BL/6 background, and obtained heterozygous mice for optineurin (Optn<sup>WT/470T</sup>), approximately half of which were TDP-43<sup>G348C</sup> positive. The latter were crossed with Optn<sup>470T/WT</sup> mice resulting in a potential double-hit ALS/FTD mouse model harboring mouse Optn<sup>470T</sup> truncation and a human TDP-43<sup>G348C</sup> transgene (Optn<sup>470T</sup>/TDP-43<sup>G348C</sup>; (Mohović, 2023)). All mice were genotyped by PCR amplification and subsequent gel electrophoreses, where we used specific primers to detect the presence of bands for Optn<sup>WT</sup> (~363 bp), Optn<sup>470T</sup> (~288 bp), and TDP-43<sup>G348C</sup> (~365 bp) (Fig. 23 A). Optineurin and TDP-43 levels were analyzed by western blotting of whole brain homogenates from mice genotyped as WT, TDP-43<sup>G348C</sup>, Optn<sup>470T</sup>, and Optn<sup>470T</sup>/TDP-43<sup>G348C</sup> (Fig. 23 B). We observed a ~5-fold lower expression of truncated optineurin compared to full-length (wild-type, WT) optineurin, with a similar expression pattern between Optn<sup>470T</sup>/TDP-43<sup>G348C</sup> and TDP-43<sup>G348C</sup> mice (Fig. 23 B, C). When analyzing TDP-43 expression, we found a ~20-fold higher expression in TDP-43<sup>G348C</sup> transgene compared to WT mice (Fig. 23 B, D). However, we observed a 30% decrease in TDP-43 expression in

Optn<sup>470T</sup>/TDP-43<sup>G348C</sup> compared to Optn<sup>470T</sup> mice, suggesting that optineurin insufficiency may have a protective function by downregulating TDP-43 levels (Fig. 23 B, D). To conclude, a new double-hit ALS/FTD Optn<sup>470T</sup>/TDP-43<sup>G348C</sup> was successfully generated and characterized by PCR and western blot. Additionally, the presence of TDP-43<sup>G348C</sup> transgene did not affect optineurin expression, whereas optineurin insufficiency reduced TDP-43 expression.

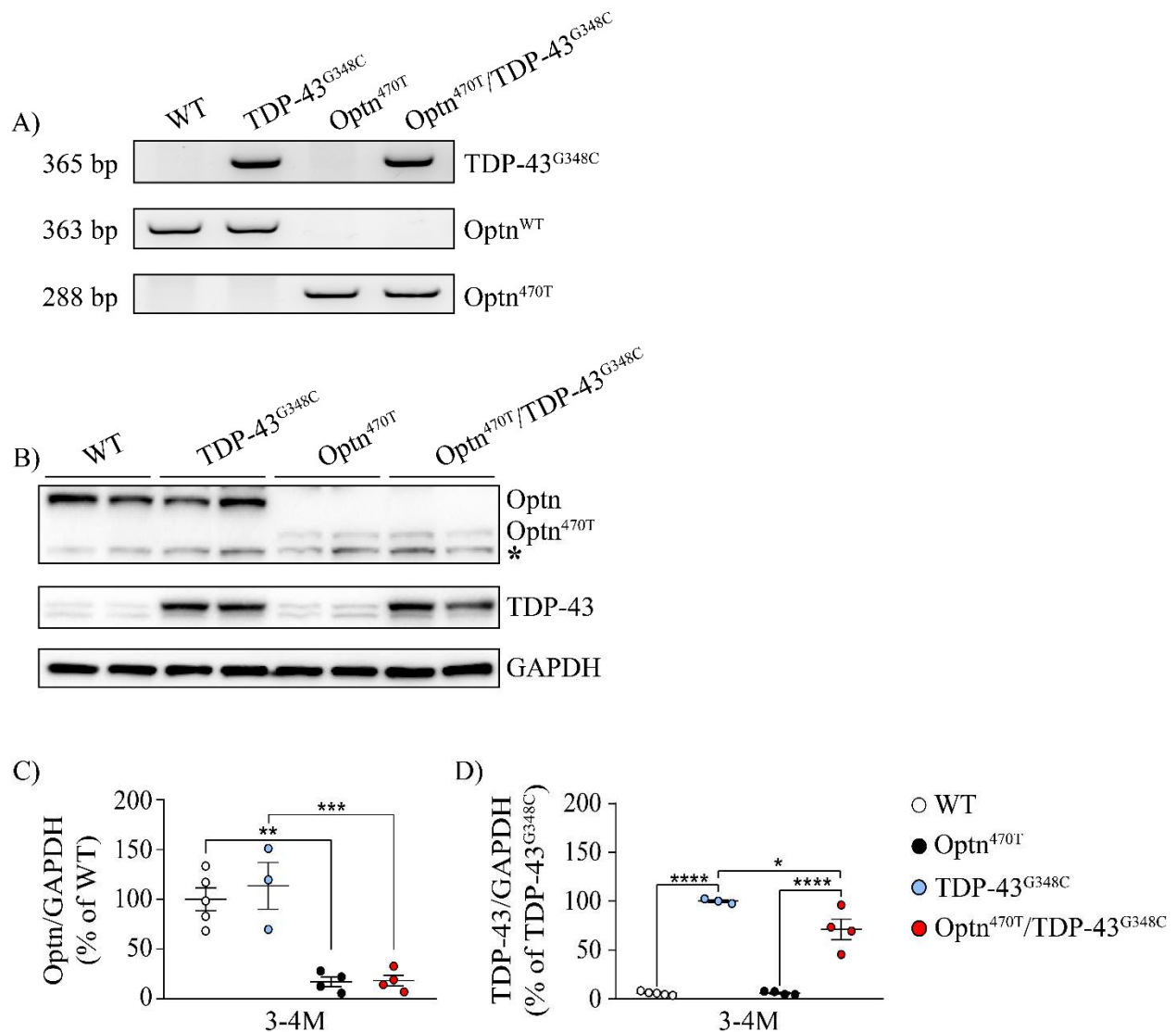


**Figure 23. Characterization of a new Optn<sup>470T</sup>/TDP-43<sup>G348C</sup> double-hit mouse model.** PCR confirmation on the agarose gel for the presence of Optn<sup>WT</sup>, Optn<sup>470T</sup> and TDP-43<sup>G348C</sup> transgene (A) in the indicated mice. Western blot analysis (B) of Optn (C) and TDP-43 (D) expression in the whole brain homogenates of young adult mice (3-4 months); results were normalized to GAPDH as the loading control and shown as % of WT (C) or TDP-43<sup>G348C</sup> (D) mice; two representative

mice of each genotype are shown. Non-specific band in (B) is marked with \*. The data is shown as average  $\pm$  SEM of 3-5 WT, Optn<sup>470T</sup>, TDP-43<sup>G348C</sup> and Optn<sup>470T</sup>/TDP-43<sup>G348C</sup> male mice, and was analyzed by one-way ANOVA; \*  $p < 0.05$ , \*\*  $p < 0.01$ , \*\*\*  $p < 0.001$ , \*\*\*\*  $p < 0.0001$ .

#### **4.4.2. NF- $\kappa$ B and TBK1 signaling activation between TDP-43<sup>G348C</sup> and WT BMDMs was comparable**

Swarup *et al* have shown hyperactivation of the NF- $\kappa$ B signaling in TDP-43<sup>G348C</sup> primary neonatal microglia on western blot and in TDP-43<sup>WT</sup> BMDMs on RT-qPCR (Swarup et al., 2011b). Nevertheless, the detailed NF- $\kappa$ B signaling analysis was not done, so we performed it on three levels: western blot, RT-qPCR and ELISA. First, we measured NF- $\kappa$ B signaling activation by I $\kappa$ B- $\alpha$  degradation and p65 phosphorylation at serine 536 (Fig. 24 A). LPS stimulation of WT BMDMs led to almost complete I $\kappa$ B- $\alpha$  degradation 15 min after stimulation, after which it started to reaccumulate at 30 min and reached basal levels by 60 min (Fig. 24 A, B). Phosphorylation of p65 in WT BMDMs peaked at 15 min upon stimulation, retained its levels at 30 min, and slightly started to decrease at 60 min (Fig. 24 A, C). Therefore, the pattern of NF- $\kappa$ B activation in TDP-43<sup>G348C</sup> BMDMs was similar to WT BMDMs. We subsequently analyzed the mRNA expression (Fig 24 D) and protein secretion (Fig. 24 E) of TNF, a major pro-inflammatory cytokine expressed upon NF- $\kappa$ B activation. *Tnf* mRNA expression, measured by RT-qPCR, peaked at 2 h upon LPS stimulation of WT BMDMs and then dropped, but remained a bit higher at 24 h compared to the basal levels (Fig. 24 D). A similar pattern of *Tnf* mRNA expression was observed in TDP-43<sup>G348C</sup> BMDMs. TNF secretion from WT BMDMs, measured by ELISA, was detected 2 h after LPS stimulation, continued to rise at 4 h, and peaked at 24 h (Fig. 24 E). TDP-43<sup>G348C</sup> BMDMs secreted a comparable amount of TNF upon LPS stimulation. Therefore, unlike Swarup *et al.*, we showed that NF- $\kappa$ B signaling was unaffected by overexpression of TDP-43<sup>G348C</sup> transgene, meaning that TDP-43 did not regulate activation of the NF- $\kappa$ B signaling.

Another signaling pathway activated by LPS stimulation is TBK1 signaling, which results in the production of IFN- $\beta$  (Perry et al., 2004). However, the role of TDP-43 in TBK1 signaling activation is still unknown. TBK1 phosphorylation at serine 172, a sign of TBK1 activation, was analyzed by western blot (Fig. 24 F). In WT BMDMs, it peaked 0.5 h upon LPS stimulation and

then started to diminish from 1 h to 4 h (Fig. 24 F, G). The same TBK1 activation pattern was observed in TDP-43<sup>G348C</sup> BMDMs. IFN- $\beta$  mRNA expression (Fig 24 H) and protein secretion (Fig. 24 I) were subsequently measured. RT-qPCR analysis revealed a peak of *Ifn- $\beta$*  mRNA expression at 2 h upon LPS stimulation, which returned to basal levels by 24 h in WT BMDMs (Fig. 24 H), with a slightly lower induction of *Ifn- $\beta$*  mRNA in TDP-43<sup>G348C</sup> BMDMs, without reaching statistical significance due to a low number of repetitions (n = 2). IFN- $\beta$  secretion in WT BMDMs was detectable at low levels in the basal state, increased at 2 h, peaked at 4 h, and dropped by 24 h after LPS stimulation (Fig. 24 I). IFN- $\beta$  secretion from TDP-43<sup>G348C</sup> BMDMs was slightly decreased compared to WT BMDMs, except at 24 h where the concentrations were similar. To conclude, TBK1 signaling activation was not affected by TDP-43<sup>G348C</sup> overexpression.



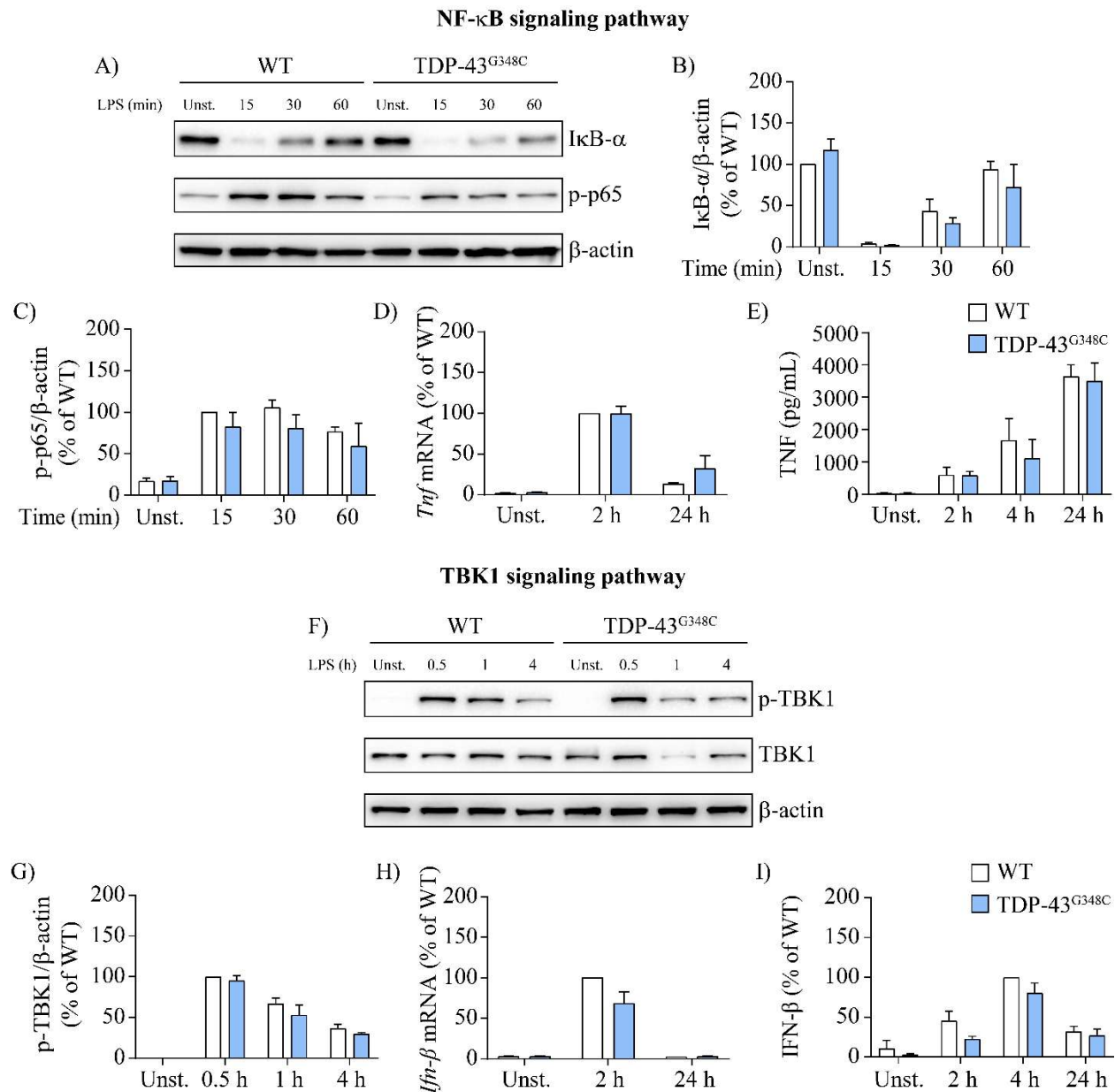


**Figure 24. TDP-43<sup>G348C</sup> and WT BMDMs showed comparable NF- $\kappa$ B and TBK1 pathway activation upon LPS stimulation.** BMDMs were generated from the bone marrow of 3-5-month-old WT and TDP-43<sup>G348C</sup> mice and stimulated with 500 ng/mL of LPS at the indicated time points. NF- $\kappa$ B signaling was analyzed by western blot (A) for I $\kappa$ B- $\alpha$  degradation (B) and p65 phosphorylation (C); results were normalized to GAPDH as the loading control and shown as % of WT unstimulated cells (B) or cells treated for 15 minutes with LPS (C). *Tnf* mRNA was analyzed by RT-qPCR, normalized to the housekeeping gene (*Gapdh*) and shown as % of WT cells treated for 2 h with LPS (D). TNF protein secretion was analyzed by ELISA (D). TBK1 signaling was

analyzed by western blot (F) for TBK1 phosphorylation (G); results were normalized to GAPDH as the loading control and shown as % of WT cells treated for 0.5 h with LPS. *Ifn-β* mRNA was analyzed by RT-qPCR, normalized to the housekeeping gene *Gapdh* and shown as % of WT cells treated 2 h with LPS (H). IFN-β protein secretion was analyzed by ELISA (I) and was shown as % of WT cells treated for 4 h with LPS. The data is shown as average ± SEM (B, C, E, G, I) or SD (D, H) from 2-3 independent experiments and was analyzed by two-way ANOVA.

#### **4.4.3. LPS stimulation of Optn<sup>470T</sup>/TDP-43<sup>G348C</sup> led to a similar NF-κB, but reduced TBK1 activation compared to TDP-43<sup>G348C</sup> BMDMs**

To test if the presence of Optn<sup>470T</sup> truncation in TDP-43<sup>G348C</sup> BMDMs will affect activation of the NF-κB and TBK1 signaling, we generated BMDMs from TDP-43<sup>G348C</sup> and Optn<sup>470T</sup>/TDP-43<sup>G348C</sup> mice, stimulated them with LPS and analyzed by western blot, RT-qPCR and ELISA. NF-κB signaling activation was measured by IκB-α degradation and p65 phosphorylation by western blot (Fig. 25 A). In TDP-43<sup>G348C</sup> BMDMs, IκB-α degradation started 0.5 h after LPS stimulation, reaccumulated at 1 h to 60% of its basal level, and remained the same at 3 h (Fig. 25 A and B). Interestingly, IκB-α expression in the basal state of Optn<sup>470T</sup>/TDP-43<sup>G348C</sup> BMDMs was higher by 45% compared to TDP-43<sup>G348C</sup> BMDMs. However, after its degradation 0.5 h after stimulation, it reaccumulated to the same levels as observed in TDP-43<sup>G348C</sup> BMDMs. Phosphorylation of p65 in TDP-43<sup>G348C</sup> BMDMs peaked at 0.5 h upon stimulation, slightly dropped at 1 h, and further decreased at 3 h (Fig. 25 A, C). *Tnf* mRNA levels peaked at 2 h upon LPS stimulation and markedly dropped by 24 h in TDP-43<sup>G348C</sup> BMDMs, with the same kinetics in Optn<sup>470T</sup>/TDP-43<sup>G348C</sup> BMDMs. (Fig. 25 D). TNF protein secretion from TDP-43<sup>G348C</sup> BMDMs started 2 h upon LPS stimulation, peaked at 6 h and remained at a similar level up to 24 h (Fig. 25 E), with an unaffected secretion pattern in Optn<sup>470T</sup>/TDP-43<sup>G348C</sup> BMDMs. Thus, we have shown that optineurin truncation in TDP-43<sup>G348C</sup> BMDMs increased basal IκB-α levels, but without affecting the NF-κB signaling activation and TNF production.

We have previously shown that optineurin plays a role as a positive regulator of TBK1 signaling and IFN-β production (Markovinovic et al., 2018; Munitic et al., 2013), so we wanted to check if the presence of a high level of human TDP-43<sup>G348C</sup> transgene will additionally affect it. TBK1

phosphorylation peaked at 0.5 h, retained its levels at 1 h, and dropped at 3 h in TDP-43<sup>G348C</sup> BMDMs (Fig. 25 F). In contrast, the phosphorylation of TBK1 was decreased in Optn<sup>470T</sup>/TDP-43<sup>G348C</sup> BMDMs. *Ifn-β* mRNA peaked at 2 h upon LPS stimulation and dropped to basal levels at 24 h in TDP-43<sup>G348C</sup> BMDMs (Fig. 25 H). In Optn<sup>470T</sup>/TDP-43<sup>G348C</sup> BMDMs, a reduced *Ifn-β* mRNA expression at 2 h was observed, although this was not statistically significant due to a limited number of repetitions (n = 2). IFN-β secretion from TDP-43<sup>G348C</sup> BMDMs started 2 h upon LPS stimulation, peaked at 6 h, and was markedly reduced by 24 h (Fig. 25 I). On the contrary, IFN-β levels were significantly reduced in Optn<sup>470T</sup>/TDP-43<sup>G348C</sup> BMDMs at 2 h and 6 h. By this, we confirmed that optineurin has retained its function as a positive regulator of the TBK1 signaling in the presence of TDP-43<sup>G348C</sup> transgene, but the potential proteotoxic stress exerted by the latter did not further affect the signaling.

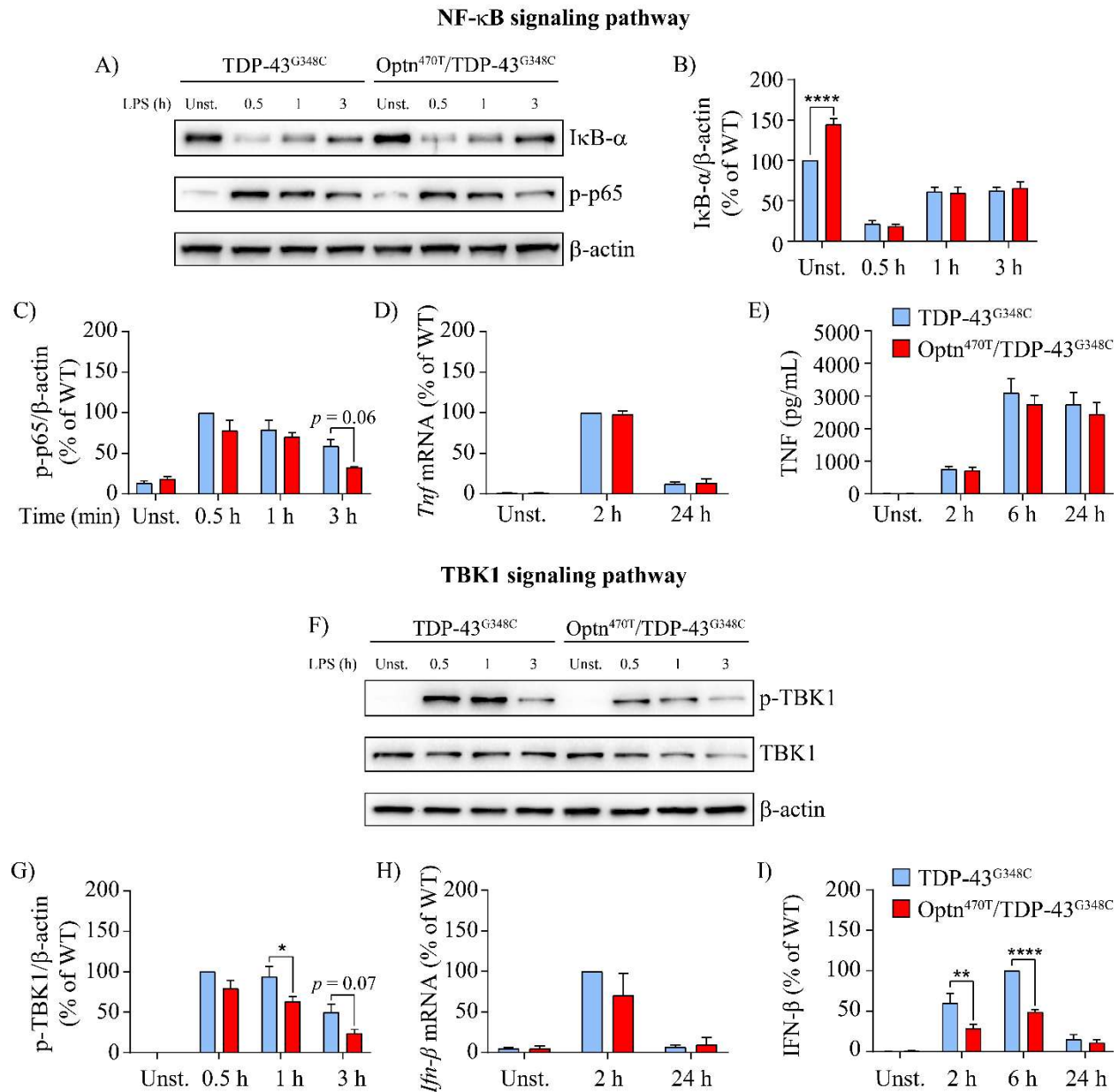


**Figure 25. Optn<sup>470T</sup>/TDP-43<sup>G348C</sup> BMDMs showed similar NF- $\kappa$ B but diminished TBK1 activation upon LPS stimulation compared to TDP-43<sup>G348C</sup> BMDMs.** BMDMs were generated from bone marrow of 3-5-month-old TDP-43<sup>G348C</sup> and Optn<sup>470T</sup>/TDP-43<sup>G348C</sup> mice and stimulated with 500 ng/mL LPS at the indicated time points. NF- $\kappa$ B signaling was analyzed by western blot (A) for I $\kappa$ B- $\alpha$  degradation (B) and p65 phosphorylation (C); results were normalized to GAPDH as the loading control and shown as % of WT unstimulated cells (B) or cells treated for 0.5 h with LPS (C). *Tnf* mRNA was analyzed by RT-qPCR, normalized to the housekeeping gene (*Gapdh*) and shown as % of WT cells treated for 2 h with LPS (D). TNF secretion was analyzed by ELISA

(D). TBK1 signaling was analyzed by western blot (F) for TBK1 phosphorylation (G); results were normalized to GAPDH as the loading control and shown as % of WT cells treated for 0.5 h with LPS. *Ifn-β* mRNA was analyzed by RT-qPCR, normalized to the housekeeping gene *Gapdh* and shown as % of WT cells treated 2 h with LPS (H). IFN-β protein secretion was analyzed by ELISA (I) and was shown as % of WT cells treated for 6 h with LPS. The data is shown as average ± SEM (B, C, E, G, I) or SD (D, H) from 2-4 independent experiments and was analyzed by two-way ANOVA; \*  $p < 0.05$ , \*\*  $p < 0.01$ , \*\*\*\*  $p < 0.0001$

#### **4.4.4. Optn<sup>470T</sup>/TDP-43<sup>G348C</sup> mice had lower body weight, and improved motor and cognitive functions compared to TDP-43<sup>G348C</sup> mice**

We let the mice of all four genotypes (WT, Optn<sup>470T</sup>, TDP-43<sup>G348C</sup> and Optn<sup>470T</sup>/TDP-43<sup>G348C</sup>) age up to 18 months to analyze the effect of TDP-43<sup>G348C</sup> on ALS and FTD-like pathology. At that time, we observed a ~10% decrease in the body weight of Optn<sup>470T</sup>/TDP-43<sup>G348C</sup> mice compared to Optn<sup>470T</sup> and TDP-43<sup>G348C</sup> mice (Fig. 26 A). To check for motor coordination, we performed rotarod (Fig. 26 B) and grid-hanging tests (Fig. 26 C). On the rotarod, we observed a prominent age-induced decline in motor function. More precisely, the time spent on rotarod dropped by 30-40% in middle-aged mice (11-15M), and by 50% in aged mice (15-18M), compared to young adult mice (6-10M). Surprisingly, this was similar for all the genotypes (Fig. 26 B), even though TDP-43<sup>G348C</sup> were reported to have ALS symptoms from 7 months onwards (Swarup et al., 2011). However, when we performed a more sensitive grid-hanging test at 18 months of age, we observed a 40% increase in time spent on a grid for Optn<sup>470T</sup>/TDP-43<sup>G348C</sup> compared to TDP-43<sup>G348C</sup> mice, without a difference between other genotypes (Fig. 26 C). We then tested the cognitive function by a novel object recognition test and observed a 16% lower preference for the novel object in TDP-43<sup>G348C</sup> compared to WT mice (Fig. 26 D). Surprisingly, in Optn<sup>470T</sup>/TDP-43<sup>G348C</sup> we observed a 10% rescue of cognitive function compared to TDP-43<sup>G348C</sup> mice (Fig. 26 D). In conclusion, the presence of optineurin truncation in TDP-43<sup>G348C</sup> mice decreased the body weight, and improved motor and cognitive functions, even though we expected worsened phenotype due to the coexistence of two ALS-linked mutations. This suggests an unexpected protective effect of optineurin in TDP-43<sup>G348C</sup> mice.

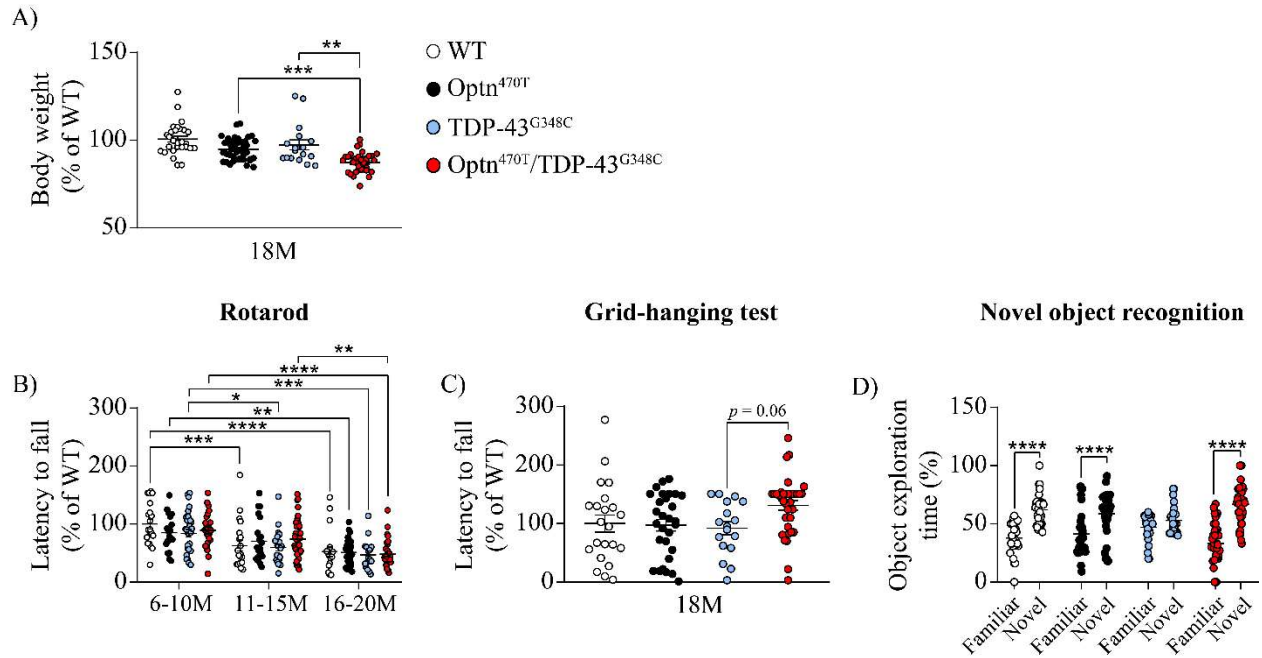


**Figure 26. Optn<sup>470T</sup>/TDP-43<sup>G348C</sup> mice had improved motor and cognitive functions and lower body weight compared to TDP-43<sup>G348C</sup> mice at 18 months of age.** Male and female mice of both sexes were analyzed at the indicated age for body weight (A; WT: 28, Optn<sup>470T</sup>: 33, TDP-43<sup>G348C</sup>: 17, Optn<sup>470T</sup>/TDP-43<sup>G348C</sup>: 39 mice), motor coordination on accelerating rotarod (B; WT: 20, 20, 19; Optn<sup>470T</sup>: 18, 21, 28; TDP-43<sup>G348C</sup>: 31, 22, 16; Optn<sup>470T</sup>/TDP-43<sup>G348C</sup>: 25, 40, 32 mice) and grid-hanging test (C; WT: 22, Optn<sup>470T</sup>: 29, TDP-43<sup>G348C</sup>: 17, Optn<sup>470T</sup>/TDP-43<sup>G348C</sup>: 35 mice), and cognitive function by novel object recognition test (D; WT: 32, Optn<sup>470T</sup>: 34, TDP-43<sup>G348C</sup>: 25, Optn<sup>470T</sup>/TDP-43<sup>G348C</sup>: 39 mice). The results were first separated according to the sex and normalized to WT mice of the same sex, and then pooled (A-C), whereas in (B) the results were expressed as % of 6-10M WT. In (D) % of preference for the familiar and novel object are shown. The data is shown as average  $\pm$  SEM and was analyzed by Kruskal-Wallis test (A, C) or two-way ANOVA (B, D); \* p < 0.05, \*\* p < 0.01, \*\*\* p < 0.001, \*\*\*\* p < 0.0001.

#### 4.4.5. LPS-mediated body weight loss and death were rescued by the presence of Optn<sup>470T</sup> truncation in TDP-43<sup>G348C</sup> mice

It was shown that two-month-old Optn<sup>470T</sup> mice had chemokine disbalance in the brain upon intraperitoneal LPS stimulation (Markovinovic et al., 2018) and that 10-month-old TDP-43<sup>G348C</sup> mice had increased mRNA expression of various pro-inflammatory cytokines (Swarup, et al.,

2011). In addition, our *in vitro* results have shown that a single dose of LPS induced neither TDP-43 cytoplasmic mislocalization (Marošević, 2022) nor cytokine disbalance in TDP-43<sup>G348C</sup> BMDMs (Fig. 27). Therefore, we administered 18-month-old WT, Optn<sup>470T</sup>, TDP-43<sup>G348C</sup> and Optn<sup>470T</sup>/TDP-43<sup>G348C</sup> mice with 1.5 mg/kg LPS for three consecutive days to try to induce TDP-43 cytoplasmic mislocalization and cytokine disbalance to aggravate the ALS/FTD phenotype. The sickness behavior was checked 24 h after each LPS administration and included measurements of the body weight (Fig. 27 A) and temperature (Fig. 27 B). We observed a gradual body weight loss upon each LPS dose in all genotypes. Mice with optineurin truncation (Optn<sup>470T</sup> and Optn<sup>470T</sup>/TDP-43<sup>G348C</sup>) have shown increased body weight loss compared to mice with WT optineurin (WT and TDP-43<sup>G348C</sup>) on the first and second day upon LPS administration (Fig. 27 A). However, on the third day, the body weight loss was still increased in Optn<sup>470T</sup> mice compared to WT mice, whereas Optn<sup>470T</sup>/TDP-43<sup>G348C</sup> and TDP-43<sup>G348C</sup> became equal, suggesting the protective effect of optineurin in the latter (Fig. 27 A). The temperature dropped slightly in every genotype on the first day of LPS administration, additionally dropped on the second day, and was kept similar on the third day, without a difference between the genotypes (Fig. 27 B). All WT and Optn<sup>470T</sup> mice survived two doses of LPS, whereas ~73% of mice survived by the third day. In contrast, TDP-43<sup>G348C</sup> mice started dying on the second day, and only 53% of mice survived by the third day, showing that they were most vulnerable to LPS-induced sepsis (Fig. 27 C). Interestingly, Optn<sup>470T</sup>/TDP-43<sup>G348C</sup> mice showed the best survival with ~88% surviving by the third day, suggesting the protective effect of optineurin truncation in TDP-43<sup>G348C</sup> mice. In conclusion, Optn<sup>470T</sup>/TDP-43<sup>G348C</sup> mice have shown decreased body weight loss and the highest survival rate by the third day upon LPS administration. Altogether, optineurin truncation showed a protective effect upon three-day LPS administration of TDP-43<sup>G348C</sup> mice.





mice. The percentages and numbers of non-T/non-B ( $T^-/B^-$ ; Fig. 17 B, E) and T cells (Fig. 28 C, F) remained similar between the genotypes. B cell percentage was slightly decreased in  $Optn^{470T}$  and  $TDP-43^{G348C}$  mice compared to WT mice, but this did not reach statistical significance. In contrast,  $Optn^{470T}/TDP-43^{G348C}$  mice had ~20% decreased B cell percentage and ~50% decreased absolute B cell number compared to  $Optn^{470T}$  mice. No differences were found in absolute B cell number between WT and  $TDP-43^{G348C}$  mice (Fig. 28 G). Therefore, we have shown here that the decreased splenocyte number in  $Optn^{470T}/TDP-43^{G348C}$  mice was largely due to the decreased presence of the B cell population. However, in future experiments, the spleens need also to be analyzed in the basal state to elucidate the reason for decreased B cell population in  $Optn^{470T}/TDP-43^{G348C}$  mice.

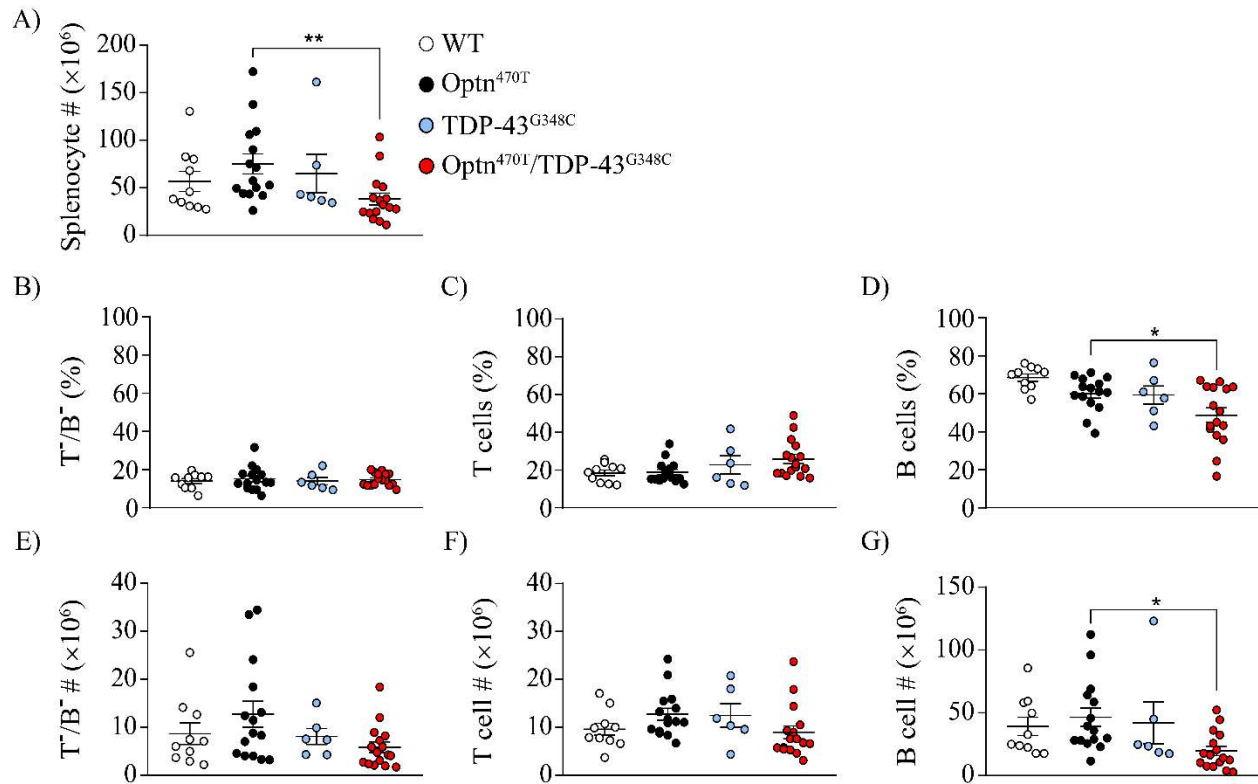


**Figure 28.** The decreased splenocyte number in  $Optn^{470T}/TDP-43^{G348C}$  compared to  $Optn^{470T}$  mice upon three-day LPS stimulation was accounted for by the loss of B lymphocytes. WT,  $Optn^{470T}$ ,  $TDP-43^{G348C}$  and  $Optn^{470T}/TDP-43^{G348C}$  at the age of 18 months were intraperitoneally administered with 1.5 mg/kg for three consecutive days, the spleens were isolated 24 h after the last dose and analyzed by the flow cytometry. The number of splenocytes (A), frequencies (%) of non-T/non-B cells (B;  $T^-/B^-$ ), T lymphocytes (C), B lymphocytes (D), and the absolute numbers of

these subsets (E-G) are shown. The data is shown as average  $\pm$  SEM of the indicated number of mice (10 WT, 15 Optn<sup>470T</sup>, 6 TDP-43<sup>G348C</sup> and 16 Optn<sup>470T</sup>/TDP-43<sup>G348C</sup>) and was analyzed by Kruskal-Wallis test (A, B, E-G) and one-way ANOVA (C, D); \*  $p < 0.05$ , \*\*  $p < 0.01$ .

#### **4.4.7. The spleens of LPS-treated Optn<sup>470T</sup>/TDP-43<sup>G348C</sup> mice had lower numbers of classical dendritic and NK cells compared to Optn<sup>470T</sup> mice**

We further analyzed the non-T/non-B population to characterize innate immune cells upon three-day LPS administration. The percentage of macrophages in Optn<sup>470T</sup>, TDP-43<sup>G348C</sup> and Optn<sup>470T</sup>/TDP-43<sup>G348C</sup> mice was slightly higher compared to WT mice, although this did not reach statistical significance due to substantial mouse-to-mouse variability. The absolute numbers of macrophages were similar between all genotypes (Fig. 29 A, B). The expression of activation markers CD86 and CD11c on macrophages was slightly lower in Optn<sup>470T</sup>, TDP-43<sup>G348C</sup> and Optn<sup>470T</sup>/TDP-43<sup>G348C</sup> mice compared to WT mice, whereas MHC-II expression was slightly increased in the presence of TDP-43<sup>G348C</sup> transgene, but without statistical significance between the genotypes (Fig. 29 C). The percentages of classical dendritic cells (cDC) were comparable between the genotypes (Fig. 29 D), whereas the number was significantly lower in Optn<sup>470T</sup>/TDP-43<sup>G348C</sup> mice compared to Optn<sup>470T</sup> mice (Fig. 18 E). CD86 and MHC-II expression were similar between the genotypes (Fig. 29 F). The percentage of neutrophils was higher in Optn<sup>470T</sup> mice compared to WT mice, with a similar trend between TDP-43<sup>G348C</sup> and Optn<sup>470T</sup>/TDP-43<sup>G348C</sup> mice (Fig. 29 G) whereas the number was lower in transgenic compared to non-transgenic mice (Fig. 29 H). The natural killer (NK) cell percentage was similar between the genotypes (Fig. 29 I), but the absolute numbers were lower in transgenic compared to non-transgenic mice (Fig. 29 J). In conclusion, Optn<sup>470T</sup>/TDP-43<sup>G348C</sup> mice had lower cDC and NK cell numbers upon consecutive LPS stimulation compared to Optn<sup>470T</sup> mice.

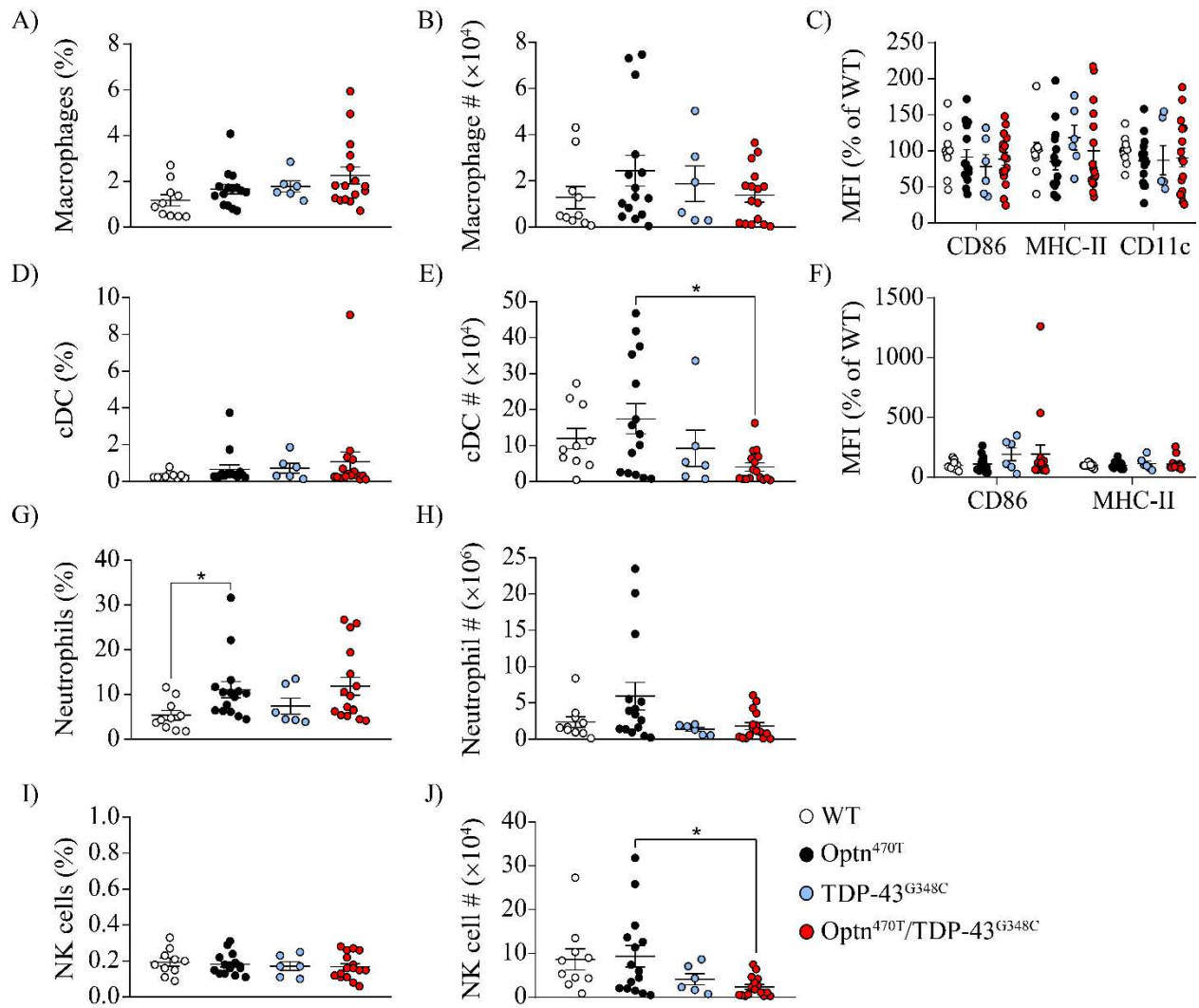


**Figure 29. Optn<sup>470T</sup>/TDP-43<sup>G348C</sup> mice had a lower number of classical dendritic and NK cells compared to Optn<sup>470T</sup> mice upon three-day LPS administration.** WT, Optn<sup>470T</sup>, TDP-43<sup>G348C</sup>, and Optn<sup>470T</sup>/TDP-43<sup>G348C</sup> at the age of 18 months were intraperitoneally stimulated with 1.5 mg/kg for three consecutive days, the spleens were isolated 24 h after the last dose and analyzed by flow cytometry. Frequencies (%) of macrophages (A), classical dendritic cells (D; cDC), neutrophils (G), NK cells (I), and their numbers (B, E, H, J) are shown. Macrophage and cDC activation were assessed by the MFI of CD86, MHC-II and CD11c activation markers (C, F). The data is shown as average ± SEM of indicated number of mice (10 WT, 15 Optn<sup>470T</sup>, 6 TDP-43<sup>G348C</sup>, and 16 Optn<sup>470T</sup>/TDP-43<sup>G348C</sup>) and was analyzed by Kruskal-Wallis test (A, B, C: MHC-II and CD86, D-H, J) and one-way ANOVA (C: CD86, I); \* p < 0.05.

#### 4.4.8. Three-day LPS administration led to increased serum CCL2 and IL-10 levels in TDP-43<sup>G348C</sup> and Optn<sup>470T</sup>/TDP-43<sup>G348C</sup> mice, respectively

To evaluate if the differences in the cytokine profiles correlated to body weight loss and survival, we measured the concentration of cytokines (IL-10, IFN- $\gamma$ ) and chemokines (CXCL10, CCL2 and CXCL1) in the sera, and in the homogenates of the whole brain and the spinal cord. C-X-C motif chemokine ligand 10 (CXCL10) levels were very high in the serum, brain, and spinal cord (Fig. 30 A-C), without a difference between the genotypes. Chemokine (C-C motif) ligand 2 (CCL2) levels in the sera were significantly increased in TDP-43<sup>G348C</sup> mice compared to WT mice, with a similar but non-significant trend between Optn<sup>470T</sup> and Optn<sup>470T</sup>/TDP-43<sup>G348C</sup> mice (Fig. 30 D). In contrast, there were no differences between the genotypes in CCL2 concentrations in the brain (Fig. 30 E) and spinal cord (Fig. 30 F). Serum CXCL1 concentrations were low for most mice (Fig. 30 G), whereas it was highly abundant in the brains (Fig. 30 H). IL-10 was detectable only in the serum and we observed that the presence of TDP-43<sup>G348C</sup> transgene increased its concentration, which was almost significant between Optn<sup>470T</sup> and Optn<sup>470T</sup>/TDP-43<sup>G348C</sup> mice (Fig. 30 I). Additionally, the presence of Optn<sup>470T</sup> truncation decreased IL-10 levels, but not to a significant extent. Lastly, IFN- $\gamma$  serum levels were low and comparable between the genotypes (Fig. 30 J). To conclude, the concentrations of the analyzed cytokines and chemokines were comparable between the genotypes, except for CCL2 and IL-10 in the serum, where they were found to be higher in TDP-43<sup>G348C</sup> and Optn<sup>470T</sup>/TDP-43<sup>G348C</sup> mice compared to non-transgenic mice, respectively. Although IL-10 is potentially neuroprotective and could explain increased survival of Optn<sup>470T</sup>/TDP-43<sup>G348C</sup>, further analyses are necessary to test if it is protective in this particular case.

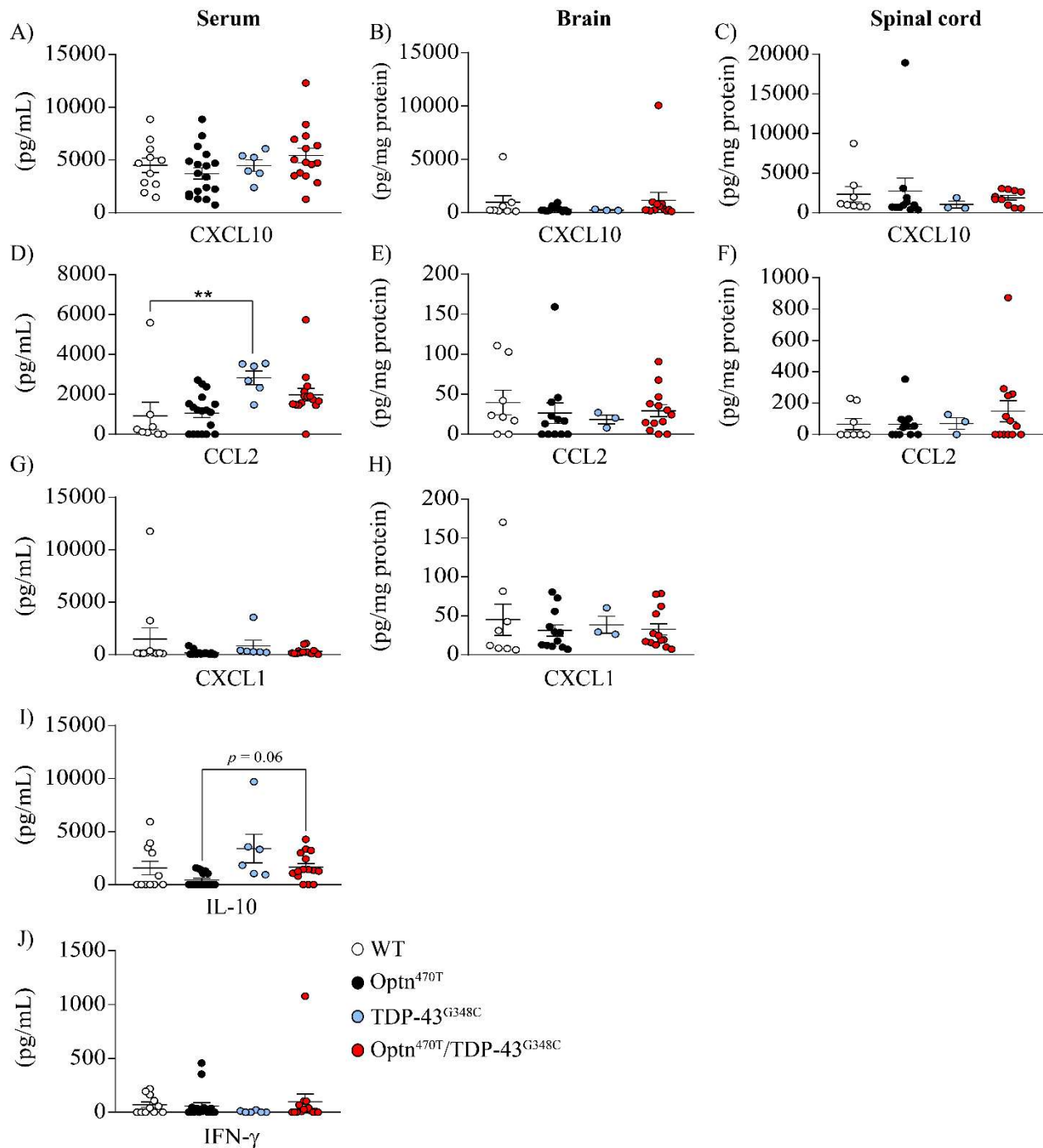


**Figure 30. Three-day LPS administration increased CCL2 and IL-10 concentrations in the serum of TDP-43<sup>G348C</sup> and Optn<sup>470T</sup>/TDP-43<sup>G348C</sup> mice, respectively.** WT, Optn<sup>470T</sup>, TDP-43<sup>G348C</sup> and Optn<sup>470T</sup>/TDP-43<sup>G348C</sup> at the age of 18 months were intraperitoneally stimulated with 1.5 mg/kg for three consecutive days. The sera, brains and spinal cords were isolated 24 h after the last dose and analyzed by Legendplex. The concentrations for CXCL10 (A-C), CCL2 (D-F), CXCL1 (G, H), IL-10 (I) and IFN-γ (J) in the sera (left column), brain (middle column) and the

spinal cord (right column) are shown. Note: final cytokine concentrations in the brain and the spinal cord were divided with the total protein concentration per sample and are depicted as mg/pg of total protein. The data is shown as average  $\pm$  SEM of mice (serum: 11 WT, 18 Optn<sup>470T</sup>, 6 TDP-43<sup>G348C</sup> and 15 Optn<sup>470T</sup>/TDP-43<sup>G348C</sup>; brain and spinal cord: 8 WT, 12 Optn<sup>470T</sup>, 3 TDP-43<sup>G348C</sup> and 13 Optn<sup>470T</sup>/TDP-43<sup>G348C</sup>) and was analyzed by one-way ANOVA (A) and Kruskal-Wallis test (B-J); \*\*  $p < 0.01$ .

## 5. Discussion

### 5.1. The role of optineurin in the central nervous system during aging

#### 5.1.1. Optn<sup>470T</sup> mice did not show ALS/FTD-like neuropathology during aging

Optineurin mutations that directly affect UBR (E478G and Q398X) were reported to be pathogenic in ALS patients, and it was proposed that excessive inflammation was the mechanism of the disease (Maruyama et al., 2010). Subsequently, it was also shown that patients bearing these mutations also develop FTD (H. Ito et al., 2011; Kamada et al., 2014). Here, we have utilized Optn<sup>470T</sup> mouse model, which mimics Q398X patient mutation, to study if aging could act as a potential second hit for the development of ALS/FTD-like phenotype. We found that aging-mediated loss of motor and cognitive abilities was not exaggerated in Optn<sup>470T</sup> mice, which we confirmed by several motor and cognitive tests shown here and in our recent publication (Mohovic, Peradinovic et al., 2023). This is consistent with the absence of ALS-like motor deficits in aged Optn<sup>-/-</sup> (Kurashige et al., 2021; Moharir & Swarup, 2022) and Optn<sup>D477N</sup> mice (Gleason et al., 2011). The only neurological deficits in Optn<sup>-/-</sup> mice were reported by Ito *et al.*, who found a decreased vertical rearing activity (i.e. lesser use of the hindlimbs) in three-month-old Optn<sup>-/-</sup> mice (Y. Ito et al., 2016). However, this phenotype was very mild and did not show a typical ALS progression. Moreover, when an open-field test was conducted by the same group, no differences in motor activity were found between WT and Optn<sup>-/-</sup> mice, further corroborating that the neurological phenotype, if any, is mild (Y. Ito et al., 2016). Surprisingly, an interesting result was recently reported by a study done in mice with conditional *OPTN* UBR truncation in glutamatergic neurons (named *OPTN<sup>fl/fl</sup>::Vglut2-Cre*, hereafter called “glutamatergic neuron-specific Optn<sup>470T</sup>”). They have observed the signs of motor and cognitive decline present already at three months of age (D. Liu et al., 2025). To point out, the same *OPTN<sup>fl/fl</sup>* floxed mouse model was generated by Munitic *et al.* (Munitic et al., 2013) and was used to generate whole body Optn<sup>470T</sup> truncation analyzed in our study. For this reason, it is not immediately clear why the glutamatergic neuron-specific Optn<sup>470T</sup> truncation would lead to ALS, while the whole-body Optn<sup>470T</sup> truncation would not (Mohovic, Peradinovic et al., 2023). There are several potential reasons for this finding. Firstly, it is important to address the role of the genetic background, since Munitic *et al.* have previously reported that Optn<sup>470T</sup> truncation in mice with mixed C57BL/6 × 129 background was embryonically lethal in majority of pups, with only 3% instead of 25% of homozygous mice born

to Optn<sup>470T</sup> heterozygous parents (Munitic et al., 2013). This effect of embryonic lethality with incomplete penetrance was lost upon further backcrossing to the C57BL/6J background (Munitic et al., 2013). Liu *et al.*, crossed the OPTN<sup>ff</sup> mice to V-glut2-Cre mice, where the latter were of mixed C57BL/6;FVB;129 background (D. Liu et al., 2025), with pure FVB and 129 mice being reported to spontaneously develop diseases such as blindness, cancer and diabetes (001800 - FVB Strain Details; 002448 - 129S1 Strain Details). Secondly, Liu *et al.* primarily focused on glaucoma, while we performed an extensive analysis of motor functions and related pathology. Their motor function analysis was conducted on a small number of mice with limited neuropathological evaluation, unlike our more detailed analysis. Additionally, Liu *et al.* combined male and female mice for their motor coordination analysis and performed neuropathological analysis at only one time point (three months), without assessing disease progression with age. Furthermore, ChAT<sup>+</sup> lower motor neuron number in WT mice reported by the authors was much lower than typically reported in the literature. It is also unclear how the lower motor neurons in glutamatergic neuron-specific Optn<sup>470T</sup> mice would be affected, as these neurons are cholinergic, not glutamatergic. Finally, an additional reason for the discrepancy between the findings in glutamatergic neuron-specific and whole body Optn<sup>470T</sup> truncation could be that in the latter the truncation in the surrounding microglia may have a protective effect. Given that some other findings in this thesis argue for a protective effect of Optn<sup>470T</sup> truncation in some settings (discussed below), this needs to be tested in future studies.

Optineurin and TBK1 act on the same signaling axis, so the mouse models carrying mutations in these genes can be compared. Of particular importance is a *Tbk1*<sup>+/-</sup> mouse model, which is a mouse model of TBK1 haploinsufficiency that represents ALS/FTD-linked loss-of-function mutations (Freischmidt et al., 2015). *Tbk1*<sup>+/-</sup> mice also did not develop motor and cognitive deficits during aging (Bruno et al., 2020), whereas the additional presence of TAK1 deletion in microglia precipitated the disease phenotype (Xu et al., 2018). This group suggested that *Tbk1*<sup>+/-</sup> mice did not develop ALS/FTD-like phenotype due to the compensation of TBK1 function by TAK1. These findings could mean that the presence of additional genetic mutations or instabilities may cause ALS, strengthening the hypothesis that ALS requires multiple steps to develop (Al-Chalabi et al., 2014).



It was reported that death  $\geq 50\%$  of motor neurons is required for ALS manifestation (Hardiman et al., 2017). Thus, we also examined Optn<sup>470T</sup> mice for potential early neuropathological changes. We found preserved neuronal numbers and absence of TDP-43 pathology in the lumbar spinal cords and the brains of Optn<sup>470T</sup> mice, which is in line with the absence of motor and cognitive deficits. The absence of neurodegeneration and/or TDP-43 pathology was also reported for Optn<sup>-/-</sup> (Y. Ito et al., 2016; Dermentzaki et al., 2019), *Tbkl*<sup>+/-</sup> (Bruno et al., 2020) and TBK1<sup>E696K</sup> (Brenner et al., 2024) mice during aging. The exceptions were Kurashige *et al.* and D. Liu *et al.* with the findings in the spinal cord of Optn<sup>-/-</sup> and glutamatergic neuron-specific Optn<sup>470T</sup> mice, respectively. The former showed neurodegeneration and TDP-43 aggregation in the spinal cord, whereas the latter showed only neurodegeneration (Kurashige et al., 2021; D. Liu et al., 2025). It is worth mentioning that both of these mouse models are of mixed genetic backgrounds, which are susceptible to certain diseases, as described above. Regarding the TDP-43 pathology, Kurashige *et al.* have used N-terminal TDP-43 antibody, for which we have shown an unusual diffuse cytoplasmic staining of motor neurons (Mohovic, Peradinovic et al., 2023). For this reason, we have additionally looked at potential pathology by using a C-terminal-specific TDP-43 antibody and an antibody against phospho-TDP-43<sup>Ser409</sup>, with the latter being specific for TDP-43 aggregates. TDP-43 was also not detected in insoluble fractions of Optn<sup>470T</sup> brains (Mohovic, Peradinovic et al., 2023). Our experiments thus showed the absence of TDP-43 pathology by several complementary methods. Similar to optineurin and TBK1, mutations in *C9ORF72* were found to be loss-of-function (DeJesus-Hernandez et al., 2011). Since ALS affects motor neurons, mice with C9orf72-specific knockout in neurons were generated (Koppers et al., 2015). In contrast to glutamatergic neuron-specific Optn<sup>470T</sup>, the neuron-specific deletion of *C9orf72* in mice did not result in neurodegeneration and TDP-43 pathology, possibly suggesting a distinct disease mechanism. We have also measured the aging-induced accumulation of lipofuscin in the motor cortex and the lumbar spinal cord and have shown no differences between WT and Optn<sup>470T</sup> mice. In conclusion, many physiological ALS mouse models carrying mutations in *Tbkl*, *Optn* or *C9orf72*, unlike the models with transgenic overexpression (ex. SOD1-G93A model) do not recapitulate typical ALS/FTD neuropathology in terms of TDP-43 aggregation and neurodegeneration. This suggests that presence of mutations in other ALS-linked genes and/or stressors is needed to precipitate the disease in mice.

Since neuroinflammation is one of the major hallmarks of ALS and inflammatory signaling was proposed to be directly affected by *OPTN* mutations, we analyzed astrocyte and microglial activation in the spinal cords and the brains of *Optn*<sup>470T</sup> mice during aging. In the spinal cord of *Optn*<sup>470T</sup> mice we observed a slight aging-induced increase in GFAP expression by immunofluorescence, but a decrease on western blot, whereas in the brain no differences were found. In aged mice and rats, astrocyte activation increases with aging, which is usually measured by GFAP expression and cell number (Sandhir et al., 2008; Boisvert et al., 2018; Tsesmelis et al., 2023). The discrepancy in GFAP expression for the spinal cord obtained by western blot and immunofluorescence could not be explained at the moment and should be further studied by comparing three- and 24-month-old mice. To analyze astrocyte activation in more depth, combination of GFAP, glutamine synthetase and Ki67 will be used, since those represent markers of proliferative astrocytes (Escartin et al., 2021). For the brain, the lack of difference in GFAP expression during aging may be caused by the region-specific GFAP expression induced by aging (Boisvert et al., 2018). This could be improved by using homogenate of a specified brain region, instead of the whole brain homogenate. The next sign of neuroinflammation that we analyzed is microgliosis, which was increased during aging in the spinal cord and the brain and was more prominent when three-month-old mice were compared to 24-month-old mice, which is in line with previous findings in mice and rats (Xie et al., 2013; Bruno et al., 2020; Jin et al., 2021). Optineurin insufficiency did not alter astrocyte and microglial activation during aging. The absence of exaggerated neuroinflammation was previously reported in *Optn*<sup>-/-</sup> mice (Slowicka et al., 2016b) and other mouse models such as *Tbkl*<sup>+/-</sup> (Bruno et al., 2020; Brenner et al., 2024) and mice with neuron-specific knockout of *C9orf72* (Koppers et al., 2015), suggesting that loss-of-function mutations in immune-regulating genes are not sufficient to alter aging-induced neuroinflammation in mice. We have also analyzed the levels of TNF and IFN- $\beta$  and found that their secretion was not impaired in *Optn*<sup>470T</sup> mice. However, the opposite was found for TNF levels in spinal cords of *Optn*<sup>-/-</sup> mice, where its level was increased by 15% compared to WT mice (Y. Ito et al., 2016), which may be the result from different optineurin mutation. Indeed, the differences between results obtained from *Optn*<sup>470T</sup> and *Optn*<sup>-/-</sup> could suggest that protein insufficiency and deficiency may have a distinct impact on the disease pathogenesis. However, the direct reason for discrepancies between optineurin deficiency and insufficiency mouse models cannot be made since different analyses were performed in those mice. In addition, some groups derived their own *Optn*<sup>-/-</sup> mouse

by deleting different exons (e.g. Kurashige *et al.* vs Ito *et al.*), which may be the reason for differences between those groups. For example, the previous study has shown that floxing of exons 2 and 3 did not lead to optineurin deletion, but rather N-terminal truncation Optn<sup>Δ157</sup> due to the presence of an alternative open reading frame (Meena et al., 2016). Notably, we were the first who analyzed optineurin levels during aging. The levels of WT protein increased during aging, whereas the truncated form (Optn<sup>470T</sup>) did not. This may be due to aging-induced inflammation, since an increase in optineurin levels were reported upon inflammatory stimulation (Sudhakar et al., 2009; J. Wang et al., 2021). This increase in WT optineurin protein levels could perhaps suggest its protective function in terms of preventing cytokine and chemokine imbalance, reported for its insufficiency (Markovinovic et al., 2018).

### **5.1.2. Optineurin insufficiency did not alter phagocytosis in primary myeloid cells**

Here we have shown that optineurin insufficiency did not impair phagocytosis in primary BMDMs and primary neonatal microglia in basal conditions and upon LPS-induced inflammation. The similar was shown by Frakes *et al.*, where they have shown that primary neonatal microglia from SOD1<sup>G93A</sup> mice did not exhibit toxic ALS-linked features, whereas adult microglia did (Frakes et al., 2014). We observed a decreased percentage of phagocytic cells during aging, which is consistent with previous findings (Natrajan et al., 2015; Wong et al., 2017), but optineurin insufficiency did not additionally affect it. LPS led to an increased accumulation of phagocytosed material, which was more pronounced in aged BMDMs. During phagocytosis in LPS-induced inflammatory conditions, TNF and IL-10 secretion were increased, whereas their concentration dropped during aging, which was more pronounced for TNF. In contrast, monocyte-derived microglia-like cells from sporadic ALS patients have shown decreased phagocytosis (Quek et al., 2022). In line with that study, primary adult microglia isolated from SOD1<sup>G93A</sup> spinal cords at symptomatic stage also showed decreased phagocytosis (Barreto-Núñez et al., 2024). Therefore, decreased phagocytosis may represent a novel ALS hallmark. Although our data suggest no effect of optineurin in phagocytosis, the drawback of our study is the lack of data on primary microglia isolated from aged Optn<sup>470T</sup> mice due to a technical problem of high autofluorescence of aged microglia, which precluded the flow cytometry-based microglia sorting (Mohovic, Peradinovic et

al., 2023). We plan to overcome this problem by isolating adult microglia by anti-CD11b beads, a specific marker of microglia in the brain.

### 5.1.3. The role of optineurin in splenic T cell polarization during aging

Pro-inflammatory T cell polarization was reported in the blood of ALS patients (Béland et al., 2020), so we performed analysis of T cell populations in the peripheral lymphoid tissues (spleens) of Optn<sup>470T</sup> mice during aging. We have previously reported a similar number and percentages of CD4<sup>+</sup> and CD8<sup>+</sup> T cells in the spleens of aged Optn<sup>470T</sup> and WT mice (Mohovic, Peradinovic et al., 2023). Here, we analyzed different T cell subsets based on cytokine production upon stimulation with PMA/Iono. We have observed an aging-induced increase in CD4<sup>+</sup>IFN- $\gamma$ <sup>+</sup> and CD4<sup>+</sup>TNF<sup>+</sup>IFN- $\gamma$ <sup>+</sup> in WT mice, which was unaffected in Optn<sup>470T</sup> male mice. However, although the CD4<sup>+</sup>TNF<sup>+</sup> cell percentages were similar at all time points in WT male mice, we found an aging-induced decline in CD4<sup>+</sup>TNF<sup>+</sup> cells in 24-month-old Optn<sup>470T</sup> males. CD4<sup>+</sup>IL-17A<sup>+</sup> T cell percentage was also significantly lower in 24-month-old Optn<sup>470T</sup> males compared to WT males. In ALS patients and SOD1<sup>G93A</sup> mice, it was reported that the presence of T<sub>H1</sub> (that produce TNF and IFN- $\gamma$ ) and T<sub>H17</sub> (that produce IL-17A) cells was increased (Beers et al., 2011; Saresella et al., 2013). Here, such proinflammatory T cell polarization was absent, which is in line with the absence of ALS disease phenotype. In contrast, the decrease of T<sub>H17</sub> cells in Optn<sup>470T</sup> males is in line with the study in which optineurin was specifically deleted in dendritic cells (Optn<sup>ADC</sup>), where the phenotype was proposed to be linked to lower expression of co-stimulatory molecules (CD80, CD86 and MHC-II) (J. Wang et al., 2021). However, we have shown an increased expression of CD86 and MHC-II in cDC in Optn<sup>470T</sup> males during aging (Mohovic, Peradinovic et al., 2023), therefore the exact link between T cell priming from DC cells in Optn<sup>470T</sup> mice is still inconclusive. Additionally, the amounts of produced TNF, IFN- $\gamma$  and IL-17A were generally unaffected by optineurin insufficiency. The prominent cytokine produced upon T cell stimulation with PMA/Iono is IL-2 (Brignall et al., 2017). The production and percentages of CD4<sup>+</sup>IL-2<sup>+</sup> cells were unaffected by optineurin insufficiency in male mice, suggesting normal response to T cell activation. In females, an increase in CD4<sup>+</sup>IFN- $\gamma$ <sup>+</sup> and CD4<sup>+</sup>TNF<sup>+</sup>IFN- $\gamma$ <sup>+</sup> cell percentage was present in both genotypes, whereas a decrease in CD4<sup>+</sup>TNF<sup>+</sup> and CD4<sup>+</sup>IL-17A<sup>+</sup> cells was absent, suggesting differences between sexes.

In contrast to CD4 T cells, an increase in CD8<sup>+</sup>TNF<sup>+</sup> cell percentage was observed in Optn<sup>470T</sup> male mice, whereas a strong aging-induced increase in CD8<sup>+</sup>IFN- $\gamma$ <sup>+</sup> and CD8<sup>+</sup>TNF<sup>+</sup>IFN- $\gamma$ <sup>+</sup> cell percentage was similar to WT males. The latter is in line with increased CD8<sup>+</sup>IFN- $\gamma$ <sup>+</sup> cell percentage during aging (Yi et al., 2019). CD8<sup>+</sup>IL-2<sup>+</sup> T cell percentage increased during aging and was not altered in Optn<sup>470T</sup> mice. The amount of cytokines on the per cell basis was unaffected in Optn<sup>470T</sup> males. In females, similar findings were observed, with less pronounced increase in CD8<sup>+</sup>TNF<sup>+</sup>IFN- $\gamma$ <sup>+</sup> cell percentage, probably due to sex differences and low number of replicates. In future studies we need to include additional female mice to be able us to conclude this issue. The role of CD8<sup>+</sup> T cells in the blood of ALS patients is still controversial, with opposing findings reported (De Marchi et al., 2021). However, in SOD1<sup>G93A</sup> mouse model, depletion of CD8<sup>+</sup> T cells was linked to decreased motor neuron death, without an effect on survival (Coque et al., 2019). In addition, they have found a similar IFN- $\gamma$  secretion between SOD1<sup>G93A</sup> and WT mice, suggesting that alteration in cytokine profile of CD8<sup>+</sup> T cells is not affected in ALS. Altogether, Optn<sup>470T</sup> mice did not develop an altered cytokine profile of CD8<sup>+</sup> T cells, which was reported in other ALS mouse models.

## **5.2. Characterization of a novel double-hit ALS/FTD mouse model during aging and upon inflammation**

### **5.2.1. Optineurin insufficiency reduces TDP-43 levels in the brains of TDP-43<sup>G348C</sup> mice**

Due to the absence of an ALS/FTD-like phenotype in Optn<sup>470T</sup> mice, we crossed them with TDP-43<sup>G348C</sup>, and we successfully obtained a novel model that carries two mutations (Optn<sup>470T</sup>/TDP-43<sup>G348C</sup> mice). We successfully confirmed all the genotypes by PCR. Next, we analyzed optineurin expression and confirmed the presence of WT and Optn<sup>470T</sup> bands, whose expression was not affected by the presence of TDP-43<sup>G348C</sup> transgene. Perhaps surprisingly, we found that TDP-43 levels were reduced in the brains of 3-4-month-old Optn<sup>470T</sup>/TDP-43<sup>G348C</sup> mice. This contrasts our findings in individual cell subsets isolated from Optn<sup>470T</sup> mouse brains, where we have shown increased TDP-43 levels in primary neonatal microglia and embryonic neurons (Prtenjaca et al., 2022; Mohović, 2023). It is important to note that those primary cells did not overexpress TDP-43. This may be in line with findings reported by Brenner *et al.*, where they have reported that

TBK1 haploinsufficiency in  $SOD1^{G93A}$  mouse model ( $SOD1^{G93A}/Tbkl^{+/-}$  mice) had toxic effects at the early stage, which transformed to a protective one at the late stage of the disease (Brenner et al., 2019). In more detail, the authors proposed that the reasons behind this were defective autophagy in the early stage and decreased neuroinflammation in the late stage of the disease in  $SOD1^{G93A}/Tbkl^{+/-}$  mice. This could explain the differences between CNS-derived primary cells from embryonic or neonatal stage compared to adult brains. Additionally, the *in vivo* and *in vitro* results may differ due to the lack of complex cell-to-cell communication in the latter. This will be further tested by immunofluorescence analysis of TDP-43 expression and aggregation in the brains, primary cells and organotypic brain slices derived from TDP-43<sup>G348C</sup> and Optn<sup>470T</sup>/TDP-43<sup>G348C</sup> mice. We speculate to find increased TDP-43 levels in embryonic/neonatal primary cells but decreased levels at the adult CNS tissue level of Optn<sup>470T</sup>/TDP-43<sup>G348C</sup> mice. Notably, the lower levels of TDP-43 transgene in Optn<sup>470T</sup>/TDP-43<sup>G348C</sup> mice could perhaps explain their improved cognitive functions during aging, and their resistance to death during the LPS challenge (further discussed below).

### **5.2.2. Optineurin insufficiency decreased LPS-induced TBK1 signaling in TDP-43<sup>G348C</sup> BMDMs and led to increased baseline I $\kappa$ B- $\alpha$ levels without affecting LPS-induced NF- $\kappa$ B signaling**

Prior to testing the role of optineurin in TDP-43<sup>G348C</sup> BMDMs, we first wanted to test the effect of TDP-43<sup>G348C</sup> transgene alone on the NF- $\kappa$ B and TBK1 signaling. The NF- $\kappa$ B pathway has been previously analyzed in that mouse model, but TBK1 pathway has not been studied (Swarup et al., 2011b). We have shown similar NF- $\kappa$ B activation and TNF production in TDP-43<sup>G348C</sup> and WT BMDMs. This contrasts the findings of Swarup *et al.*, since they have shown that TDP-43 acts as a co-activator of p65. Specifically, they demonstrated that an overexpression of WT or mutant TDP-43 in BV2 cells and primary myeloid cells (neonatal microglia and BMDMs) resulted in increased activation of the NF- $\kappa$ B signaling upon LPS stimulation (Swarup et al., 2011b). The reason may be genetic background, since these mice were of mixed C57BL/6, ICR and C3H genetic background, and the number of backcrossing on C57BL/6 background was unmentioned. Additionally, C3H mice were reported to have a mutation in TLR4 (PRR that senses LPS), making those mice more resistant to stimulation. Therefore, the effect of C3H background on primary cells

may be the reason for the difference in signaling. Another potential reason may be due to analysis of different time points. Here we performed more detailed analyses by western blot, RT-qPCR and ELISA, which strengthens our conclusions. For TBK1 signaling, we have also shown normal TBK1 activation and IFN- $\beta$  production in BMDMs derived from TDP-43<sup>G348C</sup> mice compared to WT. This is in contrast to findings obtained from MEF and THP-1 (human monocyte cell line) cells overexpressing other TDP-43 mutants, such as TDP-43<sup>WT</sup> or TDP-43<sup>Q331K</sup>, where an increased IFN- $\beta$  production was observed due to mitochondrial DNA-mediated activation of stimulator of interferon genes (STING) (Yu et al., 2020). This was also corroborated in the brains of transgenic TDP-43<sup>A315T</sup> mouse model by the same group. Overproduction of IFN- $\beta$  was also reported in an SOD1<sup>G85R</sup> mice due to STING overactivation, strengthening the toxic effect of high IFN- $\beta$  levels (Tan et al., 2022). Therefore, the difference in mutated gene may result in a different phenotype and related neuropathology. Also, the effect may be cell-specific, so the analysis of IFN- $\beta$  expression in the CNS or isolated primary cells (microglia, embryonic neurons) from TDP-43<sup>G348C</sup> mice are needed to corroborate these results.

Next, we performed the same analyses in TDP-43<sup>G348C</sup> and Optn<sup>470T</sup>/TDP-43<sup>G348C</sup> BMDMs, where we have found increased basal levels of I $\kappa$ B- $\alpha$ . I $\kappa$ B- $\alpha$  has an inhibitory effect on the NF- $\kappa$ B activation (Beg et al., 1992) and its increased expression was shown to correlate with decreased microglial activation after stroke in mice (Lalancette-Hébert et al., 2007). However, LPS-stimulated NF- $\kappa$ B activation and TNF production were not affected in Optn<sup>470T</sup>/TDP-43<sup>G348C</sup> BMDMs, suggesting that increased I $\kappa$ B- $\alpha$  levels in the basal state did not affect overall signaling, at least not in this setting. In TBK1 signaling pathway, optineurin insufficiency led to a decreased TBK1 signaling activation (measured by its autophosphorylation on serine 172) and IFN- $\beta$  production, which is consistent with other findings in primary cells derived from Optn<sup>-/-</sup>, Optn<sup>D477N</sup> and Optn<sup>470T</sup> (Gleason et al., 2011; Munitic et al., 2013; Obaid et al., 2015; Pourcelot et al., 2016; Slowicka et al., 2016b; Markovinovic et al., 2018), confirming the role of optineurin as a positive regulator of TBK1 signaling. Therefore, BMDMs generated from double-mutant Optn<sup>470T</sup>/TDP-43<sup>G348C</sup> mice exhibited activation of TBK1 signaling similar to cells from Optn<sup>470T</sup> mice. Altogether, TDP-43<sup>G348C</sup> overexpression did not affect the role of optineurin in inflammatory signaling.

### 5.2.3. **Optn<sup>470T</sup>/TDP-43<sup>G348C</sup> mice showed decreased body weight, but improved motor and cognitive functions compared to TDP-43<sup>G348C</sup> mice**

Optn<sup>470T</sup>/TDP-43<sup>G348C</sup> mice have shown decreased body weight compared to Optn<sup>470T</sup> and TDP-43<sup>G348C</sup> mice of the same age. We have recently shown that the body weight of Optn<sup>470T</sup> at 12 months of age was lower compared to WT mice, whereas the difference was lost at 24 months (Mohovic, Peradinovic et al., 2023). The loss of difference in aging mice can perhaps explain the lack of significance between WT and Optn<sup>470T</sup> mice in this study, which was done in 18-month-old mice. For TDP-43<sup>G348C</sup> mice, no data about weight was reported (Swarup et al., 2011) and we observed no significant difference in body weight compared to WT mice. In contrast, TDP-43<sup>A315T</sup> started to lose body weight from 4.5 months of age onwards and had shorter survival, which was attributed to neurodegeneration in the myenteric plexus (Herdewyn et al., 2014; Wegorzewska et al., 2009). The exact reason for lower body weight of Optn<sup>470T</sup>/TDP-43<sup>G348C</sup> mice is still unknown and presents an interesting observation for further studies. Notably, it was shown that the downregulation of TDP-43 and TBK1 affected metabolism in mice (Chiang et al., 2010; Cruz et al., 2018). Since TBK1 activation is decreased in cells with optineurin truncation, we may expect a similar effect to TBK1 deletion on metabolism in mice carrying Optn<sup>470T</sup> truncation. Additionally, the presence of Optn<sup>470T</sup> and TDP-43<sup>G348C</sup> mutations alone might not have an effect, whereas while present in the same mouse, a synergistic effect on metabolism may be achieved. This effect will be further investigated by metabolic screening including analysis of blood or urine glucose levels and liver histology. When tested on rotarod, neither Optn<sup>470T</sup>/TDP-43<sup>G348C</sup> mice nor TDP-43<sup>G348C</sup> mice developed motor deficits. This is in contrast with a previous finding where *TDP-43<sup>G298S</sup>/Tbkl<sup>+/-</sup>* have shown increased motor impairment compared to *TDP-43<sup>G298S</sup>* mice, but only in several time points (Sieverding et al., 2021). The explanation for our findings may be that we tested our mice at 18 months of age, the time point at which *TDP-43<sup>G298S</sup>/Tbkl<sup>+/-</sup>* mice also did not show impaired motor capabilities, meaning that our mice may have had a phenotype in other time points, which we missed. Other explanations may include different microbiome in our mouse facility and genetic background. On the contrary, grid-hanging test revealed that Optn<sup>470T</sup>/TDP-43<sup>G348C</sup> mice had increased time of hanging, which indicates improvement of motor functions. On the other hand, this is surprising because we expected that the presence of two ALS-linked mutations would aggravate motor function. The possible rescue of phenotype may be due to the decrease of TDP-43<sup>G348C</sup> protein levels in the brains of Optn<sup>470T</sup>/TDP-43<sup>G348C</sup> mice reported in



figure 23, but this needs to be confirmed in aged mice. Improved hanging time of Optn<sup>470T</sup>/TDP-43<sup>G348C</sup> mice may have also resulted from lower body weight. Another explanation may be a decreased denervation at the NMJ levels, which will be analyzed in the tibialis anterior muscle. We have also analyzed FTD signs by novel object recognition test and observed a decrease in cognitive function of TDP-43<sup>G348C</sup> mice, which is consistent with previous finding (Kumar et al., 2021). Surprisingly, we have observed improved cognition of Optn<sup>470T</sup>/TDP-43<sup>G348C</sup> mice compared to TDP-43<sup>G348C</sup> mice. This unexpected finding has to be further explored by the analysis of neuronal number, TDP-43 pathology and neuroinflammation in the hippocampus, a region responsible for memory. Notably, these results are in line with findings by Brenner *et al.*, where they have reported that TBK1 haploinsufficiency had toxic effect at early stage, which transformed to protective one later in the disease course of SOD1<sup>G93A</sup> mice (Brenner et al., 2019). To test this, we will assess motor and cognitive abilities of young Optn<sup>470T</sup>/TDP-43<sup>G348C</sup> mice.

#### **5.2.4. Compared to TDP-43<sup>G348C</sup> mice, Optn<sup>470T</sup>/TDP-43<sup>G348C</sup> mice had prolonged survival and decreased splenocyte number, without difference in innate immune cell activation and cytokine profiles upon *in vivo* three-day LPS administration**

We have performed a three-day intraperitoneal LPS stimulation of 18-month-old Optn<sup>470T</sup>/TDP-43<sup>G348C</sup> mice due to two reasons: 1) single intraperitoneal dose of LPS revealed a disbalance in inflammatory marker expression in the brains of Optn<sup>470T</sup> mice, without a difference in microglial activation (Markovinovic et al., 2018); 2) TDP-43<sup>G348C</sup> mice have shown the signs of neuroinflammation and increased pro-inflammatory marker expression in the spinal cords at 10 months of age (Swarup et al., 2011). Therefore, we expected that consecutive LPS administration would result in the breakdown of immune regulation in Optn<sup>470T</sup>/TDP-43<sup>G348C</sup> mice. We opted for a three-day LPS stimulation, since it was reported that chronic LPS stimulation led to nuclear loss of TDP-43 (Correia et al., 2015). We observed a stronger body weight loss in mice with optineurin truncation, whereas Optn<sup>470T</sup>/TDP-43<sup>G348C</sup> mice were more resistant to weight loss on the third day. However, an LPS-induced temperature drop of Optn<sup>470T</sup>/TDP-43<sup>G348C</sup> mice was not altered compared to other genotypes. TDP-43<sup>G348C</sup> mice showed higher mortality and weight loss upon LPS administration, which was rescued in Optn<sup>470T</sup>/TDP-43<sup>G348C</sup> mice. The increased death rate of TDP-43<sup>G348C</sup> mice may be explained by already reported increased levels of pro-inflammatory

markers (Swarup et al., 2011) and higher TDP-43<sup>G348C</sup> protein levels, as well by our observation of increased IL-6 levels in the brains and sera (data not shown), a cytokine associated with mortality (Baune et al., 2011). These cytokines could have been affected by optineurin insufficiency.

To study the reasons behind the increased survival of Optn<sup>470T</sup>/TDP-43<sup>G348C</sup> mice, we have analyzed splenic immune cell populations. We have observed unchanged T cell numbers in Optn<sup>470T</sup>/TDP-43<sup>G348C</sup> mice but found a significant decrease in B cells. This likely also explains the decreased number of splenocytes observed in those mice given that the B cells normally comprise the largest spleen cell subset. Since the mice were stimulated with LPS (stimulator of innate immune cells) and not bacteria, we did not expect such a large effect on the adaptive immune cells. It is possible that the B cell numbers were affected even prior to LPS treatment, so in future experiments spleens from Optn<sup>470T</sup>/TDP-43<sup>G348C</sup> mice will be analyzed in the basal state over time. We next analyzed innate immune cells and their activation, where we observed unchanged macrophage number and activation marker expression in the spleens of Optn<sup>470T</sup>/TDP-43<sup>G348C</sup> mice compared to Optn<sup>470T</sup> and TDP-43<sup>G348C</sup> mice. In contrast, cDC numbers were lower in Optn<sup>470T</sup>/TDP-43<sup>G348C</sup> mice, which was also reported in ALS patients (Rusconi et al., 2017). Nevertheless, the activation marker expression was unchanged. Neutrophil numbers and percentages were unchanged in Optn<sup>470T</sup>/TDP-43<sup>G348C</sup> mice, whereas NK cell numbers were decreased. These findings differ to findings in ALS patients, where increased numbers of neutrophils and NK cells were found (Murdock et al., 2016, 2017). It is important to note that the reason for discrepancies found between LPS-stimulated mice and ALS patients may be because ALS patients were analyzed in the absence of inflammation induced by bacterial agents. Overall, our results suggest that three-day LPS administration of Optn<sup>470T</sup>/TDP-43<sup>G348C</sup> mice recapitulated ALS-like innate immune profile only for dendritic cell number, whereas other cell types remained unaffected. However, to make a final conclusion, analysis of unadministered mice will be done to see how and if LPS administration made a change in immune cell repertoire.

To additionally address the potential reasons for prolonged survival of Optn<sup>470T</sup>/TDP-43<sup>G348C</sup> mice upon three-day LPS challenge, we analyzed cytokine and chemokine concentrations in the sera, brains and spinal cords upon three-day LPS administration. We did not find an alteration in concentrations of CXCL10, CXCL1 and IFN- $\gamma$ . It was unexpected that CXCL10 and CXCL1

levels were not dysbalanced in the brains and spinal cords of Optn<sup>470T</sup> mice, since their levels were reported to be down- and upregulated upon LPS stimulation, respectively (Markovinovic et al., 2018; Markovinović, 2019). The reason may be the difference in time points, since Markovinovic *et al.* have analyzed CXCL10 and CXCL1 24 h after LPS stimulation. Therefore, in future experiments, an analysis of those cytokines will be performed at an earlier time point as well. CCL2, was found to be elevated in the sera of TDP-43<sup>G348C</sup> mice, but not Optn<sup>470T</sup>/TDP-43<sup>G348C</sup> mice. In SOD1<sup>G85R</sup> mouse model was shown that the administration of an antibody against CCL2 prolonged survival (Tan et al., 2022). Therefore, elevated CCL2 levels may be the reason for earlier LPS-induced mortality of TDP-43<sup>G348C</sup> mice. Lastly, IL-10 was detected only in the serum and slightly increased in the presence of TDP-43<sup>G348C</sup> transgene but decreased in the presence of Optn<sup>470T</sup> truncation. The former recapitulates increased IL-10 levels in SOD1<sup>G93A</sup> mouse model upon LPS administration (Gravel et al., 2016), whereas the latter confirms the finding of decreased IL-10 levels in Optn<sup>470T</sup> primary neonatal microglia (Markovinovic et al., 2018). In conclusion, three-day LPS administration led to a disbalance of only CCL2 and IL-10 in the serum, whereas other cytokines and chemokines remained unaffected. Therefore, an ALS-like cytokine profile was not fully recapitulated. We will perform analyses of cytokines and chemokines at earlier time points because the peak of cytokine concentrations (e.g. TNF, IL-6, IFN- $\beta$ ), which regulate chemokine expression, usually occurs 1.5 to 3 h upon LPS stimulation and by 24 h their impact may be missed. Therefore, current cytokine analyses did not answer our question for the prolonged survival of Optn<sup>470T</sup>/TDP-43<sup>G348C</sup> mice. Other reasons for prolonged survival could be the decreased levels of TDP-43<sup>G348C</sup> protein expression, which will be confirmed by immunofluorescence of the brain and the spinal cord slices.

## 6. Conclusions

- 1) Optn<sup>470T</sup> mice have shown similar motor and cognitive functions to WT mice during aging.
- 2) Aging of Optn<sup>470T</sup> mice did not trigger ALS-like neuropathology, such as exacerbated loss of (motor) neurons, TDP-43 cytoplasmic aggregation and increased lipofuscin accumulation.
- 3) Aging led to an increase of WT, but not truncated form of optineurin.
- 4) Aging-induced neuroinflammation (measured by microglial and astrocyte activation and cytokine content) in the spinal cord and brain was unaffected by optineurin insufficiency.
- 5) Optineurin insufficiency did not affect phagocytosis of primary BMDMs and neonatal microglia.
- 6) Aged Optn<sup>470T</sup> male mice had increased CD4<sup>+</sup> T<sub>H17</sub> cell polarization and decreased percentage of CD8<sup>+</sup> TNF<sup>+</sup> T cells.
- 7) TDP-43<sup>G348C</sup> protein levels were decreased in Optn<sup>470T</sup>/TDP-43<sup>G348C</sup> mice compared to TDP-43<sup>G348C</sup> mice.
- 8) Upon LPS stimulation TDP-43<sup>G348C</sup> BMDMs showed normal NF-κB and TBK1 signaling, whereas Optn<sup>470T</sup>/TDP-43<sup>G348C</sup> mice showed unaffected NF-κB and decreased TBK1 signaling; the latter is reminiscent to the findings in primary Optn<sup>470T</sup> BMDMs, BMDCs and microglia, suggesting the absence of an effect of TDP-43<sup>G348C</sup> transgene on these signaling pathways.
- 9) Optineurin insufficiency resulted in decreased body weight and improved motor and cognitive functions of TDP-43<sup>G348C</sup> mice.
- 10) Optineurin truncation ameliorated sickness behavior and improved survival of TDP-43<sup>G348C</sup> mice upon LPS administration.
- 11) LPS-administered Optn<sup>470T</sup>/TDP-43<sup>G348C</sup> mice had lower numbers of splenic B cells, and classical dendritic and NK cells compared to Optn<sup>470T</sup> mice.
- 12) CCL2 and IL-10 serum levels were increased in TDP-43<sup>G348C</sup> and Optn<sup>470T</sup>/TDP-43<sup>G348C</sup> mice upon LPS administration, respectively.

## 7. Literature

001800—FVB Strain Details. (n.d.). Retrieved March 8, 2025, from <https://www.jax.org/strain/001800>

002448—129S1 Strain Details. (n.d.). Retrieved March 8, 2025, from <https://www.jax.org/strain/002448>

Abe, K., Aoki, M., Tsuji, S., Itoyama, Y., Sobue, G., Togo, M., Hamada, C., Tanaka, M., Akimoto, M., Nakamura, K., Takahashi, F., Kondo, K., Yoshino, H., Abe, K., Aoki, M., Tsuji, S., Itoyama, Y., Sobue, G., Togo, M., ... Yoshino, H. (2017). Safety and efficacy of edaravone in well defined patients with amyotrophic lateral sclerosis: A randomised, double-blind, placebo-controlled trial. *The Lancet Neurology*, 16(7), 505–512. [https://doi.org/10.1016/S1474-4422\(17\)30115-1](https://doi.org/10.1016/S1474-4422(17)30115-1)

Agrawal, A., & Gupta, S. (2011). Impact of aging on dendritic cell functions in humans. *Ageing Research Reviews*, 10(3), 336–345. <https://doi.org/10.1016/j.arr.2010.06.004>

Ahmad, L., Zhang, S.-Y., Casanova, J.-L., & Sancho-Shimizu, V. (2016). Human TBK1: A Gatekeeper of Neuroinflammation. *Trends in Molecular Medicine*, 22(6), 511–527. <https://doi.org/10.1016/j.molmed.2016.04.006>

Akçimen, F., Lopez, E. R., Landers, J. E., Nath, A., Chiò, A., Chia, R., & Traynor, B. J. (2023). Amyotrophic lateral sclerosis: Translating genetic discoveries into therapies. *Nature Reviews Genetics*, 24(9), 642–658. <https://doi.org/10.1038/s41576-023-00592-y>

Akizuki, M., Yamashita, H., Uemura, K., Maruyama, H., Kawakami, H., Ito, H., & Takahashi, R. (2013). Optineurin suppression causes neuronal cell death via NF-κB pathway. *Journal of Neurochemistry*, 126(6), 699–704. <https://doi.org/10.1111/jnc.12326>

Al-Chalabi, A., Andersen, P. M., Chandran, S., Chio, A., Corcia, P., Couratier, P., Danielsson, O., De Carvalho, M., Desnuelle, C., Grehl, T., Grosskreutz, J., Holmøy, T., Ingre, C., Karlsborg, M., Kleveland, G., Christoph Koch, J., Koritnik, B., KuzmaKozakiewicz, M., Laaksovirta, H., ... Van Den Berg, L. H. (2017). July 2017 ENCALs statement on edaravone. *Amyotrophic Lateral Sclerosis and Frontotemporal Degeneration*, 18(7–8), 471–474. <https://doi.org/10.1080/21678421.2017.1369125>

Al-Chalabi, A., Calvo, A., Chio, A., Colville, S., Ellis, C. M., Hardiman, O., Heverin, M., Howard, R. S., Huisman, M. H. B., Keren, N., Leigh, P. N., Mazzini, L., Mora, G., Orrell, R. W., Rooney, J., Scott, K. M., Scotton, W. J., Seelen, M., Shaw, C. E., ... Pearce, N. (2014). Analysis of amyotrophic lateral sclerosis as a multistep process: A population-based modelling study. *The Lancet Neurology*, 13(11), 1108–1113. [https://doi.org/10.1016/S1474-4422\(14\)70219-4](https://doi.org/10.1016/S1474-4422(14)70219-4)

Al-Chalabi, A., & Lewis, C. M. (2011). Modelling the Effects of Penetrance and Family Size on Rates of Sporadic and Familial Disease. *Human Heredity*, 71(4), 281–288. <https://doi.org/10.1159/000330167>

Anborgh, P. H., Godin, C., Pampillo, M., Dhami, G. K., Dale, L. B., Cregan, S. P., Truant, R., & Ferguson, S. S. G. (2005). Inhibition of Metabotropic Glutamate Receptor Signaling by the Huntingtin-binding Protein Optineurin. *Journal of Biological Chemistry*, 280(41), 34840–34848. <https://doi.org/10.1074/jbc.M504508200>

Andrews, J. A., Jackson, C. E., Heiman-Patterson, T. D., Bettica, P., Brooks, B. R., & Pioro, E. P. (2020). Real-world evidence of riluzole effectiveness in treating amyotrophic lateral sclerosis. *Amyotrophic Lateral Sclerosis and Frontotemporal Degeneration*, 21(7–8), 509–518. <https://doi.org/10.1080/21678421.2020.1771734>

Arai, T., Hasegawa, M., Akiyama, H., Ikeda, K., Nonaka, T., Mori, H., Mann, D., Tsuchiya, K., Yoshida, M., Hashizume, Y., & Oda, T. (2006). TDP-43 is a component of ubiquitin-positive tau-negative inclusions in frontotemporal lobar degeneration and amyotrophic lateral sclerosis. *Biochemical and Biophysical Research Communications*, 351(3), 602–611. <https://doi.org/10.1016/j.bbrc.2006.10.093>

Arenzana-Seisdedos, F., Turpin, P., Rodriguez, M., Thomas, D., Hay, R. T., Virelizier, J.-L., & Dargemont, C. (1997). Nuclear localization of I kappa B alpha promotes active transport of NF-kappa B from the nucleus to the cytoplasm. *Journal of Cell Science*, 110(3), 369–378. <https://doi.org/10.1242/jcs.110.3.369>

Ayala, Y. M., De Conti, L., Avendaño-Vázquez, S. E., Dhir, A., Romano, M., D'Ambrogio, A., Tollervey, J., Ule, J., Baralle, M., Buratti, E., & Baralle, F. E. (2011). TDP-43 regulates its mRNA levels through a negative feedback loop. *The EMBO Journal*, 30(2), 277–288. <https://doi.org/10.1038/emboj.2010.310>

- Bang, J., Spina, S., & Miller, B. L. (2015). Frontotemporal dementia. *The Lancet*, 386(10004), 1672–1682. [https://doi.org/10.1016/S0140-6736\(15\)00461-4](https://doi.org/10.1016/S0140-6736(15)00461-4)
- Barreto-Núñez, R., Béland, L., Boutej, H., Picher-Martel, V., Dupré, N., Barbeito, L., & Kriz, J. (2024). Chronically activated microglia in ALS gradually lose their immune functions and develop unconventional proteome. *Glia*, 72(7), 1319–1339. <https://doi.org/10.1002/glia.24531>
- Baune, B. T., Rothermundt, M., Ladwig, K. H., Meisinger, C., & Berger, K. (2011). Systemic inflammation (Interleukin 6) predicts all-cause mortality in men: Results from a 9-year follow-up of the MEMO Study. *AGE*, 33(2), 209–217. <https://doi.org/10.1007/s11357-010-9165-5>
- Beers, D. R., & Appel, S. H. (2019). Immune dysregulation in amyotrophic lateral sclerosis: Mechanisms and emerging therapies. *The Lancet. Neurology*, 18(2), 211–220. [https://doi.org/10.1016/S1474-4422\(18\)30394-6](https://doi.org/10.1016/S1474-4422(18)30394-6)
- Beers, D. R., Henkel, J. S., Xiao, Q., Zhao, W., Wang, J., Yen, A. A., Siklos, L., McKercher, S. R., & Appel, S. H. (2006). Wild-type microglia extend survival in PU.1 knockout mice with familial amyotrophic lateral sclerosis. *Proceedings of the National Academy of Sciences*, 103(43), 16021–16026. <https://doi.org/10.1073/pnas.0607423103>
- Beers, D. R., Zhao, W., Liao, B., Kano, O., Wang, J., Huang, A., Appel, S. H., & Henkel, J. S. (2011). Neuroinflammation modulates distinct regional and temporal clinical responses in ALS mice. *Brain, Behavior, and Immunity*, 25(5), 1025–1035. <https://doi.org/10.1016/j.bbi.2010.12.008>
- Beers, D. R., Zhao, W., Wang, J., Zhang, X., Wen, S., Neal, D., Thonhoff, J. R., Alsuliman, A. S., Shpall, E. J., Rezvani, K., & Appel, S. H. (2017). ALS patients' regulatory T lymphocytes are dysfunctional, and correlate with disease progression rate and severity. *JCI Insight*, 2(5). <https://doi.org/10.1172/jci.insight.89530>
- Beg, A. A., Ruben, S. M., Scheinman, R. I., Haskill, S., Rosen, C. A., & Baldwin, A. S. (1992). I kappa B interacts with the nuclear localization sequences of the subunits of NF-kappa B: A mechanism for cytoplasmic retention. *Genes & Development*, 6(10), 1899–1913. <https://doi.org/10.1101/gad.6.10.1899>

Béland, L.-C., Markovinovic, A., Jakovac, H., De Marchi, F., Bilic, E., Mazzini, L., Kriz, J., & Munitic, I. (2020). Immunity in amyotrophic lateral sclerosis: Blurred lines between excessive inflammation and inefficient immune responses. *Brain Communications*, 2(2), fcaa124. <https://doi.org/10.1093/braincomms/fcaa124>

Boillée, S., Yamanaka, K., Lobsiger, C. S., Copeland, N. G., Jenkins, N. A., Kassiotis, G., Kollias, G., & Cleveland, D. W. (2006). Onset and Progression in Inherited ALS Determined by Motor Neurons and Microglia. *Science*, 312(5778), 1389–1392. <https://doi.org/10.1126/science.1123511>

Boisvert, M. M., Erikson, G. A., Shokhirev, M. N., & Allen, N. J. (2018). The Aging Astrocyte Transcriptome from Multiple Regions of the Mouse Brain. *Cell Reports*, 22(1), 269–285. <https://doi.org/10.1016/j.celrep.2017.12.039>

Brenner, D., Sieverding, K., Bruno, C., Lüningschrör, P., Buck, E., Mungwa, S., Fischer, L., Brockmann, S. J., Ulmer, J., Bliedehäuser, C., Philibert, C. E., Satoh, T., Akira, S., Boillée, S., Mayer, B., Sendtner, M., Ludolph, A. C., Danzer, K. M., Lobsiger, C. S., ... Weishaupt, J. H. (2019). Heterozygous Tbk1 loss has opposing effects in early and late stages of ALS in mice. *Journal of Experimental Medicine*, 216(2), 267–278. <https://doi.org/10.1084/jem.20180729>

Brenner, D., Sieverding, K., Srinidhi, J., Zellner, S., Secker, C., Yilmaz, R., Dyckow, J., Amr, S., Ponomarenko, A., Tunaboyle, E., Douahem, Y., Schlag, J. S., Rodríguez Martínez, L., Kislinger, G., Niemann, C., Nalbach, K., Ruf, W. P., Uhl, J., Hollenbeck, J., ... Weishaupt, J. H. (2024). A TBK1 variant causes autophagolysosomal and motoneuron pathology without neuroinflammation in mice. *Journal of Experimental Medicine*, 221(5), e20221190. <https://doi.org/10.1084/jem.20221190>

Brignall, R., Cauchy, P., Bevington, S. L., Gorman, B., Pisco, A. O., Bagnall, J., Boddington, C., Rowe, W., England, H., Rich, K., Schmidt, L., Dyer, N. P., Travis, M. A., Ott, S., Jackson, D. A., Cockerill, P. N., & Paszek, P. (2017). Integration of Kinase and Calcium Signaling at the Level of Chromatin Underlies Inducible Gene Activation in T Cells. *The Journal of Immunology*, 199(8), 2652–2667. <https://doi.org/10.4049/jimmunol.1602033>

Brown, R. H., & Al-Chalabi, A. (2017). Amyotrophic Lateral Sclerosis. *New England Journal of Medicine*, 377(2), 162–172. <https://doi.org/10.1056/NEJMra1603471>



Bruijn, L. I., Houseweart, M. K., Kato, S., Anderson, K. L., Anderson, S. D., Ohama, E., Reaume, A. G., Scott, R. W., & Cleveland, D. W. (1998). Aggregation and Motor Neuron Toxicity of an ALS-Linked SOD1 Mutant Independent from Wild-Type SOD1. *Science*, 281(5384), 1851–1854. <https://doi.org/10.1126/science.281.5384.1851>

Bruno, C., Sieverding, K., Freischmidt, A., Satoh, T., Walther, P., Mayer, B., Ludolph, A. C., Akira, S., Yilmazer-Hanke, D., Danzer, K. M., Lobsiger, C. S., Brenner, D., & Weishaupt, J. H. (2020). Haploinsufficiency of TANK-binding kinase 1 prepones age-associated neuroinflammatory changes without causing motor neuron degeneration in aged mice. *Brain Communications*, 2(2), fcaa133. <https://doi.org/10.1093/braincomms/fcaa133>

Bsibsi, M., Ravid, R., Gveric, D., & van Noort, J. M. (2002). Broad Expression of Toll-Like Receptors in the Human Central Nervous System. *Journal of Neuropathology & Experimental Neurology*, 61(11), 1013–1021. <https://doi.org/10.1093/jnen/61.11.1013>

Butovsky, O., Siddiqui, S., Gabriely, G., Lanser, A. J., Dake, B., Murugaiyan, G., Doykan, C. E., Wu, P. M., Gali, R. R., Iyer, L. K., Lawson, R., Berry, J., Krichevsky, A. M., Cudkowicz, M. E., & Weiner, H. L. (2012). Modulating inflammatory monocytes with a unique microRNA gene signature ameliorates murine ALS. *Journal of Clinical Investigation*, 122(9), 3063–3087. <https://doi.org/10.1172/JCI62636>

Chau, T.-L., Gioia, R., Gatot, J.-S., Patrascu, F., Carpentier, I., Chapelle, J.-P., O'Neill, L., Beyaert, R., Piette, J., & Chariot, A. (2008). Are the IKKs and IKK-related kinases TBK1 and IKK-ε similarly activated? *Trends in Biochemical Sciences*, 33(4), 171–180. <https://doi.org/10.1016/j.tibs.2008.01.002>

Chen, Z. J., Parent, L., & Maniatis, T. (1996). *Site-Specific Phosphorylation of IκBα by a Novel Ubiquitination-Dependent Protein Kinase Activity*. [https://doi.org/10.1016/s0092-8674\(00\)81064-8](https://doi.org/10.1016/s0092-8674(00)81064-8)

Chi, Z.-L., Akahori, M., Obazawa, M., Minami, M., Noda, T., Nakaya, N., Tomarev, S., Kawase, K., Yamamoto, T., Noda, S., Sasaoka, M., Shimazaki, A., Takada, Y., & Iwata, T. (2010). Overexpression of optineurin E50K disrupts Rab8 interaction and leads to a progressive retinal degeneration in mice. *Human Molecular Genetics*, 19(13), 2606–2615. <https://doi.org/10.1093/hmg/ddq146>

- Chiang, P.-M., Ling, J., Jeong, Y. H., Price, D. L., Aja, S. M., & Wong, P. C. (2010). Deletion of TDP-43 down-regulates Tbc1d1, a gene linked to obesity, and alters body fat metabolism. *Proceedings of the National Academy of Sciences*, 107(37), 16320–16324. <https://doi.org/10.1073/pnas.1002176107>
- Chiu, I. M., Phatnani, H., Kuligowski, M., Tapia, J. C., Carrasco, M. A., Zhang, M., Maniatis, T., & Carroll, M. C. (2009). Activation of innate and humoral immunity in the peripheral nervous system of ALS transgenic mice. *Proceedings of the National Academy of Sciences*, 106(49), 20960–20965. <https://doi.org/10.1073/pnas.0911405106>
- Clark, K., Pegg, M., Plater, L., Sorcek, R. J., Young, E. R. R., Madwed, J. B., Hough, J., McIver, E. G., & Cohen, P. (2011). Novel cross-talk within the IKK family controls innate immunity. *Biochemical Journal*, 434(1), 93–104. <https://doi.org/10.1042/BJ20101701>
- Clement, A. M., Nguyen, M. D., Roberts, E. A., Garcia, M. L., Boillee, S., Rule, M., McMahon, A. P., Doucette, W., Siwek, D., Ferrante, R. J., & Jr, R. H. B. (2003). *Wild-Type Nonneuronal Cells Extend Survival of SOD1 Mutant Motor Neurons in ALS Mice*. 302.
- Clucas, J., & Meier, P. (2023). Roles of RIPK1 as a stress sentinel coordinating cell survival and immunogenic cell death. *Nature Reviews Molecular Cell Biology*, 24(11), 835–852. <https://doi.org/10.1038/s41580-023-00623-w>
- Coque, E., Salsac, C., Espinosa-Carrasco, G., Varga, B., Degauque, N., Cadoux, M., Crabé, R., Virenque, A., Soulard, C., Fierle, J. K., Brodovitch, A., Libralato, M., Végh, A. G., Venteo, S., Scamps, F., Boucraut, J., Laplaud, D., Hernandez, J., Gergely, C., ... Raoul, C. (2019). Cytotoxic CD8<sup>+</sup> T lymphocytes expressing ALS-causing SOD1 mutant selectively trigger death of spinal motoneurons. *Proceedings of the National Academy of Sciences*, 116(6), 2312–2317. <https://doi.org/10.1073/pnas.1815961116>
- Correia, A. S., Patel, P., Dutta, K., & Julien, J.-P. (2015). Inflammation Induces TDP-43 Mislocalization and Aggregation. *PLOS ONE*, 10(10), e0140248. <https://doi.org/10.1371/journal.pone.0140248>

- Crosio, C., Valle, C., Casciati, A., Iaccarino, C., & Carri, M. T. (2011). Astroglial Inhibition of NF- $\kappa$ B Does Not Ameliorate Disease Onset and Progression in a Mouse Model for Amyotrophic Lateral Sclerosis (ALS). *PLoS ONE*, 6(3), e17187. <https://doi.org/10.1371/journal.pone.0017187>
- Cruz, V. H., Arner, E. N., Wynne, K. W., Scherer, P. E., & Brekken, R. A. (2018). Loss of Tbk1 kinase activity protects mice from diet-induced metabolic dysfunction. *Molecular Metabolism*, 16, 139–149. <https://doi.org/10.1016/j.molmet.2018.06.007>
- De Majo, M., Topp, S. D., Smith, B. N., Nishimura, A. L., Chen, H.-J., Gkazi, A. S., Miller, J., Wong, C. H., Vance, C., Baas, F., Ten Asbroek, A. L. M. A., Kenna, K. P., Ticozzi, N., Redondo, A. G., Esteban-Pérez, J., Tiloca, C., Verde, F., Duga, S., Morrison, K. E., ... Shaw, C. E. (2018). ALS-associated missense and nonsense TBK1 mutations can both cause loss of kinase function. *Neurobiology of Aging*, 71, 266.e1-266.e10. <https://doi.org/10.1016/j.neurobiolaging.2018.06.015>
- De Marchi, F., Franjkic, T., Schito, P., Russo, T., Nimac, J., Chami, A. A., Mele, A., Vidatic, L., Kriz, J., Julien, J.-P., Apic, G., Russell, R. B., Rogelj, B., Cannon, J. R., Baralle, M., Agosta, F., Hecimovic, S., Mazzini, L., Buratti, E., & Munitic, I. (2023). Emerging Trends in the Field of Inflammation and Proteinopathy in ALS/FTD Spectrum Disorder. *Biomedicines*, 11(6), Article 6. <https://doi.org/10.3390/biomedicines11061599>
- De Marchi, F., Munitic, I., Amedei, A., Berry, J. D., Feldman, E. L., Aronica, E., Nardo, G., Van Weehaeghe, D., Niccolai, E., Prtenjaca, N., Sakowski, S. A., Bendotti, C., & Mazzini, L. (2021). Interplay between immunity and amyotrophic lateral sclerosis: Clinical impact. *Neuroscience and Biobehavioral Reviews*, 127, 958–978. <https://doi.org/10.1016/j.neubiorev.2021.06.027>
- DeJesus-Hernandez, M., Mackenzie, I. R., Boeve, B. F., Boxer, A. L., Baker, M., Rutherford, N. J., Nicholson, A. M., Finch, N. A., Flynn, H., Adamson, J., Kouri, N., Wojtas, A., Sengdy, P., Hsiung, G.-Y. R., Karydas, A., Seeley, W. W., Josephs, K. A., Coppola, G., Geschwind, D. H., ... Rademakers, R. (2011). Expanded GGGGCC Hexanucleotide Repeat in Noncoding Region of C9ORF72 Causes Chromosome 9p-Linked FTD and ALS. *Neuron*, 72(2), 245–256. <https://doi.org/10.1016/j.neuron.2011.09.011>
- Demestre, M., Pullen, A., Orrell, R. W., & Orth, M. (2005). ALS-IgG-induced selective motor neurone apoptosis in rat mixed primary spinal cord cultures. *Journal of Neurochemistry*, 94(1), 268–275. <https://doi.org/10.1111/j.1471-4159.2005.03184.x>

- Deng, H. X., Hentati, A., Tainer, J. A., Iqbal, Z., Cayabyab, A., Hung, W. Y., Getzoff, E. D., Hu, P., Herzfeldt, B., & Roos, R. P. (1993). Amyotrophic lateral sclerosis and structural defects in Cu,Zn superoxide dismutase. *Science (New York, N.Y.)*, 261(5124), 1047–1051. <https://doi.org/10.1126/science.8351519>
- Deng, L., Wang, C., Spencer, E., Yang, L., Braun, A., You, J., Slaughter, C., Pickart, C., & Chen, Z. J. (2000). *Activation of the IkappaB Kinase Complex by TRAF6 Requires a Dimeric Ubiquitin-Conjugating Enzyme Complex and a Unique Polyubiquitin Chain.*
- Dermentzaki, G., Politi, K. A., Lu, L., Mishra, V., Pérez-Torres, E. J., Sosunov, A. A., McKhann, G. M., Lotti, F., Shneider, N. A., & Przedborski, S. (2019). Deletion of Ripk3 Prevents Motor Neuron Death In Vitro but not In Vivo. *eNeuro*, 6(1). <https://doi.org/10.1523/ENEURO.0308-18.2018>
- Dominguez, J., Yu, J. T., Tan, Y. J., Ng, A., De Guzman, M. F., Natividad, B., Daroy, M. L., Cano, J., Yu, J., Lian, M. M., Zeng, L., Lim, W. K., Foo, J. N., & Ng, A. S. L. (2021). Novel Optineurin Frameshift Insertion in a Family With Frontotemporal Dementia and Parkinsonism Without Amyotrophic Lateral Sclerosis. *Frontiers in Neurology*, 12, 645913. <https://doi.org/10.3389/fneur.2021.645913>
- Du, Y., Zhao, W., Thonhoff, J. R., Wang, J., Wen, S., & Appel, S. H. (2020). Increased activation ability of monocytes from ALS patients. *Experimental Neurology*, 328, 113259. <https://doi.org/10.1016/j.expneurol.2020.113259>
- Ea, C.-K., Deng, L., Xia, Z.-P., Pineda, G., & Chen, Z. J. (2006). Activation of IKK by TNFalpha requires site-specific ubiquitination of RIP1 and polyubiquitin binding by NEMO. *Molecular Cell*, 22(2), 245–257. <https://doi.org/10.1016/j.molcel.2006.03.026>
- Eichhoff, G., Busche, M. A., & Garaschuk, O. (2008). In vivo calcium imaging of the aging and diseased brain. *European Journal of Nuclear Medicine and Molecular Imaging*, 35(S1), 99–106. <https://doi.org/10.1007/s00259-007-0709-6>
- Engelhardt, J. I., & Appel, S. H. (1990). IgG Reactivity in the Spinal Cord and Motor Cortex in Amyotrophic Lateral Sclerosis. *Archives of Neurology*, 47(11), 1210–1216. <https://doi.org/10.1001/archneur.1990.00530110068019>

- Es, M. A. van, Hardiman, O., Chio, A., Al-Chalabi, A., Pasterkamp, R. J., Veldink, J. H., & Berg, L. H. van den. (2017). Amyotrophic lateral sclerosis. *The Lancet*, 390(10107), 2084–2098. [https://doi.org/10.1016/S0140-6736\(17\)31287-4](https://doi.org/10.1016/S0140-6736(17)31287-4)
- Escartin, C., Galea, E., Lakatos, A., O’Callaghan, J. P., Petzold, G. C., Serrano-Pozo, A., Steinhäuser, C., Volterra, A., Carmignoto, G., Agarwal, A., Allen, N. J., Araque, A., Barbeito, L., Barzilai, A., Bergles, D. E., Bonvento, G., Butt, A. M., Chen, W.-T., Cohen-Salmon, M., ... Verkhratsky, A. (2021). Reactive astrocyte nomenclature, definitions, and future directions. *Nature Neuroscience*, 24(3), Article 3. <https://doi.org/10.1038/s41593-020-00783-4>
- Fitzgerald, K. A., Rowe, D. C., Barnes, B. J., Caffrey, D. R., Visintin, A., Latz, E., Monks, B., Pitha, P. M., & Golenbock, D. T. (2003). LPS-TLR4 signaling to IRF-3/7 and NF-kappaB involves the toll adapters TRAM and TRIF. *The Journal of Experimental Medicine*, 198(7), 1043–1055. <https://doi.org/10.1084/jem.20031023>
- Frakes, A. E., Ferraiuolo, L., Haidet-Phillips, A. M., Schmelzer, L., Braun, L., Miranda, C. J., Ladner, K. J., Bevan, A. K., Foust, K. D., Godbout, J. P., Popovich, P. G., Guttridge, D. C., & Kaspar, B. K. (2014). Microglia Induce Motor Neuron Death via the Classical NF-κB Pathway in Amyotrophic Lateral Sclerosis. *Neuron*, 81(5), 1009–1023. <https://doi.org/10.1016/j.neuron.2014.01.013>
- Franceschi, C., Bonafè, M., Valensin, S., Olivieri, F., De Luca, M., Ottaviani, E., & De Benedictis, G. (2000). Inflamm-aging: An Evolutionary Perspective on Immunosenescence. *Annals of the New York Academy of Sciences*, 908(1), 244–254. <https://doi.org/10.1111/j.1749-6632.2000.tb06651.x>
- Franceschi, C., Garagnani, P., Parini, P., Giuliani, C., & Santoro, A. (2018). Inflammaging: A new immune–metabolic viewpoint for age-related diseases. *Nature Reviews Endocrinology*, 14(10), 576–590. <https://doi.org/10.1038/s41574-018-0059-4>
- Freischmidt, A., Wieland, T., Richter, B., Ruf, W., Schaeffer, V., Müller, K., Marroquin, N., Nordin, F., Hübers, A., Weydt, P., Pinto, S., Press, R., Millecamps, S., Molko, N., Bernard, E., Desnuelle, C., Soriani, M.-H., Dorst, J., Graf, E., ... Weishaupt, J. H. (2015). Haploinsufficiency of TBK1 causes familial ALS and fronto-temporal dementia. *Nature Neuroscience*, 18(5), 631–636. <https://doi.org/10.1038/nn.4000>

- Fukushi, M., Ohsawa, R., Okinaka, Y., Oikawa, D., Kiyono, T., Moriwaki, M., Irie, T., Oda, K., Kamei, Y., Tokunaga, F., Sotomaru, Y., Maruyama, H., Kawakami, H., & Sakaguchi, T. (2023). Optineurin deficiency impairs autophagy to cause interferon beta overproduction and increased survival of mice following viral infection. *PLOS ONE*, 18(6), e0287545. <https://doi.org/10.1371/journal.pone.0287545>
- Garofalo, S., Coccozza, G., Porzia, A., Inghilleri, M., Raspa, M., Scavizzi, F., Aronica, E., Bernardini, G., Peng, L., Ransohoff, R. M., Santoni, A., & Limatola, C. (2020). Natural killer cells modulate motor neuron-immune cell cross talk in models of Amyotrophic Lateral Sclerosis. *Nature Communications*, 11(1), 1773. <https://doi.org/10.1038/s41467-020-15644-8>
- Ginhoux, F., Greter, M., Leboeuf, M., Nandi, S., See, P., Gokhan, S., Mehler, M. F., Conway, S. J., Ng, L. G., Stanley, E. R., Samokhvalov, I. M., & Merad, M. (2010). Fate Mapping Analysis Reveals That Adult Microglia Derive from Primitive Macrophages. *Science*, 330(6005), 841–845. <https://doi.org/10.1126/science.1194637>
- Gleason, C. E., Ordureau, A., Gourlay, R., Arthur, J. S. C., & Cohen, P. (2011). Polyubiquitin Binding to Optineurin Is Required for Optimal Activation of TANK-binding Kinase 1 and Production of Interferon  $\beta$ . *Journal of Biological Chemistry*, 286(41), 35663–35674. <https://doi.org/10.1074/jbc.M111.267567>
- Gong, Y. H., Parsadanian, A. S., Andreeva, A., Snider, W. D., & Elliott, J. L. (2000). Restricted Expression of G86R Cu/Zn Superoxide Dismutase in Astrocytes Results in Astrocytosis But Does Not Cause Motoneuron Degeneration. *The Journal of Neuroscience*, 20(2), 660–665. <https://doi.org/10.1523/JNEUROSCI.20-02-00660.2000>
- Gotkine, M., De Majo, M., Wong, C. H., Topp, S. D., Michaelson-Cohen, R., Epsztejn-Litman, S., Eiges, R., Y, Y. L., Kanaan, M., Shaked, H. M., Alahmady, N., Vance, C., Newhouse, S. J., Breen, G., Nishimura, A. L., Shaw, C. E., & Smith, B. N. (2021). A recessive S174X mutation in Optineurin causes amyotrophic lateral sclerosis through a loss of function via allele-specific nonsense-mediated decay. *Neurobiology of Aging*, 106, 1–6. <https://doi.org/10.1016/j.neurobiolaging.2021.05.009>

- Graber, D. J., Hickey, W. F., & Harris, B. T. (2010). Progressive changes in microglia and macrophages in spinal cord and peripheral nerve in the transgenic rat model of amyotrophic lateral sclerosis. *Journal of Neuroinflammation*, 7(1), 8. <https://doi.org/10.1186/1742-2094-7-8>
- Gravel, M., Béland, L.-C., Soucy, G., Abdelhamid, E., Rahimian, R., Gravel, C., & Kriz, J. (2016). IL-10 Controls Early Microglial Phenotypes and Disease Onset in ALS Caused by Misfolded Superoxide Dismutase 1. *Journal of Neuroscience*, 36(3), 1031–1048. <https://doi.org/10.1523/JNEUROSCI.0854-15.2016>
- Grossman, M., Seeley, W. W., Boxer, A. L., Hillis, A. E., Knopman, D. S., Ljubenov, P. A., Miller, B., Piguet, O., Rademakers, R., Whitwell, J. L., Zetterberg, H., & Van Swieten, J. C. (2023). Frontotemporal lobar degeneration. *Nature Reviews Disease Primers*, 9(1), 40. <https://doi.org/10.1038/s41572-023-00447-0>
- Gudkov, S. V., Burmistrov, D. E., Kondakova, E. V., Sarimov, R. M., Yarkov, R. S., Franceschi, C., & Vedunova, M. V. (2023). An emerging role of astrocytes in aging/neuroinflammation and gut-brain axis with consequences on sleep and sleep disorders. *Ageing Research Reviews*, 83, 101775. <https://doi.org/10.1016/j.arr.2022.101775>
- Guo, Q., Jin, Y., Chen, X., Ye, X., Shen, X., Lin, M., Zeng, C., Zhou, T., & Zhang, J. (2024). NF- $\kappa$ B in biology and targeted therapy: New insights and translational implications. *Signal Transduction and Targeted Therapy*, 9(1), 53. <https://doi.org/10.1038/s41392-024-01757-9>
- Guo, S., Wang, H., & Yin, Y. (2022). Microglia Polarization From M1 to M2 in Neurodegenerative Diseases. *Frontiers in Aging Neuroscience*, 14, 815347. <https://doi.org/10.3389/fnagi.2022.815347>
- Gurney, M. E., Pu, H., Chiu, A. Y., Dal Canto, M. C., Polchow, C. Y., Alexander, D. D., Caliendo, J., Hentati, A., Kwon, Y. W., & Deng, H. X. (1994). Motor neuron degeneration in mice that express a human Cu,Zn superoxide dismutase mutation. *Science (New York, N.Y.)*, 264(5166), 1772–1775. <https://doi.org/10.1126/science.8209258>
- Häcker, H., Redecke, V., Blagoev, B., Kratchmarova, I., Hsu, L.-C., Wang, G. G., Kamps, M. P., Raz, E., Wagner, H., Häcker, G., Mann, M., & Karin, M. (2006). Specificity in Toll-like receptor

signalling through distinct effector functions of TRAF3 and TRAF6. *Nature*, 439(7073), 204–207. <https://doi.org/10.1038/nature04369>

Hardiman, O., Al-Chalabi, A., Chio, A., Corr, E. M., Logroscino, G., Robberecht, W., Shaw, P. J., Simmons, Z., & van den Berg, L. H. (2017). Amyotrophic lateral sclerosis. *Nature Reviews Disease Primers*, 3(1), Article 1. <https://doi.org/10.1038/nrdp.2017.71>

Hattula, K., & Peränen, J. (2000). FIP-2, a coiled-coil protein, links Huntingtin to Rab8 and modulates cellular morphogenesis. *Current Biology*, 10(24), 1603–1606. [https://doi.org/10.1016/S0960-9822\(00\)00864-2](https://doi.org/10.1016/S0960-9822(00)00864-2)

Henkel, J. S., Beers, D. R., Wen, S., Rivera, A. L., Toennis, K. M., Appel, J. E., Zhao, W., Moore, D. H., Powell, S. Z., & Appel, S. H. (2013). Regulatory T-lymphocytes mediate amyotrophic lateral sclerosis progression and survival. *EMBO Molecular Medicine*, 5(1), 64–79. <https://doi.org/10.1002/emmm.201201544>

Henkel, J. S., Engelhardt, J. I., Siklós, L., Simpson, E. P., Kim, S. H., Pan, T., Goodman, J. C., Siddique, T., Beers, D. R., & Appel, S. H. (2004). Presence of dendritic cells, MCP-1, and activated microglia/macrophages in amyotrophic lateral sclerosis spinal cord tissue. *Annals of Neurology*, 55(2), 221–235. <https://doi.org/10.1002/ana.10805>

Herdewyn, S., Cirillo, C., Van Den Bosch, L., Robberecht, W., Vanden Berghe, P., & Van Damme, P. (2014). Prevention of intestinal obstruction reveals progressive neurodegeneration in mutant TDP-43 (A315T) mice. *Molecular Neurodegeneration*, 9(1), 24. <https://doi.org/10.1186/1750-1326-9-24>

Hou, Y., Dan, X., Babbar, M., Wei, Y., Hasselbalch, S. G., Croteau, D. L., & Bohr, V. A. (2019). Ageing as a risk factor for neurodegenerative disease. *Nature Reviews Neurology*, 15(10), Article 10. <https://doi.org/10.1038/s41582-019-0244-7>

Hu, H., & Sun, S.-C. (2016). Ubiquitin signaling in immune responses. *Cell Research*, 26(4), 457–483. <https://doi.org/10.1038/cr.2016.40>

Inukai, Y., Nonaka, T., Arai, T., Yoshida, M., Hashizume, Y., Beach, T. G., Buratti, E., Baralle, F. E., Akiyama, H., Hisanaga, S., & Hasegawa, M. (2008). Abnormal phosphorylation of Ser409/410



of TDP-43 in FTL-DU and ALS. *FEBS Letters*, 582(19), 2899–2904. <https://doi.org/10.1016/j.febslet.2008.07.027>

Ito, H., Nakamura, M., Komure, O., Ayaki, T., Wate, R., Maruyama, H., Nakamura, Y., Fujita, K., Kaneko, S., Okamoto, Y., Ihara, M., Konishi, T., Ogasawara, K., Hirano, A., Kusaka, H., Kaji, R., Takahashi, R., & Kawakami, H. (2011). Clinicopathologic study on an ALS family with a heterozygous E478G optineurin mutation. *Acta Neuropathologica*, 122(2), 223–229. <https://doi.org/10.1007/s00401-011-0842-y>

Ito, Y., Ofengeim, D., Najafov, A., Das, S., Saberi, S., Li, Y., Hitomi, J., Zhu, H., Chen, H., Mayo, L., Geng, J., Amin, P., DeWitt, J. P., Mookhtiar, A. K., Florez, M., Ouchida, A. T., Fan, J., Pasparakis, M., Kelliher, M. A., ... Yuan, J. (2016). RIPK1 mediates axonal degeneration by promoting inflammation and necroptosis in ALS. *Science*, 353(6299), 603–608. <https://doi.org/10.1126/science.aaf6803>

Jin, C., Shao, Y., Zhang, X., Xiang, J., Zhang, R., Sun, Z., Mei, S., Zhou, J., Zhang, J., & Shi, L. (2021). A Unique Type of Highly-Activated Microglia Evoking Brain Inflammation via Mif/Cd74 Signaling Axis in Aged Mice. *Aging and Disease*, 12(8), 2125. <https://doi.org/10.14336/AD.2021.0520>

Jo, M., Lee, S., Jeon, Y.-M., Kim, S., Kwon, Y., & Kim, H.-J. (2020). The role of TDP-43 propagation in neurodegenerative diseases: Integrating insights from clinical and experimental studies. *Experimental & Molecular Medicine*, 52(10), 1652–1662. <https://doi.org/10.1038/s12276-020-00513-7>

Kachaner, D., Filipe, J., Laplantine, E., Bauch, A., Bennett, K. L., Superti-Furga, G., Israël, A., & Weil, R. (2012). Plk1-Dependent Phosphorylation of Optineurin Provides a Negative Feedback Mechanism for Mitotic Progression. *Molecular Cell*, 45(4), 553–566. <https://doi.org/10.1016/j.molcel.2011.12.030>

Kamada, M., Izumi, Y., Ayaki, T., Nakamura, M., Kagawa, S., Kudo, E., Sako, W., Maruyama, H., Nishida, Y., Kawakami, H., Ito, H., & Kaji, R. (2014). Clinicopathologic features of autosomal recessive amyotrophic lateral sclerosis associated with optineurin mutation. *Neuropathology*, 34(1), 64–70. <https://doi.org/10.1111/neup.12051>

- Kawamata, T., Akiyama, H., Yamada, T., & McGeer, P. L. (1992). *Immunologic Reactions in Amyotrophic Lateral Sclerosis Brain and Spinal Cord Tissue*. 140(3).
- Komander, D., & Rape, M. (2012). The Ubiquitin Code. *Annual Review of Biochemistry*, 81(1), 203–229. <https://doi.org/10.1146/annurev-biochem-060310-170328>
- Koppers, M., Blokhuis, A. M., Westeneng, H., Terpstra, M. L., Zundel, C. A. C., Vieira De Sá, R., Schellevis, R. D., Waite, A. J., Blake, D. J., Veldink, J. H., Van Den Berg, L. H., & Pasterkamp, R. J. (2015). C9orf72 ablation in mice does not cause motor neuron degeneration or motor deficits. *Annals of Neurology*, 78(3), 426–438. <https://doi.org/10.1002/ana.24453>
- Kovalenko, A., Chable-Bessia, C., & Cantarella, G. (2003). *The tumour suppressor CYLD negatively regulates NF- $\kappa$ B signalling by deubiquitination*. 424.
- Kriz, J., Nguyen, M. D., & Julien, J.-P. (2002). Minocycline Slows Disease Progression in a Mouse Model of Amyotrophic Lateral Sclerosis. *Neurobiology of Disease*, 10(3), 268–278. <https://doi.org/10.1006/nbdi.2002.0487>
- Kumar, S., Phaneuf, D., Cordeau, P., Boutej, H., Kriz, J., & Julien, J.-P. (2021). Induction of autophagy mitigates TDP-43 pathology and translational repression of neurofilament mRNAs in mouse models of ALS/FTD. *Molecular Neurodegeneration*, 16(1), 1. <https://doi.org/10.1186/s13024-020-00420-5>
- Kurashige, T., Kuramochi, M., Ohsawa, R., Yamashita, Y., Shioi, G., Morino, H., Kamada, M., Ayaki, T., Ito, H., Sotomaru, Y., Maruyama, H., & Kawakami, H. (2021). Optineurin defects cause TDP43-pathology with autophagic vacuolar formation. *Neurobiology of Disease*, 148, 105215. <https://doi.org/10.1016/j.nbd.2020.105215>
- Kwiatkowski, T. J., Bosco, D. A., LeClerc, A. L., Tamrazian, E., Vanderburg, C. R., Russ, C., Davis, A., Gilchrist, J., Kasarskis, E. J., Munsat, T., Valdmanis, P., Rouleau, G. A., Hosler, B. A., Cortelli, P., De Jong, P. J., Yoshinaga, Y., Haines, J. L., Pericak-Vance, M. A., Yan, J., ... Brown, R. H. (2009). Mutations in the *FUS/TLS* Gene on Chromosome 16 Cause Familial Amyotrophic Lateral Sclerosis. *Science*, 323(5918), 1205–1208. <https://doi.org/10.1126/science.1166066>

- Kwon, H. S., & Koh, S.-H. (2020). Neuroinflammation in neurodegenerative disorders: The roles of microglia and astrocytes. *Translational Neurodegeneration*, 9(1), 42. <https://doi.org/10.1186/s40035-020-00221-2>
- Lalancette-Hébert, M., Gowing, G., Simard, A., Weng, Y. C., & Kriz, J. (2007). Selective Ablation of Proliferating Microglial Cells Exacerbates Ischemic Injury in the Brain. *The Journal of Neuroscience*, 27(10), 2596–2605. <https://doi.org/10.1523/JNEUROSCI.5360-06.2007>
- Laplantine, E., Fontan, E., Chiaravalli, J., Lopez, T., Lakisic, G., Véron, M., Agou, F., & Israël, A. (2009). NEMO specifically recognizes K63-linked poly-ubiquitin chains through a new bipartite ubiquitin-binding domain. *The EMBO Journal*, 28(19), 2885–2895. <https://doi.org/10.1038/emboj.2009.241>
- Lee, S., & Kim, H.-J. (2015). Prion-like Mechanism in Amyotrophic Lateral Sclerosis: Are Protein Aggregates the Key? *Experimental Neurobiology*, 24(1), 1–7. <https://doi.org/10.5607/en.2015.24.1.1>
- Leger, M., Quiedeville, A., Bouet, V., Haelewyn, B., Boulouard, M., Schumann-Bard, P., & Freret, T. (2013). Object recognition test in mice. *Nature Protocols*, 8(12), Article 12. <https://doi.org/10.1038/nprot.2013.155>
- Li, D., & Wu, M. (2021). Pattern recognition receptors in health and diseases. *Signal Transduction and Targeted Therapy*, 6(1), 291. <https://doi.org/10.1038/s41392-021-00687-0>
- Li, F., Xie, X., Wang, Y., Liu, J., Cheng, X., Guo, Y., Gong, Y., Hu, S., & Pan, L. (2016). Structural insights into the interaction and disease mechanism of neurodegenerative disease-associated optineurin and TBK1 proteins. *Nature Communications*, 7(1), 12708. <https://doi.org/10.1038/ncomms12708>
- Li, Q., & Barres, B. A. (2018). Microglia and macrophages in brain homeostasis and disease. *Nature Reviews Immunology*, 18(4), 225–242. <https://doi.org/10.1038/nri.2017.125>
- Li, X., Li, C., Zhang, W., Wang, Y., Qian, P., & Huang, H. (2023). Inflammation and aging: Signaling pathways and intervention therapies. *Signal Transduction and Targeted Therapy*, 8(1), 239. <https://doi.org/10.1038/s41392-023-01502-8>

- Li, Y., Kang, J., & Horwitz, M. S. (1998). Interaction of an Adenovirus E3 14.7-Kilodalton Protein with a Novel Tumor Necrosis Factor Alpha-Inducible Cellular Protein Containing Leucine Zipper Domains. *Molecular and Cellular Biology*, 18(3), 1601–1610. <https://doi.org/10.1128/MCB.18.3.1601>
- Liao, B., Zhao, W., Beers, D. R., Henkel, J. S., & Appel, S. H. (2012). Transformation from a neuroprotective to a neurotoxic microglial phenotype in a mouse model of ALS. *Experimental Neurology*, 237(1), 147–152. <https://doi.org/10.1016/j.expneurol.2012.06.011>
- Lin, M., Ji, X., Lv, Y., Cui, D., & Xie, J. (2023). The Roles of TRAF3 in Immune Responses. *Disease Markers*, 2023, 1–11. <https://doi.org/10.1155/2023/7787803>
- Lincecum, J. M., Vieira, F. G., Wang, M. Z., Thompson, K., De Zutter, G. S., Kidd, J., Moreno, A., Sanchez, R., Carrion, I. J., Levine, B. A., Al-Nakhala, B. M., Sullivan, S. M., Gill, A., & Perrin, S. (2010). From transcriptome analysis to therapeutic anti-CD40L treatment in the SOD1 model of amyotrophic lateral sclerosis. *Nature Genetics*, 42(5), 392–399. <https://doi.org/10.1038/ng.557>
- Ling, S.-C., Polymenidou, M., & Cleveland, D. W. (2013). Converging Mechanisms in ALS and FTD: Disrupted RNA and Protein Homeostasis. *Neuron*, 79(3), 416–438. <https://doi.org/10.1016/j.neuron.2013.07.033>
- Lino, M. M., Schneider, C., & Caroni, P. (2002). Accumulation of SOD1 Mutants in Postnatal Motoneurons Does Not Cause Motoneuron Pathology or Motoneuron Disease. *The Journal of Neuroscience*, 22(12), 4825–4832. <https://doi.org/10.1523/JNEUROSCI.22-12-04825.2002>
- Liu, D., Webber, H. C., Bian, F., Xu, Y., Prakash, M., Feng, X., Yang, M., Yang, H., You, I.-J., Li, L., Liu, L., Liu, P., Huang, H., Chang, C.-Y., Liu, L., Shah, S. H., La Torre, A., Welsbie, D. S., Sun, Y., ... Hu, Y. (2025). Optineurin-facilitated axonal mitochondria delivery promotes neuroprotection and axon regeneration. *Nature Communications*, 16(1), 1789. <https://doi.org/10.1038/s41467-025-57135-8>
- Liu, T., Zhang, L., Joo, D., & Sun, S.-C. (2017). NF-κB signaling in inflammation. *Signal Transduction and Targeted Therapy*, 2(1), 17023. <https://doi.org/10.1038/sigtrans.2017.23>
- Liu, Z., Chen, P., Gao, H., Gu, Y., Yang, J., Peng, H., Xu, X., Wang, H., Yang, M., Liu, X., Fan, L., Chen, S., Zhou, J., Sun, Y., Ruan, K., Cheng, S., Komatsu, M., White, E., Li, L., ... Hu, R. (2014).

Ubiquitylation of Autophagy Receptor Optineurin by HACE1 Activates Selective Autophagy for Tumor Suppression. *Cancer Cell*, 26(1), 106–120. <https://doi.org/10.1016/j.ccr.2014.05.015>

Liu, Z., Li, H., Hong, C., Chen, M., Yue, T., Chen, C., Wang, Z., You, Q., Li, C., Weng, Q., Xie, H., & Hu, R. (2018). ALS-Associated E478G Mutation in Human OPTN (Optineurin) Promotes Inflammation and Induces Neuronal Cell Death. *Frontiers in Immunology*, 9, 2647. <https://doi.org/10.3389/fimmu.2018.02647>

Lomen-Hoerth, C., Anderson, T., & Miller, B. (2002). The overlap of amyotrophic lateral sclerosis and frontotemporal dementia. *Neurology*, 59(7), 1077–1079. <https://doi.org/10.1212/WNL.59.7.1077>

López-Otín, C., Blasco, M. A., Partridge, L., Serrano, M., & Kroemer, G. (2013). The Hallmarks of Aging. *Cell*, 153(6), 1194–1217. <https://doi.org/10.1016/j.cell.2013.05.039>

López-Otín, C., Blasco, M. A., Partridge, L., Serrano, M., & Kroemer, G. (2023). Hallmarks of aging: An expanding universe. *Cell*, 186(2), 243–278. <https://doi.org/10.1016/j.cell.2022.11.001>

Ma, X., Helgason, E., Phung, Q. T., Quan, C. L., Iyer, R. S., Lee, M. W., Bowman, K. K., Starovasnik, M. A., & Dueber, E. C. (2012). Molecular basis of Tank-binding kinase 1 activation by transautophosphorylation. *Proceedings of the National Academy of Sciences*, 109(24), 9378–9383. <https://doi.org/10.1073/pnas.1121552109>

Mackenzie, I. R. A., Bigio, E. H., Ince, P. G., Geser, F., Neumann, M., Cairns, N. J., Kwong, L. K., Forman, M. S., Ravits, J., Stewart, H., Eisen, A., McClusky, L., Kretzschmar, H. A., Monoranu, C. M., Highley, J. R., Kirby, J., Siddique, T., Shaw, P. J., Lee, V. M.-Y., & Trojanowski, J. Q. (2007). Pathological TDP-43 distinguishes sporadic amyotrophic lateral sclerosis from amyotrophic lateral sclerosis with SOD1 mutations. *Annals of Neurology*, 61(5), 427–434. <https://doi.org/10.1002/ana.21147>

Marín-Rubio, J. L., Raote, I., Inns, J., Dobson-Stone, C., & Rajan, N. (2023). CYLD in health and disease. *Disease Models & Mechanisms*, 16(6), dmm050093. <https://doi.org/10.1242/dmm.050093>

Markovinović, A. (2019). *NEUROINFLAMMATION IN MICE WITH OPTINEURIN INSUFFICIENCY* [Info:eu-repo/semantics/doctoralThesis, University of Rijeka. Department of Biotechnology]. <https://urn.nsk.hr/urn:nbn:hr:193:538797>

Markovinovic, A., Cimbri, R., Ljutic, T., Kriz, J., Rogelj, B., & Munitic, I. (2017). Optineurin in amyotrophic lateral sclerosis: Multifunctional adaptor protein at the crossroads of different neuroprotective mechanisms. *Progress in Neurobiology*, 154, 1–20. <https://doi.org/10.1016/j.pneurobio.2017.04.005>

Markovinovic, A., Ljutic, T., Béland, L.-C., & Munitic, I. (2018). Optineurin Insufficiency Disbalances Proinflammatory and Anti-inflammatory Factors by Reducing Microglial IFN- $\beta$  Responses. *Neuroscience*, 388, 139–151. <https://doi.org/10.1016/j.neuroscience.2018.07.007>

Marošević, M. (2022). *Interaction of optineurin and TDP-43 in cell models of amyotrophic lateral sclerosis* [Info:eu-repo/semantics/masterThesis, University of Rijeka. Department of Biotechnology]. <https://urn.nsk.hr/urn:nbn:hr:193:791592>

Maruyama, H., Morino, H., Ito, H., Izumi, Y., Kato, H., Watanabe, Y., Kinoshita, Y., Kamada, M., Nodera, H., Suzuki, H., Komure, O., Matsuura, S., Kobatake, K., Morimoto, N., Abe, K., Suzuki, N., Aoki, M., Kawata, A., Hirai, T., ... Kawakami, H. (2010). Mutations of optineurin in amyotrophic lateral sclerosis. *Nature*, 465(7295), 223–226. <https://doi.org/10.1038/nature08971>

Masrori, P., & Van Damme, P. (2020). Amyotrophic lateral sclerosis: A clinical review. *European Journal of Neurology*, 27(10), 1918–1929. <https://doi.org/10.1111/ene.14393>

Matejuk, A., & Ransohoff, R. M. (2020). Crosstalk Between Astrocytes and Microglia: An Overview. *Frontiers in Immunology*, 11, 1416. <https://doi.org/10.3389/fimmu.2020.01416>

Mattson, M. P., & Arumugam, T. V. (2018). Hallmarks of Brain Aging: Adaptive and Pathological Modification by Metabolic States. *Cell Metabolism*, 27(6), 1176–1199. <https://doi.org/10.1016/j.cmet.2018.05.011>

McCauley, M. E., & Baloh, R. H. (2019). Inflammation in ALS/FTD pathogenesis. *Acta Neuropathologica*, 137(5), 715–730. <https://doi.org/10.1007/s00401-018-1933-9>

McGeer, P. L., McGeer, E. G., Kawamata, T., Yamada, T., & Akiyama, H. (1991). Reactions of the Immune System in Chronic Degenerative Neurological Diseases. *Canadian Journal of*

*Neurological Sciences / Journal Canadien Des Sciences Neurologiques*, 18(S3), 376–379.  
<https://doi.org/10.1017/S0317167100032479>

Mead, R. J., Shan, N., Reiser, H. J., Marshall, F., & Shaw, P. J. (2022). Amyotrophic lateral sclerosis: A neurodegenerative disorder poised for successful therapeutic translation. *Nature Reviews Drug Discovery*, 1–28. <https://doi.org/10.1038/s41573-022-00612-2>

Meena, N. P., Zhu, G., Mittelstadt, P. R., Giardino Torchia, M. L., Pourcelot, M., Arnoult, D., Ashwell, J. D., & Munitic, I. (2016). The TBK1-binding domain of optineurin promotes type I interferon responses. *FEBS Letters*, 590(10), 1498–1508. <https://doi.org/10.1002/1873-3468.12176>

Milošević, M., Milićević, K., Božić, I., Lavrnja, I., Stevanović, I., Bijelić, D., Dubaić, M., Živković, I., Stević, Z., Giniatullin, R., & Andjus, P. (2017). Immunoglobulins G from Sera of Amyotrophic Lateral Sclerosis Patients Induce Oxidative Stress and Upregulation of Antioxidative System in BV-2 Microglial Cell Line. *Frontiers in Immunology*, 8, 1619. <https://doi.org/10.3389/fimmu.2017.01619>

Minegishi, Y., Iejima, D., Kobayashi, H., Chi, Z.-L., Kawase, K., Yamamoto, T., Seki, T., Yuasa, S., Fukuda, K., & Iwata, T. (2013). Enhanced optineurin E50K–TBK1 interaction evokes protein insolubility and initiates familial primary open-angle glaucoma. *Human Molecular Genetics*, 22(17), 3559–3567. <https://doi.org/10.1093/hmg/ddt210>

Mittelbrunn, M., & Kroemer, G. (2021). Hallmarks of T cell aging. *Nature Immunology*, 22(6), 687–698. <https://doi.org/10.1038/s41590-021-00927-z>

Moharir, S. C., & Swarup, G. (2022). Optineurin deficiency induces patchy hair loss but it is not sufficient to cause amyotrophic lateral sclerosis in mice. *Biochimica et Biophysica Acta (BBA) - Molecular Basis of Disease*, 1868(10), 166470. <https://doi.org/10.1016/j.bbadis.2022.166470>

Mohović, N. (2023). *Crosstalk of TDP-43 and Optineurin in Amyotrophic Lateral Sclerosis Models* [Info:eu-repo/semantics/doctoralThesis, University of Rijeka. Department of Biotechnology]. <https://urn.nsk.hr/urn:nbn:hr:193:697776>

Mohovic, N., Peradinovic, J., Markovinovic, A., Cimbro, R., Minic, Z., Dominovic, M., Jakovac, H., Nimac, J., Rogelj, B., & Munitic, I. (2023). Neuroimmune characterization of optineurin

insufficiency mouse model during ageing. *Scientific Reports*, 13(1), Article 1. <https://doi.org/10.1038/s41598-023-38875-3>

Moreland, R. J., Dresser, M. E., Rodgers, J. S., Roe, B. A., Conaway, J. W., Conaway, R. C., & Hanas, J. S. (2000). Identification of a transcription factor IIIA-interacting protein. *Nucleic Acids Research*, 28(9), 1986–1993. <https://doi.org/10.1093/nar/28.9.1986>

Morton, S., Hesson, L., Pegg, M., & Cohen, P. (2008). Enhanced binding of TBK1 by an optineurin mutant that causes a familial form of primary open angle glaucoma. *FEBS Letters*, 582(6), 997–1002. <https://doi.org/10.1016/j.febslet.2008.02.047>

Moss, C. E., Phipps, H., Wilson, H. L., & Kiss-Toth, E. (2023). Markers of the ageing macrophage: A systematic review and meta-analysis. *Frontiers in Immunology*, 14, 1222308. <https://doi.org/10.3389/fimmu.2023.1222308>

Munitic, I., Torchia, M. L. G., Meena, N. P., Zhu, G., Li, C. C., & Ashwell, J. D. (2013). Optineurin Insufficiency Impairs IRF3 but Not NF- $\kappa$ B Activation in Immune Cells. *The Journal of Immunology*, 191(12), 6231–6240. <https://doi.org/10.4049/jimmunol.1301696>

Murdock, B. J., Bender, D. E., Kashlan, S. R., Figueroa-Romero, C., Backus, C., Callaghan, B. C., Goutman, S. A., & Feldman, E. L. (2016). Increased ratio of circulating neutrophils to monocytes in amyotrophic lateral sclerosis. *Neurology Neuroimmunology & Neuroinflammation*, 3(4), e242. <https://doi.org/10.1212/NXI.0000000000000242>

Murdock, B. J., Zhou, T., Kashlan, S. R., Little, R. J., Goutman, S. A., & Feldman, E. L. (2017). Correlation of Peripheral Immunity With Rapid Amyotrophic Lateral Sclerosis Progression. *JAMA Neurology*, 74(12), 1446–1454. <https://doi.org/10.1001/jamaneurol.2017.2255>

Nagabhushana, A., Bansal, M., & Swarup, G. (2011). Optineurin Is Required for CYLD-Dependent Inhibition of TNF $\alpha$ -Induced NF- $\kappa$ B Activation. *PLOS ONE*, 6(3), e17477. <https://doi.org/10.1371/journal.pone.0017477>

Nakanishi, H., & Wu, Z. (2009). Microglia-aging: Roles of microglial lysosome- and mitochondria-derived reactive oxygen species in brain aging. *Behavioural Brain Research*, 201(1), 1–7. <https://doi.org/10.1016/j.bbr.2009.02.001>



Nakazawa, S., Oikawa, D., Ishii, R., Ayaki, T., Takahashi, H., Takeda, H., Ishitani, R., Kamei, K., Takeyoshi, I., Kawakami, H., Iwai, K., Hatada, I., Sawasaki, T., Ito, H., Nureki, O., & Tokunaga, F. (2016). Linear ubiquitination is involved in the pathogenesis of optineurin-associated amyotrophic lateral sclerosis. *Nature Communications*, 7(1), Article 1. <https://doi.org/10.1038/ncomms12547>

Naor, S., Keren, Z., Bronshtein, T., Goren, E., Machluf, M., & Melamed, D. (2009). Development of ALS-like disease in SOD-1 mice deficient of B lymphocytes. *Journal of Neurology*, 256(8), 1228–1235. <https://doi.org/10.1007/s00415-009-5097-3>

Natrajan, M. S., de la Fuente, A. G., Crawford, A. H., Linehan, E., Nuñez, V., Johnson, K. R., Wu, T., Fitzgerald, D. C., Ricote, M., Bielekova, B., & Franklin, R. J. M. (2015). Retinoid X receptor activation reverses age-related deficiencies in myelin debris phagocytosis and remyelination. *Brain*, 138(12), 3581–3597. <https://doi.org/10.1093/brain/awv289>

Neumann, M., Sampathu, D. M., Kwong, L. K., Truax, A. C., Micsenyi, M. C., Chou, T. T., Bruce, J., Schuck, T., Grossman, M., Clark, C. M., McCluskey, L. F., Miller, B. L., Masliah, E., Mackenzie, I. R., Feldman, H., Feiden, W., Kretzschmar, H. A., Trojanowski, J. Q., & Lee, V. M.-Y. (2006). Ubiquitinated TDP-43 in frontotemporal lobar degeneration and amyotrophic lateral sclerosis. *Science (New York, N.Y.)*, 314(5796), 130–133. <https://doi.org/10.1126/science.1134108>

Obaid, R., Wani, S. E., Azfer, A., Hurd, T., Jones, R., Cohen, P., Ralston, S. H., & Albagha, O. M. E. (2015). Optineurin Negatively Regulates Osteoclast Differentiation by Modulating NF- $\kappa$ B and Interferon Signaling: Implications for Paget's Disease. *Cell Reports*, 13(6), 1096–1102. <https://doi.org/10.1016/j.celrep.2015.09.071>

O'Loughlin, T., Kruppa, A. J., Ribeiro, A. L. R., Edgar, J. R., Ghannam, A., Smith, A. M., & Buss, F. (2020). OPTN recruitment to a Golgi-proximal compartment regulates immune signalling and cytokine secretion. *Journal of Cell Science*, 133(12), jcs239822. <https://doi.org/10.1242/jcs.239822>

Ou, S. H., Wu, F., Harrich, D., García-Martínez, L. F., & Gaynor, R. B. (1995). Cloning and characterization of a novel cellular protein, TDP-43, that binds to human immunodeficiency virus type 1 TAR DNA sequence motifs. *Journal of Virology*, 69(6), 3584–3596. <https://doi.org/10.1128/jvi.69.6.3584-3596.1995>

Özoğuz, A., Uyan, Ö., Birdal, G., Iskender, C., Kartal, E., Lahut, S., Ömür, Ö., Agim, Z. S., Eken, A. G., Sen, N. E., Kavak, P., Saygı, C., Sapp, P. C., Keagle, P., Parman, Y., Tan, E., Koç, F., Deymeer, F., Oflazer, P., ... Başak, A. N. (2015). The distinct genetic pattern of ALS in Turkey and novel mutations. *Neurobiology of Aging*, 36(4), 1764.e9-1764.e18. <https://doi.org/10.1016/j.neurobiolaging.2014.12.032>

Paolicelli, R. C., Sierra, A., Stevens, B., Tremblay, M.-E., Aguzzi, A., Ajami, B., Amit, I., Audinat, E., Bechmann, I., Bennett, M., Bennett, F., Bessis, A., Biber, K., Bilbo, S., Blurton-Jones, M., Boddeke, E., Brites, D., Brône, B., Brown, G. C., ... Wyss-Coray, T. (2022). Microglia states and nomenclature: A field at its crossroads. *Neuron*, 110(21), 3458–3483. <https://doi.org/10.1016/j.neuron.2022.10.020>

Parvizi, T., Klotz, S., Keritam, O., Caliskan, H., Imhof, S., König, T., Haider, L., Traub-Weidinger, T., Wagner, M., Brunet, T., Brugger, M., Zimprich, A., Rath, J., Stögmänn, E., Gelpi, E., & Cetin, H. (2024). Clinical heterogeneity within the ALS-FTD spectrum in a family with a homozygous optineurin mutation. *Annals of Clinical and Translational Neurology*, 11(6), 1579–1589. <https://doi.org/10.1002/acn3.52075>

Perry, A. K., Chow, E. K., Goodnough, J. B., Yeh, W.-C., & Cheng, G. (2004). Differential Requirement for TANK-binding Kinase-1 in Type I Interferon Responses to Toll-like Receptor Activation and Viral Infection. *The Journal of Experimental Medicine*, 199(12), 1651–1658. <https://doi.org/10.1084/jem.20040528>

Pohl, C., & Dikic, I. (2019). Cellular quality control by the ubiquitin-proteasome system and autophagy. *Science*, 366(6467), 818–822. <https://doi.org/10.1126/science.aax3769>

Polymenidou, M., & Cleveland, D. W. (2011). The Seeds of Neurodegeneration: Prion-like Spreading in ALS. *Cell*, 147(3), 498–508. <https://doi.org/10.1016/j.cell.2011.10.011>

Pottier, C., Rampersaud, E., Baker, M., Wu, G., Wu, J., McCauley, J. L., Zuchner, S., Schule, R., Bermudez, C., Hussain, S., Cooley, A., Wallace, M., Zhang, J., Taylor, J. P., Benatar, M., & Rademakers, R. (2018). Identification of compound heterozygous variants in OPTN in an ALS-FTD patient from the CReATe consortium: A case report. *Amyotrophic Lateral Sclerosis & Frontotemporal Degeneration*, 19(5–6), 469–471. <https://doi.org/10.1080/21678421.2018.1452947>

- Pourcelot, M., Zemirli, N., Silva Da Costa, L., Loyant, R., Garcin, D., Vitour, D., Munitic, I., Vazquez, A., & Arnoult, D. (2016). The Golgi apparatus acts as a platform for TBK1 activation after viral RNA sensing. *BMC Biology*, *14*(1), 69. <https://doi.org/10.1186/s12915-016-0292-z>
- Poyet, J.-L., Srinivasula, S. M., Lin, J., Fernandes-Alnemri, T., Yamaoka, S., Tsichlis, P. N., & Alnemri, E. S. (2000). Activation of the I $\kappa$ B Kinases by RIP via IKK $\gamma$ /NEMO-mediated Oligomerization. *Journal of Biological Chemistry*, *275*(48), 37966–37977. <https://doi.org/10.1074/jbc.M006643200>
- Pramatarova, A., Laganière, J., Roussel, J., Brisebois, K., & Rouleau, G. A. (2001). Neuron-Specific Expression of Mutant Superoxide Dismutase 1 in Transgenic Mice Does Not Lead to Motor Impairment. *The Journal of Neuroscience*, *21*(10), 3369–3374. <https://doi.org/10.1523/JNEUROSCI.21-10-03369.2001>
- Prasad, A., Bharathi, V., Sivalingam, V., Girdhar, A., & Patel, B. K. (2019). Molecular Mechanisms of TDP-43 Misfolding and Pathology in Amyotrophic Lateral Sclerosis. *Frontiers in Molecular Neuroscience*, *12*, 25. <https://doi.org/10.3389/fnmol.2019.00025>
- Prtenjaca, N. (2020). Optineurin Dysfunction in Amyotrophic Lateral Sclerosis: Why So Puzzling? *Periodicum Biologorum*, *121–122*(1–2), 23–34. <https://doi.org/10.18054/pb.v121-122i1-2.10627>
- Prtenjaca, N., Rob, M., Alam, M. S., Markovinovic, A., Stuani, C., Buratti, E., & Munitic, I. (2022). Optineurin Deficiency and Insufficiency Lead to Higher Microglial TDP-43 Protein Levels. *International Journal of Molecular Sciences*, *23*(12), Article 12. <https://doi.org/10.3390/ijms23126829>
- Pulko, V., Davies, J. S., Martinez, C., Lanteri, M. C., Busch, M. P., Diamond, M. S., Knox, K., Bush, E. C., Sims, P. A., Sinari, S., Billheimer, D., Haddad, E. K., Murray, K. O., Wertheimer, A. M., & Nikolich-Zugich, J. (2016). Human memory T cells with a naive phenotype accumulate with aging and respond to persistent viruses. *Nature Immunology*, *17*(8), 966–975. <https://doi.org/10.1038/ni.3483>
- Quek, H., Cuní-López, C., Stewart, R., Colletti, T., Notaro, A., Nguyen, T. H., Sun, Y., Guo, C. C., Lupton, M. K., Roberts, T. L., Lim, Y. C., Oikari, L. E., La Bella, V., & White, A. R. (2022). ALS monocyte-derived microglia-like cells reveal cytoplasmic TDP-43 accumulation, DNA damage,

and cell-specific impairment of phagocytosis associated with disease progression. *Journal of Neuroinflammation*, 19(1), 58. <https://doi.org/10.1186/s12974-022-02421-1>

Rahighi, S., Ikeda, F., Kawasaki, M., Akutsu, M., Suzuki, N., Kato, R., Kensche, T., Uejima, T., Bloor, S., Komander, D., Randow, F., Wakatsuki, S., & Dikic, I. (2009). Specific Recognition of Linear Ubiquitin Chains by NEMO Is Important for NF- $\kappa$ B Activation. *Cell*, 136(6), 1098–1109. <https://doi.org/10.1016/j.cell.2009.03.007>

Rezaie, T., Child, A., Hitchings, R., Brice, G., Miller, L., Coca-Prados, M., Héon, E., Krupin, T., Ritch, R., Kreutzer, D., Crick, R. P., & Sarfarazi, M. (2002). Adult-Onset Primary Open-Angle Glaucoma Caused by Mutations in Optineurin. *Science*, 295(5557), 1077–1079. <https://doi.org/10.1126/science.1066901>

Rezaie, T., & Sarfarazi, M. (2005). Molecular cloning, genomic structure, and protein characterization of mouse optineurin☆. *Genomics*, 85(1), 131–138. <https://doi.org/10.1016/j.ygeno.2004.10.011>

Richter, B., Sliter, D. A., Herhaus, L., Stolz, A., Wang, C., Beli, P., Zaffagnini, G., Wild, P., Martens, S., Wagner, S. A., Youle, R. J., & Dikic, I. (2016). Phosphorylation of OPTN by TBK1 enhances its binding to Ub chains and promotes selective autophagy of damaged mitochondria. *Proceedings of the National Academy of Sciences*, 113(15), 4039–4044. <https://doi.org/10.1073/pnas.1523926113>

Ringholz, G. M., Appel, S. H., Bradshaw, M., Cooke, N. A., Mosnik, D. M., & Schulz, P. E. (2005). Prevalence and patterns of cognitive impairment in sporadic ALS. *Neurology*, 65(4), 586–590. <https://doi.org/10.1212/01.wnl.0000172911.39167.b6>

Rob, M. (2018). *Karakterizacija uloge optineurina u regulaciji upalnih signala u mikroglijalnim i neuronalnim staničnim linijama* [Info:eu-repo/semantics/masterThesis, University of Rijeka. Department of Biotechnology]. <https://urn.nsk.hr/urn:nbn:hr:193:162533>

Rosen, D. R., Siddique, T., Patterson, D., Figlewicz, D. A., Sapp, P., Hentati, A., Donaldson, D., Goto, J., O'Regan, J. P., Deng, H.-X., Rahmani, Z., Krizus, A., McKenna-Yasek, D., Cayabyab, A., Gaston, S. M., Berger, R., Tanzi, R. E., Halperin, J. J., Herzfeldt, B., ... Brown, R. H. (1993).

Mutations in Cu/Zn superoxide dismutase gene are associated with familial amyotrophic lateral sclerosis. *Nature*, 362(6415), 59–62. <https://doi.org/10.1038/362059a0>

Rusconi, M., Gerardi, F., Santus, W., Lizio, A., Sansone, V. A., Lunetta, C., Zanoni, I., & Granucci, F. (2017). Inflammatory role of dendritic cells in Amyotrophic Lateral Sclerosis revealed by an analysis of patients' peripheral blood. *Scientific Reports*, 7(1), 7853. <https://doi.org/10.1038/s41598-017-08233-1>

Sahlender, D. A., Roberts, R. C., Arden, S. D., Spudich, G., Taylor, M. J., Luzio, J. P., Kendrick-Jones, J., & Buss, F. (2005). Optineurin links myosin VI to the Golgi complex and is involved in Golgi organization and exocytosis. *The Journal of Cell Biology*, 169(2), 285–295. <https://doi.org/10.1083/jcb.200501162>

Sako, W., Ito, H., Yoshida, M., Koizumi, H., Kamada, M., Fujita, K., Hashizume, Y., Izumi, Y., & Kaji, R. (2012). Nuclear factor k B expression in patients with sporadic amyotrophic lateral sclerosis and hereditary amyotrophic lateral sclerosis with optineurin mutations. *Clinical Neuropathology*, 31(11), 418–423. <https://doi.org/10.5414/NP300493>

Samadhiya, S., Sardana, V., Bhushan, B., Maheshwari, D., Goyal, R., & Pankaj. (2022). Assessment of Therapeutic Response of Edaravone and Riluzole Combination Therapy in Amyotrophic Lateral Sclerosis Patients. *Annals of Indian Academy of Neurology*, 25(4), 692–697. [https://doi.org/10.4103/aian.aian\\_1083\\_21](https://doi.org/10.4103/aian.aian_1083_21)

Sandhir, R., Onyszchuk, G., & Berman, N. E. J. (2008). Exacerbated glial response in the aged mouse hippocampus following controlled cortical impact injury. *Experimental Neurology*, 213(2), 372–380. <https://doi.org/10.1016/j.expneurol.2008.06.013>

Saresella, M., Piancone, F., Tortorella, P., Marventano, I., Gatti, A., Caputo, D., Lunetta, C., Corbo, M., Rovaris, M., & Clerici, M. (2013). T helper-17 activation dominates the immunologic milieu of both amyotrophic lateral sclerosis and progressive multiple sclerosis. *Clinical Immunology*, 148(1), 79–88. <https://doi.org/10.1016/j.clim.2013.04.010>

Schwamborn, K., Weil, R., Courtois, G., Whiteside, S. T., & Israël, A. (2000). Phorbol Esters and Cytokines Regulate the Expression of the NEMO-related Protein, a Molecule Involved in a NF-

$\kappa$ B-independent Pathway. *Journal of Biological Chemistry*, 275(30), 22780–22789. <https://doi.org/10.1074/jbc.M001500200>

Sharma, S., tenOever, B. R., Grandvaux, N., Zhou, G.-P., Lin, R., & Hiscott, J. (2003). Triggering the Interferon Antiviral Response Through an IKK-Related Pathway. *Science*, 300(5622), 1148–1151. <https://doi.org/10.1126/science.1081315>

Sieverding, K., Ulmer, J., Bruno, C., Satoh, T., Tsao, W., Freischmidt, A., Akira, S., Wong, P. C., Ludolph, A. C., Danzer, K. M., Lobsiger, C. S., Brenner, D., & Weishaupt, J. H. (2021). Hemizygous deletion of *Tbkl* worsens neuromuscular junction pathology in TDP-43G298S transgenic mice. *Experimental Neurology*, 335, 113496. <https://doi.org/10.1016/j.expneurol.2020.113496>

Sikora, E., Bielak-Zmijewska, A., Dudkowska, M., Krzystyniak, A., Mosieniak, G., Wesierska, M., & Wlodarczyk, J. (2021). Cellular Senescence in Brain Aging. *Frontiers in Aging Neuroscience*, 13, 646924. <https://doi.org/10.3389/fnagi.2021.646924>

Slowicka, K., Vereecke, L., Mc Guire, C., Sze, M., Maelfait, J., Kolpe, A., Saelens, X., Beyaert, R., & van Loo, G. (2016). Optineurin deficiency in mice is associated with increased sensitivity to Salmonella but does not affect proinflammatory NF- $\kappa$ B signaling. *European Journal of Immunology*, 46(4), 971–980. <https://doi.org/10.1002/eji.201545863>

Slowicka, K., Vereecke, L., & Van Loo, G. (2016). Cellular Functions of Optineurin in Health and Disease. *Trends in Immunology*, 37(9), 621–633. <https://doi.org/10.1016/j.it.2016.07.002>

Sudhakar, C., Nagabhushana, A., Jain, N., & Swarup, G. (2009). NF- $\kappa$ B Mediates Tumor Necrosis Factor  $\alpha$ -Induced Expression of Optineurin, a Negative Regulator of NF- $\kappa$ B. *PLoS ONE*, 4(4), e5114. <https://doi.org/10.1371/journal.pone.0005114>

Sun, S.-C., Ganchi, P. A., Ballard, D. W., & Greene, W. C. (1993). *NF-KB Controls Expression of Inhibitor IKBa: Evidence for an Inducible Autoregulatory Pathway*. 259.

Sundaramoorthy, V., Walker, A. K., Tan, V., Fifita, J. A., Mccann, E. P., Williams, K. L., Blair, I. P., Guillemin, G. J., Farg, M. A., & Atkin, J. D. (2015). Defects in optineurin- and myosin VI-mediated cellular trafficking in amyotrophic lateral sclerosis. *Human Molecular Genetics*, 24(13), 3830–3846. <https://doi.org/10.1093/hmg/ddv126>

Swarup, V., Phaneuf, D., Bareil, C., Robertson, J., Rouleau, G. A., Kriz, J., & Julien, J.-P. (2011). Pathological hallmarks of amyotrophic lateral sclerosis/frontotemporal lobar degeneration in transgenic mice produced with TDP-43 genomic fragments. *Brain*, 134(9), 2610–2626. <https://doi.org/10.1093/brain/awr159>

Swarup, V., Phaneuf, D., Dupré, N., Petri, S., Strong, M., Kriz, J., & Julien, J.-P. (2011). Deregulation of TDP-43 in amyotrophic lateral sclerosis triggers nuclear factor  $\kappa$ B-mediated pathogenic pathways. *Journal of Experimental Medicine*, 208(12), 2429–2447. <https://doi.org/10.1084/jem.20111313>

Talbott, E. O., Malek, A. M., & Lacomis, D. (2016). The epidemiology of amyotrophic lateral sclerosis. In *Handbook of Clinical Neurology* (Vol. 138, pp. 225–238). Elsevier. <https://doi.org/10.1016/B978-0-12-802973-2.00013-6>

Tan, H. Y., Yong, Y. K., Xue, Y. C., Liu, H., Furihata, T., Shankar, E. M., & Ng, C. S. (2022). cGAS and DDX41-STING mediated intrinsic immunity spreads intercellularly to promote neuroinflammation in SOD1 ALS model. *iScience*, 25(6), 104404. <https://doi.org/10.1016/j.isci.2022.104404>

Tang, Y., & Le, W. (2016). Differential Roles of M1 and M2 Microglia in Neurodegenerative Diseases. *Molecular Neurobiology*, 53(2), 1181–1194. <https://doi.org/10.1007/s12035-014-9070-5>

*Tissue expression of OPTN - Summary—The Human Protein Atlas*. (n.d.). Retrieved March 6, 2025, from <https://www.proteinatlas.org/ENSG00000123240-OPTN/tissue>

Tokunaga, F., Sakata, S., Saeki, Y., Satomi, Y., Kirisako, T., Kamei, K., Nakagawa, T., Kato, M., Murata, S., Yamaoka, S., Yamamoto, M., Akira, S., Takao, T., Tanaka, K., & Iwai, K. (2009). Involvement of linear polyubiquitylation of NEMO in NF- $\kappa$ B activation. *Nature Cell Biology*, 11(2), 123–132. <https://doi.org/10.1038/ncb1821>

Toth, R. P., & Atkin, J. D. (2018). Dysfunction of Optineurin in Amyotrophic Lateral Sclerosis and Glaucoma. *Frontiers in Immunology*, 9, 1017. <https://doi.org/10.3389/fimmu.2018.01017>

Trias, E., King, P. H., Si, Y., Kwon, Y., Varela, V., Ibarburu, S., Kovacs, M., Moura, I. C., Beckman, J. S., Hermine, O., & Barbeito, L. (2018). Mast cells and neutrophils mediate peripheral motor

pathway degeneration in ALS. *JCI Insight*, 3(19), e123249. <https://doi.org/10.1172/jci.insight.123249>

Tsesmelis, K., Maity-Kumar, G., Croner, D., Sprissler, J., Tsesmelis, M., Hein, T., Baumann, B., & Wirth, T. (2023). Accelerated aging in mice with astrocytic redox imbalance as a consequence of SOD2 deletion. *Aging Cell*, 22(9), e13911. <https://doi.org/10.1111/accel.13911>

Tu, D., Zhu, Z., Zhou, A. Y., Yun, C., Lee, K.-E., Toms, A. V., Li, Y., Dunn, G. P., Chan, E., Thai, T., Yang, S., Ficarro, S. B., Marto, J. A., Jeon, H., Hahn, W. C., Barbie, D. A., & Eck, M. J. (2013). Structure and Ubiquitination-Dependent Activation of TANK-Binding Kinase 1. *Cell Reports*, 3(3), 747–758. <https://doi.org/10.1016/j.celrep.2013.01.033>

Tumbarello, D. A., Waxse, B. J., Arden, S. D., Bright, N. A., Kendrick-Jones, J., & Buss, F. (2012). Autophagy receptors link myosin VI to autophagosomes to mediate Tom1-dependent autophagosome maturation and fusion with the lysosome. *Nature Cell Biology*, 14(10), 1024–1035. <https://doi.org/10.1038/ncb2589>

Tümer, Z., Bertelsen, B., Gredal, O., Magyari, M., Nielsen, K. C., LuCamp, Grønskov, K., & Brøndum-Nielsen, K. (2012). A novel heterozygous nonsense mutation of the OPTN gene segregating in a Danish family with ALS. *Neurobiology of Aging*, 33(1), 208.e1-208.e5. <https://doi.org/10.1016/j.neurobiolaging.2011.07.001>

Tuzlak, S., Dejean, A. S., Iannaccone, M., Quintana, F. J., Waisman, A., Ginhoux, F., Korn, T., & Becher, B. (2021). Repositioning TH cell polarization from single cytokines to complex help. *Nature Immunology*, 22(10), 1210–1217. <https://doi.org/10.1038/s41590-021-01009-w>

Vaibhava, V., Nagabhushana, A., Chalasani, M. L. S., Sudhakar, C., Kumari, A., & Swarup, G. (2012). Optineurin mediates negative regulation of Rab8 function by TBC1D17, a GTPase activating protein. *Journal of Cell Science*, jcs.102327. <https://doi.org/10.1242/jcs.102327>

Van Blitterswijk, M., Van Vught, P. W. J., Van Es, M. A., Schelhaas, H. J., Van Der Kooi, A. J., De Visser, M., Veldink, J. H., & Van Den Berg, L. H. (2012). Novel optineurin mutations in sporadic amyotrophic lateral sclerosis patients. *Neurobiology of Aging*, 33(5), 1016.e1-1016.e7. <https://doi.org/10.1016/j.neurobiolaging.2011.05.019>



- Vance, C., Rogelj, B., Hortobágyi, T., De Vos, K. J., Nishimura, A. L., Sreedharan, J., Hu, X., Smith, B., Ruddy, D., Wright, P., Ganesalingam, J., Williams, K. L., Tripathi, V., Al-Saraj, S., Al-Chalabi, A., Leigh, P. N., Blair, I. P., Nicholson, G., De Belleruche, J., ... Shaw, C. E. (2009). Mutations in FUS, an RNA Processing Protein, Cause Familial Amyotrophic Lateral Sclerosis Type 6. *Science*, 323(5918), 1208–1211. <https://doi.org/10.1126/science.1165942>
- Volk, A. E., Weishaupt, J. H., Andersen, P. M., Ludolph, A. C., & Kubisch, C. (2018). Current knowledge and recent insights into the genetic basis of amyotrophic lateral sclerosis. *Medizinische Genetik*, 30(2), 252–258. <https://doi.org/10.1007/s11825-018-0185-3>
- von Bernhardt, R., Eugénin-von Bernhardt, L., & Eugénin, J. (2015). Microglial cell dysregulation in brain aging and neurodegeneration. *Frontiers in Aging Neuroscience*, 7. <https://doi.org/10.3389/fnagi.2015.00124>
- Wagner, S., Carpentier, I., Rogov, V., Kreike, M., & Ikeda, F. (2008). Ubiquitin binding mediates the NF- $\kappa$ B inhibitory potential of ABIN proteins. <https://doi.org/10.1038/sj.onc.1211042>
- Wang, C., Deng, L., Hong, M., Akkaraju, G. R., Inoue, J., & Chen, Z. J. (2001). TAK1 is a ubiquitin-dependent kinase of MKK and IKK. *Nature*, 412(6844), 346–351. <https://doi.org/10.1038/35085597>
- Wang, J., Wang, J., Hong, W., Zhang, L., Song, L., Shi, Q., Shao, Y., Hao, G., Fang, C., Qiu, Y., Yang, L., Yang, Z., Wang, J., Cao, J., Yang, B., He, Q., & Weng, Q. (2021). Optineurin modulates the maturation of dendritic cells to regulate autoimmunity through JAK2-STAT3 signaling. *Nature Communications*, 12(1), Article 1. <https://doi.org/10.1038/s41467-021-26477-4>
- Wang, Y., Szretter, K. J., Vermi, W., Gilfillan, S., Rossini, C., Cella, M., Barrow, A. D., Diamond, M. S., & Colonna, M. (2012). IL-34 is a tissue-restricted ligand of CSF1R required for the development of Langerhans cells and microglia. *Nature Immunology*, 13(8), 753–760. <https://doi.org/10.1038/ni.2360>
- Watanabe, M., Dykes-Hoberg, M., Cizewski Culotta, V., Price, D. L., Wong, P. C., & Rothstein, J. D. (2001). Histological Evidence of Protein Aggregation in Mutant SOD1 Transgenic Mice and in Amyotrophic Lateral Sclerosis Neural Tissues. *Neurobiology of Disease*, 8(6), 933–941. <https://doi.org/10.1006/nbdi.2001.0443>

- Wegorzewska, I., Bell, S., Cairns, N. J., Miller, T. M., & Baloh, R. H. (2009). TDP-43 mutant transgenic mice develop features of ALS and frontotemporal lobar degeneration. *Proceedings of the National Academy of Sciences*, 106(44), 18809–18814. <https://doi.org/10.1073/pnas.0908767106>
- Weinstein, S. L., Finn, A. J., Davé, S. H., Meng, F., Lowell, C. A., Sanghera, J. S., & DeFranco, A. L. (2000). Phosphatidylinositol 3-kinase and mTOR mediate lipopolysaccharide-stimulated nitric oxide production in macrophages via interferon-beta. *Journal of Leukocyte Biology*, 67(3), 405–414. <https://doi.org/10.1002/jlb.67.3.405>
- Wenisch, C., Patruta, S., Daxböck, F., Krause, R., & Hörl, W. (2000). Effect of age on human neutrophil function. *Journal of Leukocyte Biology*, 67(1), 40–45. <https://doi.org/10.1002/jlb.67.1.40>
- Wertz, I. E., O'Rourke, K. M., Zhou, H., Eby, M., Aravind, L., Seshagiri, S., Wu, P., Wiesmann, C., Baker, R., Boone, D. L., Ma, A., Koonin, E. V., & Dixit, V. M. (2004). *De-ubiquitination and ubiquitin ligase domains of A20 downregulate NF- $\kappa$ B signalling*. 430.
- Wild, P., Farhan, H., McEwan, D. G., Wagner, S., Rogov, V. V., Brady, N. R., Richter, B., Korac, J., Waidmann, O., Choudhary, C., Dötsch, V., Bumann, D., & Dikic, I. (2011). Phosphorylation of the Autophagy Receptor Optineurin Restricts Salmonella Growth. *Science*, 333(6039), 228–233. <https://doi.org/10.1126/science.1205405>
- Wilson, D. M., Cookson, M. R., Van Den Bosch, L., Zetterberg, H., Holtzman, D. M., & Dewachter, I. (2023). Hallmarks of neurodegenerative diseases. *Cell*, 186(4), 693–714. <https://doi.org/10.1016/j.cell.2022.12.032>
- Wong, C. K., Smith, C. A., Sakamoto, K., Kaminski, N., Koff, J. L., & Goldstein, D. R. (2017). Aging Impairs Alveolar Macrophage Phagocytosis and Increases Influenza-Induced Mortality in Mice. *The Journal of Immunology*, 199(3), 1060–1068. <https://doi.org/10.4049/jimmunol.1700397>
- Wu, C.-J., Conze, D. B., Li, T., Srinivasula, S. M., & Ashwell, J. D. (2006). Sensing of Lys 63-linked polyubiquitination by NEMO is a key event in NF- $\kappa$ B activation. *Nature Cell Biology*, 8(4), 398–406. <https://doi.org/10.1038/ncb1384>

- Xie, F., Zhang, J.-C., Fu, H., & Chen, J. (2013). Age-related decline of myelin proteins is highly correlated with activation of astrocytes and microglia in the rat CNS. *International Journal of Molecular Medicine*, 32(5), 1021–1028. <https://doi.org/10.3892/ijmm.2013.1486>
- Xu, D., Jin, T., Zhu, H., Chen, H., Ofengeim, D., Zou, C., Mifflin, L., Pan, L., Amin, P., Li, W., Shan, B., Naito, M. G., Meng, H., Li, Y., Pan, H., Aron, L., Adiconis, X., Levin, J. Z., Yankner, B. A., & Yuan, J. (2018). TBK1 Suppresses RIPK1-Driven Apoptosis and Inflammation during Development and in Aging. *Cell*, 174(6), 1477-1491.e19. <https://doi.org/10.1016/j.cell.2018.07.041>
- Yamanaka, K., Chun, S. J., Boillee, S., Fujimori-Tonou, N., Yamashita, H., Gutmann, D. H., Takahashi, R., Misawa, H., & Cleveland, D. W. (2008). Astrocytes as determinants of disease progression in inherited amyotrophic lateral sclerosis. *Nature Neuroscience*, 11(3), 251–253. <https://doi.org/10.1038/nn2047>
- Yi, H.-S., Kim, S. Y., Kim, J. T., Lee, Y.-S., Moon, J. S., Kim, M., Kang, Y. E., Joung, K. H., Lee, J. H., Kim, H. J., Chun, K., Shong, M., & Ku, B. J. (2019). T-cell senescence contributes to abnormal glucose homeostasis in humans and mice. *Cell Death & Disease*, 10(3), 249. <https://doi.org/10.1038/s41419-019-1494-4>
- Yu, C.-H., Davidson, S., Harapas, C. R., Hilton, J. B., Mlodzianoski, M. J., Laohamonthonkul, P., Louis, C., Low, R. R. J., Moecking, J., Nardo, D. D., Balka, K. R., Calleja, D. J., Moghaddas, F., Ni, E., McLean, C. A., Samson, A. L., Tyebji, S., Tonkin, C. J., Bye, C. R., ... Masters, S. L. (2020). TDP-43 Triggers Mitochondrial DNA Release via mPTP to Activate cGAS/STING in ALS. *Cell*, 183(3), 636-649.e18. <https://doi.org/10.1016/j.cell.2020.09.020>
- Zandi, E., Rothwarf, D. M., Delhase, M., Hayakawa, M., & Karin, M. (1997). *The IkappaB kinase complex (IKK) contains two kinase subunits, IKKalpha and IKKbeta, necessary for IkappaB phosphorylation and NF-kappaB activation*. [https://doi.org/10.1016/s0092-8674\(00\)80406-7](https://doi.org/10.1016/s0092-8674(00)80406-7)
- Zhang, J., Liu, L., Li, M., Liu, H., Gong, X., Tang, Y., Zhang, Y., Zhou, X., Lin, Z., Guo, H., & Pan, L. (2024). Molecular Basis of the Recognition of the Active Rab8a by Optineurin. *Journal of Molecular Biology*, 436(22), 168811. <https://doi.org/10.1016/j.jmb.2024.168811>

- Zhang, R., Gascon, R., Miller, R. G., Gelinas, D. F., Mass, J., Hadlock, K., Jin, X., Reis, J., Narvaez, A., & McGrath, M. S. (2005). Evidence for systemic immune system alterations in sporadic amyotrophic lateral sclerosis (sALS). *Journal of Neuroimmunology*, 159(1–2), 215–224. <https://doi.org/10.1016/j.jneuroim.2004.10.009>
- Zhao, W., Beers, D. R., Hooten, K. G., Sieglaff, D. H., Zhang, A., Kalyana-Sundaram, S., Traini, C. M., Halsey, W. S., Hughes, A. M., Sathe, G. M., Livi, G. P., Fan, G.-H., & Appel, S. H. (2017). Characterization of Gene Expression Phenotype in Amyotrophic Lateral Sclerosis Monocytes. *JAMA Neurology*, 74(6), 677. <https://doi.org/10.1001/jamaneurol.2017.0357>
- Zhu, G., Wu, C.-J., Zhao, Y., & Ashwell, J. D. (2007). Optineurin Negatively Regulates TNF $\alpha$ -Induced NF- $\kappa$ B Activation by Competing with NEMO for Ubiquitinated RIP. *Current Biology*, 17(16), 1438–1443. <https://doi.org/10.1016/j.cub.2007.07.041>

## 8. Abbreviations

$\Delta$ ex5; deletion of exon 5

aa; amino acids

ALS; amyotrophic lateral sclerosis

Arg1; arginase 1

BMDC; bone marrow dendritic cells

BMDM; bone marrow-derived macrophages

BV2; mouse microglial cell line

CC; coil-coiled

CCL; chemokine (C-C motif) ligand

cDC; classical dendritic cells

CNS; central nervous system

ChAT; choline acetyltransferase

CSF1; colony-stimulating factor 1

CSF1R; colony-stimulating factor 1 receptor

CXCL; C-X-C motif chemokine ligand

CYLD; cylindromatosis

C9ORF72; chromosome 9 open reading frame 72

DAMPs; danger-associated molecular patterns

DC; dendritic cells

DI; discrimination index

FDA; U.S. Food and Drug Administration Agency

FIP-2; 14.7K-interacting protein 2

FTD; frontotemporal dementia

FUS; fused in sarcoma

GFAP; glial fibrillary acidic protein

HEK293; human embryonic kidney 293

Htt; huntingtin

IFN; interferon

IGF-1; insulin growth factor-1

I $\kappa$ B- $\alpha$ ; inhibitor of  $\kappa$ B- $\alpha$

IKK; inhibitor of  $\kappa$ B kinase

IL; interleukin

IRF; interferon regulatory factor

J774.1; mouse macrophage cell line

K; lysine

LIR; LC3-interacting domain

LPS; lipopolysaccharide

LUBAC; linear ubiquitin chain assembly complex

M; methionine

MAPT; microtubule-associated protein tau

MEFs; mouse embryonic fibroblasts

MFI; mean fluorescence intensity

mGluR1a; metabotropic glutamate receptor type 1a

MYPT1; myosin phosphatase target subunit 1

NEMO; NF- $\kappa$ B essential modulator

NES; nuclear export signal

Neuro2A; mouse neuroblastoma cell line

NF- $\kappa$ B; nuclear factor- $\kappa$ B

NK; natural killer cells

NLS; nuclear localization signal

NSC-34; mouse motor neuron-like cell line

NTG; normal tension glaucoma

OPTN; optineurin

PAMPs; pathogen-associated molecular patterns

POAG; primary open angle glaucoma

PRRs; pattern recognition receptors

RANKL; receptor activator of nuclear factor  $\kappa$ B ligand

RIPK1; receptor-interacting serine/threonine protein kinase 1

RGC-5; mouse retinal ganglion cell line

RPE; human retinal pigment epithelium cells

RRM; RNA recognition motif

SOD1; superoxide dismutase 1

STAT; signal transducer and activator of transcription

STING; stimulator of interferon genes

TAK1; transforming growth factor  $\beta$ -activated kinase 1

TBK1; TANK-binding kinase 1

TDP-43; TAR DNA-binding protein 43

TFIIIA-intP; transcription factor IIIA

TGF- $\beta$ ; transforming growth factor  $\beta$

Th; helper T cells

TLR; Toll-like receptor

TNF; tumor necrosis factor

TNFR1; tumor necrosis factor receptor 1

TRAF; tumor necrosis factor receptor-associated factor

TRIF; TIR-domain-containing adapter-inducing IFN- $\beta$

TRAM; TRIF-related adaptor molecule

Treg; regulatory T cells

UBAN; ubiquitin-binding region of ABIN proteins and NEMO

UBR; ubiquitin-binding region

UPS; ubiquitin-proteasomal system

Q/N; glutamine/asparagine-rich region

WT; wild-type

ZF; zinc finger



## 9. List of figures

|  |    |
|--|----|
| Figure 1. Central nervous system regions and neurons affected in ALS. ....   | 1  |
| Figure 2. Most frequent genes affected by mutations in ALS. ....   | 4  |
| Figure 3. ALS/FTD represents a spectrum disorder, rather than distinct diseases. ....  | 5  |
| Figure 4. Protein domains and interaction partners of optineurin. ....   | 9  |
| Figure 5. Optineurin mutations found in ALS, FTD and both. ....  | 11 |
| Figure 6. Microglial phenotypes and their characteristic markers. ....   | 15 |
| Figure 7. NF- $\kappa$ B signaling upon TLR4 stimulation with LPS. ....  | 20 |
| Figure 8. The proposed role of optineurin in the NF- $\kappa$ B signaling pathway. ....  | 22 |
| Figure 9 TBK1 signaling pathway. ....  | 25 |
| Figure 10. The proposed role of optineurin in the TBK1 signaling pathway. ....   | 27 |
| Figure 11. TDP-43 protein domains. ....  | 29 |
| Figure 12. Phagocytosis assay setup. ....  | 59 |
| Figure 13. Gating strategy for <i>in vitro</i> T cell restimulation. ....  | 63 |
| Figure 14. Gating strategy for analysis of spleens upon consecutive LPS stimulation. ....  | 63 |
| Figure 15. Gating strategy for phagocytosis assay. ....  | 64 |
| Figure 16. Aging did not accelerate motor and cognitive decline in Optn <sup>470T</sup> mice. ....   | 67 |
| Figure 17. Aging did not trigger ALS-like neuropathology in Optn <sup>470T</sup> mice. ....  | 70 |
| Figure 18. Optineurin levels increased during aging in the spinal cord, but its insufficiency did not increase microgliosis. ....  | 73 |
| Figure 19. Optineurin insufficiency led to an increase of aging-induced Iba1 expression in the brain homogenates, but similar cytokine profiles. ....  | 76 |
| Figure 20. Optineurin insufficiency did not affect basal and inflammatory phagocytosis neither in BMDMs during aging nor in primary neonatal microglia. ....                                       | 78 |
| Figure 21. Male Optn <sup>470T</sup> , but not female mice, had similar T <sub>H1</sub> but decreased T <sub>H17</sub> CD4 <sup>+</sup> T cell polarization during aging compared to WT mice. .... | 82 |
| Figure 22. Aging induced an increase in CD8 <sup>+</sup> T cells positive for TNF in Optn <sup>470T</sup> male mice, whereas IFN- $\gamma$ and IL-2 were similar to WT mice. ....                  | 84 |
| Figure 23. Characterization of a new Optn <sup>470T</sup> /TDP-43 <sup>G348C</sup> double-hit mouse model. ....  | 85 |
| Figure 24. TDP-43 <sup>G348C</sup> and WT BMDMs showed comparable NF- $\kappa$ B and TBK1 pathway activation upon LPS stimulation. ....  | 88 |

|   |     |
|---|-----|
| Figure 25. Optn <sup>470T</sup> /TDP-43 <sup>G348C</sup> BMDMs showed similar NF-κB but diminished TBK1 activation upon LPS stimulation compared to TDP-43 <sup>G348C</sup> BMDMs. ....                               | 91  |
| Figure 26. Optn <sup>470T</sup> /TDP-43 <sup>G348C</sup> mice had improved motor and cognitive functions and lower body weight compared to TDP-43 <sup>G348C</sup> mice at 18 months of age. ....                     | 93  |
| Figure 27. The presence of Optn <sup>470T</sup> truncation in TDP-43 <sup>G348C</sup> mice had a protective effect against LPS-induced body weight loss and death. ....   | 95  |
| Figure 28. The decreased splenocyte number in Optn <sup>470T</sup> /TDP-43 <sup>G348C</sup> compared to Optn <sup>470T</sup> mice upon three-day LPS stimulation was accounted for by the loss of B lymphocytes. .... | 96  |
| Figure 29. Optn <sup>470T</sup> /TDP-43 <sup>G348C</sup> mice had a lower number of classical dendritic and NK cells compared to Optn <sup>470T</sup> mice upon three-day LPS administration. ....                    | 98  |
| Figure 30. Three-day LPS administration increased CCL2 and IL-10 concentrations in the serum of TDP-43 <sup>G348C</sup> and Optn <sup>470T</sup> /TDP-43 <sup>G348C</sup> mice, respectively. ....                    | 100 |

## 10. List of tables

|   |    |
|---|----|
| Table 1. List of optineurin interaction partners and their cellular function. ....  | 7  |
| Table 2. Summary of findings regarding the role of optineurin in the NF- $\kappa$ B signaling.....  | 22 |
| Table 3. Summary of findings regarding the role of optineurin in the TBK1 signaling.....  | 27 |
| Table 4. List of primary antibodies used in western blot (WB) and immunofluorescence (IF). ..   | 40 |
| Table 5. List of secondary antibodies used in western blot (WB) and immunofluorescence (IF).  | 41 |
| Table 6. List of antibodies used for IFN- $\beta$ ELISA. ....   | 41 |
| Table 7. Antibodies used for staining surface markers by flow cytometry. ....   | 42 |
| Table 8. Antibodies used for intracellular staining by flow cytometry. ....   | 42 |
| Table 9. PCR reaction mixes per one sample for amplification of WT and Optn <sup>470T</sup> and TDP-43 <sup>G348C</sup> DNA fragments. .... | 45 |
| Table 10. PCR programs for genotyping. ....   | 45 |
| Table 11. Primers used for PCR, ordered from Metabion at stock concentration of 100 $\mu$ M. ....   | 46 |
| Table 12. Reverse transcription reaction mix. ....  | 54 |
| Table 13. Reverse transcription PCR program. ....   | 55 |
| Table 14. RT-qPCR master mix. ....  | 55 |
| Table 15. List of primers used for RT-qPCR.....   | 56 |
| Table 16. RT-qPCR program.....  | 56 |

## 11. Biography



### Josip Peradinović

📍 **Work :** Radmile Matejcic 2, 51000, RIJEKA, Croatia

✉ **Email:** [josip.peradinovic@biotech.uniri.hr](mailto:josip.peradinovic@biotech.uniri.hr)

**Place of birth:** Rijeka, Croatia **Nationality:** Croatian

#### WORK EXPERIENCE

[ 15 Oct 2020 – Current ]

##### PhD candidate

*Faculty of Biotechnology and Drug Development*

**City:** Rijeka | **Country:** Croatia

Field of research: Investigating the role of optineurin in immune-mediated pathologies

#### EDUCATION AND TRAINING

[ 15 Oct 2020 – Current ]

##### PhD candidate

*Faculty of Biotechnology and Drug development*

**City:** Rijeka, Croatia |

Programme: Medicinal Chemistry

[ 2018 – 2020 ]

##### Master of Biotechnology in Medicine

*Faculty of Biotechnology and Drug Development*

**City:** Rijeka, Croatia |

GPA: 4.727 (*Summa cum laude*) (max 5.00)

**Master's thesis:** The cell-specific role of optineurin in TLR4- and ER stress-mediated activation of the NF- $\kappa$ B pathway

[ 2015 – 2018 ]

##### Bachelor of Biotechnology and Drug Research

*Faculty of Biotechnology and Drug Development*

**City:** Rijeka, Croatia | **Country:** Croatia |

GPA: 4.621 (*Cum laude*) (max 5.00)

**Bachelor's thesis:** Tripyridylporphyrins in photodynamic inactivation of *Legionellae*

[ 2015 – 2018 ]

##### Grammar School eugen Kunicic

**City:** Opatija, Croatia |

[ 2003 – 2011 ]

##### Elementary School dr. Andrija Mohorovicic

**City:** Matulji, Croatia |

#### AWARDS AND SCHOLARSHIPS

Croatian Academy of sciences and Arts Grant

"Investigating the role of optineurin during viral infection of primary neurons"

6. December 2024. – 6. December 2025.

##### ERASMUS+ Mobility

ERASMUS+ Mobility

Internship at the University of Ulm, Department of Neurology

Mentor: David Brenner, MD, PhD

Research focus: The role of Tbk1 haploinsufficiency in ALS mouse model

08. January – 08. March 2024.

Bursary for "FluoMicro@ICGEB - Practical Course of Fluorescence Microscopy and high throughput imaging" attendance

04. - 06. October 2022.

Selvita's bursary for attendance at HDBMB conference: FROM SCIENCE TO KNOWLEDGE

28. September – 01. October 2022.

Scholarship for successful students of city of Matulji

2016. - 2020.

## PUBLICATIONS

---

Nikolina Mohovic\*, Josip Peradinovic\*, Andrea Markovinovic, Raffaello Cimbri, Zeljka Minic, Marin Dominovic, Hrvoje Jakovac, Jerneja Nimac, Boris Rogelj & Ivana Munitic; Neuroimmune characterization of optineurin insufficiency mouse model during ageing. *Sci Rep.* 13, 11840 (2023); (Q1, IF = 4.996); <https://doi.org/10.1038/s41598-023-38875-3> \* These authors contributed equally

Josip Peradinovic, Nikolina Mohovic, Katarina Bulic, Andrea Markovinovic, Raffaello Cimbri and Ivana Munitic. Ageing-Induced Decline in Primary Myeloid Cell Phagocytosis Is Unaffected by Optineurin Insufficiency. *Biology* 2023, 12(2), 240; <https://doi.org/10.3390/biology12020240>

Prtenjača N, Dominović M, Peradinović J, Šajn R, Markovinović A, Munitić I (2020), Optineurin Dysfunction in Amyotrophic Lateral Sclerosis: Why So Puzzling? *Periodicum Biologorum*. 2021 Mar; 1-2. doi: 10.18054./pb.v121-122i1-2.10627

## SCIENTIFIC CONFERENCES

---

### 8th RIJEKA FORUM ON NEURODEGENERATIVE DISEASES

Poster presentation: "Neuroimmune characterization of aged mice with optineurin insufficiency" 16. - 17. September 2024.

### Science and Us

Oral presentation: "Immunity in optineurin insufficiency mouse model during aging: From the central nervous system to the periphery" 16. - 18. June 2024.

### ENCALS - European Network to Cure ALS

Poster presentation: "Neuroimmune characterization of aged mice with optineurin insufficiency" 11. - 14. July 2023.

### International Congress of the Croatian Society of Biochemistry and Molecular Biology HDBMB22: FROM SCIENCE TO KNOWLEDGE

Poster presentation: "Neuroimmune characterization of optineurin insufficiency mouse model" 28. September – 01. October 2022.

**Joint ICGEB – ALS Society of Canada Symposium on Inflammation & Proteinopathy in ALS/FTD Spectrum Disorder**

Poster presentation: "Characterization of optineurin insufficiency mice during ageing" 30. June - 03. July 2022.

**Croatian Immunological Society - Annual meeting**

Oral and poster presentation "Neuroimmune characterization of optineurin insufficiency mouse model" 23. - 25. September 2021.

**3rd Symposium of Physiology and Pathology of neuroglia (Online)**

Oral presentation: "The cell-specific role of optineurin in the NF- $\kappa$ B pathway" 24. - 25. November 2020.

**Sanitas - Student congress of health protection**

Poster presentation: „Photodynamic inactivation as a novel approach in eradication of *Legionella*" 5. - 6. April 2019.

**TRAININGS**

---

**FluoMicro@ICGEB - Practical Course of Fluorescence Microscopy and high throughput imaging**

Organized by: The International Centre for Genetic Engineering and Biotechnology (ICGEB) 04. - 06. October 2022.

**Flow cytometry: from basic principles to advanced applications (Online)**

Organized by: The International Centre for Genetic Engineering and Biotechnology (ICGEB) 28. - 30. September 2021.

**Winter school "Basics of Scientific Writing"**

2. - 3. March 2018.

**SCIENCE POPULARIZATION**

---

**4th Symposium PosteRi**

Poster evaluation committee  
05. October 2024.

**Presentation of Laboratory for Molecular Immunology**

Faculty of Biotechnology and Drug Research Open Days  
2021., 2023., 2024.

**The night of investigators**

27. September 2019.

**LABORATORY EXPERIENCE**

---

[ Sep 2019 – Jul 2020 ] **Master Student Researcher**

Mentor: Associate Professor Ivana Munitic, MD, PhD

|                              |   |
|------------------------------|---|
|                              | <p>Co-mentor: Assistant Professor Jelena Ban, PhD<br/> Laboratory for Molecular Immunology<br/> Department of Biotechnology, University of Rijeka, Croatia</p>  |
| [ Oct 2019 – Nov 2019 ]      | <p><b>Student Teaching Fellow, course: Immunology</b><br/> Help with experiments<br/> Laboratory for Molecular Immunology<br/> Department of Biotechnology, University of Rijeka, Croatia</p>   |
| [ Mar 2018 – May 2018 ]      | <p><b>Bachelor Student Researcher</b><br/> Mentor: Associate Professor Nela Malatesti, PhD<br/> Co-mentor: Associate Professor Ivana Gobin, PhD<br/> Department for Microbiology and Parasitology<br/> Medical School, University of Rijeka, Croatia</p> <p><b>Volunteer in Research</b><br/> Laboratory for Natural Products and Metabolomics<br/> Department of Biotechnology, University of Rijeka, Croatia</p> <p>July 2017. - September 2017.,<br/> July 2016. - September 2016.</p> |
| <b>LABORATORY TECHNIQUES</b> | <hr/> <p>Work with cell lines and primary cells (microglia, astrocytes, bone marrow, neurons), protein isolation from cells and tissues, protein quantification, western blot, ELISA, RT-qPCR, photoinactivation test on bacteria, flow cytometry, motor and behavioral tests on mice, immunofluorescence</p>   |
| <b>MEMBERSHIPS</b>           | <hr/> <p>Croatian Immunological Society<br/> September 2021. -</p> <p>Croatian Society of Biochemistry and Molecular Biology<br/> October 2021. -</p>   |
| <b>COMPUTATIONAL SKILLS</b>  | <hr/> <p><b>Computational skills</b><br/> <i>In silico</i> analysis: Avogadro, Chemaxon Marvin, PyMOL, Chimera, VMD, GROMACS<br/> MS Office (Word, Excel, PowerPoint), Adobe Illustrator, Adobe Photoshop<br/> A plasmid Editor (ApE) software - used for cloning<br/> GraphPad Prism</p>   |
| <b>LANGUAGE SKILLS</b>       | <hr/> <p><b>Mother tongue(s):</b> Croatian</p>  |

**Other language(s):**

**English**

LISTENING C1 READING C1 WRITING C1

SPOKEN PRODUCTION C1 SPOKEN INTERACTION C1

**Russian**

LISTENING B1 READING B1 WRITING B1

SPOKEN PRODUCTION A2 SPOKEN INTERACTION A2

*Levels: A1 and A2: Basic user; B1 and B2: Independent user; C1 and C2: Proficient user*

## **DRIVING LICENCE**

---

**Cars:** B